Functional Characterisation Of Novel Plasmodium falciparum Proteins And Their Role In Erythrocyte Invasion.

Benjamin Liffner

Research Centre for Infectious Diseases

Department of Molecular and Biomedical Sciences

School of Biological Sciences

University of Adelaide

August 2020

A thesis submitted by

Benjamin Liffner

to

The University of Adelaide,

for fulfilment of the requirements for

Doctor of Philosophy in Biological Sciences

in the Department of Molecular and Biomedical Sciences,

School of Biological Sciences.

Abstract

Malaria caused by *Plasmodium falciparum* is responsible for the deaths of hundreds of thousands of children every year, and imparts an overwhelming economic burden on the world's poorest countries. All symptoms of malaria are caused during the asexual blood-stage of the *P. falciparum* lifecycle, which is reliant on merozoite invasion of host red blood cells (RBCs). Due to its essentiality for parasite survival, and its exposure to the host immune system, merozoite invasion is an attractive target for the development of antimalarial therapeutics. Merozoite invasion is coordinated by a series of secretory organelles, of which the largest and most well characterised are the rhoptries. Previous studies into rhoptry proteins have been strongly foccused on antigens that are secreted from the rhoptries during invasion; primarily due to their promise as vaccine candidates. As such, very little is known about proteins that coordinate rhoptry biogenesis, structure, or function.

Prior to this study the *P. falciparum* proteins Pf3D7_0210600 and Pf3D7_0405200, hereafter referred to as *P. falciparum* Cytosolically Exposed Rhoptry Leaflet Interacting proteins (PfCERLI) 1 and 2, were largely uncharacterised proteins that previous studies had suggested may play a role in merozoite invasion. We hypothesised that PfCERLI1 and PfCERLI2 were rhoptry proteins that shared an evolutionary relationship and were both essential for merozoite invasion. We aimed to test these hypotheses through bioinformatic analyses, immunofluorescence microscopy, and gene disruption or inducible knockdown.

Bioinformatic and phylogenetic analyses showed that *cerli1* and *cerli2* arose through an ancestral gene duplication of *cerli1* that was present in the most recent common ancestor of haematozoa and coccidia. Analysis of the structure of CERLI proteins revealed

they possess a conserved motif with the consensus sequence PHISE/DxxP that we have termed PHIS, along with conserved C2 and Pleckstrin homology (PH) domains that are likely ito have a role in membrane association.

Using selection linked integration targeted gene disruption (SLI-TGD) we determined that both *Pfcerli1* and *Pfcerli2* were refractory to gene deletion and likely important for blood-stage growth. To assess their functions, we used an inducible protein knockdown system whereby the addition of glucosamine (GLCN) results in specific mRNA degradation prior to translation. Knockdown of either CERLI1 or CERLI2 resulted in growth inhibition caused by an inability of merozoites to invade RBCs. Immunofluorescnce microscopy and biochemical techniques revealed that both proteins are peripheral membrane proteins that localise to the cytosolic face of the rhoptry bulb.

Rhoptry secretion assays showed that knockdown of PfCERLI1, but not PfCERLI2, leads to a defect in the secretion of key rhoptry antigens. By contrast, electron microscopy analysis of rhoptry size indicated a significant increase in rhoptry length following PfCERLI2 knockdown, but no change with PfCERLI1 knockdown. Semi-quantiative super-resolution microscopy analysis determined that knockdown of PfCERLI1 alters rhoptry antigen distribution, and it was shown that both PfCERLI1 and PfCERLI2 knockdown inhibit processing of key rhoptry antigens.

The findings of these studies show that the previously uncharacterised proteins, PfCERLI1 and PfCERLI2, are related rhoptry proteins whose functions are essential for maintaining rhoptry morphology, rhoptry secretion, and rhoptry antigen processing.

Declaration

I certify that this work contains no material which has been accepted for the award of any other degree or diploma in my name, in any university or other tertiary institution and, to the best of my knowledge and belief, contains no material previously published or written by another person, except where due reference has been made in the text. In addition, I certify that no part of this work will, in the future, be used in a submission in my name, for any other degree or diploma in any university or other tertiary institution without the prior approval of the University of Adelaide and where applicable, any partner institution responsible for the joint-award of this degree.

I acknowledge that copyright of published works contained within this thesis resides with the copyright holder(s) of those works.

I also give permission for the digital version of my thesis to be made available on the web, via the University's digital research repository, the Library Search and also through web search engines, unless permission has been granted by the University to restrict access for a period of time.

I acknowledge the support I have received for my research through the provision of an Australian Government Research Training Program Scholarship.

Signature: **Date:** 26th August 2020

Publications

Peer-reviewed publications to support this thesis:

1.**Liffner B**, Frölich S, Heinemann GK, Liu B, Dixon MWA, Gilberger T, Wilson DW. (2020). PfCERLI1 is a conserved rhoptry associated protein essential for *Plasmodium falciparum* merozoite invasion of erythrocytes. *Nature Communications*.

Manuscripts in preparation to support this thesis:

1. **Liffner B**, Balbin JM, Heinemann GK, Strauss J, Liu B, Dixon MWA, Gilberger T, Wilson DW. *Pfcerli2* arose through duplication of *Pfcerli1* and is essential for merozoite invasion by the malaria parasite *Plasmodium falciparum*.

Other publications from this candidature:

1. Burda PC, Corsskey T, Lauk K, Zuborg A, Söhnchen C, **Liffner B**, Wilcke L, Strauss J, Jeffries C, Svergun D, Wilson DW, Wilmanns M, Gilberger T. Structural analysis reveals a lipocalin in the malaria parasite *Plasmodium falciparum* that is essential for parasite proliferation. *Cell Reports*.

2. Wichers JS, Scholz J, Strauss J, Witt S, Lill A, Ehnold L, Neupert N, **Liffner B**, Lühken R, Petter M, Lorenzen S, Wilson DW, Löw C, Lavazec C, Bruchhaus I, Tannich E, Gilberger TW, Bachmann A. (2019). Dissecting the gene expression, localization,

membrane topology and function of the *Plasmodium falciparum* STEVOR protein family. *mBio*.

3. Geiger M, Brown C, Wichers JS, Strauss J, **Liffner B**, Wilcke L, Lemcke S, Wilson DW, Filarsky M, Burda PC, Zhang K, Junoop M, Gilberger T. (2019). Structural insights into PfARO and characterization of its interaction with PfAIP. *Journal of Molecular Biology*.

Other accepted manuscript from this candidature:

1. Burns A, Sleebs B, Ghizal S, De Paoli A, Anderson D, **Liffner B**, Harvey R, Beeson JG, Creek DJ, Goodman CD, McFadden GI, Wilson DW. Retargeting azithromycin-like compounds as antimalarials with dual modality. Accepted at BMC Biology (BMCB-D-20-00228).

Communications

The results of this thesis were presented at the following scientific conferences:

1. **Liffner B**, Burns A, Wilson W. Characterising the role of PfROMP in erythrocyte invasion and sexual development of the malaria parasite, *Plasmodium falciparum.* Adelaide Protein Group Student Awards 2017, Adelaide, Australia. Poster Presentation.

2. **Liffner B**, Frölich S, Balbin JM, Lemcke S, Alder A, Gilberger T, Wilson DW. Understanding how the malaria parasite, *Plasmodium* falciparum, invades red blood cells. German Academic Exchange Service (DAAD) alumni meeting 2018, Melbourne, Australia. Poster presentation.

3. **Liffner B**, Heinemann GK, Gilbeger T, Wilson DW. Functional and structural insights into related essential rhoptry proteins. Biology and Pathology of the Malaria Parasite 2019, Heidelberg, Germany. Poster presentation and flash talk.

4. **Liffner B**, Frölich S, Beeson J, Gilberger T, Wilson DW. Genetic analysis of a conserved protein reveals an important role in *Plasmodium falciparum* merozoite invasion of the host cell. Biology and Pathology of the Malaria Parasite 2019, Heidelberg, Germany. Poster presentation and flash talk.

5. **Liffner B**, Frölich S, Liu B, Dixon MWA, Gilbeger T, Wilson DW. Functional analysis of a conserved rhoptry protein reveals an essential role in erythrocyte invasion by *Plasmodium* falciparum merozoites. Gordon Research Seminar: Malaria, 2019, Les Diablerets, Switzerland. Poster presentation.

6. **Liffner B**, Frölich S, Dixon MWA, Gilberger T, Wilson DW. Identification of a novel rhoptry protein that is essential for merozoite invasion. Malaria in Melbourne 2019, Melbourne, Australia. Oral presentation.

7. **Liffner B**, Frölich S, Balbin JM, Wilson DW. A novel malaria parasite protein essential for invasion. Institute for Photonics and Advanced Sensing Student Awards 2020, Adelaide, Australia. Oral presentation.

8. **Liffner B**, Frölich S, Dixon MWA, Heinemann G, Liu B, Ralph SA, Gilberger T, Wilson DW. Identification of a novel malaria merozoite protein that is essential for rhoptry secretion. Molecular Approaches to Malaria 2020, Lorne, Australia. Poster presentation.

9. **Liffner B,** Frölich S, Balbin JM, Strauss J, Dixon MWA, Heinemann G, Liu B, Ralph SA, Gilberger T, Wilson DW. Identification of related *P. falciparum* merozoite proteins that are essential for rhoptry secretion. Australian Society for Parasitology conference 2020. Oral Presentation.

Acknowledgments

The last three and a half years have been a rollercoaster of ups, downs, and roundabouts. Through it all though, I've learned, seen, and done things I couldn't previously have imagined, and this has made it worth all the while. I've often thought about how few people in this world wake up each morning and are excited for the day of work ahead of them. For my PhD giving me the opportunity to pursue a career where this is my reality, I am endlessly indebted.

To Danny, I can't say how much your guidance has shaped not only my future career, but me as a person. So often you went out of your way to do things that would help me immensely, even if it provided no benefit, or maybe even made it more difficult, for you. It is this selflessness, and the consant drive to try make things better for those around you, that I admire most. Thank you for giving me so many wonderful opportunities, and for making the Wilson Lab the place on earth I most enjoy being.

To Tim, thankyou for the amazing hospitality in Hamburg. My six months there was some of the best times I've ever had. Even if what I actually planned to there experimentally was a cataclysmic failure, I have learned so much from my time there, and Hamburg will always feel like a home away from home. To the rest of the BNI/CSSB crew, especially Stephan, Paul, and Michael, thankyou for making my time in Hamburg so enjoyable. I hope we cross paths again many times in the future.

To the members of the Wilson Lab past and present: Amy, Issy, Sonja, Miguel, Jill, Ornella, Maria and Helin, sorry for distracting you from getting any work done with facts

about jellyfish, or a rant about why time is an imperial measurement. Working with you all has been an absolute blast, you've made the lab such a fun environment. The consistently high standard of our snacks, along with the lunch schedule will be something I will hold all my future colleagues to.

To the RCID members past and present, all our collaborators, and the malaria community more broadly, thankyou for the comeradery over the past few years and holding me and everybody else to a high standard of work. A particular thankyou to James, and the members of the Paton Lab, for generously hosting us in your lab space for the first year and a bit of my PhD.

To my best mates out of the lab: Isaac, Juan, Matt, Matt, Tim, Francis, Noah, and Dec, thanks for all the great times and support.

To my beautiful partner Tahlia, I couldn't have done this without you. You keep me grounded, and on track when things are not going well. The last few years has involved a lot of awkward working hours, periods with little time off, and us spending months apart. I can't thankyou enough for taking that in your stride and being so accepting of the difficulties of my career path. To Vince, Sandra, Alessia, and Lara, thankyou for everything you've done for me over the past few years. Being in a family environment, when I don't get to see my only family together very frequently, is something I've really cherished.

Finally to my family, Mum Dad, Dylan, Stacey, Joel, Rebecca, Nic, Amy, Farmor, Farfar, Tayah, Callie, Kai and Magnus, the last few years have been tough, but we have been strong together. Although geographically distant, we are close in thought and feeling. To Granny, one of the last things you told me was to travel the world and chase my dreams. I hope I've made you proud. Limitless undying love.

Table of Contents

List of Tables

Chapter 3 Tables

Chapter 5 Tables

List of Figures

Chapter 1 Figures

Chatper 3 Figures

Chapter 4 Figures

Chapter 5 Figures

Abbreviations

ACß	Adenylyl/Adenylate cyclase beta
ACT	Artemisinin combination therapy
AIP	ARO interacting protein
AMA	Apical membrane antigen
ARO	Armadillo repeats only
BLAST	Basic local alignment search tool
BSA	Bovine serum albumin
C1	Compound 1
cDNA	Complementary DNA
CERLI	Cytosolically exposed rhoptry leaflet interacting protein
CRISPR	Clustered regularly interspersed small palindromic repeats
CSP	Circumsporozoite protein
CyRPA	Cysteine-rich protective antigen
DAPI	4’,6-diamidino-2phenylindole, dihydrochloride
DHFR	Dihydrofolate reductase
DNA	Deoxyribonucleic acid
E64	*trans*-Epoxysuccinyl-L-leucylamido(4-guanidino)butane

EBA	Erythrocyte binding antigen
EDTA	Ethylenediaminetetraacetic acid
ELISA	Enzymye-linked immunosorbent assay
EMP	Erythrocyte membrane protein
ERC	Endoplamsic reticulum-resident calcium binding protein
EtBr	Ethidum bromide
EV	Evacuoles
EXP	Exported protein
FITC	Fluorescein isothiocyanate
GAP	Glideosome associated protein
gDNA	Genomic DNA
GFP	Green fluorescent protein
GLCN	Glucosamine
GLCN6P	Glucosamine-6-phosphate
GlmS	Glucosamine-6-phosphate riboswitch ribozyme
Gly	Glycophorin
GPI	Glycophosphatidylinositol
HA	Haemagglutinin

HEPES	4-(2-hydroxyethyl)-1-piperazineethanesulfonic acid
HPI	Hours post-invasion
HSP	Heat shock protein
IMC	Inner-membrane complex
IP4	1,3,4,5-tetrakisphosphate
IRS	Indoor residual spraying
ITASSER	Iterative threading assembly refinement
ITN	Insecticide treated bednet
KD	Knock down
KO	Knock out
LOMETS	Local meta-threading-server
LSM	Laser scanning microscope
MACS	Magnet-activated cell sorting
MCC	Mander's correlation coefficient
MOP	Merozoite organising protein
MSP	Merozoite surface protein
Myo	Myosin
NAG	N-acetylglucosamine

PBS	Phosphate buffered saline
PCC	Pearson’s correlation coefficient
PCR	Polymerase chain reaction
PE	Phycoerythrin
PFA	Paraformaldehyde
PH	Pleckstrin homology
PIP3	Phosphatidylinositol (3,4,5)-trisphosphate
PLL	Poly-L-lysine
PPM	Parasite plasma membrane
PTEX	Plasmodium translocon of exported proteins
PV	Parasitophorous vacuole
PVM	Parasitophorous vacuole membrane
RAMA	Rhoptry associated membrane antigen
RAP	Rhoptry associated protein
RBC	Red blood cell
RBW	Riboswitch
RESA	Ring-expressed surface antigen
RH	Reticulocyte binding homologue

RHOP	Rhoptry protein
RhopH	Rhoptry heavy protein
Ripr	RH5-interacting protein
RNA	Ribonucleic acid
RON	Rhoptry neck protein
RPMI	Roswell Park Memorial Institute
SDS	Sodium dodecyl sulphate
SLI-TGD	Selection linked integration – targeted gene disruption
SoD	Superoxide dismutatse
SP	Signal peptide
TBS	Tris-buffered saline
TCA	Trichloroacetic acid
TEM	Transmission electron microscopy
Tx100	Triton-X-100
UPGMA	Unweighted pair group method with arithmetic mean
UTR	Untranslated region
WHO	World Health Organization

Chapter 1: Introduction

Global burden of malaria

Malaria is caused by single-celled apicomplexan parasites of the genus *Plasmodium* and is transmitted to humans by female *Anopheles* mosquitoes (Cowman, Healer et al. 2016). Malaria results in both significant morbidity and mortality in endemic countries, with approximately half the world's population at risk of malaria. This public health burden leads to significant socioeconomic stress on many of the world's poorest countries (World Health Organization 2019). Due to its overwhelming burden, the World Health Organization, with governmental and philanthropic partners, have set a goal of malaria eradication (Gates 2007, Gates 2007).

Human malaria parasites

Several malaria parasites are known to cause disease in humans, with *Plasmodium falciparum, P. vivax, P. malariae, P. ovale curtisi,* and *P. ovale walikeri* typically considered as human malaria parasites (Cowman, Healer et al. 2016). Additionally, *P. knowlesi* (Singh, Kim Sung et al. 2004), *P. simium* (Brasil, Zalis et al. 2017), and *P. cynomolgi* (Hartmeyer, Stensvold et al. 2019) have recently been identified as emerging zoonotic malaria parasites that have spilled over from either macaques (genus: *Macaca*) or howler monkeys (genus: *Alouatta*). While significant differences exist between the biology, evolutionary history, and clinical presentations of these parasites, all are transmitted to humans through the bite of an infected female *Anopheles* mosquito (Cowman, Healer et al. 2016).

Epidemiology

It is estimated that there were 228 million cases of malaria in 2018 that caused 405,000 deaths with children under the age of five representing 67% of malaria deaths (World Health Organization 2019). Additionally, malaria imparts a significant health burden on both pregnant mothers and infants with 872,000 low birthweight births caused by malaria in pregnancy (World Health Organization 2019). Malaria is predominantly present in the world's tropical and sub-tropical regions, with 87 countries currently listed as being malaria endemic (World Health Organization 2019). Sub-Saharan Africa is the most heavily affected region in the world in terms of malaria mortality, with 94% of all malaria deaths occurring there (World Health Organization 2019). *P. falciparum* is the most prevalent parasite in sub-Saharan Africa, where it accounts for 99.7% of all malaria cases (World Health Organization 2019). *P. vivax* is much more common outside of Africa with ~50% of cases in South-East Asia and 75% of cases in the Americas caused by this parasite (World Health Organization 2019). Malaria is endemic in Australia's nearest neighbour, Papua New Guinea, where it is a leading cause of childhood mortality and hospitalisation (World Health Organization 2016).

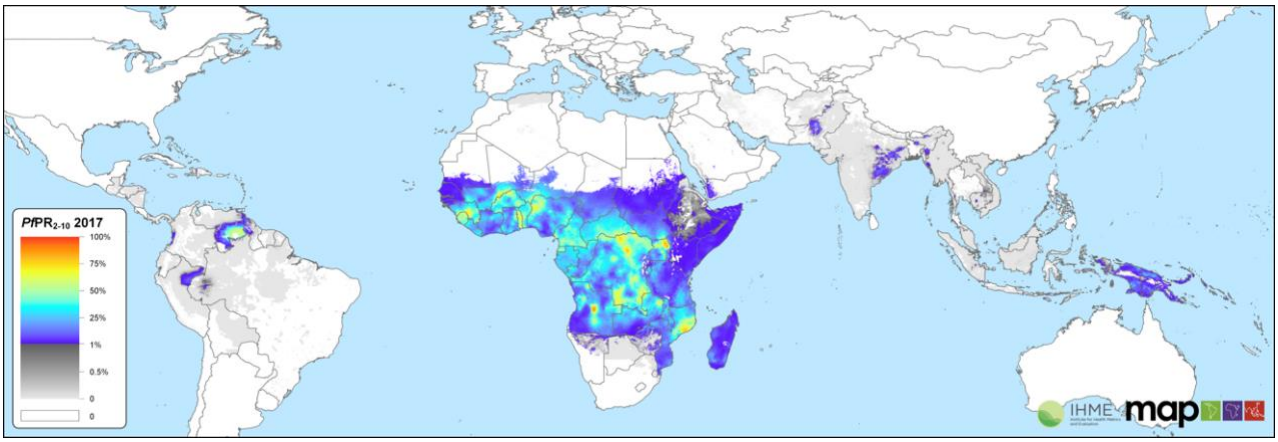

Figure 1.1: Global endemicity of *P. falciparum*.

P. falciparum infection prevalence in children aged 2 to 10 in the year 2017. Figure replicated from the Malaria Atlas Project (https://malariaatlas.org/) (Weiss, Lucas et al. 2019).

In areas where malaria is highly endemic, like much of sub-Saharan Africa, children typically suffer multiple infections and go on to develop non-sterilising naturally acquired immunity by adulthood (Doolan, Dobaño et al. 2009). In lower transmission areas, this naturally acquired immunity often fails to develop and so adults are commonly infected in these areas (Pinkevych, Petravic et al. 2012). Additionally, naturally acquired immunity is not lifelong and wanes when a previously immune individual leaves a malaria endemic area for an extended period of time (Pinkevych, Petravic et al. 2012). Moreover, asymptomatic infections that are enabled by non-sterilising natural immunity provide a significant reservoir of community transmission that can continue all year (Chaumeau, Kajeechiwa et al. 2019).

Malaria often causes intense epidemics upon breakdown of economic or social systems, healthcare systems, mass migration events (Abeku 2007) and with changes in weather patterns (Loevinsohn 1994). Malaria transmission is intrinsically linked to the prevalence and breeding behaviour of *Anopheles* mosquitoes, which varies greatly around the world largely according to

local climate and weather events. Additionally, different *Anopheles* spp. have vastly different capacities as vectors for different species of human-infecting *Plasmodium* (Gunasekaran, Sahu et al. 2014). As such, malaria transmission changes significantly over time, but it is thought that climate change may introduce malaria and increase its intensity in many areas of the world (Caminade, Kovats et al. 2014). Of most immediate concern are those who live in the higher altitude cooler climates of already malaria endemic countries (Betuela, Maraga et al. 2012), which are often densely populated; such as the New Guinea and Ethiopian Highlands. It is predicted that an increase of 1°C in global mean temperature would result in an increase of 410,000 (15% increase) cases each year in Ethiopia alone (Siraj, Santos-Vega et al. 2014). While it is difficult to predict how climate change may alter malaria transmission in many different localities, this poses a significant hurdle for the future eradication of malaria.

Clinical presentation of malaria

Malaria can present clinically with an extremely broad range and severity of symptoms that are influenced by the *Plasmodium* species causing the infection, host age, sex and parasite burden, among others (Svenson, MacLean et al. 1995). Typically, malaria is an uncomplicated febrile illness that manifests as fever, headaches and chills that recur approximately every 24, 48, or 72 (*P. knowlesi, P. falciparum*/*P. vivax*/*P. ovale, P. malariae* respectively) hours according to the *Plasmodium* species causing the infection (Svenson, MacLean et al. 1995, McKenzie, Jeffery et al. 2001, Singh, Kim Sung et al. 2004, Cowman, Healer et al. 2016). These recurring fevers are typically self-limiting and in malaria endemic areas, children will typically become infected multiple times throughout their childhood (Doolan, Dobaño et al. 2009). Following multiple rounds of infection, non-sterilising immunity develops whereby individuals may harbour significant numbers of parasites but remain asymptomatic (Doolan, Dobaño et al. 2009). Asymptomatic

carriers represent an important infectious reservoir, as they can still transmit the parasite but are unlikely to receive antimalarial therapeutics.

While most cases of malaria are uncomplicated and self-limiting, approximately 1% of those infected will go on to develop significant, life threatening, complications that are known collectively as severe malaria (Marsh, Forster et al. 1995). Severe malaria is typically characterised as presenting with neurological complications (cerebral malaria), severe anaemia, metabolic acidosis, or a combination of the three (Marsh, Forster et al. 1995, Dondorp 2005). Patients who present with more than one of these three distinct clinical manifestations have significantly worse prognoses than those with only one (Marsh, Forster et al. 1995). Additionally, malaria can manifest clinically in many different ways including acute renal failure (Das 2008), multiple organ failure (Krishnan and Karnad 2003), or liver failure (Viriyavejakul, Khachonsaksumet et al. 2014), however the mechanisms for these manifestations are either poorly understood or related to one of the three aforementioned manifestations of severe malaria.

Anaemia

Malaria can result in anaemia both directly, through destruction of infected red blood cells (RBCs) as well as indirectly, through enhanced clearance of uninfected RBCs and a decrease in erythropoiesis (White 2018). While severe anaemia is a common cause of hospitalisation in children with severe malaria, nearly all children in highly malaria endemic areas are anaemic (White 2018). The high prevalence of anaemia due to malaria, as well as other causes of anaemia such as malnutrition or hookworm, is thought to impart a significant developmental burden on affected children (Lozoff, Beard et al. 2006, Georgieff 2011).

The prevalence of malaria in historically malaria endemic regions of the world has strongly selected for genetic traits that are protective against malaria with sickle cell anaemia the most well

studied of these (Weatherall 2008, Casanova 2015, Williams 2016). While these traits were selected because they inhibited parasite replication and therefore protected to a certain degree against malaria, they also decrease oxygen carrying capacity of RBCs and themselves either lead to exacerbate anaemia. Sickle cell anaemia is estimated to have contributed directly to ~114,000 deaths in 2015 (GBD 2015 Mortality and Causes of Death Collaborators 2016) and while sickle cells are resistant to infection, it is thought that many of these aneamia deaths were still triggered by malaria (White 2018). Furthermore, glucose-6-phosphate dehydrogenase (G6PD) deficiency, which was likely selected for in humans because it imparts partial protection from malaria is now present in over 400 million people worldwide (Cappellini and Fiorelli 2008) and leaves patients at an increased risk of severe malarial anaemia (White 2018).

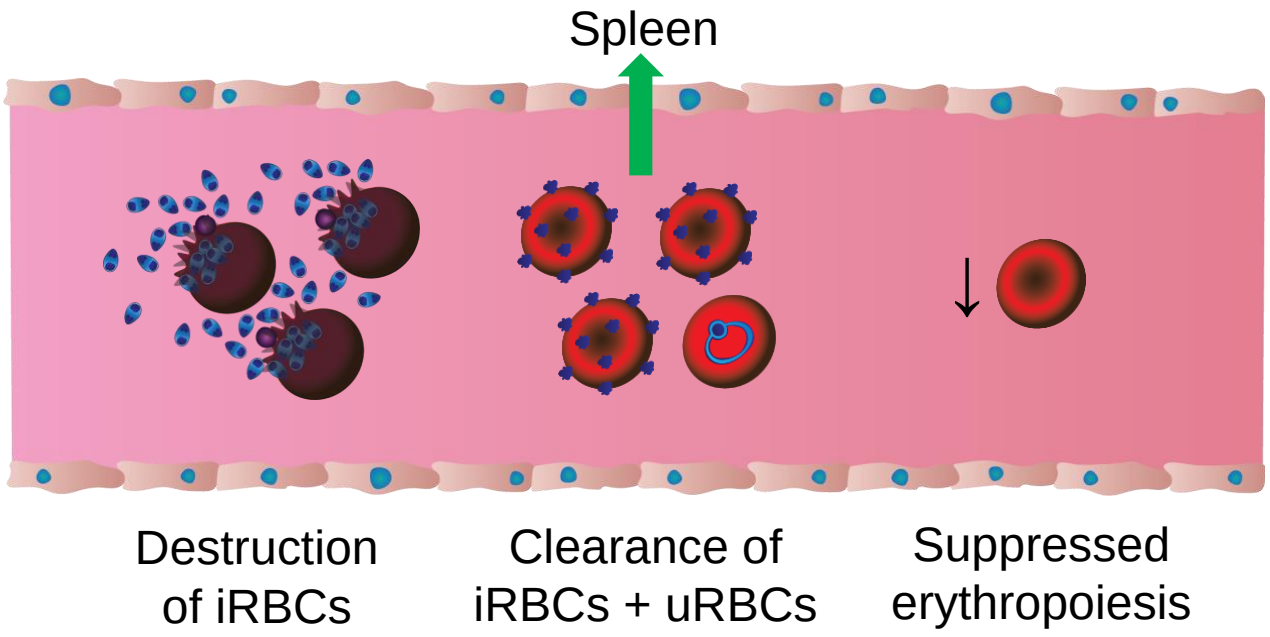

Figure 1.2: Mechanism of anaemia caused by malaria parasites.

Malarial anaemia is caused through multiple mechanisms including: destruction of infected RBCs (iRBCs) during schizont rupture, increased splenic clearance of both uninfected RBCs (uRBCs) and iRBCs, and an inhibition of erythropoiesis.

Metabolic acidosis and respiratory distress

Malaria causes a significant decrease in the oxygen carrying capacity of RBCs, and parasites can also form clusters of both infected and uninfected RBCs, a process known as rosetting, that can decrease circulation to particular parts of the body (Chotivanich, Udomsangpetch et al. 1998). Such a decrease in the local availability of oxygen can promote reliance on anaerobic glycolysis by affected tissues (Planche, Dzeing et al. 2005). Anaerobic glycolysis produces lactic acid, which in turn can decrease blood pH resulting in acidosis. Additionally, it is thought that the antimalarial immune response, hypotension and dehydration can contribute significantly to metabolic acidosis (Sasi, Burns et al. 2007). Severe metabolic acidosis is a strong predictor of poor patient outcomes, as metabolic acidosis can lead to complications in multiple organs (English, Sauerwein et al. 1997). The most common complication of metabolic acidosis, however, is respiratory distress (Taylor, Hanson et al. 2012). As well as an increased respiratory rate, due to poor oxygen transfer, malaria can increase alveolar capillary permeability, which allows buildup of fluid in the lungs and can cause either acute lung injury (ALI) or acute respiratory distress syndrome (ARDS) (Mohan, Sharma et al. 2008). Treatment of ARDS or ALI in malaria patients can be complicated by the fact that this pathology may no longer be principally driven by parasites at the point of hospital admission. As such, malaria patients with respiratory complications may not respond well to antimalarial therapeutics, meaning intubation and mechanical ventilation is often required (Mohan, Sharma et al. 2008).

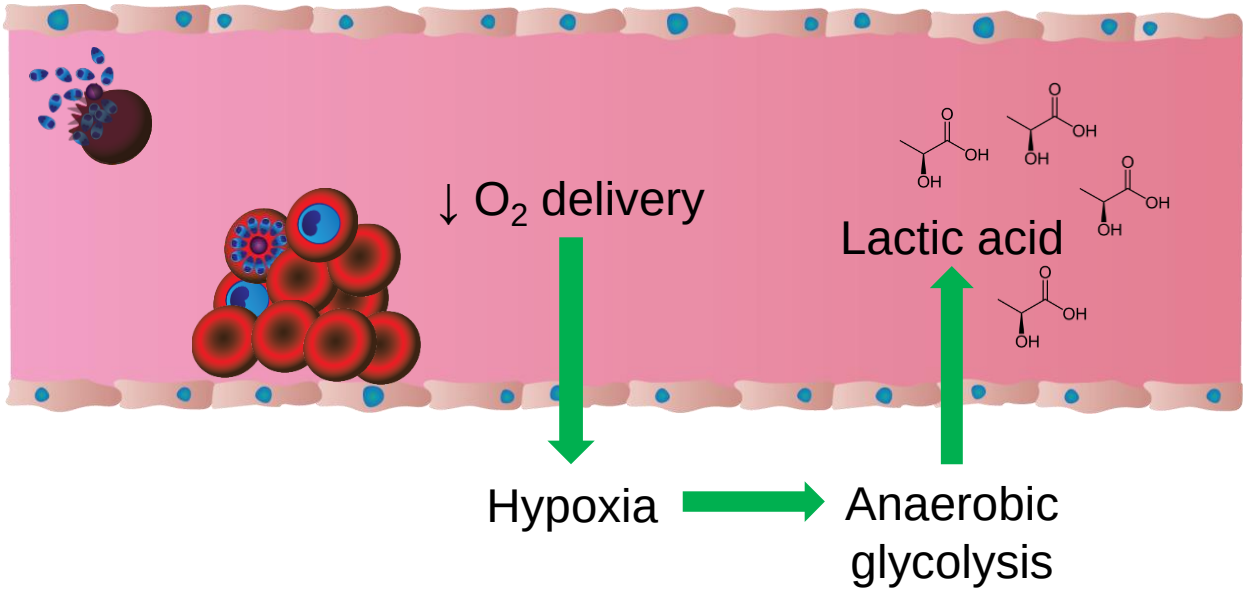

Figure 1.3: Mechanism of metabolic acidosis caused by malaria parasites.

Malarial anaemia decreases oxygen delivery to cells systemically. Additionally, parasites can sequester in capillaries, inhibiting blood flow and therefore oxygen delivery locally. Decreased oxygen delivery promotes the hypoxia response in affected cells, which shifts their metabolism towards anaerobic glycolysis. Lactic acid, a product of increased anaerobic glycolysis, is secreted into the blood and increases blood pH; leading to acidosis.

Cerebral malaria

Malaria parasites can cause encephalitis, or cerebral malaria, by crossing the blood brain barrier (BBB) and rosetting or adhering to endothelial vasculature (Chotivanich, Udomsangpetch et al. 1998, Dondorp 2005, Cowman, Healer et al. 2016). BBB permeability is thought to be increased by metabolic acidosis, and so often patients with cerebral malaria also have metabolic acidosis (English, Sauerwein et al. 1997, Sasi, Burns et al. 2007). Parasite adhesion to endothelial vasculature can promote swelling in the brain, while rosetting decreases blood flow to the brain (Cowman, Healer et al. 2016). Patients suffering cerebral malaria commonly present with impaired consciousness, seizures, and eventually coma that is regularly fatal if left untreated (Dondorp 2005). For patients who do recover from cerebral malaria, they often suffer life-long cognitive and neurological deficits (Dondorp 2005).

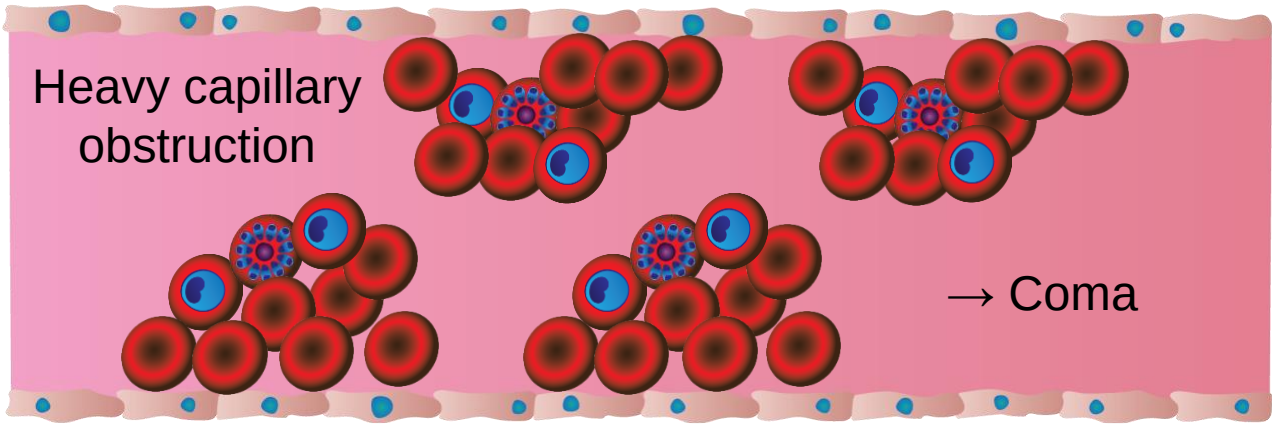

Figure 1.4: Mechanism of cerebral malaria caused by *P. falciparum*.

P. falciparum can adhere to cerebral endothelium, a process known as cytoadherence. Cytoadherence results in a significant reduction in blood flow through cerebral capillaries. Additionally, presence of parasites in the cerebral capillaries leads to inflammation. These two mechanisms together lead to cerebral malaria and potentially coma.

Malaria in pregnancy

During pregnancy, malaria parasites can adhere to placental vasculature and alter pregnancy outcomes (Rogerson 2017). Additionally, this makes pregnant women more susceptible to severe malaria (Rogerson 2017). Malaria can influence the pregnancy outcomes both indirectly, by affecting the health of the mother, or directly by adhering to placental vasculature (Tarning 2016), which results in both placental inflammation and a reduction in oxygen availability (Tarning 2016). Placental adhesion can cause intrauterine growth restriction, premature delivery, low birth weight and stillbirth (Tarning 2016). Despite the significant complications of malaria in pregnancy, there is no conclusive evidence that babies born to infected mothers are themselves infected. Therefore, it is thought that malaria parasites cannot cross the placenta into the fetus. In highly malaria endemic regions, most women will be clinically immune to malaria by their first pregnancy, however they exhibit an increased susceptibility to disease while pregnant (Cutts, Agius et al. 2020). For women in malaria endemic areas, the increased susceptibility of malaria in pregnancy is typically reduced following multiple pregnancies; known as maternal immunity (Cutts, Agius et al. 2020). As mothers are typically clinically immune to malaria, they confer temporary immunity to their newborn babies, which is thought to be mediated by transfer of antibodies through breast milk (Cutts, Agius et al. 2020). Transfer of maternal antibodies is thought to protect newborn children form malaria in their first few months of life (Dobbs and Dent 2016). Once the child's immune system begins to mature and the influence of maternal antibodies wanes, they become susceptible to infection (Dobbs and Dent 2016).

Plasmodium parasite lifecycle

Humans are infected with *Plasmodium* parasites when a female *Anopheles* mosquito takes a blood meal and injects sporozoite stage parasites subcutaneously (Cowman, Healer et al. 2016). Sporozoites migrate from the site of the blood meal, through the circulatory system, into the liver; where they invade hepatocytes (Cowman, Healer et al. 2016). Once inside a hepatocyte, the parasite undergoes multiple rounds of asexual division to form a structure known as a hepatic schizont, which contains tens of thousands of daughter merozoites (Cowman, Healer et al. 2016). In addition to forming merosomes, *P. vivax*, along with potentially *P. ovale curtisi* and *walikeri*, have the ability to go into a state of dormancy known as the hypnozoite (Garnham 1980, Hulden and Hulden 2011). Hypnozoites can remain dormant from a period of months to years without causing any clinical symptoms prior to clinical relapse (Hulden and Hulden 2011). It is thought that the hypnozoite stage allows these parasites to maintain an infectious reservoir in temperate regions where the mosquito breeding season is not long lived (Hulden and Hulden 2011). Following maturation, which occurs over approximately 7-14 days, merosomes rupture, releasing the contained daughter merozoites into the blood stream to initiate the blood stage of the lifecycle. No pattern associated molecular patterns (PAMPs) or damage associated molecular patterns (DAMPs) have been identified for liver stage parasites, and so it is thought that all symptoms of clinical malaria are driven by the blood stage of infection.

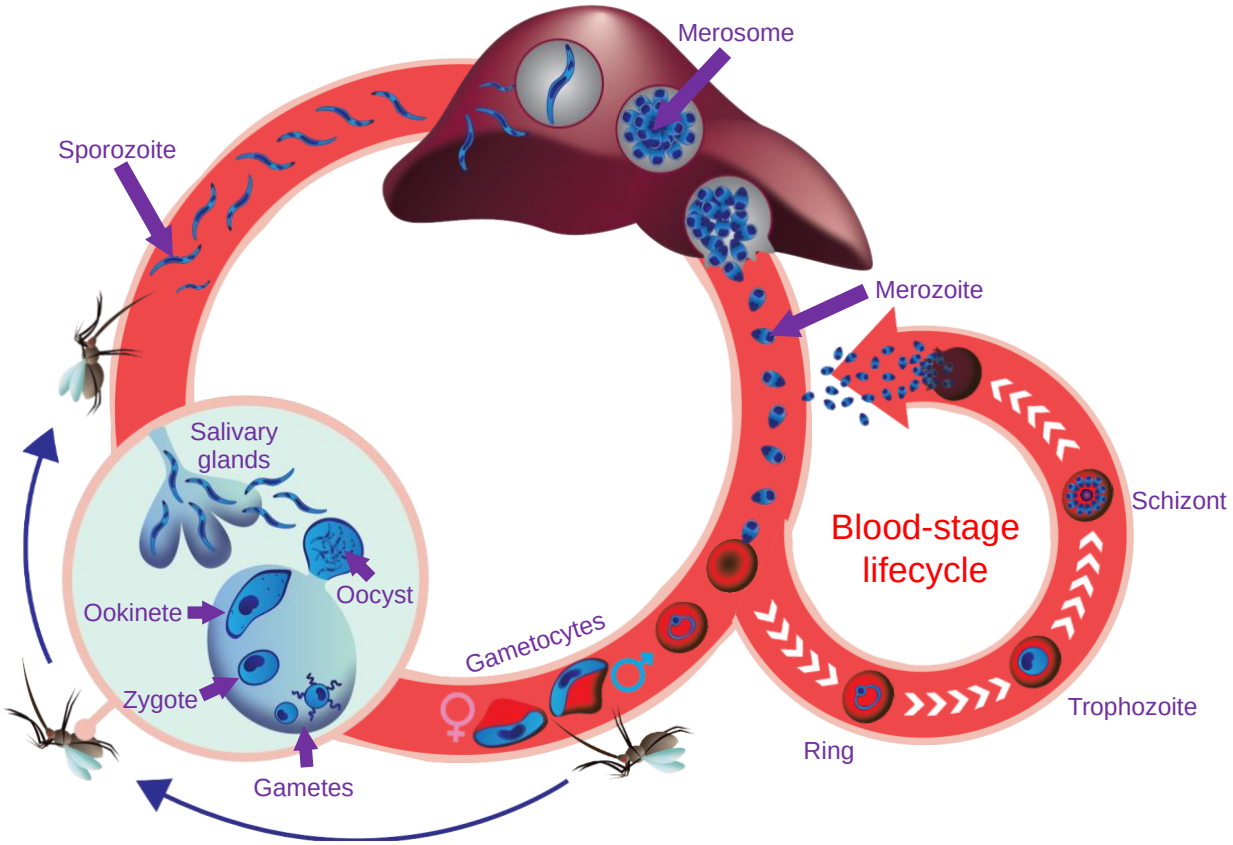

Figure 1.5: *Plasmodium falciparum* lifecycle.

P. falciparum sporozoites are transmitted to humans during a blood meal from an infected Anopheles mosquito. Sporozoites migrate to the liver, where they invade hepatocytes. Following hepatocyte invasion, the parasite develops into a structure known as a merosome, which contains thousands of merozoites. Once mature, the merosome ruptures and releases these merozoites into the blood stream where they invade red blood cells. Following merozoite invasion, the parasite progresses through the ring and trophozoite morphological stages. Trophozoites begin to divide and form new daughter merozoites, which are contained within a schizont. Approximately 48 hours following merozoite invasion, mature schizonts rupture and release merozoites back into the blood stream to invade new red blood cells. This asexual blood stage is responsible for all clinical symptoms of malaria. A small proportion of blood stage parasites commit to sexual development, where they form either female or male gametocytes. Gametocytes are taken up by a mosquito during a blood meal, where they rapidly transition to gametes that fuse into a zygote. Zygotes transition to an invasive ookinete, which invades the mosquito midgut wall to form an oocyst. New sporozoites develop inside the oocyst and once mature, the oocyst ruptures and sporozoites migrate to the salivary glands ready to be transmitted to a human in the next blood meal.

Following their release from merosomes, merozoites recognise, migrate towards and infect host RBCs (Cowman, Tonkin et al. 2017, Yahata, Hart et al. 2020). During the process of invasion, the merozoite pulls the RBC membrane around itself to form a parasitophorous vacuole (PV) that it will reside inside for the remainder of the blood stage (Burns, Balbin et al. 2019). Newly invaded merozoites rapidly differentiate into a ring stage parasite, which undertakes modification of the RBC so that it is conducive to parasite growth (Cowman, Healer et al. 2016). The primary amino acid source of blood stage parasites is haemoglobin, which it catabolises and converts into the inert crystal haemozoin before storage inside a specialized organelle known as the food or digestive vacuole (FV/DV) (Coronado, Nadovich et al. 2014). The ring stage parasite converts into a trophozoite stage parasite, where the parasite drastically increases in size and begins to take up the majority of the RBC cytosol. Following significant growth in the trophozoite stage, the parasite undertakes multiple rounds of asynchronous DNA replication and closed mitosis (without cytokinesis) in a process known as schizogony (Gerald, Mahajan et al. 2011, Matthews, Duffy et al. 2018). During schizogony both the mitochondria and the apicoplast, a remnant plastid of cyanobacterial origin, also replicate (Preiser, Wilson et al. 1996, Milton and Nelson 2016). Additionally, the parasite begins to form micronemes, dense granules, and rhoptries, which are specialised organelles that coordinate host cell invasion (Cowman and Crabb 2006). At the completion of schizogony, there is a singular round of synchronized cytokinesis such that 8-32 (species dependent) new daughter merozoites are formed that each contain their own set of organelles and unique parasite plasma membrane (PPM) (Gerald, Mahajan et al. 2011). Mature schizonts first rupture their PVM and then the erythrocyte membrane, releasing daughter merozoites into the circulatory system to invade new RBCs (Dowse, Koussis et al. 2008).

Asexually replicating blood stage parasites cannot infect mosquitoes, and so a small proportion of asexual parasites commit to sexual development by undergoing a process known as gametocytogenesis (Talman, Domarle et al. 2004, Ngotho, Soares et al. 2019). Gametocytogenesis is highly divergent between human infecting *Plasmodium* parasites, with *P. falciparum* gametocytes forming elongated 'falciform' parasites in the bone marrow that only emerge after approximately 14 days of maturation (Talman, Domarle et al. 2004, Ngotho, Soares et al. 2019). Gametocytogenesis occurs much more rapidly in other species, with gametocytes typically visible in peripheral blood smears as soon as parasites can be seen (Ngotho, Soares et al. 2019). Once both mature male and female gametocytes are present in circulation, they can be taken up during a mosquito blood meal where the change of temperature triggers male gametocytes to enter a process known as exflagellation where they form male gametes that go on to fuse with female gametes; forming a zygote (Guttery, Holder et al. 2012, Ngotho, Soares et al. 2019). Following zygote formation, the parasite rapidly differentiates into an invasive ookinete, which invades the mosquito midgut wall to form a replicative oocyst where new sporozoites develop (Guttery, Holder et al. 2012). Mature sporozoites rupture out from the oocyst and migrate through the mosquito haemolymph into the salivary glands (Kojin and Adelman 2019). Sporozoites then undergo a complicated series of invasion and protein coat shedding events that permit them to translocate from the basal lamina of the salivary gland into the salivary gland duct where they reside until the female *Anopheles* mosquito takes another blood meal to continue the parasite lifecycle (Sinnis and Sim 1997, Ghosh and Jacobs-Lorena 2009, Kojin and Adelman 2019).

Malaria control strategies and challenges

Recent progress in malaria control

Following tremendous global mortality caused by malaria during both World Wars, the United States of America established malaria control as a primary goal. Conducted by the Federal Communicable Disease Center (now Centers for Disease Control and Prevention) of the United States, the national malaria eradication program was established in 1947 and by 1951 malaria had been eradicated from the continental US (Nájera, González-Silva et al. 2011, Centers for Disease Control and Prevention 2018, Centers for Disease Control and Prevention 2018). Optimistic following the success of the US, the WHO announced the Global Malaria Eradication Programme (GMEP) in 1955, which primarily focused mosquito-targeting interventions using the insecticide dichloro-diphenyl-trichloroethane (DDT) (Nájera, González-Silva et al. 2011). While malaria was drastically reduced, or even eradicated, in many nations during the GMEP reliance on such intensive measures with very few alternative interventions led to epidemic resurgence of malaria in many areas; most notably Ceylon (now Sri Lanka) who had been malaria free for four years (Nájera, González-Silva et al. 2011). Due to unsatisfactory progress, emergence of drug resistance, and increasing malaria epidemics, the program was formally disbanded in 1969.

In 2000, the WHO again placed malaria control high on its agenda with the establishment of the Millennium Development Goals, where Goal 6 was "Combat HIV/AIDS, malaria and other disease" (United Nations 2000, Cibulskis, Alonso et al. 2016). Following the development of novel antimalarial drugs and long-lasting insecticide-treated bed nets (LLINs), the Bill & Melinda Gates Foundation announced their agenda for malaria eradication in 2007 (Gates 2007, Gates 2007). This intensified focus on malaria eradication, with support from multiple industry, academic, and philanthropic partners, has led to great reductions in malaria morbidity and mortality; with a 13%

reduction in malaria cases and a 52% reduction in deaths since 2000 (World Health Organization 2015, Cibulskis, Alonso et al. 2016). Since 2015, Algeria, Krygyzstan, Uzbekistan, Argentina, Paraguay, Sri Lanka, and The Maldives have all be certified as malaria-free with a further 18 countries on track for elimination by the end of 2020 (World Health Organization 2019). Despite these successes, however, greater than 100 countries remain malaria endemic and most countries where malaria has been eliminated were previously low transmission areas.

Mosquito-targeting interventions

Historically the most effective form of malaria prevention has been the use of insecticides, principally in the form of indoor residual spraying (IRS) or through the use of LLINs. Following a blood meal, an infected female mosquito will typically rest on a wall nearby the person who was fed upon to digest her blood meal (Sherrard-Smith, Skarp et al. 2019). IRS involves spraying the internal walls of dwellings with long-lasting insecticides that will kill infected females following a blood meal; preventing malaria transmission. In many malaria endemic areas, people sleep under a bed net that has been impregnated with long-lasting pyrethroid insecticides, which are considered very safe for humans. LLINs work directly by preventing the person sleeping underneath from being bitten, which drastically reduces local incidence of malaria when a large enough proportion of the population uses them. While mosquito-targeting interventions currently represent the most cost-effective strategy for preventing malaria, they provide no protection for those who are infected.

Antimalarial therapeutics

Effective antimalarial therapeutics, which typically target asexually replicating parasites to resolve disease symptoms, have been used for approximately 400 years, since the Quechua people

of South America discovered that chewing on the bark of *Cinchona* trees can cure fevers (Fluckiger and Hanburg 1874). *Cinchona* bark remained the only effective remedy for malaria until its active ingredient, quinine, was isolated in 1820 (Tse, Korsik et al. 2019). Despite over 400 years of clinical use, quinine remains in use today, typically when administered intravenously. The 20th century saw the development of many new antimalarial drugs. Chloroquine, a quinine derivative, was introduced in 1945 and acted as the primary antimalarial therapeutic during the GMEP and remained the gold-standard for malaria treatment until the 1990s (Nájera, González-Silva et al. 2011, Tse, Korsik et al. 2019). Proguanil, primaquine, sulfadoxine-pyrimethamine, mefloquine and atovaquone were all developed as antimalarials following chloroquine and many remain in use for some circumstances, such as for travelers (Trish and Tony 2007, Tse, Korsik et al. 2019). The current gold-standard treatments for malaria are artemisinin combination therapies (ACTs) that partner the fast-acting artemisinin, a sweet wormwood (*Artemsinina annua*) derived compound developed in 1972 (Qinghaosu Antimalaria Coordinating Research Group 1979), with a slower acting partner drug. ACTs are currently the recommended therapy for use in all malaria endemic countries by the WHO (World Health Organization 2015).

Chemoprophylaxis

While the aforementioned drugs were developed for treatment of symptomatic malaria, seasonal malaria transmission, travel, and the burden of malaria in pregnancy have led to the development of chemoprophylatic therapeutics to prevent malaria. Across the Sahel, a hot and dry region between the Sahara Desert and Sudanian Savanna, malaria transmission only occurs during the approximately 3-month rainy season. Seasonal malaria chemoprevention (SMC) has been used in this area, where children are treated routinely with sulfadoxine-pyrimethamine and amodiaquine. SMC has been shown to reduce severe malaria by up to 75% in regions with such highly seasonal transmission (World Health Organization 2012, World Health Organization 2017). As both

pregnant women and unborn babies are highly susceptible to malaria, sulfadoxine-pyrimethamine is also used for intermittent preventative treatment in pregnancy (IPTp) (World Health Organization 2017). The WHO recommends IPTp for 20 highly endemic countries in Sub-Saharan Africa, and its implementation has led to significant improvements in both maternal and fetal health outcomes (World Health Organization 2013). For malaria-naïve travelers entering endemic areas during periods of malaria transmission, malaria prophylaxis may be recommended (Trish and Tony 2007). A combination of atovaquone and proguanil (Malarone™), mefloquine, or the antibiotic doxycycline are routinely prescribed for travelers to malaria endemic areas and are effective for short-term stays (Trish and Tony 2007).

Rapid diagnostics

A crucial aspect of malaria control is knowing who is infected and doing so early so that antimalarial drugs can be administered. Traditionally, malaria diagnostics were performed by analysing blood from the patient by light microscopy, which would likely occur at a district healthcare centre and be performed by a trained specialist (Cunningham, Jones et al. 2019). The majority of the burden of malaria occurs in low- or middle-income countries, whose healthcare systems are primarily based on local primary health care as a district healthcare centre may be hours or days travel away. Considering this reliance on locally based primary healthcare, large populations in malaria endemic areas are unable to access microscopy-based diagnostics when they are infected. Furthermore, microscopy-based diagnostics often provide false negative results for patients whose parasite burden is low. Rapid diagnostic tests (RDTs) have recently been deployed globally, which detect abundant secreted parasite proteins such as histidine rich protein (HRP) 2 (Moody 2002). RDTs use a single drop of blood from the patient, require very little expertise to operate, and produce a sensitive result in 15-30 minutes (Moody 2002, Cunningham, Jones et al.

2019). For these reasons, RDTs have been recommended by the WHO to diagnose malaria, particularly in Sub-Saharan Africa where approximately 75% of malaria diagnoses were made by RDT in 2017 (World Health Organization 2019).

Vaccine development

Only two pathogens have been intentionally eradicated by humans, smallpox (*Variola virus*) (World Health Organization 1980) and rinderpest (*Rinderpest morbillivirus*) (Food and Agriculture Organisation of the United Nations and World Organisation for Animal Health 2011) and both were achieved using highly effective vaccines. Malaria eradication has largely been impeded by the lack of a highly effective vaccine that provides long-lasting protection in spite of malaria vaccine development being an area of extreme interest for many decades. While no vaccine for malaria is currently in widespread use, RTS,S (Mosquirix™), was licensed in 2015. In Phase III clinical trials, following four vaccinations, RTS,S conferred modest protection in at risk age groups with a 20.3% reduction in clinical malaria in infants and 35.2% in young children and similar protection against severe malaria (Gosling and von Seidlein 2016, Mahmoudi and Keshavarz 2017). Modelling studies have suggested that implementation of RTS,S could reduce malaria deaths by up to 580 per 100,000 vaccinated children and cases by up to 80,000 per 100,000 vaccinated children over a 10 year period (Penny, Galactionova et al. 2015). While even a modest reduction in malaria burden, such as that provided by RTS,S could reduce malaria morbidity and mortality significantly across the globe, it is unlikely RTS,S alone could be used to achieve the goal of malaria eradication.

Challenges to malaria control

For all the advancements made in therapeutic and public health interventions against malaria in recent years, significant hurdles are yet to be overcome. Current challenges to malaria control, now and in the future, are biological, economic, technological, and cultural. Overcoming these challenges to achieve malaria eradication will require a coordinated approach from the academic, governmental, industrial and philanthropic sectors.

Insecticide resistance

Routine use of insecticides for malaria control places a significant selective pressure on mosquitoes. As such, resistance has emerged amongst *Anopheles* mosquitoes to currently used insecticides, with individual mosquito populations resistant to all insecticide classes widespread across many malaria endemic areas (Collins, Vaselli et al. 2019, Sherrard-Smith, Skarp et al. 2019). Resistance can occur in the form of molecular resistance, where mutations that arise in mosquito populations are selected because they decrease sensitivity to insecticides (Ingham, Anthousi et al. 2020). Additionally, mosquitoes can be behaviorally resistant, whereby their feeding behavior is altered to prevent exposure to insecticides (Sougoufara, Diédhiou et al. 2014). Previous studies have shown that the introduction of LLINs, which protect the user while they sleep, can promote *Anopheles funestans* to switch its biting tendency to earlier in the day before people go to sleep and therefore, decrease the effectiveness of LLINs (Sougoufara, Diédhiou et al. 2014).

Antimalarial resistance

While a number of highly effective antimalarial drugs have been developed, and are currently in use, resistance has developed against all currently licensed antimalarial drugs. Historically, the emergence and rapid spread of chloroquine resistance contributed significantly to the abandonment of the GMEP and resulted in large increases in global malaria mortality (Nájera,

González-Silva et al. 2011). In 2009, artemisinin resistance was identified in the Greater Mekong Sub-region and was found to be associated with treatment failure (Dondorp, Nosten et al. 2009). Artemisinin is typically administered in combination therapies, and since 2009, parasites resistant against all licensed ACTs have been identified (Rosenthal 2018, Tse, Korsik et al. 2019). Additionally, molecular epidemiology studies have identified the most common artemisinin resistance-conferring mutations (*Kelch13* C580Y/R549T) in *P. falciparum* isolates from India (Das, Saha et al. 2018), Guyana (Mathieu, Cox et al. 2020) and Papua New Guinea (Miotto, Sekihara et al. 2020) among other nations (Rosenthal 2018). While all of these have been shown to increase artemisinin resistance *in vitro* it is currently unclear the extent to which artemisinin resistance contributes to treatment failure outside of the Greater Mekong Sub-region. Presently, artemisinin resistance has not been shown to contribute to treatment failure in Africa but in the case of chloroquine, resistance emerged in the Greater Mekong Sub-region before spreading to Africa (Rosenthal 2018). With the very real threat of significantly reduced effectiveness of ACTs looming for sub-Saharan Africa, the most malaria endemic region on earth, development of novel antimalarial therapeutics is essential for ongoing malaria control.

RDT-negative parasites

RDTs have made malaria diagnostics far more accessible and effective for people living in rural areas of low- or middle-income countries, particularly in sub-Saharan Africa. As positive diagnoses from RDTs likely mean the patient receives a dose of antimalarial drugs, RDT detection imparts a significant selective pressure on parasite survival. In many places it was noticed that microscopically confirmed malaria cases were being diagnosed as false negatives using RDTs. Most RDTs detect the protein HRP2 and it was subsequently determined that these false-negatives were being caused by parasites that lacked *hrp2* (Moody 2002, Berhane, Anderson et al. 2018). HRP2-negative parasites are widespread in many parts of the world, with HRP2 negativity

approaching 100% in some regions (Berhane, Anderson et al. 2018). Microscopy diagnosis provides a reliable backup in places where HRP2-negativity is high, however the aforementioned difficulties with microscopic diagnosis impede its effectiveness. In order to combat HRP2-negative parasites, and provide cheap and rapid diagnostics for the future, development of new RDTs is vital.

Waning vaccine efficacy

RTS,S vaccination only demonstrated modest efficacy in both children and infants and is therefore unlikely to play a major role in an eradication program. The limited efficacy that RTS,S did demonstrate, however, also waned significantly over time. In children vaccinated at 5-17 months, 33 months following RTS,S vaccination, vaccinated children were 19% more likely to have a severe malaria event than those not vaccinated (Gosling and von Seidlein 2016, Mahmoudi and Keshavarz 2017). Additionally, vaccine efficacy for all clinical malaria cases in both children and infants fell to only 8% over the same time period (Gosling and von Seidlein 2016, Mahmoudi and Keshavarz 2017), indicating that while RTS,S may prompt immunity in a modest proportion of those vaccinated, this immunity is not durable over time. Importantly, this waning of immunity would mean that if an infant was vaccinated with RTS,S and developed immunity, this immunity would likely wane before they reach the age of five and therefore make them again susceptible in the most at risk age range. Hope for vaccine development is found in the observation that most adults in malaria endemic areas develop non-sterilising immunity following multiple rounds of infection (Doolan, Dobaño et al. 2009). Naturally acquired immunity to malaria, however, is not durable and so for the development of a malaria vaccine to be used for eradication it will likely need to elicit immunity that is durable on a scale of decades.

While RTS,S targets the liver-invading sporozoite stage of the lifecycle, promising vaccines both in development and clinical trials target the RBC-invasive merozoite stage of the lifecycle.

Following schizont rupture, merozoite antigens are directly exposed in the bloodstream and as such can be directly targeted by the host immune response. Merozoite vaccine candidates include the merozoite surface proteins (MSP) 1 and 2. Additionally, merozoites secrete antigens from specialised organelles known as rhoptries and micronemes that interact with RBCs. Currently, no vaccines against merozoite antigens have been licensed for use. An MSP2 vaccine was shown to reduce parasite density by 62 % in a Phase 2b clinical trial (Genton, Betuela et al. 2002), however its effectiveness was limited by the presence of non-protected MSP2 genotypes. Currently, the rhoptry protein reticulocyte-binding protein homologue 5 (RH5) is considered the most promising blood-stage vaccine candidate (Payne, Silk et al. 2017).

Merozoite invasion of host RBCs

With antimalarial drug resistance spreading and the lack of an effective vaccine, development of novel antimalarial therapeutic and vaccine targets is of critical importance. An important target for vaccine development and an emerging target for drug development is merozoite invasion of RBCs. After merozoites are released from the schizont, and before invading RBCs, they are directly exposed to the bloodstream and the host immune response (Cowman, Tonkin et al. 2017).

Throughout the blood stage of the lifecycle, *P. falciparum* resides inside a RBC that does not express major histocompatibility complex (MHC) I or II and as such cannot be killed by cytotoxic T lymphocytes (CTLs). Thus, blood stage malaria is considered to elicit a weak cell-mediated immune response (Kurup, Butler et al. 2019). It has long been known, however, that transfer of serum immunoglobulin from naturally immune individuals can confer non-sterilising immunity to malaria (Cohen, Mc et al. 1961, Beeson, Drew et al. 2016). It is thought that this natural immunity to malaria occurs through either directly neutralising or functional antibodies that

recognise *P. falciparum* proteins on the surface of infected RBCs or on the surface of the merozoite following schizont rupture (Beeson, Drew et al. 2016, Teo, Feng et al. 2016). This potential for antibodies targeting merozoite proteins, along with its essentiality for parasite survival and disease progression has highlighted invasion as an attractive target for the development of novel antimalarial therapeutics and vaccine candidates.

Merozoites contain a series of organelles that are involved specifically in invasion, which are known as the exonemes, micronemes, rhoptries, and dense granules (Cowman and Crabb 2006, Cowman, Tonkin et al. 2017). Prior to schizont rupture, merozoites release the contents of an organelle known as the exonemes (Yeoh, O'Donnell et al. 2007, Dowse, Koussis et al. 2008). The exonemes contain a subtilisin-like protease known as SUB1 that process a family of proteins known as the serine-rich antigens (SERA), which in turn result in the rupture of the PVM followed by the RBC membrane; releasing the merozoites (Yeoh, O'Donnell et al. 2007, Dowse, Koussis et al. 2008).

Following schizont rupture, merozoites initiate a weak, reversible, attachment to the RBC, which is thought to be mediated by a family of proteins known as merozoite surface proteins (MSPs) (Beeson, Drew et al. 2016, Burns, Balbin et al. 2019). Following initial RBC recognition, the merozoite reorients such that its apical surface contacts the RBC membrane. After reorientation, the merozoite secretes the contents of its micronemes along with the contents of the rhoptry neck, which is the most apically located portion of the rhoptry.

Micronemal antigens, including erythrocyte binding antigens (EBAs) and apical membrane antigen 1 (AMA1), along with rhoptry neck antigens reticulocyte-like binding homologues (RHs) and rhoptry neck proteins (RONs) interact in a coordinated fashion to recognise the host RBC (Beeson, Drew et al. 2016). AMA1 and the RON complex (RON2-4) form an irreversible tight junction between the merozoite and RBC (Vulliez-Le Normand, Tonkin et al. 2012). Following

tight junction formation, the contents of the rhoptry bulb, the more basally located portion of the rhoptry, are secreted into the cytosol of the RBC along with the contents of the dense granules.

Recent evidence suggests that merozoites use a process called ‘gliding motility’ to migrate toward uninfected RBCs (Yahata, Hart et al. 2020). Gliding motility is achieved through an actin-myosin based motor known as the glideosome, which is part of a flattened cisternal membranous compartment known as the inner-membrane complex (IMC) (Baum, Richard et al. 2006). Merozoites then utilise the force generated by the actin-myosin based motor, the glideosome, to pull the RBC membrane around itself and form a host-derived PV(Keeley and Soldati 2004, Weiss, Gilson et al. 2015). Following successful invasion, the host RBC undergoes echinocytosis whereby the RBC membrane temporarily distorts before returning to its previous shape (Weiss, Gilson et al. 2015).

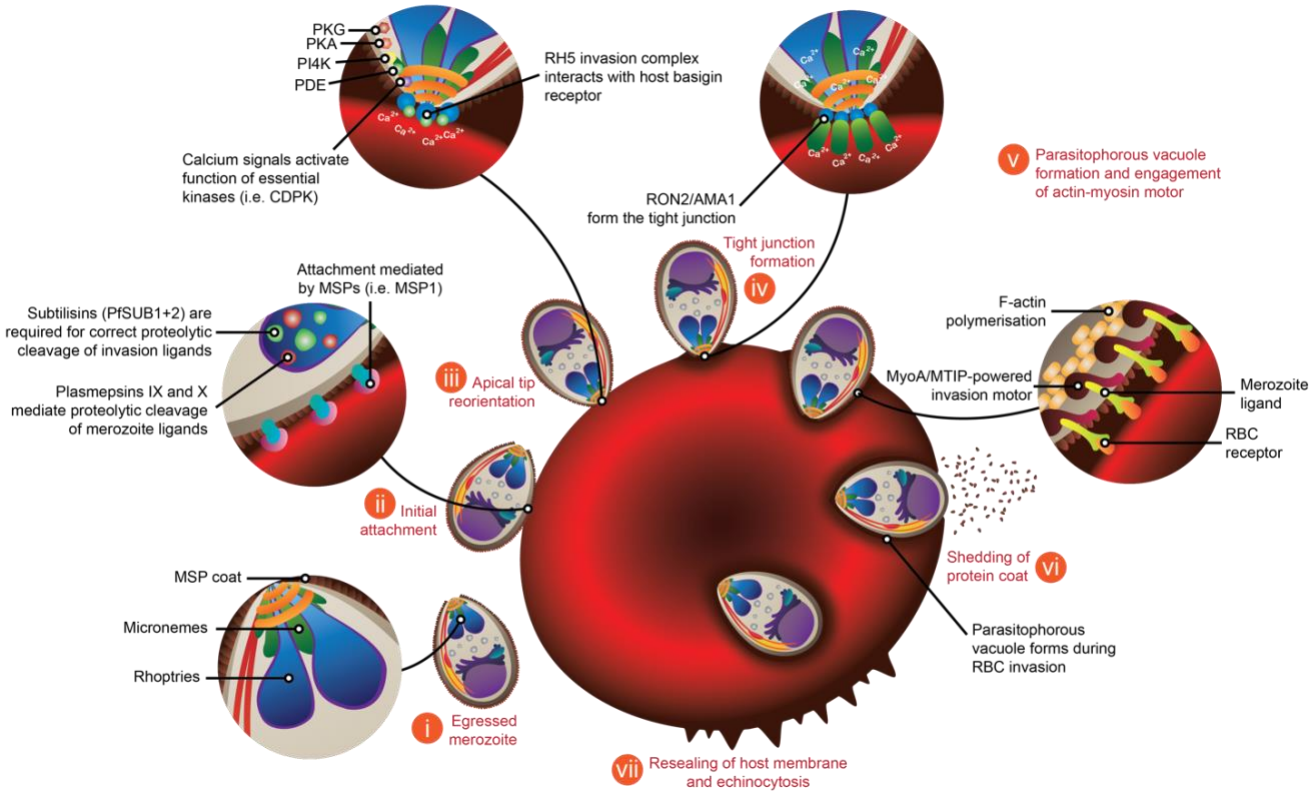

Figure 1.6: *Plasmodium falciparum* invasion of RBCs. Figure adapted from (Burns, Balbin et al. 2019)

Merozoite invasion begins when the newly egressed merozoite forms a weak initial attachment with the RBC membrane, which is coordinated by merozoite surface proteins (MSPs). The merozoite then reorients itself such that its apical tip contacts the RBC membrane. After reorientation, the merozoite secretes ligands from the micronemes and rhoptry neck that form an irreversible tight junction between the merozoite and RBC. Once the tight junction has been established, the merozoite secretes the contents of the rhoptry bulb into the RBC to remodel the cell and help establish the parasitophorous vacuole membrane (PVM). The merozoite then uses an actin-myosin based motor complex to pull the RBC membrane around itself, which results in the shedding of the MSP coat and the internalisation of the merozoite. Following the completion of invasion, the RBC membrane reseals and the infected cell undergoes a process known as echinocytosis, where the RBC membrane temporarily deforms.

Secreted merozoite antigens

Many of the parasite proteins that are involved in invasion are functionally redundant and not always required for invasion. EBA-175 and EBA-140 bind to the human RBC receptors glycophorin A (Adams, Sim et al. 1992) and glycophorin C (Maier, Duraisingh et al. 2003), respectively, however neither of these interactions are essential for parasite survival (Weiss, Gilson et al. 2015). Additionally, many of the proteins that are secreted form the merozoite are targets of strong antibody selection and as such their amino acid sequences are highly polymorphic between parasite isolates. Furthermore, some merozoite proteins, particularly MSPs, are either members of multigene families or thought to be expressed at levels considerably higher than is required for their function and act as an ‘antigenic smokescreen’ to prevent antibody inhibition (Anders 1986). Many of the initial merozoite antigens taken into vaccine development exhibited one or more of these characteristics and as such initial vaccine trials against merozoite antigens showed little to no efficacy (Sagara, Dicko et al. 2009, Salamanca, Gómez et al. 2019).

An ideal merozoite vaccine candidate would be essential for invasion, lowly expressed and lowly polymorphic. While many merozoite proteins do not have these characteristics, some do such as the leading vaccine candidate RH5 (Ragotte, Higgins et al. 2020). RH5 forms a complex with the micronemal proteins cysteine rich protective antigen (CyRPA) and RH5 interacting protein (Ripr) and binds to the RBC receptor basigin (cluster of differentiation (CD) 147) (Wong, Huang et al. 2019). All three proteins in this complex are essential for invasion, and antibodies targeting them offer strain-transcendent invasion inhibitory activity. Anti-RH5 human monoclonal antibodies have been identified that potentiate other invasion inhibitory antibodies by slowing the process of invasion (Alanine, Quinkert et al. 2019). Merozoite invasion occurs in approximately 30 seconds, and so it has been previously suggested that the antibody concentrations required to successfully block such a rapid process would be unattainable in infants; the most at risk age group (Payne, Silk et al. 2017, Alanine, Quinkert et al. 2019). It is thought that this potentiation holds great promise for the development of either a vaccine, or therapeutic monoclonal antibody, that would both inhibit invasion directly but also enhance the host antimalarial response.

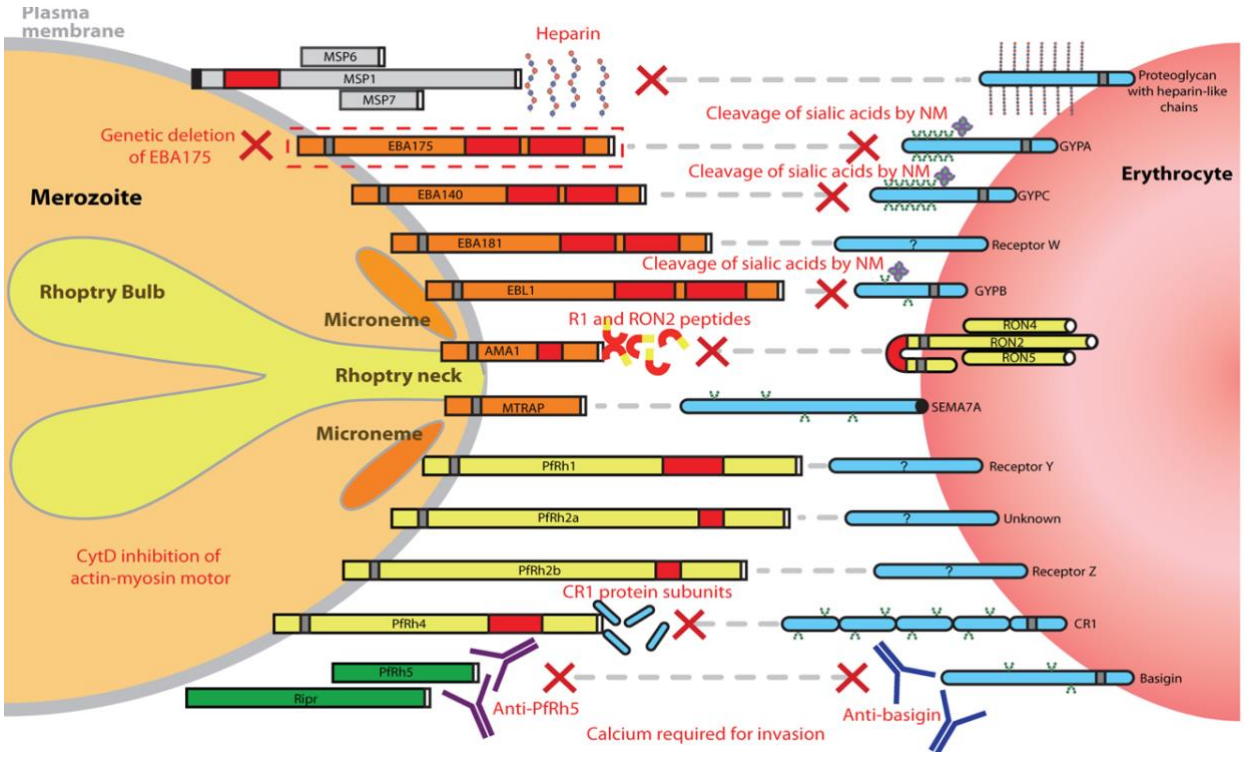

Figure 1.7: Merozoite antigens and RBC receptors. Adapted from (Weiss, Gilson et al. 2015).

Merozoite invasion involves the coordinated interaction of many P. falciparum antigens and RBC receptors. Proteins in blue represent RBC receptors, proteins in yellow represent rhoptry neck proteins, proteins in orange represent microneme proteins, proteins in grey represent merozoite surface proteins, proteins in green represent members of the RH5 complex.

Micronemal proteins

Microneme secretion is thought to occur following the secretion of the exonemes and most micronemal proteins interact with the host RBC at very early stages of invasion prior to tight junction formation (Cowman, Tonkin et al. 2017). A single merozoite may contain many micronemes and it was initially thought that the contents of individual micronemes were homogenous and all were secreted at the approximately the same time. Recent studies, however, suggest that micronemes are non-homogenous, with some containing particular antigens but lacking others (Absalon, Blomqvist et al. 2018, Ebrahimzadeh, Mukherjee et al. 2019).

Additionally, it is thought that micronemes that containing certain contents can be secreted earlier or later than others (Absalon, Blomqvist et al. 2018, Ebrahimzadeh, Mukherjee et al. 2019). Micronemes contain a number of leading vaccine candidates including the erythrocyte binding antigens, and apical membrane antigen 1.

Erythrocyte binding antigens

The Erythrocyte binding antigen (EBA) family includes EBA-140, EBA-175, EBA-181, EBL-1, and the pseudogene EBA-165, which are characterised by their exonic structure along with two Duffy binding domains at their N-termini (Maier, Baum et al. 2009, Beeson, Drew et al. 2016). It is thought that the EBAs may facilitate early interactions with the RBC to allow the tight junction to form, or by helping to establish the tight junction directly. With the exception of EBA-165, all members of the EBA family localise to the micronemes and play an active role in merozoite invasion (Maier, Baum et al. 2009, Beeson, Drew et al. 2016). In *P. falciparum*, *EBA-165* contains two frame shift mutations, preventing the production of full-length protein. When these frame shift mutations are corrected, however, EBA-165 has been shown to bind to ape RBCs, but not human RBCs, suggesting its pseudogenization may have been driven by divergence of *P. falciparum* from the other *Laverania* (Proto, Siegel et al. 2019). Individually, none of the EBAs are essential for merozoite invasion, however their disruption can alter the kinetics of invasion. EBA-175, EBL-1, and EBA-140 have been shown to bind to the glycophorins A, B, and C, respectively, on the surface of human RBCs (Adams, Sim et al. 1992, Maier, Duraisingh et al. 2003, Maier, Baum et al. 2009, Mayer, Cofie et al. 2009, Beeson, Drew et al. 2016). EBA-181 has been shown to bind to an RBC receptor that is sialidated, but which receptor this is currently unknown (Gilberger, Thompson et al. 2003, Mayer, Mu et al. 2004, Maier, Baum et al. 2009, Beeson, Drew et al. 2016). It is thought that merozoites can attempt to invade an RBC using one specific pathway, which would correspond with one EBA. Disruption of that individual EBA, say EBA-175, leads to an inability to invade

using glycophorin A, preventing these parasites from entering a RBC using this receptor. Inhibition of one particular pathway will then select for merozoites invading using a separate pathway where EBA-175 is not required. Thus EBA-175 becomes dispensable for merozoite invasion through antigen switching (Reed, Caruana et al. 2000).

EBA-175 is by far the most well studied of the EBAs and recent studies have shown that EBA-175 binding to glycophorin A results in a biophysical change to the RBC that correlates directly with parasite invasion efficiency (Koch, Wright et al. 2017). This data has led to speculation that EBA binding may actually make the RBC more permissive to invasion (Koch, Wright et al. 2017). Following invasion, secreted EBA-175 has been shown to bind to glycophorin A of uninfected cells and promote RBC clustering (Paing, Salinas et al. 2018). It is thought that this EBA-175-mediated clustering provides a selective advantage to parasites as it may bring infected RBCs in closer contact with uninfected RBCs and additionally may form a physical barrier from antibodies (Paing, Salinas et al. 2018). Secretion of EBA-175 and EBA-140 containing micronemes has recently been shown to be controlled by phosphoinositide binding protein (PH2) and it is hypothesised that PH2 may coordinate fusion between the micronemal membrane and PPM (Ebrahimzadeh, Mukherjee et al. 2019).

Apical membrane antigen 1

Apical membrane antigen (AMA) 1 is likely the most well studied micronemal protein as it is essential in *P. falciparum* and plays a key role in invasion biology across Apicomplexa (Triglia, Healer et al. 2000). It is thought that AMA1 is secreted earlier than most other micronemal antigens from 'egress-related' micronemes, which lack EBAs (Absalon, Blomqvist et al. 2018). Following schizont rupture, surface AMA1 interacts with the RON2/4/5 complex of rhoptry origin, which is embedded in the RBC membrane. More specifically, the exposed ectodomain of AMA1 binds RON2 and it is thought that this interaction leads to the formation of the tight junction (Srinivasan,

Beatty et al. 2011). A synthetic peptide inhibitor known as R1, which mimics the RON2 binding region, has been developed that inhibit the AMA1-RON2 interaction and tight junction formation (Wang, MacRaild et al. 2014). R1 and related peptides provides a useful tool for understanding the dynamics of tight junction formation and mechanisms of invasion inhibition. It has also been shown that knockdown of AMA1 results in a defect in the resealing of the RBC membrane following invasion, suggesting that AMA1 may have an additional function following tight junction initiation (Yap, Azevedo et al. 2014). Unlike EBA-175 and EBA-140, AMA1 secretion is not influenced by PH2 disruption, suggesting that AMA1 and EBA containing micronemes may be separate (Ebrahimzadeh, Mukherjee et al. 2019).

AMA1 is produced as an 88 kDa pro-protein that is processed to a 66 kDa species localising to the micronemes (Narum and Thomas 1994, Hodder, Crewther et al. 1996, Beeson, Drew et al. 2016). Prior to schizont rupture AMA1 is phosphorylated and translocated from the micronemes to the merozoite surface (Beeson, Drew et al. 2016, Absalon, Blomqvist et al. 2018).

Dense granule proteins

Unlike most rhoptry and micronemal proteins, dense granule proteins typically do not play an active role in the invasion process but instead are involved with remodelling the RBC. *P. falciparum* remodels its host RBC to decorate the RBC surface with functional proteins that allow avoidance of splenic clearance through cytoadhesion and to alter RBC membrane properties. Dense granule proteins are therefore secreted directly into the cytosol of the RBC following tight junction formation and most either interact with the RBC membrane are involved in formation of the nascent PVM.

<u>*Plasmodium* translocon of exported proteins</u>

In order to be placed into the RBC membrane, parasite produced proteins need to cross the PPM, PVM, RBC cytosol and finally RBC membrane. Needing to cross three distinct membranes would impart significant structural hurdles on many proteins. In order to facilitate transfer of parasite proteins from the PVM into the RBC cytosol, the merozoite secretes dense granule proteins that form the *Plasmodium* translocon of exported proteins (PTEX). PTEX allows proteins that need to cross the PVM into the RBC cytosol to unfold and pass through a pore that PTEX makes in the PVM before refolding in the RBC cytosol. PTEX is thought to have three core proteins, exported protein (EXP) 2, heat shock protein (HSP) 101 and PTEX150 (de Koning-Ward, Gilson et al. 2009, Bullen, Charnaud et al. 2012, Ho, Beck et al. 2018), along with three accessory proteins, PV1 (Morita, Nagaoka et al. 2018), thioredoxin (TRX) 2 (de Koning-Ward, Gilson et al. 2009, Morita, Nagaoka et al. 2018) and PTEX88 (Chisholm, McHugh et al. 2016). EXP2, HSP101, PTEX150, and PV1 are known to localise to the dense granules and are secreted into the RBC cytosol during invasion before fusing with the PVM (Bullen, Charnaud et al. 2012, Morita, Nagaoka et al. 2018). It is not currently understood how the PTEX components initially embed themselves into the PV, but PTEX forms as a complex where EXP2 forms a pore through the PVM (Ho, Beck et al. 2018). Attached to the PV cytosol side of EXP2 is PTEX150, to which HSP101 is attached (Ho, Beck et al. 2018). Once assembled, PTEX processes proteins that contain a *Plasmodium* export element (PEXEL), which is cleaved during translocation through the endoplasmic reticulum (Boddey, O'Neill et al. 2016). PTEX utilises adenosine triphosphate (ATP) as its energy source for this cleavage, as HSP101 is an ATPase (de Koning-Ward, Gilson et al. 2009, Chisholm, McHugh et al. 2016). It is currently unclear what the function of PTEX150 is, however it is hypothesised to play a structural role in the translocon(Chisholm, McHugh et al. 2016, Ho, Beck et al. 2018).

Ring-infected erythrocyte surface antigen

Ring-infected erythrocyte surface antigen (RESA) is a dense granule protein that is involved in RBC remodelling following merozoite invasion (Aikawa, Torii et al. 1990, Foley, Tilley et al. 1991, Mills, Diez-Silva et al. 2007, Pei, Guo et al. 2007). RESA is a 155 kDa protein that falls into a family of proteins known as *Plasmodium* helical interspersed subtelomeric (PHIST) proteins, based on a domain shared between many exported *P. falciparum* proteins. Additionally, RESA possesses a J domain, which was first characterised in the chaperone DnaJ, leading to speculation that RESA may act as a chaperone. During invasion, RESA is secreted from the dense granules into the RBC cytosol and associates with the RBC membrane upon phosphorylation. RESA has been shown to bind to RBC spectrin, which increases cellular rigidity and decrease RBC permissivity for subsequent events of merozoite invasion (Foley, Tilley et al. 1991, Pei, Guo et al. 2007). It is also thought that this increase in cellular rigidity caused by RESA protects infected RBCs from damage caused by the increased temperatures associated with malarial fevers (Mills, Diez-Silva et al. 2007).

RESA belongs to a family of at least 7 paralogues of RESA-like genes (Aurrecoechea, Brestelli J Fau - Brunk et al. 2008). It is unclear what drove the diversificiation of this family of genes. Most of the RESA-like proteins, however, have been shown to localise to the erythrocyte membrane and some have been shown to interact with the RBC cytoskeleton (Tarr, Moon et al. 2014). Individually, many of the RESA-like proteins are not essential during *in vitro* parasite culture (Zhang, Wang et al. 2018) but it is possible that they exhibit functional redundancy similar to the EBAs during invasion. Additionally, it is possible that RBC stabilising properties of RESA and the RESA-like proteins, which may be essential during *in vivo* conditions of fever or immune clearance, are less important for *in vitro* parasite survival.

Rhoptry proteins

Rhoptry proteins can be stored in one of two distinct structural compartments of the rhoptries, the neck, or the bulb. Rhoptry neck antigens, similar to micronemal antigens, are secreted early during merozoite invasion and typically facilitate initial interactions between the RBC and merozoite. Rhoptry bulb antigens, similar to dense granule proteins, are secreted later during invasion and are generally thought to be involved in host cell remodelling and PVM establishment.

Rhoptry associated membrane antigen

Rhoptry associated membrane antigen (RAMA) is produced as an 170 kDa pro-protein in trophozoites, during nascent rhoptry development, then is processed to a 60 kDa form in mature parasites (Topolska, Lidgett et al. 2004). RAMA localises to the inner leaflet of the rhoptry bulb membrane through a glycosylphoshatidylinositol (GPI) anchor and is trafficked to the nascent rhoptry bulb by sortilin (Topolska, Lidgett et al. 2004, Hallée, Boddey et al. 2018). It is thought that RAMA, in turn, may act as a chaperone for other rhoptry proteins, as its interactions with rhoptry-associated protein (RAP) 1 and Rhoptry heavy (RhopH) 3, leads to trafficking of these proteins to the nascent rhoptry (Topolska, Lidgett et al. 2004, Richard, Kats et al. 2009). Secretion of RAMA occurs following tight junction formation and it is thought that RAMA initially binds to the RBC membrane before being internalised as a component of the PVM. RAMA has been shown to be essential for blood stage survival (Sanders, Kats et al. 2006), however its function is currently unknown. Recent studies have suggested, contrary to previous reports, that RAMA is required for trafficking rhoptry neck proteins rather than rhoptry bulb proteins (Sherling, Perrin et al. 2019). Additionally, it was shown that in RAMA induced knockout parasites rhoptry neck biogenesis is inhibited, which leads to an invasion defect and a failure for RBCs to undergo echinocytosis (Sherling, Perrin et al. 2019). It is currently unclear how the use of anti-RAMA antibodies in

previous compared to an induced knockout in more recent studies may have influenced the observed phenotypes.

Rhoptry associated protein complex

The low molecular weight rhoptry complex contains the rhoptry associated proteins (RAP) RAP1, RAP2, and RAP3 (Baldi, Good et al. 2002). RAP1 is the most well studied of the three, with RAP3 being identified comparatively recently (Baldi, Good et al. 2002) relative to RAP1 (Schofield, Bushell et al. 1986) and 2 (Ridley, Lahm et al. 1991, Baldi, Andrews et al. 2000). RAP1 is formed as a an approximately 90 kDa pro-protein that contains an N-terminal signal peptide (SP). RAP1 is trafficked to the nascent rhoptry by RAMA and then localises to the rhoptry bulb(Richard, Kats et al. 2009). Following its trafficking to the rhoptries, RAP1 is processed by both SUB1 and plasmepsin IX (PMIX) to a 67 kDa mature protein (Silmon de Monerri, Flynn et al. 2011, Nasamu, Glushakova et al. 2017, Favuzza, de Lera Ruiz et al. 2020). The final RAP1 processing event is thought to occur extremely late in schizont development, possibly during schizont rupture, as this processed form is largely found only in free merozoites (Bushell, Ingram et al. 1988, Howard, Narum et al. 1998). RAP1 has previously been shown to be secreted from the rhoptry bulb into the RBC cytosol (Riglar, Richard et al. 2011) following tight junction formation and while it is thought to have a role in PVM establishment, its function is unclear.

RAP1 is not essential for *P. falciparum* blood-stage growth, however its disruption leads to the inhibition of RAP2 rhoptry trafficking (Baldi, Andrews et al. 2000). RAP2 is much smaller than RAP1, at only 42 kDa, and shares no obvious sequence homology with RAP1. As RAP1 knockout inhibits RAP2 trafficking, it is thought that the low molecular weight rhoptry complex forms during rhoptry biogenesis (Baldi, Andrews et al. 2000). Like RAP1, RAP2 is also secreted into the RBC cytosol during invasion and it is possible that the two remain in complex during this process (Suarez, Lentini et al. 2019). Previous studies have suggested that RAP2, unlike RAP1, is

essential for *in vitro* growth as it has not been successfully disrupted (Cowman, Baldi et al. 2000), however the observation that RAP1 knockout leads to RAP2 mislocalisation has led to suggestion that it may not be essential (Baldi, Andrews et al. 2000). Speculation over the essentiality of RAP2 is further confused by the fact that *RAP2* and *RAP3* are paralogues in the *Laverania* subgenus of *Plasmodium* with species outside of this subgenus containing only a single *RAP2/3* gene (Baldi, Good et al. 2002). RAP3 has been shown not to be essential for blood stage growth, however it is thought that this is because it can be functionally complemented by RAP2 (Baldi, Good et al. 2002). While it is currently unclear if *P. falciparum* RAP2 or RAP3 are essential for blood stage growth of *P. falciparum*, recent studies of RAP2 in *P. berghei* show its knockdown strongly attenuates parasite growth by causing a PVM defect following invasion (Bushell, Gomes et al. 2017, Ghosh, Kennedy et al. 2017, Niikura, Inoue et al. 2018).

High molecular weight rhoptry complex

Following merozoite invasion the newly invaded parasite generates new permeability pathways (NPPs), which are essential for allowing nutrient uptake during blood-stage development (Ekland, Akabas et al. 2011). Of these NPPs, the most well characterised is the *Plasmodium* surface anion channel (PSAC), which is present on the infected RBC surface and allows import of amino acids, ions and vitamins (Staines, Rae et al. 2000, Staines, Ellory et al. 2001, Ekland, Akabas et al. 2011). The rhoptry heavy (RhopH) protein complex consists of three members, RhopH1, RhopH2, and RhopH3, which are involved with NPP/PSAC establishment following merozoite invasion (Zainabadi 2016, Counihan, Chisholm et al. 2017, Sherling, Knuepfer et al. 2017). RhopH1 was initially thought to be a single protein, also known as cytoadherence-linked asexual gene (*clag*) 3, however it has subsequently been shown that *clag* has expanded through multiple duplication events to five known *clag* genes in *P. falciparum*, *clag 2, 3.1, 3.2, 8* and *9* (Counihan, Kalanon et al. 2013). It is not clear what the functional or evolutionary importance of this gene expansion is.

Following the initial identification of the RhopH complex (Cooper, Ingram et al. 1988), the *clag* genes (RhopH1) were identified as playing key roles in cytoadherence through binding to the endothelial receptor CD36 (Holt, Gardiner et al. 1999, Ocampo, Rodríguez et al. 2005). It was subsequently shown that this inhibition of cytoadherence was associated with the inability for newly invaded parasites to form NPPs and PSAC (Ling, Florens et al. 2004, Zainabadi 2016). While it is likely that RhopH1 is important for parasite survival *in vivo*, deletion of any of the individual *clag* genes has little influence on *in vitro* growth (Comeaux, Coleman et al. 2011). Disruption of *clag 3.2* has been shown to result in an upregulation of *clag 3.1* expression, while disruption of both *clag 3.1* and *3.2* was strongly inhibitory to parasite growth. It has therefore been suggested that many of the *clag* genes are functionally redundant (Comeaux, Coleman et al. 2011).

It is not currently understood how the RhopH complex allows for the formation of NPPs and PSAC. The RhopH complex localises to the rhoptry bulb in merozoites and is secreted into the RBC cytosol following tight junction formation (Ling, Florens et al. 2004, Kaneko, Lim et al. 2005). It is thought that the RhopH complex then facilitates the establishment of NPPs and PSAC to allow for nutrient import into newly invaded parasites. While the role of RhopH1 in NPP/PSAC establishment has been understood for some time, RhopH2 and RhopH3 were only recently shown to also be important for the process (Counihan, Chisholm et al. 2017, Sherling, Knuepfer et al. 2017). Recent studies have shown that RhopH2 is essential for nutrient import following invasion and also that it binds to the RBC cytoskeleton, potentially providing a mechanism for NPP/PSAC establishment (Counihan, Chisholm et al. 2017). RhopH3 has recently been shown also to be essential for NPP/PSAC establishment, however its conditional truncation was also shown to have a directly inhibitory effect on merozoite invasion; suggesting RhopH3 may have multiple functions (Sherling, Knuepfer et al. 2017).

Reticulocyte binding homologues

The reticulocyte binding homologue (Rh) family are classified based on their similarity to the *P. vivax* reticulocyte binding proteins (RBPs) 1 and 2, and contain the members Rh1, Rh2a, Rh2b, Rh3, Rh4, and Rh5. Rh5 is distinct from the other members of the Rh family in that it lacks a transmembrane domain and has low sequence homology, while Rh3 is thought to be a pseudogene. Rh2a and Rh2b are paralogues whose amino acid sequences are identical for the first ~2700 amino acids and only differ in an ~500 amino acid region towards their C-termini (Dvorin, Bei et al. 2010). All Rh family members have been shown to localise to the rhoptry neck of merozoites and are thought to be secreted prior to tight junction formation and mediate early interactions with the RBC (Rayner , Vargas-Serrato et al. 2001, Stubbs, Simpson et al. 2005, Triglia, Duraisingh et al. 2005, Dvorin, Bei et al. 2010). It has also been suggested that the Rh family may trigger the release of the EBAs from the micronemes, although the mechanism for this is unclear (Rayner , Vargas-Serrato et al. 2001). Rh5 has been shown to be essential for merozoite invasion, while Rh1,2a,2b, and 4 are dispensable (Stubbs, Simpson et al. 2005, Triglia, Duraisingh et al. 2005, Dvorin, Bei et al. 2010, Aniweh, Suurbaar et al. 2020). Rh4 binds to human complement receptor 1 (CR1) (Tham, Wilson et al. 2010) while Rh5 binds to the human receptor basigin (Crosnier, Bustamante et al. 2011). Rh1, 2a, and 2b have all been shown to bind the RBC surface, however the receptors to which they bind are unknown (Rayner , Vargas-Serrato et al. 2001, Triglia, Duraisingh et al. 2005, Dvorin, Bei et al. 2010). It is thought that the three non-essential Rh proteins may contribute to functional redundancy characteristic of invasion pathway switching along with the EBAs (Rayner , Vargas-Serrato et al. 2001).

Rh5-CyRPA-Ripr complex

The Rh5-CyRPA-Ripr complex has been studied intensely in recent years due to its interest as a vaccine candidate. Rh5 is present only in the *Lavernia* subgenus of *Plasmodium,* and while CyRPA and Ripr are found outside *Laverania*, their functions outside *P. falciparum* are not

understood (Galaway, Yu et al. 2019). Rh5 is produced as a 63 kDa pro-protein and localises to the rhoptry neck. Rh5 is subsequently cleaved into a 45 kDa mature protein that is secreted during the process of invasion. CyRPA and Ripr are micronemal antigens that form a complex with Rh5 whereby CyRPA binds to the N-terminus of RH5 and Ripr in turn binds to CyRPA (Chen, Xu et al. 2014, Chen, Xu et al. 2017, Wong, Huang et al. 2019). Once the Rh5-CyRPA-Ripr complex has formed, Rh5 binds basigin using its C-terminus, triggering an increase in RBC calcium (Chen, Xu et al. 2014, Wright, Hjerrild et al. 2014, Wong, Huang et al. 2019). It is thought that upon basigin binding, Rh5 inserts into the RBC membrane where it, along with Ripr forms a pore between the RBC membrane and PPM that may be where merozoite antigens are secreted into the RBC cytosol (Chen, Xu et al. 2014, Wong, Huang et al. 2019). The suggestion that the Rh5-CyRPA-Ripr complex forms a pore between the merozoite and RBC, however, has been questioned as the structural and biochemical properties of Rh5 are thought not to be permissive for membrane insertion or unfolding (Ragotte, Higgins et al. 2020). As the Rh5-basigin interaction is of great importance to *P. falciparum* invasion it has been suggested, by constructing ancestral *Rh5* genes through comparison with *Laverania Rh5* sequences, that an *Rh5* polymorphism may have been a key step in the evolution of *P. falciparum* (Galaway, Yu et al. 2019).

It is currently unclear how the Rh5-CyRPA-Ripr complex associates with the PPM during invasion, and while it was initially thought CyRPA contained a GPI-anchor(Reddy, Amlabu et al. 2015), this was later shown not to be the case (Volz, Yap et al. 2016, Ragotte, Higgins et al. 2020). The N-terminus of Rh5 has recently been shown to interact with the GPI-anchored protein P113 and it is thought that this interaction may allow anchoring of the complex to the PPM during invasion (Galaway, Drought et al. 2017). It is not known whether the entire Rh5-CyRPA-Ripr complex is capable of interacting with P113 and whether this protein does indeed act as the membrane anchor for the complex.

Rhoptry neck proteins

The rhoptry neck (RON) family comprises a group of proteins that share a common name but have no universally shared features. Currently characterised RON proteins in *P. falciparum* are RON2, RON3, RON4, RON5, RON6, and RON12. The numbers assigned to each of the RON proteins roughly reflects the order that they were discovered in, but this is complicated by the fact that many RONs were identified and named first in *Toxoplasma gondii* and lack a *Plasmodium* homologue. *P. falciparum* RON2, RON4, and RON5 localise to the rhoptry neck and form the RON complex that is involved with tight junction formation (Alexander, Arastu-Kapur et al. 2006, Morahan, Sallmann et al. 2009, Richard, MacRaild et al. 2010, Curtidor, Patiño et al. 2011, Curtidor, Patiño et al. 2014). RON6 and RON12 localise to the rhoptry neck but are not members of the RON complex (Proellocks, Kats et al. 2009, Knuepfer, Suleyman et al. 2014). RON3 localises to the rhoptry bulb in *P. falciparum* and is not a member of the canonical RON complex (Ito, Han et al. 2011).

For the RONs involved in the RON complex (RON2, RON4, and RON5) they are secreted from the rhoptry neck early in merozoite invasion (Vulliez-Le Normand, Tonkin et al. 2012). The RON complex then embeds into the RBC membrane such that RON4 and RON5 are exposed to the RBC cytosol while RON2 spans the RBC membrane and has a large extracellular region (Vulliez-Le Normand, Tonkin et al. 2012, Delgadillo, Parker et al. 2016). Following its secretion from the micronemes, AMA1 binds to the exposed region of RON2 and this allows the formation of the tight junction (Cao, Kaneko et al. 2009, Richard, MacRaild et al. 2010, Vulliez-Le Normand, Tonkin et al. 2012, Delgadillo, Parker et al. 2016). It is unclear mechanistically how the AMA1-RON complex interaction facilitates tight junction formation. The AMA1-RON complex interaction is non-redundant and as such, RON2, RON4, and RON5 are all essential for blood stage growth.

RON6 is 950 amino acid protein that contains an N-terminal SP, followed by three repeat regions, a *Plasmodium* conserved region, and a cysteine rich region at its C-terminus (Proellocks, Kats et al. 2009). RON6 has been shown to localise to the rhoptry neck by both immunofluorescence and immunoelectron microscopy and it is thought to be essential for blood stage growth (Proellocks, Kats et al. 2009). Additionally it has been shown that RON6 is secreted during invasion and goes on to localise at the newly formed PVM in newly invaded ring stage parasites (Proellocks, Kats et al. 2009). Currently, the function of RON6 and whether it has any binding partners is unknown. RON12 is a 315 amino acid protein that, like RON6, contains an N-terminal SP and localises to the rhoptry neck (Knuepfer, Suleyman et al. 2014). Unlike all of the other RONs in *P. falciparum*, however, RON12 lacks a functional homologue outside of *Plasmodium* (Knuepfer, Suleyman et al. 2014). RON12 is secreted from the rhoptry neck during invasion where it is thought to form a soluble component of the nascent PV (Knuepfer, Suleyman et al. 2014, Ito, Takashima et al. 2019). It is currently unclear what the function of RON12 is and while RON12 is not essential for blood stage growth *in vitro*, RON12-null parasites exhibit a severe growth defect (Knuepfer, Suleyman et al. 2014).

RON3 is a 2215 amino acid protein that contains an N-terminal SP, three transmembrane domains and a coiled coil region (Ito, Han et al. 2011). After being named for its *T. gondii* homologue, RON3 was shown to localise to the rhoptry bulb in *P. falciparum* by both immunofluorescence and immunoelectron microscopy (Ito, Han et al. 2011, Zhao, Chang et al. 2014). Despite its distinct localisation, RON3 has been shown to bind to both RON2 and RON4 (Ito, Han et al. 2011). Its interactions with RON2 and RON4 have led to speculation that there may be a non-canonical RON complex that lacks RON5 (Ito, Han et al. 2011). It is not known what the significance of this complex is to merozoite invasion as the function of RON3 is currently unknown.

Rhoptries of Apicomplexa

Rhoptries are the largest of the secretory organelles of Apicomplexa and they vary across the phylum in their number, size, and contents. In all Apicomplexa, however, rhoptries are always the largest of the secretory organelles and possess both a neck and bulb, giving them the distinct 'club-shape' for which they are named. In *Plasmodium*, merozoites and sporozoites contain two rhoptries, while ookinetes, the other invasive stage, lack rhoptries entirely. The close relative of *Plasmodium, Babesia*, is thought to contain three rhoptries in its merozoites (Kawai, Igarashi et al. 1999), while *Theileria* is thought to contain six rhoptries per merozoite (Shaw and Tilney 1992). Distantly related to the aforementioned Apicomplexa, *Cryptosporidium* merozoites and sporozoites contain only a single rhoptry, which may be due to their vastly divergent process of invasion (Tetley, Brown et al. 1998). Rhoptries have been most well studied, in *Toxoplasma gondii* whose tachyzoites contain 8-12 rhoptries (Boothroyd and Dubremetz 2008). It is generally thought that this high number of rhoptries is related to the extremely broad host range and cellular tropism exhibited by *T. gondii* and that in any particular invasion event only a subset of all the rhoptries actively participate (Boothroyd and Dubremetz 2008).

Rhoptry evolution

Apicomplexans evolved from free-living photosynthetic organisms but now comprise only obligate intracellular parasites (Gubbels and Duraisingh 2012). The evolutionary origin of rhoptries is not entirely clear, but it is most widely accepted that rhoptries are divergent lysosomes (Ngô, Yang et al. 2004, Gubbels and Duraisingh 2012). A lysosomal origin is supported by their development from Golgi-derived vesicles that are acidic and electron dense (Ngô, Yang et al. 2004). Furthermore, homologues of many proteins that are associated with endosomes in other organisms localise to the rhoptries in Apicomplexa (Ngô, Yang et al. 2004). It is not entirely clear

what drove the evolution of rhoptries, however it is clear that rhoptries, or rhoptry-like organelles, emerged prior to divergence of Apicomplexa from the other alveolates as rhoptries are present in Perkinsozoa and Dinoflagellata (Klaus and Norbert 2010, Gubbels and Duraisingh 2012). It is therefore likely that the most recent common ancestor of all Myzozoa, the superphylum that comprises Apicomplexa, Dinoflagellates, Chromerida, and Perkinsozoa, possessed a rhoptry-like organelle. While modern Apicomplexa are obligate intracellular parasites, Dinoflagellates can be photosynthetic, predatory, or a combination of the two (Schnepf and Elbrächter 1992, Stoecker 1999). Dinoflagellate predation occurs through a process known as myzocytosis, or cellular vampirism, where rhoptry-like organelles are used to attach to prey cells and form a pore through which the dinoflagellate obtains nutrients (Schnepf and Deichgräber 1984, Coats 1999, Gubbels and Duraisingh 2012). Myzocytosis is not the preferred method of feeding for all dinoflagellates, as many photosynthesise, but most photosynthetic dinoflagellates are capable of myzocytosis (Schnepf and Elbrächter 1992). It has therefore been suggested that early rhoptries may have evolved as a strategy for cellular predation and have since evolved into essential secretory organelles for host cell invasion by obligate intracellular parasites (Gubbels and Duraisingh 2012, Klinger, Nisbet et al. 2013).

Rhoptry biogenesis

In spite of their importance to survival and the invasion biology of all apicomplexan parasites, very little is known about rhoptry biogenesis. It has been shown that the nascent rhoptry develops through fusion of Golgi-derived vesicles, but what allows these vesicles to form rhoptries is currently unknown (Bannister, Hopkins et al. 2000, Counihan, Kalanon et al. 2013). Furthermore, it is not known what the trigger for rhoptry biogenesis is, although most rhoptry proteins begin being transcribed in mid-trophozoite stage parasites. It is thought that the Golgi-

derived vesicles that go on to form the rhoptries carry cargo that is trafficked through the classical secretory pathway, as most rhoptry proteins contain an N-terminal signal peptide (Howard and Schmidt 1995, Deponte, Hoppe et al. 2012, Counihan, Kalanon et al. 2013). Additionally it has been shown that treatment with brefeldin A, an inhibitor of transport between the endoplasmic reticulum and Golgi (Chardin and McCormick 1999), prevents rhoptry biogenesis (Howard and Schmidt 1995, Ghoneim 2013). The nascent rhoptry lacks the eventual neck/bulb distinction, instead starting out as a round organelle (Bannister, Hopkins et al. 2000, Counihan, Chisholm et al. 2017). It is not known when or how the rhoptry eventually adopts its final structure. However, it is thought that at the point of Golgi release the cargo are specifically targeted to either the developing rhoptry neck or bulb; as opposed to transport to the rhoptry and subsequent distribution to its different compartments (Counihan, Kalanon et al. 2013).

Most, but not all, rhoptry antigens have signal peptides that traffic them to the developing rhoptry through the classical secretory pathway. For Golgi-trafficked antigens, it has been shown that RAMA and sortilin can act as chaperones for rhoptry bulb-destined cargo such as RAP1, RAP2, and RhopH3 (Richard, Kats et al. 2009, Hallée, Boddey et al. 2018). RAMA is transcribed earlier than most other rhoptry proteins and localises to the ER and Golgi in parasites that have not started forming their rhoptries yet. It is thought that RAMA only acts as a chaperone for rhoptry bulb proteins and it has been speculated that there may be equivalent(s) proteins that act as chaperones for rhoptry neck antigens (Counihan, Kalanon et al. 2013). Rhoptry neck biogenesis occurs following bulb biogenesis and so it is likely that a rhoptry neck chaperone would be expressed later than RAMA and possibly only be expressed once rhoptry bulb development has begun. Pf34 has been proposed as a rhoptry neck equivalent to RAMA, based on its GPI-anchor but this has not been shown experimentally (Counihan, Kalanon et al. 2013). Rhoptry proteins that lack signal peptides, such as armadillo repeats only (ARO), can localise to the rhoptries using

acylation motifs (Cabrera, Herrmann et al. 2012). However, ARO localises to the cytosolic face of the rhoptry membrane, rather than the rhoptry lumen. Localisation by acylation motifs, such as palmitoylation could either occur at the Golgi, in vesicles that will form the nascent rhoptry, or directly at protein's destination on the rhoptry. For ARO, the first 20 amino acids of its N-terminus are sufficient to target it to the rhoptries and this targeting is coordinated by both myristoylation and palmitoylation (Cabrera, Herrmann et al. 2012). It is currently unclear if ARO is palmitoylated and attached to the Golgi membrane during rhoptry-destined vesicle development, or if ARO is palmitoylated directly at the rhoptry membrane.

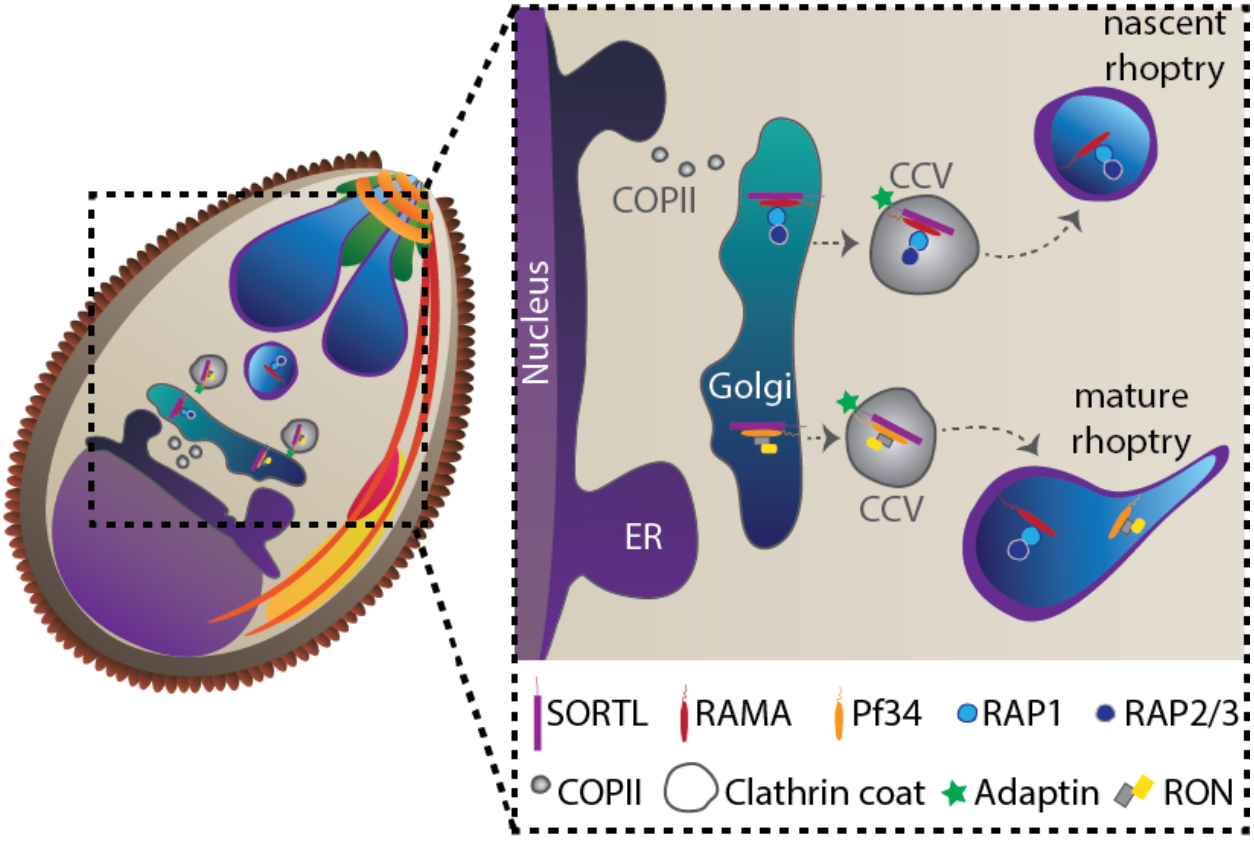

Figure 1.8: Rhoptry biogenesis in *P. falciparum*. Figure adapted from (Counihan, Kalanon et al. 2013).

Rhoptry proteins that contain a signal peptide are co-translationally inserted by the Sec translocon at the endoplasmic reticulum and subsequently trafficked to the Golgi in vesicles coated with COPII. In the Golgi, it is thought that sortillin-like protien (SORTL) binds to rhoptry-associated membrane antigen (RAMA), and that RAMA in turn binds specific rhoptry cargo, such as the rhoptry associated proteins (RAP). This rhoptry-destined cargo buds from the Golgi in clathrin coated vesicles (CCV), which travel towards the apical end of the parasite and fuse to form the nascent rhoptry. It is thought that the rhoptry bulb forms first, with cargo destined to be rhoptry neck proteins arriving later, with Pf34 thought to target rhoptry neck cargo such as the rhoptry neck (RON) proteins in a similar manner to RAMA.

Rhoptry structure

In *P. falciparum* Rhoptries are divided into a narrow neck region and a larger bulb with the neck positioned at the apical tip of the merozoite (Hanssen, Dekiwadia et al. 2013). Rhoptries are typically around 500 nm in length (neck to bulb) and the rhoptry bulb has a diameter of approximately 200 nm (Hanssen, Dekiwadia et al. 2013). It has been estimated using electron microscopy that *P. falciparum* rhoptries have a volume of between 3.5×10^7 and 6.1×10^7 nm^3 and that they comprise between 2% and 7% of the merozoite volume, with this variation due to fixation techniques (Hanssen, Dekiwadia et al. 2013). It is not currently known what differentiates the rhoptry bulb from the rhoptry neck, or how rhoptry antigens are compartmentalised as no membrane exists between the two (Zuccala, Gout et al. 2012). Using conventional electron microscopy techniques, the rhoptry neck appears more electron dense than the bulb (Hanssen, Dekiwadia et al. 2013). While this was thought to indicate differences in composition between the rhoptry neck and bulb, it has been suggested to be a staining artefact (Hanssen, Dekiwadia et al. 2013). Once merozoite invasion begins, the electron density difference between rhoptry neck and bulb disappears, which is thought to relate to the secretion of neck antigens (Hanssen, Dekiwadia et al. 2013). During *P. falciparum* invasion, the two rhoptries of the merozoite fuse together, leaving one rhoptry at the completion of invasion, which still maintains its neck and bulb structure (Hanssen, Dekiwadia et al. 2013). As the rhoptries maintain their overall structure following fusion

and secretion, it has been suggested that the rhoptry structure is supported by either an internal or external scaffold (Hanssen, Dekiwadia et al. 2013). It is currently unclear, however, what the composition of this scaffold might be.

Rhoptry fusion, secretion, and disassembly

In the mature merozoite, the rhoptries exist as two club-shaped organelles that have distinct bulb and neck regions (Bannister, Hopkins et al. 2000, Hanssen, Dekiwadia et al. 2013). During the process of invasion, the rhoptry neck fuses to the PPM, which allows the initial secretion of the rhoptry neck antigens that coordinate early RBC recognition and attachment (Hanssen, Dekiwadia et al. 2013). It is currently unknown what proteins control this rhoptry-PPM fusion event, but it is though that may involve snap receptor (SNARE) proteins as they perform similar functions in other systems (Suarez, Lentini et al. 2019). It is thought that at the initial fusion event rhoptry neck antigens, but not rhoptry bulb antigens, are secreted (Hanssen, Dekiwadia et al. 2013, Suarez, Lentini et al. 2019). Once the tight junction has been established and invasion progresses, rhoptry bulb antigens are then thought to be secreted into the RBC and contribute to formation and modification of the nascent PVM (Hanssen, Dekiwadia et al. 2013). It has been hypothesised that the rhoptry bulb contents are secreted into RBCs inside lipid-rich bodies or vesicles that are likely of rhoptry origin (Håkansson, Charron et al. 2001, Boothroyd and Dubremetz 2008, Riglar, Richard et al. 2011, Hanssen, Dekiwadia et al. 2013). It is unclear how the parasite coordinates its secretion such that neck antigens are secreted first and bulb antigens secreted later. Additionally, the trigger for rhoptry secretion or how the force required for secretion is generated are currently unknown. It has been suggested that changes in intracellular calcium, cyclic AMP (cAMP), or intracellular potassium may be the proximate trigger for rhoptry secretion, however, it is unclear what ultimately

regulates rhoptry secretion (Gubbels and Duraisingh 2012, Collins, Hackett et al. 2013, Gao, Gunalan et al. 2013, Dawn, Singh et al. 2014, Patel, Perrin et al. 2019).

In addition to the fusion of the rhoptry neck to the PPM, during the process of invasion the two rhoptries fuse together, leaving a single rhoptry that remains differentiated into bulb and neck regions (Hanssen, Dekiwadia et al. 2013). It is not known how the fusion between rhoptries relates to rhoptry secretion, but the two rhoptries are thought to fuse at the rhoptry neck first. Following neck fusion, the rhoptry temporarily exists with two bulbs but only a single fused neck. Once the tight junction has formed and the merozoite begins to actively invade the RBC, this structure transitions to only a single club shaped rhoptry by the completion of invasion (Hanssen, Dekiwadia et al. 2013). As rhoptry secretion proceeds, the volume of this single fused rhoptry steadily decreases until, at the completion of invasion, the rhoptry is approximately 25% of its initial volume (Hanssen, Dekiwadia et al. 2013), coinciding with secretion of rhoptry antigens, which may contribute to decreased rhoptry volume (Hanssen, Dekiwadia et al. 2013). An additional observation following rhoptry fusion is that the single rhoptry contains membranous whorls (Bannister, Hopkins et al. 2000, Hanssen, Dekiwadia et al. 2013). It is currently unclear if these whorls are byproducts of rhoptry membrane or rhoptry-PPM fusion, if they form the vesicle-like structures that facilitate rhoptry bulb secretion into the RBC, or a combination of the two.

The final key aspect of rhoptry biology following merozoite invasion is rhoptry disassembly. In spite of their high electron density in merozoites, the rhoptries are completely absent shortly after the completion of invasion (Sachanonta, Chotivanich et al. 2011). Rhoptry disassembly has not yet been explored experimentally and as such, we currently have no understanding of how and when rhoptries disassemble following invasion. Furthermore, what proteins coordinate rhoptry disassembly and its importance to the survival of the newly invaded ring stage parasite are unknown.

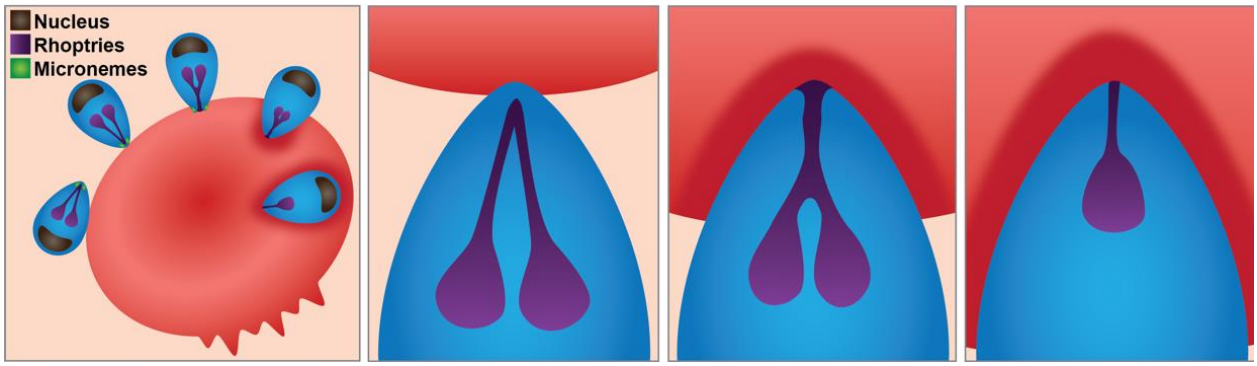

Figure 1.9: Rhoptry fusion in *P. falciparum*.

When merozoites are released following schizont rupture, the rhoptries exist as two separate club-shaped organelles with distinct neck and bulb regions. Once the merozoite recognises a RBC, the rhoptries begin to fuse together at the rhoptry neck. Additionally, the rhoptry neck fuses to the parasite plasma membrane, which allows secretion of rhoptry contents. As invasion proceeds, the rhoptries continue to fuse together and at the completion of invasion only a single, fully-fused rhoptry remains. When invasion has been completed, the rhoptry maintains its neck and bulb distinction but is considerably smaller, which is thought to be caused by the secretion of its contents.

Cytosolically exposed rhoptry-interacting proteins

There is currently a relatively good understanding of secreted rhoptry antigens and their functions or phenotypes, predominantly due to their attractiveness as vaccine candidates. By contrast, little is known about the dynamic biology of rhoptries at the point of merozoite invasion with almost nothing known at a molecular level about the proteins involved in coordinating rhoptry structure, fusion, secretion, or disassembly. Much of this unexplored biology involves dynamic interactions either between the two rhoptries, or with the rhoptry and other parts of the cell such as the PPM during the process of merozoite invasion. Rhoptry proteins that have been studied due to their promise as vaccine candidates are secreted from the rhoptry lumen and are therefore unlikely to coordinate any of these dynamic interactions that involve the cytosolic surface of the rhoptries. By contrast, proteins that localise to the cytosolic surface of the rhoptries, hereafter referred to as

cytosolically exposed rhoptry-interacting proteins (C-RIPs), possess a unique localisation that allows them to mediate interactions between the rhoptries. Additionally, C-RIPs could coordinate interactions between the rhoptries and other parts of the merozoite, such as the PPM, IMC, or cytoskeletal elements, which could facilitate movement or force generation. C-RIPs are therefore likely to have roles in coordinating fusion between rhoptries, rhoptry-PPM fusion during secretion, rhoptry disassembly post invasion, force generation during secretion, and maintaining structure of the rhoptry. Despite their likely key functions, only six putative C-RIPs have been characterised in Apicomplexa, with the potential that many other C-RIPs coordinate key rhoptry functions.

Armadillo Repeats Only (ARO)

Armadillo Repeats Only (ARO) was the first characterised C-RIP and is a 31 kDa protein that is comprised of armadillo (ARM) repeats (Cabrera, Herrmann et al. 2012, Mueller, Klages et al. 2013, Mueller, Samoo et al. 2016, Geiger, Brown et al. 2019). A crystal structure for ARO (1.8 Å, PDB: 5EWP), the first rhoptry protein whose structure has been determined by X-ray crystallography, was recently determined and showed that PfARO is a monomer that contains 5 ARM repeats (Geiger, Brown et al. 2019). Each ARM repeat is comprised of three alpha helices and they stack in a head-to-tail manner, which gives an overall right-handed superhelix structure to ARO (Geiger, Brown et al. 2019). The final helix from each ARM repeat interact forming a concave surface, giving ARO a ‘kidney bean’ shape (Geiger, Brown et al. 2019). ARO contains loops between helix 2 and 3 of ARM repeat 1, and between helix 11 and 12 of ARM repeat 4, which have been identified as likely sites for protein-protein interactions considering their conservation among Apicomplexa (Geiger, Brown et al. 2019).

ARO localises to the cytosolic face of the rhoptry bulb, and this localisation is coordinated exclusively by myristolation and palmitoylation motifs at is N-terminus that are both essential and sufficient for rhoptry targeting (Cabrera, Herrmann et al. 2012, Mueller, Klages et al. 2013, Geiger,

Brown et al. 2019). It has been shown that palmitoylation of ARO is caused by the rhoptry resident palmitoyl transferase DHHC7 (Beck, Fung et al. 2013). ARO is essential for growth in *P. falciparum*, and its knockdown has been shown to prevent positioning of rhoptries at the apical tip of *T. gondii* tachyzoites (Mueller, Klages et al. 2013, Mueller, Samoo et al. 2016). Knockdown did not directly alter rhoptry biogenesis, as the rhoptries fully formed, however they localised to the cytoplasm rather than at the apical tip (Beck, Fung et al. 2013, Mueller, Klages et al. 2013). TgARO knockdown is inhibitory to invasion but has no effect on tachyzoite egress (Beck, Fung et al. 2013). Disruption of ARM repeats 3 and 4 (2 and 3 in PfARO) have been shown to significantly attenuate parasite growth and also result in the mislocalised rhoptry phenotype (Mueller, Samoo et al. 2016). Additionally, disruption of ARM repeat 6 (5 in PfARO) has been shown to result in a clustered rhoptry phenotype, rather than mislocalised, but this too leads to parasite growth inhibition (Mueller, Samoo et al. 2016).

Immunoprecipitation experiments in *T. gondii* have showed that TgARO interacts with adenylyl cyclase beta (ACß), Myosin F (MyoF), and a protein whose function was previously unknown, ARO interacting protein (AIP) (Mueller, Klages et al. 2013). Upon disruption of ARM repeats 3 and 4, TgACß expression becomes undetectable, suggesting its localisation is dependent upon TgARO (Mueller, Samoo et al. 2016). When ARM repeat 6 of TgARO was disrupted TgACß localised to the clustered rhoptries, however it was not detected by immunoprecipitation and so it is currently unclear what role ARM repeat 6 of TgARO plays in TgACß interaction (Mueller, Samoo et al. 2016). It has been hypothesised that the interaction between ARO and ACß implicates a role for calcium signaling and protein kinase A (PKA) activation in rhoptry apical targeting (Mueller, Klages et al. 2013). A direct interaction between ARO and AIP has not been shown in *P. falciparum*. Despite this, deletion of the loop region in ARM repeat 1 (ARM repeat 2 in TgARO) of PfARO leads to a cytosolic, rather than rhoptry, distribution of PfAIP (Geiger, Brown et al.

2019). Furthermore, mutation of H_{72} and W_{74} of PfARO, two conserved residues in the ARM repeat 1 loop, also result in PfAIP mislocalisation without altering PfARO localisation (Geiger, Brown et al. 2019). Despite this specific mislocalisation, proximity dependent biotinylation of PfAIP did not identify PfARO as an interacting partner (Geiger, Brown et al. 2019). It has been suggested that in *P. falciparum* the ARO/AIP interaction may be transient and occur only during rhoptry biogenesis, as PfAIP localises to the rhoptry neck and PfARO to the rhoptry bulb (Geiger, Brown et al. 2019). Reciprocal immunoprecipitations between TgARO and TgMyoF suggested the two interact with each other (Mueller, Klages et al. 2013). Additionally, treatment of tachyzoites with butanedione monoxime (BDM), an inhibitor of myosin ATPase, also resulted in a rhoptry mislocalisation phenotype, suggesting rhoptry positioning is dependent on an actin-myosin motor (Mueller, Klages et al. 2013). Furthermore, both TgARO and PfARO are structurally similar to the myosin chaperone uncoordinated mutant number 45 (UNC-45) (Lee, Melkani et al. 2014) and so it has been suggested that ARO may bind MyoF similar to UNC-45 (Mueller, Samoo et al. 2016, Geiger, Brown et al. 2019).

ARO Interacting Protein (AIP)

AIP was first identified through immunoprecipitation experiments with ARO in *T. gondii* tachyzoites (Mueller, Klages et al. 2013). Subsequently, bioinformatic analyses identified a homologue of AIP in *P. falciparum* and showed that AIP is conserved amongst all genera of alveolates (Geiger, Brown et al. 2019). Despite its conservation across alveolates, AIP is variable in size with TgAIP 822 amino acids in length and PfAIP 421 amino acids in length (Geiger, Brown et al. 2019). It is not clear if this variation in amino acid length imparts any functional significance, as no characterised domains are present in either PfAIP or TgAIP (Geiger, Brown et al. 2019). TgAIP has been shown to localise to the cytosolic face of the rhoptry neck/bulb junction, rather than uniformly distributed across the rhoptry neck (Mueller, Klages et al. 2013, Mueller, Samoo et

al. 2016). PfAIP by contrast, localises to the cytosolic face of the apical end of the rhoptry neck and shows no colocalisation with the rhoptry bulb residing PfARO by immunofluorescence microscopy (Geiger, Brown et al. 2019).

Knockout of TgAIP resulted in loss of ACß expression as detected by Western blot, however TgARO localisation was not influenced and the rhoptries were still positioned at the apical tip (Mueller, Samoo et al. 2016). Lack of a rhoptry positioning phenotype suggests that TgAIP and TgACß are not involved in rhoptry positioning. Additionally, these data suggest that ARO is likely to directly interact with AIP and that AIP, in turn, directly interacts with ACß (Mueller, Samoo et al. 2016). While TgAIP is not essential, as it has been knocked out, it has not been determined whether TgAIP knockout attenuates parasite growth in any way. PfAIP has been shown to be essential for blood stage growth and conditional mislocalisation of PfAIP results in a direct inhibition of merozoite invasion (Geiger, Brown et al. 2019). It is thought that ARO may act as a chaperone for AIP during rhoptry biogenesis and that both ARO and AIP coordinate to interact with ACß (Mueller, Samoo et al. 2016, Geiger, Brown et al. 2019). While the function of AIP is not known, it is thought that it has a role downstream of rhoptry biogenesis or positioning and may be involved with rhoptry secretion (Mueller, Samoo et al. 2016, Geiger, Brown et al. 2019).

Adenylyl Cyclase Beta (ACß)

Adenylyl, or adenylate, cyclases are a family of enzymes that are extremely diverse in structure and amino acid sequence, but are characterised by their enzymatic activity that catalyses the conversion of ATP to cAMP and pyrophosphate (Hanoune and Defer 2001, Linder and Schultz 2003). cAMP is frequently used as a secondary messenger and its role has been most well studied in the context of protein kinase A (PKA) (Taylor, Beuchler et al. 1990). PKA is a family of kinase with extremely broad substrate specificities whose ability to phosphorylate proteins is dependent on intracellular cAMP concentration (Taylor, Beuchler et al. 1990). *P. falciparum* possesses two

adenylyl cyclases, alpha and beta, with ACß the only adenylyl cyclase expressed in *P. falciparum* asexual blood stages (Salazar, Bank et al. 2012, Patel, Perrin et al. 2019). ACß is a large protein of 2279 amino acids, however, the catalytic domain is contained in the first 700 amino acids of the protein (Salazar, Bank et al. 2012). ACß lacks any transmembrane domains, unlike most adenylyl cyclases, but has been shown to localise to the cytosolic face of the rhoptry neck (Salazar, Bank et al. 2012, Mueller, Samoo et al. 2016, Patel, Perrin et al. 2019). It has been suggested that like TgAIP, TgACß may concentrate at the rhoptry neck/bulb junction (Mueller, Samoo et al. 2016). It is not known how ACß associates with the rhoptry membrane.

PfACß has been shown to be enzymatically active when bound to a Mn^{2+} cofactor, and inactive in the presence of Mg^{2+} (Salazar, Bank et al. 2012). Additionally, its enzymatic activity was shown to be highly sensitive to pH, with optimum activity observed at 7.5 and dropping sharply with much variation from this (Salazar, Bank et al. 2012). Due to its high sensitivity to changes in pH, it has been suggested that PfACß may act as the parasite's pH sensor and could contribute to the significant decreases in *in vitro* parasite growth outside a pH range of 7.1-7.5 (Salazar, Bank et al. 2012).

PfACß is essential for blood stage growth, with conditional knockout showing this protein to also have a direct role in merozoite invasion (Patel, Perrin et al. 2019). Conditional knockout of PfACß also results in delayed egress, but this was not thought to contribute greatly to growth inhibition (Patel, Perrin et al. 2019). It has been suggested that ACß is activated by the increase in intracellular K^+ that occurs when the merozoite is released into the blood plasma following schizont rupture (Dawn, Singh et al. 2014). Following ACß activation, it is thought that there is an increase in cAMP, which in turn activates PKA and leads to microneme secretion (Dawn, Singh et al. 2014). Importantly, this study localised PfACß to the cytoplasm of merozoites, whereas multiple other studies using a combination of endogenous tagging and antibody detection have localised ACß to

the rhoptries (Dawn, Singh et al. 2014, Mueller, Samoo et al. 2016, Patel, Perrin et al. 2019). Furthermore, a subsequent study showed efficient microneme secretion in PfACß conditional knockout merozoites (Patel, Perrin et al. 2019). It was noted, however, that conditional knockout of ACß lead to an inability of merozoites to shed AMA1 from their surface and this may contribute to the invasion defect caused by ACß disruption (Patel, Perrin et al. 2019). Of note, ACß conditional knockdown did not alter secretion of the rhoptry antigen Rh2b (Patel, Perrin et al. 2019).

As the only adenylyl cyclase expressed in *P. falciparum* blood stages, and therefore potentially the only source of cAMP in the parasite, conditional disruption of PfACß leads to a large number of changes to protein phosphorylation in merozoites (Patel, Perrin et al. 2019). Hundreds of proteins were significantly hypophosphorylated following ACß conditional disruption (Patel, Perrin et al. 2019). Moreover, the importance of the vast majority of these phosphorylation sites are completely unknown. Of note, ACß conditional knockout led to the hypophosphorylation of ARO, AIP, RAMA RON2, and AMA1 (Patel, Perrin et al. 2019). It has been shown that phosphorylation of AMA1 results in a change in its structure and that this may be what prevents AMA1 shedding upon ACß disruption (Patel, Perrin et al. 2019). While ACß is an extremely important protein for parasite survival, many aspects of its biology are not understood. Only a relatively small fraction of the total ACß amino acid sequence encodes an enzymatic function and it is not clear what the function(s) of the N-terminal ~1400 amino acids may be. Additionally, it is not clear what the functional significance of ACß's rhoptry localisation is as the production of cAMP results in a systemic response throughout the merozoite rather than a local change in rhoptry cAMP concentration.

Merozoite organising protein (MOP)

P. falciparum Merozoite organising protein (PfMOP) is a large, 1826 amino acid, containing protein that was first identified in a screen for egress associated proteins (Dvorin, Martyn et al. 2010). Like PfARO, PfMOP contains an ARM repeat, but lacks a transmembrane domain, signal peptide, or acylation motifs (Absalon, Robbins et al. 2016). PfMOP has been shown to localise to the apical tip of merozoites, likely the rhoptry neck, and is exposed to the cytosol (Absalon, Robbins et al. 2016). PfMOP is essential for blood stage growth and its knockdown strongly inhibits parasite growth (Absalon, Robbins et al. 2016). More specifically, knockdown of PfMOP leads to a decrease in the number of fully-formed merozoites per schizont (Absalon, Robbins et al. 2016). PfMOP deficient parasites failed to properly segment, with many merozoites containing multiple sets of organelles (Absalon, Robbins et al. 2016). Notably, merozoites that did form in full in PfMOP deficient schizonts were capable of invading normally, indicating PfMOP does not play a direct role in invasion (Absalon, Robbins et al. 2016). It has been shown that PfMOP deficient merozoites fail to completely form the IMC and it is thought that this may cause the merozoite segmentation defect (Absalon, Robbins et al. 2016). Furthermore, PfMOP knockdown inhibited AMA1 surface translocation, suggesting that PfMOP-mediated IMC formation may be important for AMA1 translocation (Absalon, Robbins et al. 2016). It is currently unclear how PfMOP may mediate IMC formation or what significance its rhoptry localisation has for this suspected function.

Myosin F (MyoF)

Myosins comprise a protein superfamily where the common features are the ability to bind actin, hydrolyse ATP, and generate movement (Sellers 2000). Force/movement generation by myosins is used in a wide variety of biological processes including muscle contraction, cellular motility, and in Apicomplexa; generation of force required for host cell invasion (Sellers 2000, Tyska and Warshaw 2002, Robert-Paganin, Robblee et al. 2019). Myosin F (MyoF) in *P.*

falciparum is a 2160 amino acid containing protein with a myosin head domain at its N-terminus, followed by a series of IQ motifs and seven WD40 repeat domains at its C-terminus (Foth, Goedecke et al. 2006, Jacot, Daher et al. 2013). MyoF was first identified through a screen of conserved apicomplexan myosins (Foth, Goedecke et al. 2006) and TgMyoF has been shown to localise broadly throughout the parasite with foci at the apicoplast and apical tip (Jacot, Daher et al. 2013). Knockdown of TgMyoF led to a rhoptry mislocalisation phenotype, similar to TgARO knockdown, and resulted in the formation of residual bodies containing non-functional rhoptries (Jacot, Daher et al. 2013). Additionally, TgMyoF knockdown led to defects in centrosomal positioning and apicoplast division suggesting that TgMyoF likely has multiple independent functions (Jacot, Daher et al. 2013).

TgMyoF and TgARO have been shown to interact with each other through immunoprecipitation experiments and this interaction is dependent on ARM repeats 3 and 4 (ARM repeats 2 and 3 in PfARO) (Mueller, Klages et al. 2013, Mueller, Samoo et al. 2016). Based upon their interaction and similar phenotypes following knockdown, it has been suggested that TgMyoF and TgARO form a complex, potentially including TgAIP, that leads to the apical positioning of rhoptries (Mueller, Klages et al. 2013). Although MyoF is known to be essential for blood stage growth (Wall, Zeeshan et al. 2019), evidence to date does not yet support that this mechanism of rhoptry positioning also occurs in *P. falciparum*. Proximity dependent biotinylation assays suggest that PfAIP does not interact with either PfARO or PfMyoF in schizonts (Geiger, Brown et al. 2019). Moreover, PfAIP and PfARO have non-overlapping localisations, making it unlikely that they form a stable complex (Geiger, Brown et al. 2019). It is possible, however, that the ARO/AIP/MyoF interaction, and therefore rhoptry positioning, could be transient and occur earlier in the parasite lifecycle than could be detected by proximity dependent biotinylation.

Ferlin 2

Ferlins are a family of proteins that are comprised of multiple tandem C2 domains and are typically involved in membrane fusion events (Martens 2010, Lek, Evesson et al. 2012). Ferlin 2 was recently characterised in *T. gondii*, and is a 1426 amino acid containing protein that has five C2 domains, along with a putative degenerate C2 domain, and a C-terminal transmembrane domain (Coleman, Saha et al. 2018). Ferlin 2 shows a dynamic localisation whereby in intracellular parasites it localises predominantly to the cytosolic face of the IMC, with additional foci in the conoid (Coleman, Saha et al. 2018). In extracellular parasites, however, Ferlin 2 localised to the cytoplasmic face of the rhoptry membrane (Coleman, Saha et al. 2018). Conditional knockdown of TgFerlin 2 completely attenuated the ability of *T. gondii* to form plaques *in vitro*, suggesting TgFerlin 2 is essential for the lytic cycle of *T. gondii* (Coleman, Saha et al. 2018). It was subsequently shown that TgFerlin 2 knockdown strongly inhibited tachyzoite invasion without a defect in egress or host cell attachment (Coleman, Saha et al. 2018). While it was initially hypothesised that Ferlin 2 may be involved with microneme secretion, this was shown not to be the case (Coleman, Saha et al. 2018). Further analysis revealed that TgFerlin 2 leads to a significant defect in rhoptry secretion without altering rhoptry biogenesis, morphology or apical positioning (Coleman, Saha et al. 2018). Due to the canonical role of ferlins in binding Ca^{2+} (Martens 2010, Lek, Evesson et al. 2012), the authors suggested Ferlin 2 may act a calcium sensor that regulates rhoptry secretion in response to increases in intracellular calcium (Coleman, Saha et al. 2018). Typically, membrane fusion events similar to the rhoptry-PPM fusion event involve SNARE proteins (Martens 2010). Despite this, no rhoptry resident SNARE has been characterised amongst Apicomplexa. Therefore, it is thought that Ferlin 2 may be directly involved with the fusion of the rhoptry and PPM and that this function is essential for rhoptry secretion (Coleman, Saha et al. 2018). Ferlin 2 has a homologue in *P. falciparum*, which is thought to be essential for blood stage growth, however it has not been well characterised (Zhang, Wang et al. 2018).

Cytosolically exposed rhoptry leaflet interacting proteins

Prior to the work described in this thesis, relatively little was known about the two *P. falciparum* proteins Pf3D7_0210600 and Pf3D7_0405200, hereafter referred to as *Plasmodium falciparum* cytosolically exposed rhoptry leaflet interacting protein (PfCERLI) 1 and 2 respectively. Moreover, PfCERLI1 and 2 had not been linked as potential orthologue prior to work undertaken in my BSc Honours year (Liffner 2016). I observed that PfCERLI1 is the most similar protein to PfCERLI2 in the *P. falciparum* Isolate 3D7 proteome, although their sequence identity is only 15% at the amino acid level (Leahy 2015, Liffner 2016). Additionally, I identified that PfCERLI1 and PfCERLI2 have overall similar protein secondary structures and share a motif of unknown function towards their N-terminus, with the consensus sequence PHISE/DxxP, we have termed PHIS (Liffner 2016) Protein structure modelling suggested that both PfCERLI1 and PfCERLI2 possessed an approximately 100 amino acid stretch of antiparallel ß-sheets towards their N-terminii (Liffner 2016). No further analyses were made regarding the similarities between PfCERLI1 and 2, and no functional or evolutionary significance of these similarities was concluded.

Cytosolically exposed rhoptry leaflet interacting protein 1

PfCERLI1 is a 446 amino acid containing protein, which prior to our studies was thought to contain a putative signal peptide at its N-terminus but no other domains (Aurrecoechea, Brestelli J Fau - Brunk et al. 2008). Early studies identified PfCERLI1 based on its stage of expression in schizonts, along with its putative signal peptide, as potentially involved in merozoite invasion (Hu, Cabrera et al. 2009, Zenonos, Rayner et al. 2014). It was shown that recombinant PfCERLI1 reacts, albeit poorly, with sera from adults from malaria-endemic areas, suggesting PfCERLI1 may be a target of the antimalarial immune response (Zenonos, Rayner et al. 2014). A previous study had

also shown using GFP-tagging and live cell microscopy that PfCERLI1 displays an apical localisation in merozoites (Hu, Cabrera et al. 2009). Prior to the work presented in this thesis, along with previous work conducted in our laboratory, however, no functional characterisation of PfCERLI1 had been performed.

In preliminary BSc Honours studies conducted by myself and a previous student, expression of *Pfcerli1* was placed under the control of the glucosamine-inducible ribozyme knockdown system *GlmS* (Prommana, Uthaipibull et al. 2013) whereby addition of glucosamine (GLCN) results in specific degradation of the mRNA of a gene of interest and protein knockdown (Leahy 2015, Liffner 2016). Preliminary results from these undergraduate studies suggested that PfCERLI1 was important for blood stage malaria parasite growth and may have a role in merozoite invasion (Liffner 2016). Preliminary studies suggested PfCERLI1 was exposed to the merozoite cytosol and low resolution immunofluorescence analysis supported an apical localisation that had previously been suggested using a PfCERLI1-GFP fusion protein (Hu, Cabrera et al. 2009, Leahy 2015, Liffner 2016).

Cytosolically exposed rhoptry leaflet interacting protein 2

PfCERLI2 is an approximately 580 amino acid protein that has a C-terminal decapeptide tandem repeat, whose copy number is between 9 and 18 in sequenced *P. falciparum* isolates (Aurrecoechea, Brestelli J Fau - Brunk et al. 2008). PfCERLI2 was not previously identified as having any functional domains and was predicted to lack a signal peptide (Aurrecoechea, Brestelli J Fau - Brunk et al. 2008). PfCERLI2 was first identified as a target of a monoclonal antibody named M26-32 and was therefore initially named *P. falciparum* M26-32 antibody recognised antigen (PfMag-1) (Gao, Li et al. 2009). It was reported that M26-32 inhibited merozoite invasion *in vitro* and immunofluorescence assays using M26-32 showed a merozoite surface localisation for

this antibody (Gao, Li et al. 2009). The antibody M26-32 was shown to be reactive against the C-terminal decapeptide repeat of PfCERLI2 and while the functions of these kinds of repeats are unknown, they are common in *P. falciparum* (Gao, Li et al. 2009, Davies, Nofal et al. 2017). Previous studies had identified that M26-32 recognises multiple proteins in *P. falciparum*, (Cheng, Jones et al. 1991) and not just PfCERLI2 specifically. Therefore, it is possible that both the merozoite surface localisation and *in vitro* growth inhibition could be due to the targeting of proteins other than PfCERLI2.

Preliminary studies in our laboratory using a GLCN-inducible knockdown system suggested that PfCERLI2 is important for both blood stage growth and invasion (Leahy 2015, Liffner 2016). PfCERLI2 is relatively lowly expressed (Aurrecoechea, Brestelli J Fau - Brunk et al. 2008, Lopez-Barragan, Lemieux J Fau - Quinones et al. 2011) and this low expression creates difficulties for analysis of PfCERLI2 using traditional protein detection methods (Leahy 2015, Liffner 2016). As such, the localisation of PfCERLI2 and the phenotype upon knockdown was not characterised in detail.

Chapter 2: Aims & Hypotheses

While rhoptries are essential for host cell invasion by apicomplexan parasites, previous studies have focused primarily on secreted rhoptry antigens with little known about the proteins that control important aspects of rhoptry biology. This disparity between the number of characterised secreted rhoptry antigens, and rhoptry proteins with other functions has largely been driven by the potential of secreted antigens as vaccine candidates. Despite this, understanding of how rhoptries fuse together, what coordinates rhoptry-PPM fusion, and what controls and generates the force required for rhoptry secretion are vital fundamental questions of invasion biology that are currently unanswered. Moreover, identification and characterisation of rhoptry proteins may provide targets for the future development of antimalarials with novel mechanisms of action. In order to address these current gaps in the literature of invasion and rhoptry biology, this thesis will functionally characterise PfCERLI1 and PfCERLI2 and test the hypothesis that:

PfCERLI1 and PfCERLI2 are evolutionarily related proteins that have key roles in rhoptry biology and merozoite invasion

The primary goal of the studies presented in this thesis are to enhance our understanding of the currently poorly characterised proteins PfCERLI1 and PfCERLI2 in the blood stage of *P. falciparum* and therefore the specific aims to address the aforementioned hypotheses are:

1. Conduct a thorough bioinformatic analysis and construct phylogenies of PfCERLI1, PfCERLI2, and their homologues in other closely related organisms.
2. Determine the localisation of PfCERLI1 using immunofluorescence microscopy, and characterise the function of PfCERLI1 by assessing the phenotype of PfCERLI1 knockdown parasites.

3. Determine the localisation of PfCERLI2 using immunofluorescence microscopy, and characterise the function of PfCERLI2 by assessing the phenotype of PfCERLI2 knockdown parasites.

Chapter 3: Materials & Methods

A detailed description of all materials and methods relevant to this thesis is presented here. Additionally, each of the results chapters (4 & 5), are presented as manuscripts that have their own, more concise, materials and methods descriptions.

Plasmid construction and generation of genetically modified parasites

Plasmid construction

Pfcerli1^{HAGlmS} and *Pfcerli2*^{HAGlmS} riboswitch transfection vectors were prepared from a PTEX150^{HAGlmS} plasmid backbone (Prommana, Uthaipibull et al. 2013, Elsworth, Matthews et al. 2014). A 767 base pair homology region of *Pfcerli1* was PCR amplified from the 3' end of the genomic sequence of 3D7 genomic DNA (gDNA) using the primers *Pfcerli1* 5' F RBW (GGT**AGATCT**CATATCAAATTTGGTTCTTGAAG) and *Pfcerli1* 3' R RBW (GGT**CTGCAGC**ATCACTATAGTTGTACATATTTTTGC). A 758 base pair homology region of *Pfcerli2* was PCR amplified from the 3' end of the genomic sequence of 3D7 gDNA using the primers *Pfcerli2* 5' F RBW (GGT**AGATCT**GAAGGAATCTTTTGGAGATGAGC) and *Pfcerli2* 3' R RBW (GGT**CTGCAGC**TATATTTTGTATGGTATTTTCTAATTGTGC). Each of the resulting PCR products were digested with the restriction enzymes Bgl II and Pst I (indicated in bold in primer sequence) and cloned into the PTEX150-^{HAGlmS} vector (Elsworth, Matthews et al. 2014).

To generate *Pfcerli1*$^{HAGlmS/GFP}$ and *Pfcerli2*$^{HAGlmS/GFP}$ parasite lines, which express cytosolic GFP, the pHGBrHrBl-1/2 GFP plasmid was used, without modification (Wilson, Crabb et al. 2010)

For disruption of *Pfcerli1* and *Pfcerli2* using the selection linked integration – targeted gene disruption (SLI-TGD) system, a source SLI-TGD vector (Pf3D7_1463000 SLI-TGD) was used (Birnbaum, Flemming et al. 2017). A homology region of *Pfcerli1* was PCR amplified using the primers *Pfcerli1* SLI-TGD F (GGT**GCGGCCGC**GATACTCACAACATATTATATCTTGG) and *Pfcerli1* SLI-TGD R (GGT**ACGCGT**CATACCTCTATGTGTACTTTGTTCTG). A 771bp homology region of *Pfcerli2* was PCR amplified using the primers *Pfcerli2* SLI-TGD F (GGT**GCGGCCGCT**CCACATATAAGTGATTTCGAGCC) and *Pfcerli2* SLI-TGD R (GGT**ACGCGT**CCTTGCACACTTCTTGTCC). Both PCR products, and the SLI-TGD vector were then digested with Not I and Mlu I (restriction sites in bold), and ligated together.

To generate the *Pfcerli1*^{NoSP} pArl1a plasmid, which contained a GFP-tagged copy of *Pfcerli1* without its putative signal peptide, under the control of the schizont-specific *ama1* promoter, *Pfcerli1*^{NoSP} was amplified from 3D7 cDNA using the primers *Pfcerli1* No SP F (GGT**GGTACC**ATGAGAAACCGTGAGTTATTTC) and the reverse primer *Pfcerli1* R (GGT**CCTAGG**ATCACTATAGTTGTACATATTTTTGC. The resulting PCR product was digested using the Kpn I and Avr II (restriction sites in bold), and ligated into thr pArl1a plasmid backbone (Crabb, Rug et al. 2004).

Transfection

P. falciparum 3D7 parasites were transfected using either red blood cell loading, or direct schizont electroporation (Wu, Sifri et al. 1995, Moraes Barros, Gibson et al. 2017). pHGBrHrBl-1/2 GFP, *Pfcerli1*^{HAGlmS}, and *Pfcerli2*^{HAGlmS} plasmids were transfected by red blood cell loading, while *Pfcerli1*^{NoSP}pArl1a, *Pfcerli1* SLI-TGD, and *Pfcerli2* SLI-TGD plasmids were transfected by direct schizont electroporation.

Red blood cell loading transfection

Uninfected red blood cells were centrifuged at 1500 rcf for 1 minute, before washing in incomplete cytomix (0.895% w/v KCl, 0.0017% w/v $CaCl_2$, 0.076% w/v ethylene glycol-bis(ß-aminoethyl ether)-N,N,N',N'-tetraacetic acid (EGTA), 0.102% $MgCl_2$, 0.0871% w/v K_2HPO_4, 0.708% w/v HEPES). Red blood cells were then resuspended in cytomix containing 200 µg of ethanol-precipitated plasmid DNA, incubated in a 0.2 cm cuvette (Bio-Rad) on ice for 30 minutes, and electroporated (Bio-Rad) at 0.31 kV with a capitance of 960 µF. Following electroporation, red blood cells were washed twice with culture media and transferred to a 10 mL dish, which contained schizonts purified by magnet activated cell sorting.

Direct schizont electroporation

Schizont stage parasites were purified from 30 mL of parasite culture at approximately 3% haematocrit and ~5% parasiteamia using percoll purification. Subsequently, 90 µL of P3 primary cell solution was added to 50 µg of ethanol-precipitated plasmid DNA that had been re-dissolved in 10 µL TE (10 mM Tris HCl, 1 mM EDTA, pH 8). 10 µL of purified schizonts was then added before transferring the transfection mixture to a 0.2 cm cuvette (Bio-Rad). Schizonts were then electroporated using a Nucleofector X (Lonza) using program FP158, before being mixed with uninfected red blood cells and shaking at 700 rpm at 37 °C for 45 minutes. Transfected schizonts were than transferred to a 5 mL culture dish with fresh media.

Parasite maintenance and drug selection following transfection

One day following transfection, parasite cultures began drug selection to select for plasmid uptake and construct integration where appropriate. *Pfcerli1*^{HAGlmS} and *Pfcerli2*^{HAGlmS} are single crossover recombination plasmids, which require three cycles of selection with 5 nM WR99210 (Jacobus Pharmaceuticals). The *Pfcerli1*^{NoSP}pArl1a transfection vector remains as an episome and so following transfection, cultures were treated with 5 nm WR99210 consistently until resistant

parasites were observed by Giemsa smear. Parasites that had previously been transfected with *Pfcerli1*^{HAGlmS} or *Pfcerli2*^{HAGlmS} that were subsequently transfected with the episomal cytosolic GFP expressing plasmid pHGBrHrBl-1/2, were selected for using 5 μg/mL blasticidin-S-deaminase HCl (Merck Millipore). *Pfcerli1* and *Pfcerli2* SLI-TGD parasites were first selected on 5 nM WR99210, for plasmid uptake. After WR99210 resistant parasites were seen by microscopy, selection of parasites that had successfully integrated of the plasmid into the genome was selected for using 400 μg/mL G418 sulphate (geneticin, Thermo Fisher).

Parasite gDNA extraction

To harvest parasite gDNA, schizont stage parasite cultures were saponin lysed. Parasite gDNA was then extracted from saponin lysed parasites using either the Wizard® Genomic DNA Purification Kit (Promega), or the PureLink® Genomic DNA Mini Kit (Invitrogen), according to the manufacturer's protocols. Concentration and purity of gDNA were determined by loading 1 μL of gDNA onto a Thermo Scientific NanoDrop 1000 spectrophotometer, with the output read on the "Nucleic Acid" setting.

Construct integration assessment

To confirm integration of the *Pfcerli1*^{HAGlmS} and *Pfcerli2*^{HAGlmS} constructs into the parasite genome, gDNA was harvested from transfected and WR99210 selected parasites, including cloned lines. The *Pfcerli1* locus was amplified with the forward primer *Pfcerli1* 5' F RBW (GGT**AGATCT**CATATCAAATTTGGTTCTTGAAG) and either the *Pfcerli1* 3' R RBW (GGT**CTGCAGC**ATCACTATAGTTGTACATATTTTTGC) reverse primer (amplifies wildtype gDNA sequence) or the *Glms R* (GAAATCCTTACGGCTGTGATCTG) reverse primer (amplifies DNA only upon *Pfcerli1*$^{HAG\mathit{lmS}}$ integration). The Pfcerli2 locus was amplified with the forward

primer *Pfcerli2* 5' F RBW (GGT**AGATCT**GAAGGAATCTTTTGGAGATGAGC) and either the *Pfcerli2* 3' R RBW (GGT**CTGCAGC**TATATTTTGTATGGTATTTTCTAATTGTGC) reverse primer (amplifies wildtype gDNA sequence) or the *GlmS* R reverse primer (amplifies DNA only upon *Pfcerli2*^{HAGlmS} integration).

In vitro culture of *P. falciparum*

P. falciparum parasite lines

All experiments in this thesis used either 3D7 *P. falciparum* lab-adapted parasites (Walliker, Quakyi et al. 1987) or genetically modified 3D7 derivatives. 3D7 was derived from the parental line NF54 by limiting dilution cloning (Walliker, Quakyi et al. 1987). NF54 is a parasite of probable West African origin that was derived from a patient in The Netherlands (Delemarre and van der Kaay 1979, Ponnudurai, Leeuwenberg et al. 1981). 3D7 is the most well studied *P. falciparum* strain, with the curated 3D7 genome being the *P. falciparum* reference genome (Aurrecoechea, Brestelli J Fau - Brunk et al. 2008). 3D7 has an approximately 44 hr lifecycle, expands ~5.5 fold per cycle, expresses functional knobs, and has some capacity to undergo gametocytogenesis.

Continuous culture of *P. falciparum*

Parasite culture was performed in a Class II biosafety cabinet, with parasites cultured inside 5 mL, 10 mL, or 30 mL dishes, or 175cm^2 0.2 µm filtered cell culture flasks (Corning). O^+ blood, (Australian Red Cross Blood Service), was used to culture parasites in media that contained 0.5 % v/v Albumax (Gibco), 52 µM gentamycin (Gibco), 367 µM hypoxanthine (Sigma-Aldrich), 2 mM Glutamax (L-glutamine), 2 mM sodium bicarbonate ($NaHCO_3$), and RPMI-HEPES (Gibco) at pH

7.2. Parasite dishes and flasks were stored in sealable gas boxes, which were filled with 1 % oxygen (O_2), 4 % carbon dioxide (CO_2) and 94 % nitrogen (N_2) and incubated at 37 °C (Trager and Jensen 1976).

Determination and maintenance of parasitaeamia

Parasite cultures were maintained at approximately 3% haematocrit $(\frac{volume\ of\ red\ blood\ cells}{volume\ of\ culture\ media}) \times 100$ in 5 mL, 10 mL and 30 mL dishes. Percentage parasitaemia $(\frac{number\ of\ parasitise\ red\ blood\ cells}{number\ of\ unparasitised\ red\ blood\ cells}) \times 100$ was estimated by smearing approximately 2 µL of parasite culture onto a glass microscopy slide (Paul Marienfeld GmbH & Co.), fixing in 100% v/v methanol and staining in 10% v/v Giemsa's azur eosin methylene blue solution (Merck). Giemsa staining allows for differentiation between parasitised and unparasitised red blood cells, and also allows differentiation of each of the intracellular morphological stages. Fixed and stained slides were then viewed using a light microscope at 1000x (10x eyepiece 100x objective) magnification under oil immersion. Typically >500 red blood cells were counted and the parasitaemia of the culture estimated. Parasite cultures were typically kept below 5% trophozoite-stage parasitaemia, to prevent exhaustion of the culture media. To control parasitaemia, cultures were routinely subcultured by removing a defined proportion parasitised red blood cells and replacing them with uninfected red blood cells.

Cryopreservation of parasite lines

Parasite cultures were cryopreserved for future use by centrifuging the culture at 550 rcf for 5 minutes, removing the supernatant and resuspending the pellet in 2 x pellet volume of glycerolyte 57 solution (45% v/v glycerol, 16 mg/mL sodium lactate, 0.3 mg/mL potassium chloride (KCl), 0.52 mg/mL monosodium phosphate, 1.24 mg/mL disodium phosphate). Cultures

were then transferred to cryotubes (Nunc, Thermo-Fisher Scientific) and stored at either -80 °C, for short-term storage, or in liquid nitrogen for long-term storage.

Thawing of cryopreserved cultures

Cryopreserved parasites were removed from -80 °C, or liquid nitrogen, storage and thawed to room temperature by hand, before being resuspended and transferred into a 10 mL tube. Parasites were resuspended in 2 x pellet volume of 3.5% w/v sodium chloride (NaCl) solution and centrifuged at 550 rcf for 5 minutes before supernatant removal. Subsequently, parasites were resuspended in a 1:1 mixture of the 3.5% w/v sodium chloride solution and 1 x phosphate buffered saline (PBS). Following resuspension, the culture was again centrifuged at 550 rcf for 5 minutes and the supernatant removed, with the pellet being resuspended in 10 mL of parasite culture media and placed in a new culture dish.

Sorbitol synchronisation

Treatment of *P. falciparum* trophozoites or schizonts with D-sorbitol causes lysis, but short-term treatment does not lyse ring-stages. Sorbitol was, therefore, used to remove trophozoites and schizonts from parasite cultures; leaving a synchronous ring-stage culture (Lambros and Vanderberg 1979). For sorbitol synchronisation parasite cultures were transferred from a culture dish into a tube and centrifuged at 550 rcf for 5 minutes. The resultant supernatant was removed and the pellet was resuspended in 37 ^{o}C 5% w/v D-sorbitol before incubation at 37 ^{o}C for 10 minutes. Following this incubation, parasites were again centrifuged at 550 rcf for 5 minutes before removal of supernatant and resuspension in culture media. Sorbitol synchronisation was the primary form of parasite lifecycle synchronisation used in this study.

Heparin synchronisation

Heparin has previously been shown to be a potent inhibitor of merozoite invasion (Wilson, Langer et al. 2013) and this ability of heparin to inhibit invasion was used to synchronise parasite cultures. Heparin sodium (Pfizer) was added to parasite cultures at 10 μL/mL, a concentration that is almost completely inhibitory to invasion (Boyle, Wilson et al. 2010, Wilson, Langer et al. 2013); preventing further merozoite invasion and therefore tightening the window of parasite lifecycle synchronisation. Heparin was subsequently washed off of parasites by replacing the culture medium, allowing the next cycle of rupture and invasion to occur.

Percoll® synchronisation

Percoll® is a solution of colloidal silica particles coated in polyvinylpyrrolidone (PVP), which is frequently used in density gradients to separate objects based on size by centrifugation (Pertoft, Wärmegård et al. 1978). Based on their differing densities, the different stages of the *P. falciparum* lifecycle, along with uninfected red blood cells, can be separated using Percoll® gradients (Rivadeneira, Wasserman et al. 1983, Childs, Miao et al. 2013). To enrich for mature schizont stage parasites for use in transfection, parasite culture supernatants were removed and the resulting pellet resuspended in ~3 mL of 37 ºC culture medium, before being gently loaded over a tube containing 5 mL of 37 ºC 70% v/v Percoll® (Sigma-Aldrich). Cultures were then centrifuged for 15 minutes at 1200 rcf with low brake to prevent disruption of the Percoll®/media interface. Following centrifugation, the culture supernatant and Percoll® separate into two distinct layers. Uninfected red blood cells, along with ring-stage parasites, concentrate at the bottom of the Percoll® layer, while late-trophozoite and schizont-stage parasites concentrate at the interface between the Percoll® and culture supernatant layers. The supernatant layer was removed, and the

schizont-containing interface was transferred to a new tube containing fresh culture medium. These schizonts were then prepared for transfection, as described previously.

Magnet activated cell sorting

P. falciparum utilises haemoglobin from the host red blood cell as its primary source of amino acids. As haeme byproducts are toxic to the parasite, it converts digested haemaoglobin into the inert crystal haemozoin, which is magnetic (Paul, Roath et al. 1981). Therefore, as the parasite progresses through its blood-stage lifecycle, it becomes increasingly magnetic. Using this premise, late-stage trophozoites and schizonts can be separated and purified from whole parasite culture using magnet activated cell sorting (MACS). High parasitaemia culture from a 175 cm^2 flask (Corning) was harvested and resuspended in ~30 mL of incomplete media (RPMI only). Using a pre-washed MACS column (Miltenyi Biotechnology), parasite culture was run slowly through the column. Due to the magnetism of the haemozoin crystal, late-trophozoite and schizont stage parasites are held in the column while uninfected red blood cells, and early stage parasites, were eluted. The column was then removed from the magnet and purified trophozoites and schizonts were eluted into a new culture dish. Successful purification was confirmed by microscopy analysis of giemsa stained smears.

Quantification of parasite growth and invasion with CERLI knockdown

Parasite growth assays

To assess the impact of PfCERLI1 or PfCERLI2 knockdown on parasite growth, PfCERLI1^{HAGlmS}, PfCERLI2^{HAGlmS}, or 3D7 WT parasites were synchronised to ring stages and assays were set up in 96-well U-bottom plates at 1% parasitaemia and 1% haematocrit in a volume

of 45 μL as described previously (Boyle, Wilson et al. 2010). 5 μL of 10x concentration D-(+)-Glucosamine hydrochloride (GLCN) (Sigma-Aldrich), or complete media, was added to make a final volume of 50 μL. Assay plates were then incubated under standard culture conditions for 72 hours, until trophozoite-stage the following cycle. Plates were then centrifuged at 330 rcf for 2 minutes to pellet parasite culture, with the supernatant removed and the pellets resuspended in 10 μg/mL ethidium bromide (Bio-Rad). Following ~10 minutes of staining with ethidium bromide, parasites were washed twice in 1x PBS and resuspended in a final volume of 200 μL (0.25% final haematocrit). After resuspension, the trophozoite-stage parasiteaemia of each of the cultures was determined using a BD Biosciences LSR II flow cytometer. Red blood cells were gated on using forward and side scatter, while trophozoite-stage parasites were gated on using forward scatter and the 488 nm laser with the PE filter (Figure 3.1). Culture parasitaemia was determined using FlowJo Version 10 (Tree Star), and % growth inhibtion was measured as the mean change in parasitaemia compared to the media control.

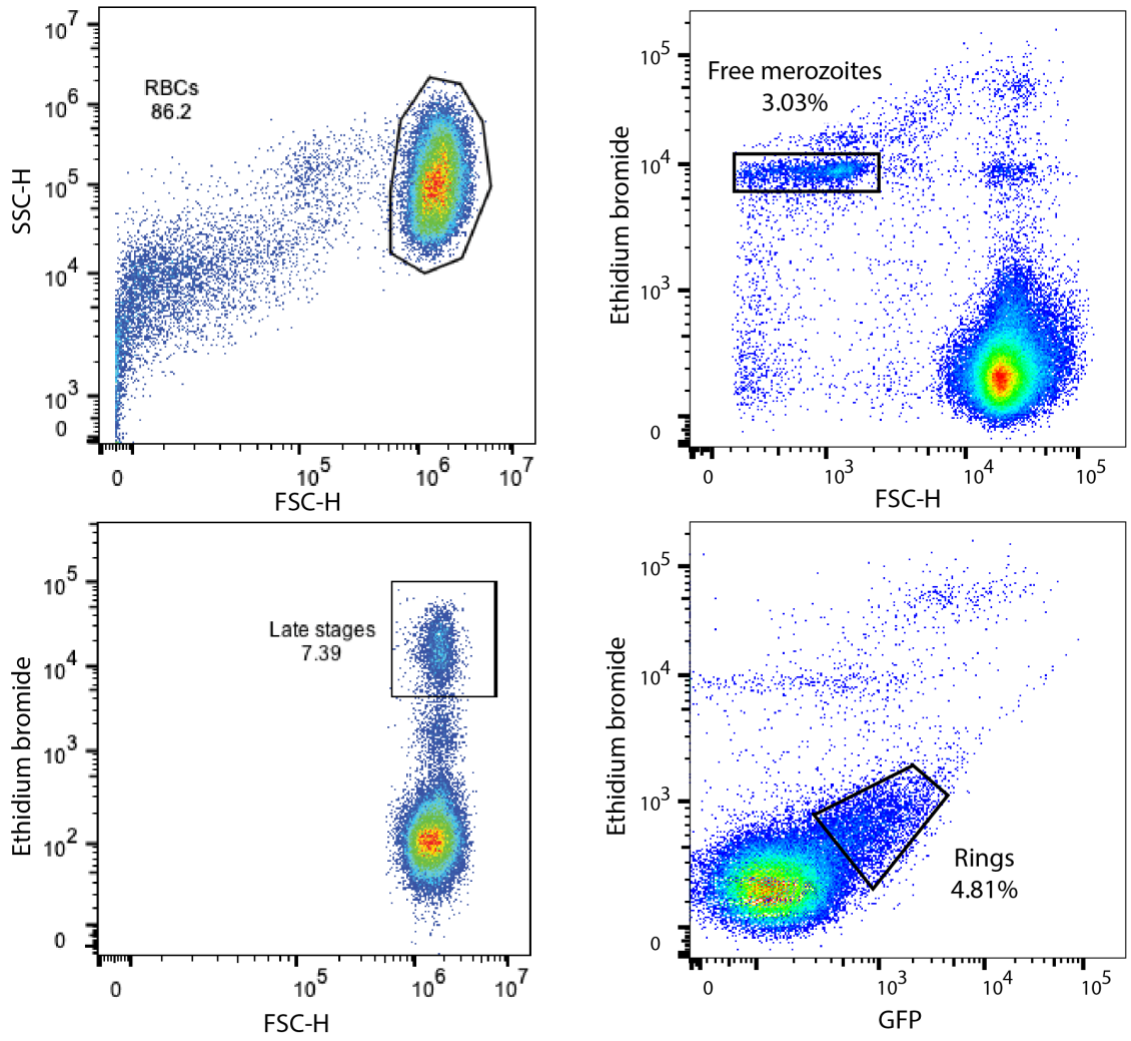

Figure 3.1: Representative flow cytometry gating plots for identification of different lifecycle stages.

Representative flow cytometry gating stratergies used to identify RBC, free merozoite, late stage, and ring stage populations. Free merozoite and ring stage gating stratergies have been replicated from the gating stratergy described in Figure 4.10.

Egress and invasion assay

To determine whether knockdown of PfCERLI1 or PfCERLI2 had an influence on parasite growth between merozoite egress and invasion, PfCERLI1$^{HAGlmS/GFP}$ and PfCERLI2$^{HAGlmS/GFP}$ were set up in 96-well U-bottom plates as described for growth assays but with minor modification. For

egress and invasion assays, cultures were set up at late trophozoite-stages, and incubated only for 24 hours, until early ring-stages the following cycle. 150 μL of 5 μg/mL ethidium bromide was then added to each of the cultures (0.25% final haematocrit), without washing, and left to stain for ~30 minutes before assessing parasitaemia by flow cytometry. Red blood cells and trophozoite-stage parasites were gated as described for growth assays, while ring stage parasites were gated as $FITC^{high}$ PE^{low}, and free merozoites gated as PE^{high} outside of the red blood cell gate (Figure 3.1). Invasion inhibtion (%) was measured as the mean change in ring-stage parasiteamia compared to the media control.

Schizont rupture assay

To determine whether knockdown of PfCERLI1 or PfCERLI2 altered the ability of schizonts to rupture, $PfCERLI1^{HAGlmS}$ and $PfCERLI2^{HAGlmS}$ parasites were synchronised to ring-stages and set up into duplicate 96-well U-bottom plates, either in the presence or absence of GLCN, as described for growth assays. After ~24 hours of incubation (pre-rupture), the late trophozoite and schizont-stage parasitaemia was determined for one of the two duplicate plates, as previously described. After a further 6 hours of incubation (post-rupture), the schizont-stage parasitaemia of the second of the duplicate plates was determined. To estimate the percentage of schizonts that ruptured over the 6 hour incubation window, the following equation was used:

$$\%\ schizont\ rupture = \left(\frac{post - rupture\ schizontaemia}{pre - rupture\ schizontaemia}\right) \times\ 100$$

Ring-stage retention assay

To determine if successfully invaded PfCERLI1 KD merozoites developed and survived the following cycle, synchronous $PfCERLI1^{HAGlmS/GFP}$ ring-stage parasites were set up in duplicate plates, and either treated with GLCN or left untreated, as described for growth assays. Following

48 hours of incubation, ring-stage parasitaemia was determined in the first of the duplicate plates plate using flow-cytometry. In the duplicate plate, GLCN was either washed out or left unwashed and heparin, which is a potent inhibitor of merozoite invasion (Boyle, Wilson et al. 2010, Wilson, Langer et al. 2013), was added to all wells to prevent further invasion events. 36 hours later, trophozoite-stage parasitaemia was determined by flow cytometry. To determine the percentage of rings that were retained from ring to trophozoite stages, the following calculation was used:

$$\left(\frac{Trophozoites\ (\%\ RBCs)}{Rings\ (\%\ RBCs)}\right) \times 100.$$

Bound merozoite assay

To assess the proportion of merozoites that fail to invade, and whether they established the tight junction, synchronous ring-stage parasites were incubated with GLCN until schizont rupture. Following schizont rupture, Giemsa-stained smears of these cultures were blinded by an independent person and then counted to determine the number of bound merozoites and newly invaded rings in each treatment.

Microscopy sample preparation, imaging and analysis

Schizont development assessment

To determine the number of merozoites produced by each fully formed schizont after knockdown of either PfCERLI1 or PfCERLI2 protein expression, ring-stage parasites were either treated with GLCN, or left untreated until schizont-stage the same cycle. Schizont-stage cultures were then matured for ~5 hours in the presence of 10 μM E64 (Sigma-Aldrich); a cysteine protease-inhibitor that prevents schizonts from rupturing the erythrocyte membrane (Collins, Hackett et al. 2017).Thin smears were made of E64 treated cultures, which were methanol fixed and stained with

Giemsa (Merck Millipore) before being blinded by an independent person in the laboratory. A blinded assessment of the number of merozoites per fully-formed schizont was performed by light microscopy on 20 schizonts per biological replicate. All schizonts where the merozoites wee counted were fully matured, with individual segmented merozoites visible.

Live-cell microscopy preparation of PfCERLI1^{NoSP}pArl1a for GFP localisation in live parasites

To determine the localisation of fluorescent fusion proteins, schizont stage parasites were centrifuged at 1500 rcf for 1 minute with the culture medium removed and the culture resuspended in 300 nM 4', 6-diamidino-2phenylindole, dihydrochloride (DAPI). Following 15 minutes of incubation at room temperature with DAPI, the culture was again centrifuged at 1500 rcf and washed in 1x PBS. PBS was removed from the culture until the culture was at a haematocrit of ~50%. ~4 μL of this culture was then dispensed along the length of a glass microscopy slide and a #1.5H high-precision coverslip was placed on top of it. Localisation of PfCERLI1^{NoSP}GFP was determined using a Zeiss AxioImager M1 with a 100x objective lens (1.4 NA) and a 10x eyepiece. Images were captured using a Hamamatsu Orca C4742-95 camera.

Immunofluorescence microscopy sample preparation

For immunofluorescence microscopy, schizont stage cultures were pelleted from culture media at 1500 rcf for 1 minute and then washed three times in 1 x PBS. Following washing, parasite cultures were resuspended in a fixative of 4% v/v paraformaldehyde (PFA) (Sigma-Aldrich) and 0.01 % v/v glutaraldehyde (Electron Microscopy Sciences), and subsequently fixed for 30 minutes at room temperature with gentle shaking. Following fixation, cultures were again centrifuged at 1500 rcf for 1 minute, with the fixative removed and the culture resuspended in 1x PBS for storage

at 4 ºC. Following fixation of parasite cultures, #1.5H high-precision coverslips (Carl Zeiss, Oberkochen, Germany) were treated with 0.01% v/v poly-L-lysine solution (Sigma-Aldrich) for 10 minutes at room temperature. ~200 μL of fixed parasite culture was settled on the poly-L-lysine coated coverslips for 1 hour at room temperature and subsequently permeabilised with 0.1 % v/v Triton-X-100 (Sigma-Aldrich) for 10 minutes. Coverslips were subsequently blocked using a solution of 3 % bovine serum albumin (BSA) (Sigma-Aldrich) in PBS either for 1 hour at room temperature with shaking, or overnight at 4 ºC without shaking. After blocking, coverslips were incubated with primary antibodies in antibody diluent (1 % w/v BSA in PBS, 0.05 % v/v Tween-20), either for 1 hour at room temperature with shaking, or overnight at 4 ºC without shaking. Following primary antibody incubation, cells were washed three times with PBS-Tween-20 (0.1 % v/v) and subsequently incubated with secondary antibodies in antibody diluent for 1 hour at room temperature with shaking in the dark. After secondary antibody incubation, coverslips were washed three times in PBS-Tween-20 and post-fixed with 4% w/v PFA for 5 minutes at room temperature. Following post-fixing, coverslips were ethanol dehydrated with three sequential treatments of 70, 90, and 100 % v/v ethanol each for 3 minutes. Coverslips were then air dried and mounted using ProLong® Gold (refractive index 1.4) antifade solution with DAPI (ThermoFisher Scientific). The mounting media was cured overnight, and coverslips were typically imaged the following day. This method of sample preparation was used for both conventional confocal and super-resolution microscopy analyses. Details of specific primary and secondary antibodies, along with their concentrations can be found in Table 3.1, or the Materials and Methods sections of Chapters 4 and 5.

Antibody name	Host species	Biological target	Concentration used	Reference/ manufacturer
Anti-HA (ab9111)	Chicken	HA-tag	1/500	abcam
Anti-RAP1 (7H8)	Mouse	RAP1 (rhoptry bulb)	1/500	(Schofield, Bushell et al. 1986)
Anti-GAP45 (R728K)	Rabbit	GAP45 (inner-membrane complex)	1/750	(Baum, Richard et al. 2006)
Anti-CyRPA (8A7)	Mouse	CyRPA (micronemes)	1/500	(Chen, Xu et al. 2017)
Anti-RON4	Rabbit	RON4 (rhoptry neck)	1/500	(Richard, MacRaild et al. 2010)
Anti-MSP1-19	Rabbit	MSP1-19 (merozoite surface)	1/500	(O'Donnell, Saul et al. 2000)
Anti-AMA1 (1F9)	Mouse	AMA1 (micronemes)	1/500	(Coley, Parisi et al. 2006)
Anti-HA-Biotin (3F10)	Rat	HA-tag	1/1000	Roche
Anti-chicken IgY Alexa Fluor 488	Goat	Chicken IgY	1/400	Invitrogen
Streptavidin Alexa Fluor 488 Conjugate	N/A	Biotin	1/400	Invitrogen
Anti-mouse IgG Alexa Fluor 555	Goat	Mouse IgG	1/400	Invitrogen
Anti-mouse IgG Alexa Fluor 594	Goat	Mouse IgG	1/400	Invitrogen
Anti-rabbit IgG Alexa Fluor 647	Goat	Rabbit IgG	1/400	Invitrogen

Table 3.1: Primary and secondary antibodies used for immunofluorescence microscopy.

Prior to all immunofluorescence microscopy analyses, antibody concentrations were optimised by preparing samples with a dilution series of each primary antibody. Additionally, a no antibody control was prepared to assess background for that particular channel. For anti-HA antibodies, additional control samples were prepared that were blocked using HA peptides. Once the optimum concentration of each primary antibody had been determined using these controls, this concentration was used across all experiments presented in this thesis.

Confocal microscopy

Following sample preparation, conventional confocal microscopy was performed using an Olympus FV3000 microscope equipped with a 100X MPLAPON oil objective (NA 1.4). Coverslips were typically stained with four fluorescent probes (DAPI and three secondary antibodies). Images were typically captured using the 405 nm, 488 nm, 561 nm, and 633 nm lasers. Three-dimensional images were made by taking Z-stack images with a step size of 0.43 μm using a sequential scan (scan zoom = 10, without line averaging).

Super-resolution microscopy

All super-resolution microscopy presented in these studies used Airyscan microscopy, which was performed using a Zeiss LSM800 AxioObserver Z1 microscope (Carl Zeiss, Obekochen, Germany) fitted with an Airyscan detector. Parasites were visualised using a Plan-Apochromat 63X (NA 1.4) M27 oil objective. Images were captured using the 405 nm, 408nm, 594nm, and 633nm lasers. Three-dimensonal images were made by taking Z-stack images with a step size of 0.16 μm. Prior to super-resolution analysis, this microscope was routinely calibrated to correct for chromatic and spherical aberrations using TetraSpeck^{TM} Fluorescent Microspheres (Life Technologies) mounted on #1.5H coverslips (Carl Zeiss, Oberkochen, Germany) with a density of

~2.3 x 10^{10} particles/mL. For super-resolution processing, images were captured using a pixel resolution of 0.04 μm in XY and once completed, images were processed using Airyscan processing in ZEN Black (Carl Zeiss, Obekochen, Germany).

Transmission electron microscopy

For transmission electron microscopy (TEM) analysis, synchronous parasite cultures were cultured until schizont stages and incubated with 4-[2-(4-fluorophenyl)-5-(1-methylpiperidine-4-yl)-1H-pyrrol-3-yl] pyridine (compound 1) (Taylor, McRobert et al. 2010), which is a potent inhibitor of PVM rupture, for 5 hours to ensure similar age of parasites. Following Compound 1 treatment, mature schizonts were purified using Percoll® as previously described. Purified schizonts were fixed in 2.5 % v/v glutaraldehyde (Electron Microscopy Sciences) in PBS overnight at 4°C. Cells were pre-embedded in agarose and fixed in 2% osmium tetroxide reduced in 1.5% potassium ferricyanide in 0.15 M sodium cacodylate buffer for 1 hr at room temperature. Subsequently, the cells were dehydrated in a graded series of ethanol- H_2O mixtures, followed by progressive infiltration with EPON resin and embedding; 70 nm sections were prepared using an ultramicrotome (Leica EM UC7, Leica Microsystems). The sections were poststained with 4% uranyl acetate in water and Reynold's lead citrate. Thin sections were observed on a transmission electron microscope at 200 kV (Tecnai G2 F30, FEI).

Immunogold transmission electron microscopy

For immunogold TEM, parasites cultures were prepared as described for standard TEM, but following Percoll® purification, they were fixed in 1% v/v glutaraldehyde (Electron Microscopy Sciences) in RPMI-HEPES. Following fixation, samples were ethanol dehydrated and embedded in LRGold resin. Ultrathin sections were cut, as described above, and these sections

were stained with mouse anti-HA 12CA5 (Roche) and subsequently 18 nm colloidal gold conjugated AffiniPure Goat Anti-Mouse IgG (Jackson ImmunoResearch). After antibody staining, sections were post-stained using uranyl acetate and lead citrate and visualised using a Talos L120C electron microscope.

General image processing and presentation

For images presented as representative images in this thesis, following their capture they were converted into .ims file format for analysis using Imaris (v9 BitPlane Inc, Switzerland). For consistency, DAPI was always false coloured blue, while the 488 nm channel was false coloured green, the 561 or 594 channel false coloured red, and the 633 channel false coloured magenta. For conventional confocal microscopy, a background subtraction and gaussian filtering were performed. Super-resolution images were presented as representative images without any modification.

Quantitative microscopy analysis

Chapter 4 involves extensive quantitative microscopy analysis including object identification, colocalisation, and diameter measurements. As these methods were the first of their kind applied to *P. falciparum*, highly detailed methods are provided in the methods and materials section and the supplementary methods section of Chapter 4.

Parasite protein lysate preparation and analysis

Saponin lysis

Typically 5-30 mL of parasite culture was pelleted at 440 rcf for 5 minutes with the supernatant removed and the culture washed in 1x PBS. Following washing, parasite cultures were resuspended in 2 x culture volume of 0.15 % w/v saponin (Sigma-Aldrich) in PBS, containing CØmplete protease inhibitors (Roche) and allowed to lyse on ice for 10 minutes. Cultures were subsequently transferred to 1.5 mL Eppendorf tubes and centrifuged at 5000 rcf for 10 minutes at 4 ^{o}C. Following centrifugation, the supernatant was removed and resuspended in 0.075 % w/v saponin in PBS and centrifuged at 8000 rcf for 10 minutes at 4 ^{o}C. After the second saponin treatment, lysates were washed three times in 1 x PBS each followed by centrifgation at 15000 rcf for 10 minutes with the final supernatant removed and the remaining parasite pellet snap frozen at -80^{o}C.

Western Blot

Typically, 3 µL of DNAse I was pipetted directly onto the saponin pellet to digest parasite gDNA. Subsequently, the volume of the prepared saponin pellet was estimated and the pellet resuspended in 5 x pellet volume of 2 x reducing sample buffer (RSB) (0.125 M Tris-HCl pH 7, 4% v/v SDS, 20% v/v glycerol, 10% v/v β-mercaptoethanol, 0.002% w/v bromophenol blue). Following resuspension in 2 x RSB, lysates were diluted with MilliQ H_2O to give a final concentration of 1 x RSB. Some samples were not treated with DNAse I and to denature gDNA they were instead heated to 90^{o}C for 3 minutes. Samples were then centrifuged at 15000 rcf for 10 minutes at 4 ^{o}C.

Prepared parasite lysates, typically 5-15 μL were loaded onto an SDS-polyacrylamide gel electrophoresis (PAGE) 4-12% Bis-Tris Bolt™ gel (Invitrogen). Gel electrophoresis was used to separate parasite proteins on the basis of their molecular weight and gels were typically run at between 100-130 V for 60-90 minutes, with variation governed by the proteins that were to be detected. SDS-PAGE gels were transferred onto nitrocellulose membranes (iBlot, Invitrogen) at 20 V for 7 minutes. Membranes were subsequently blocked using either Odyssey Blocking Buffer (TBS) (LI-COR Biosciences) or 3 % w/v skim milk powder in PBS. Typically, more abundant proteins were blocked in skim milk, while less abundant proteins were blocked in Odyssey Blocking Buffer. Membranes were either blocked for 1 hour at room temperature with shaking, or overnight at 4 ^{o}C without shaking. After blocking, the blocking buffer was removed and the membrane was incubated with primary antibodies diluted in either antibody diluent (0.5 % w/v skim milk powder in PBS) or in Odyssey Blocking Buffer. Primary antibody incubation occurred for either 1 hour at room temperature with shaking, or overnight at 4 ^{o}C without shaking. Following primary antibody incubation, membranes were washed three times for 5 minutes in 0.05 % v/v Tween-20 in PBS before incubation with secondary antibodies in either antibody diluent or Odyssey Blocking Buffer. Secondary incubation occurred at room temperature for 1 hour in the dark with shaking and was followed with three PBS-Tween-20 washes. Membranes were subsequently dried and visualised using an Odyssey Infrared imaging system (LI-COR Biosciences). Details of specific primary and secondary antibodies, along with their concentrations can be found Table 3.2, along with the Methods and Materials sections of Chapter 4 and 5.

Antibody name	Host species	Biological target	Conc. used	Reference/ Manufacturer
Anti-HA (12CA5)	Mouse	HA-tag	1/4000	Roche
Anti-RAP1 (7E8)	Mouse	RAP1 (rhoptry bulb)	1/5000	(Schofield, Bushell et al. 1986)
Anti-GAP45 (R728K)	Rabbit	GAP45 (inner-membrane complex)	1/10000	(Baum, Richard et al. 2006)
Anti-RON4	Rabbit	RON4 (rhoptry neck)	1/500	(Richard, MacRaild et al. 2010)
Anti-MSP1-19	Rabbit	MSP1-19 (merozoite surface)	1/500	(O'Donnell, Saul et al. 2000)
Anti-ERC	Rabbit	ERC (Endoplasmic reticulum)	1/10000	(Albano, Berman et al. 1999)
Anti-EBA175	Rabbit	EBA175 (micronemes)	1/5000	(Lopaticki, Maier et al. 2011)
Anti-RH4 (2E8)	Mouse	RH4 (rhoptry neck)	1/2500	(Tham, Wilson et al. 2010)
Anti-EXP2	Rabbit	EXP2 (dense granules)	1/5000	(Bullen, Charnaud et al. 2012)
Anti-EXP2	Mouse	EXP2 (dense granules)	1/5000	(Bullen, Charnaud et al. 2012)
Anti-aldolase (ab207494)	Rabbit	Aldolase (cytoplasm)	1/5000	Abcam
IRDye ® 800CW goat anti-mouse	Goat	Mouse IgG	1/4000	LiCor
IRDye ® 680RD goat anti-rabbit	Goat	Rabbit IgG	1/4000	LiCor

Table 3.2: Primary and secondary antibodies used for Western blot.

Western blot quantification

Western blot quantification was performed using Image Studio Lite 5.2.5 (LI-COR Biosciences). Membranes were scanned with the 700 nm and 800 nm scanners simultaneously, with scan intensity determined by protein abundance. Typically, abundant proteins such as loading controls were scanned at an intensity of between L2.0 and 2.0, while more lowly expressed proteins such as PfCERLI1 and PfCERLI2 were scanned at an intensity of 5. Using Image Studio Lite, the band intensity was measured for all bands present on the Western blot. All bands for each particular protein were kept identical in size to minimise artefacts based on measurement area size. The band intensity (a.u.) was measured first for all bands detected using antibodies against the loading control. The loading control band intensities of each lane were then normalised to the highest band intensity among loading controls on that membrane. The band intensity for each band that was not a loading control was then multiplied by the normalised band intensity of the loading control in that lane to give a normalised band intensity. These normalised band intensities were then used to determine changes in protein expression across different treatments.

For Western blots that assessed RAP1 processing, each of the bands present when stained with anti-RAP1 antibodies were quantified individually. The signal of each band in each lane was then combined to give the total RAP1 signal. The percentage of the total RAP1 signal that each band represented was then determined by dividing the signal of each band by the total RAP1 signal and multiplying by 100. Lane normalisation was not used for these analyses, as there is no comparison between different lanes.

Proteinase K protection assay

To differentiate between organellar luminal, or cytoplasmically exposed proteins, three aliquots of 5 mL high schizontaemia cultures were pelleted at 440 rcf for 5 minutes and saponin

lysates were prepared as previously described. Of the three aliquots, one was treated with saponin only, which lyses the RBC membrane and PVM, one was treated with saponin and digitonin, which lyses the RBC membrane, PVM, and PPM (Cabrera, Herrmann et al. 2012), and one was treated with saponin, digitonin, and proteinase K. The saponin only treatment was reuspended in SoTE buffer (0.6 M sorbitol, 20 mM Tris-HCl pH 7.5, 2mM etyhlenediaminetetraacetic acid (EDTA)) while the other two treatments were resuspended in 0.02% w/v digitonin in SoTE buffer. All samples were incubated for 10 minutes on ice before being centrifugation at 1000 rcf at 4^{o}C for 10 minutes. The proteinase K treatment was then treated with 0.1 µg/µL Proteinase K (Sigma-Aldrich) in SoTE, while the other two treatments were resuspended in SoTE buffer only for 30 minutes on ice. 50 µL of 100% v/v trichloroacetic acid (TCA) was then added to all samples to deactivate the Proteinase K, which were subsequently centrifuged at 15000 rcf for 10 minutes. All samples were then washed once in 500 µL of 100 % v/v acetone before again being centrifuged at 15000 rcf for 10 minutes and snap fozen at -80^{o}C.

Proteinase K digestion, along with saponin and digitonin lysis of host and parasite membranes is represented schematically in Figure 5.5a.

Protein solubility assay

Approximately 10 mL of high parasitaemia, schizont stage cultures were saponin lysed as previously described. Saponin lysates were subsequently resuspended in 100 µL of MilliQ H_2O, snap frozen at -80^{o}C four times, and passed through a 26-gauge needle 5 times before centrifugation at 15000 rcf for 10 minutes. Following centrifugation, the supernatant was reserved, and the pellet was washed twice in MilliQ H_2O before resuspension in 100 µL 0.1 M sodium carbonate (Na_2Ca_3) for 30 minutes on ice. The sample was again centrifuged at 15000 rcf and the supernatant was reserved, with the pellet resuspended in 100 µL 0.1% v/v Triton-X-100 for 30 minutes on ice.

Following centrifugation at 15000 rcf, the supernatant was reserved, and the remaining pellet washed and resuspended in 100 μL 1 x PBS. All samples were then diluted with 100 μL 2 x RSB and analysed by Western blot.

Hypotonic lysis solubilises cytoplasmic proteins, while carbonate treatment solubilises peripheral membrane proteins. Triton-X-100 solubilises integral membrane proteins, while the remaining Triton-X-100 insoluble pellet, predominantly contains covalently lipid linked proteins; such as those with a GPI-anchor. Schematic representations of the contents of each fraction can be found in Figure 4.4b and Figure 5.5b.

Rhoptry and microneme secretion assay

Synchronous ring-stage cultures were obtained using sorbitol synchronisation and were incubated in standard culture conditions for 24 hours until early trophozoite stage. Cultures were then enzyme treated with neuraminidase (0.067 U/mL) (Sigma-Aldrich), chymotrypsin (1 mg/mL) (Worthington Biochemical Corporation, Lakewood, NJ, USA) and trypsin (1 mg/mL) (Sigma-Aldrich) to prevent merozoites from invading. Parasites were then allowed to rupture over the following 24 hours. Following rupture, cultures were centrifuged at 13,000 rcf for 10 minutes in a benchtop centrifuge with 100 μL of culture supernatant reserved, stored on ice, and the rest removed. The remaining pellet was then also placed on ice and saponin lysed. The saponin pellet was prepared as previously described, while the culture supernatant was diluted with 100 μL of 2 x RSB. Both pellet and the culture supernatant were analysed by Western blot.

Bioinformatics and statistical analysis

Statistical analysis

All statistical analyses were performed using GraphPad PRISM 7 or 8 (GraphPad Software Inc.). In all figures where p-values were calculated, the corresponding statistical test is listed in the figure legend along with the number of experiments results are pooled from.

Signal peptide prediction

PlasmoDB predicts putative signal peptides in *P. falciparum* proteins using the program SignalP3.0 (Dyrløv Bendtsen, Nielsen et al. 2004, Aurrecoechea, Brestelli J Fau - Brunk et al. 2008). Where putative signal peptides were manually predicted, the presence of a signal peptide was predicted using the program SignalP-5.0 (Almagro Armenteros, Tsirigos et al. 2019).

In silico protein structure prediction

Full length protein sequences were submitted to one of either the online strucutre prediction tools Phyre2 (Kelley, Mezulis et al. 2015) on intensive mode, or I-TASSER (Zhang 2008, Roy, Kucukural et al. 2010, Yang, Yan et al. 2014) using its default settings. In instances where ligand binding sites were predicted for putative protein domains, the residues corresponding to that protein domain were submitted to the protein-ligand binding site prediction tool COACH (Yang, Roy et al. 2012, Roy, Yang et al. 2013). Predicted protein structures were visualised, presented and imaged using either Jmol, or EzMol (Jmol , Reynolds, Islam et al. 2018). Amino acid sequences for all proteins whose structures were predicted were obtained from either PlasmoDB or EuPathDB (Aurrecoechea, Brestelli J Fau - Brunk et al. 2008, Aurrecoechea, Barreto et al. 2017).

Multiple sequence alignment and phylogenetic tree construction

All gene and amino acid sequences, along with information about gene structure, presented in this thesis derive from either PlasmoDB or EuPathDB (Aurrecoechea, Brestelli J Fau - Brunk et al. 2008, Aurrecoechea, Barreto et al. 2017). All sequence alignments at both the protein and DNA level were constructed using Geneious version 9.1.3. All protein alignments, including both pairwise and multiple sequence alignments, were constructed using the BLOSUM62 matrix and the Geneious global alignment with free end gaps. These alignments were constructed using the default gap open penalty of 12, gap extension penalty of 3, with two refinement iterations. Phylogenetic trees constructed at both the protein and DNA levels used the Jukes-Cantor genetic distance model and were built using the unweighted pair group method with arithmetic mean (UPGMA) tree build method.

Chapter 4: PfCERLI1 is a conserved rhoptry associated protein essential for *Plasmodium falciparum* merozoite invasion of erythrocytes.

Preface

Functional characterisation of PfCERLI1 and PfCERLI2 in *P. falciparum* blood stages, along with elucidating their evolutionary relationship, were the principle aims of the research in this thesis. Chapter 4 specifically deals with the functional characterisation of PfCERLI1. Here PfCERLI1 is identified and named, showing that it is a rhoptry bulb protein whose knockdown is inhibitory to rhoptry secretion and merozoite invasion. Additionally, we establish the super-resolution microscopy and colocalisation analysis pipelines that are also used in Chapter 5. Work presented in this chapter represents the first thorough characterisation of PfCERLI1. This chapter does not include any functional characterisation of PfCERLI2 but does speculate on a putative relationship between PfCERLI1 and PfCERLI2, leading to the renaming of Pf3D7_0405200 as PfCERLI2. All results presented in this chapter were published in Nature Communications on March 16th, 2020 and so the body of this chapter is presented in journal format. Following the journal formatted article is the supplementary material, where the font and layout have been modified to fit the format of this thesis. All references presented in this chapter use a numbered referencing format, as per the specifications of the journal of publication. As such, all references from this journal formatted section of this chapter are listed as they appear in that manuscript. All references from the Supplementary Information section of this chapter follow the Author-Date referencing style from the rest of this thesis and can be found in the thesis References section. Further, figures in this journal formatted manuscript are numbered 1-6, where they are mentioned outside this chapter, they represent Figures 4.1 – 4.6 to maintain consistency with the nomenclature used in the other chapters of this thesis.

Statement of Authorship

Title of Paper	PfCERLI1 is a conserved rhoptry associated protein essential for *Plasmodium falciparum* merozoite invasion of erythrocytes.
Publication Status	☒ Published ☐ Accepted for Publication ☐ Submitted for Publication ☐ Unpublished and Unsubmitted work written in manuscript style
Publication Details	Liffner B, Frolich S, Heinemann GK, Liu B, Ralph SAR, Dixon MWA, Gilberger T, Wilson DW. PfCERLI1 is a conserved rhoptry associated protein essential for *Plasmodium falciparum* merozoite invasion of erythrocytes. *Nat Commun*, 11, 1411 (2020).

Principal Author

Name of Principal Author (Candidate)	Benjamin Liffner
Contribution to the Paper	Designed and planned the study, performed experiments and generated reagents, analysed data, wrote the manuscript.
Overall percentage (%)	40
Certification:	This paper reports on original research I conducted during the period of my Higher Degree by Research candidature and is not subject to any obligations or contractual agreements with a third party that would constrain its inclusion in this thesis. I am the primary author of this paper.
Signature	Date 03/07/20

Co-Author Contributions

By signing the Statement of Authorship, each author certifies that:

i. the candidate's stated contribution to the publication is accurate (as detailed above);
ii. permission is granted for the candidate to include the publication in the thesis; and
iii. the sum of all co-author contributions is equal to 100% less the candidate's stated contribution.

Name of Co-Author	Danny Wilson
Contribution to the Paper	Study design and planning, performed analysis and generated reagents, analysed data, manuscript writing. Contribution 15%
Signature	Date 3/7/20

Name of Co-Author	Gary Heinemann
Contribution to the Paper	Generated reagents. Contribution 2.5%
Signature	Date 15/07/2020

Name of Co-Author	Sonja Frolich
Contribution to the Paper	Designed and planned the study, performed experiments and generated reagents, analysed data, manuscript writing. Contribution 30%
Signature	Date 06/08/2020

Name of Co-Author	Boyin Liu		
Contribution to the Paper	Performed transmission electron microscopy experiments Contribution 2.5%		
Signature		Date	14/07/20

Name of Co-Author	Stuart Ralph		
Contribution to the Paper	Performed Immuno electron microscopy experiments Contribution 2.5%		
Signature		Date	14/07/20

Name of Co-Author	Matthew Dixon		
Contribution to the Paper	Study design and planning Contribution 2.5%		
Signature		Date	13/07/20

Name of Co-Author	Tim Gilberger		
Contribution to the Paper	Study design and planning, manuscript writing. Contribution 5%		
Signature		Date	7.07.20

nature COMMUNICATIONS

ARTICLE

https://doi.org/10.1038/s41467-020-15127-w OPEN

PfCERLI1 is a conserved rhoptry associated protein essential for *Plasmodium falciparum* merozoite invasion of erythrocytes

Benjamin Liffner[1,8], Sonja Frölich[1,8], Gary K. Heinemann[2], Boyin Liu[3], Stuart A. Ralph[3], Matthew W.A. Dixon[3], Tim-Wolf Gilberger[4,5,6] & Danny W. Wilson[1,7✉]

The disease-causing blood-stage of the *Plasmodium falciparum* lifecycle begins with invasion of human erythrocytes by merozoites. Many vaccine candidates with key roles in binding to the erythrocyte surface and entry are secreted from the large bulb-like rhoptry organelles at the apical tip of the merozoite. Here we identify an essential role for the conserved protein *P. falciparum* Cytosolically Exposed Rhoptry Leaflet Interacting protein 1 (PfCERLI1) in rhoptry function. We show that PfCERLI1 localises to the cytosolic face of the rhoptry bulb membrane and knockdown of PfCERLI1 inhibits merozoite invasion. While schizogony and merozoite organelle biogenesis appear normal, biochemical techniques and semi-quantitative super-resolution microscopy show that PfCERLI1 knockdown prevents secretion of key rhoptry antigens that coordinate merozoite invasion. PfCERLI1 is a rhoptry associated protein identified to have a direct role in function of this essential merozoite invasion organelle, which has broader implications for understanding apicomplexan invasion biology.

[1] Research Centre for Infectious Diseases, School of Biological Sciences, University of Adelaide, Adelaide, SA 5005, Australia. [2] Experimental Therapeutics Laboratory, School of Pharmacy and Medical Sciences, University of South Australia Cancer Research Institute, Adelaide, SA 5005, Australia. [3] Department of Biochemistry and Molecular Biology, Bio21 Molecular Science and Biotechnology Institute, The University of Melbourne, Melbourne, VIC 3010, Australia. [4] Bernhard Nocht Institute for Tropical Medicine, 20359 Hamburg, Germany. [5] Centre for Structural Systems Biology, 22607 Hamburg, Germany. [6] Biology Department, University of Hamburg, 20146 Hamburg, Germany. [7] Burnet Institute, 85 Commercial Road, Melbourne, VIC 3004, Australia. [8] These authors contributed equally: Benjamin Liffner, Sonja Frölich. ✉email: Danny.wilson@adelaide.edu.au

Malaria, caused by infection with *Plasmodium* spp. parasites, results in >400,000 deaths annually with *Plasmodium falciparum* being responsible for the majority of malaria mortality[1]. *Plasmodium* parasites have a complex lifecycle with human infection beginning with transmission of the liver-cell invading sporozoite from a female Anopheline mosquito to the human host. Thousands of daughter merozoites develop in the liver-stages and are released into the blood stream where they invade erythrocytes. In the case of *P. falciparum*, the blood-stage parasite multiplies over the next 48 h, forming 16–32 merozoites that rupture out of the schizont stage parasite and infect new erythrocytes[2]. This asexual blood-stage of the parasite lifecycle causes all disease symptoms.

Erythrocyte invasion is an essential and highly co-ordinated process that begins with reversible attachment of the merozoite to the erythrocyte surface[3]. The merozoite then reorientates such that the apical tip, containing specialised invasion organelles known as the rhoptries and micronemes, contacts the erythrocyte membrane. Invasion ligands are released from the micronemes and rhoptries prior to formation of an irreversible tight-junction that binds the merozoite to the erythrocyte surface. The merozoite then engages an acto-myosin motor complex, anchored in an inner membrane complex (IMC) that lies under the merozoite plasma membrane, to pull the erythrocyte membrane around itself; thus completing invasion[2,4].

The merozoite invasion organelles harbour essential antigens that are the targets of therapeutic interventions aimed at preventing blood-stage parasite replication[3–6]. The contents of micronemes are released first and are responsible for coordinating initial attachment events[7]. The rhoptries, which are the largest of the invasion organelles, adopt a dual club-shape with bulbs further towards the basal side of the merozoite and necks at the apical tip[8]. During invasion, rhoptry neck contents are released first and initiate early interactions with erythrocyte receptors[7,9]. Rhoptry bulb contents are secreted later in the invasion process and are typically involved in parasitophorous vacuole establishment[10].

It is unclear what differentiates the rhoptry bulb from the neck, as no membrane separates them. Because the neck and bulb remain differentiated after plasma membrane fusion, it has been hypothesised that the structure of the rhoptry may be supported by a scaffold, but the components of such a scaffold are yet to be elucidated[11]. Secretion of rhoptry contents may be partially coordinated through changes in the organelle's structure during invasion. The membranes at the tip of the rhoptry neck fuse with the parasite membrane early in invasion and the two rhoptries themselves also fuse beginning at the neck[11]. At the point of erythrocyte entry, the rhoptries fully fuse into a single rhoptry (neck and bulb). The mechanisms leading to rhoptry fusion and secretion are not understood.

Approximately 30 proteins have been linked to the rhoptry[8]. Despite the rhoptries being membrane-bound organelles with dynamic functions during secretion of invasion ligands, there remains only a single protein reported to localise to the luminal face (Rhoptry associated membrane antigen[12]) and two to the cytosolic face (Armadillo repeats only[13], ARO Interacting Protein[14,15]) of the *P. falciparum* rhoptry membrane. Therefore, the drivers of rhoptry secretion and compartmentalisation are unknown. Here we describe a highly conserved *P. falciparum* protein, Pf3D7_0210600 (henceforth named *Plasmodium falciparum* Cytosolically Exposed Rhoptry Leaflet Interacting protein (PfCERLI1)), which lies on the cytosolic face of the rhoptry bulb and is essential for rhoptry secretion and merozoite invasion.

Results

PfCERLI1 is conserved and required for blood-stage growth. PfCERLI1 is a protein of 446 amino acids that is predicted to contain a signal peptide (SP) but no transmembrane domains or glycophosphatidylinositol (GPI) anchor (Fig. 1a). The RNA expression profile and predicted SP of PfCERLI1 has led to speculation that it has a role in merozoite invasion that could be targeted by vaccines[16–18]. PfCERLI1 is highly conserved among *Plasmodium* spp., with >90% identity between *P. falciparum*, *P. reichenowi* and *P. gaboni* orthologues, >75% amino acid identity across human infecting species (including the zoonotic *P. knowlesi*) and >70% when compared to distantly related species (Fig. 1b). To determine whether this conservation was due to a function essential for blood-stage survival, we attempted to disrupt the *Pfcerli1* gene using the selection linked integration-targeted gene disruption system (SLI-TGD) (Supplementary Fig. 1a)[19]. Our attempts to disrupt *Pfcerli1* were unsuccessful, suggesting PfCERLI1 is essential for *P. falciparum* blood-stage growth.

Loss of PfCERLI1 is inhibitory to blood-stage growth. In order to analyse protein expression levels and function of PfCERLI1 during blood-stage development, we made transgenic *P. falciparum* parasites with a C-terminal haemagglutinin tagged (HA) PfCERLI1 with control of protein expression achieved through a glucosamine (GLCN) inducible *GlmS* ribozyme knockdown system (PfCERLI1^{HAGlmS})[20] (Fig. 1c). The resulting PfCERLI1-^{HAGlmS} parasites were cloned and analysed by PCR to confirm plasmid integration (Fig. 1d); cloned parasites were used in all subsequent experiments. Using lysates prepared from synchronised blood-stage parasite cultures (harvested at rings, early trophozoites, late trophozoites and schizonts) probed with anti-HA antibodies, we determined that HA-tagged PfCERLI1 was most highly expressed in late schizont stages (Fig. 1e), concordant with previously published transcriptomic data[21].

To validate that the integrated *GlmS* ribozyme could control PfCERLI1 protein expression, we treated PfCERLI1^{HAGlmS} parasites with 2.5 mM GLCN and quantified changes in HA-tagged protein levels using Western blot. Treatment of synchronous parasites with 2.5 mM GLCN for ~44 h from early ring stage led to a >80% reduction in PfCERLI1 expression, whereas expression of the loading control EXP2 was unaffected (Fig. 1f; Supplementary Fig. 1b,c). In addition, immunofluorescence microscopy analysis revealed a significant reduction in HA labelling across nearly the whole PfCERLI1^{HAGlmS} parasite population, with a reduction of HA staining by ~97% (GLCN treated vs the mean of untreated parasites, Supplementary Fig. 8c). To determine whether loss of PfCERLI1 protein expression affected parasite growth, early ring stage PfCERLI1^{HAGlmS} parasites were treated with increasing concentrations (0.125 to 5 mM) of GLCN for 48 h and parasite growth assessed the following cycle. GLCN treatment led to dose-dependent growth inhibition, with 5 mM GLCN leading to an approximately 55% reduction in parasite growth (Fig. 1g). At 2.5 mM GLCN, which we found to have minimal non-specific growth inhibitory activity against 3D7 WT parasites even after 96 h of treatment (Supplementary Fig. 2a), PfCERLI1^{HAGlmS} blood-stage parasite growth was reduced by ~40% after 48 h treatment. PfCERLI1's high level of conservation and being refractory to disruption suggested an essential role in parasite growth with the stage of protein expression indicating it could be involved in erythrocyte invasion.

PfCERLI1 has an important role in merozoite invasion. In order to assess whether PfCERLI1 has a role in merozoite invasion, we co-transfected the PfCERLI1^{HAGlmS} parasites with a cytosolic green fluorescent protein (GFP) reporter plasmid (PfCERLI1$^{HAGlmS/GFP}$) that allowed accurate quantitation of new merozoite invasion events by flow cytometry[22,23]. Since

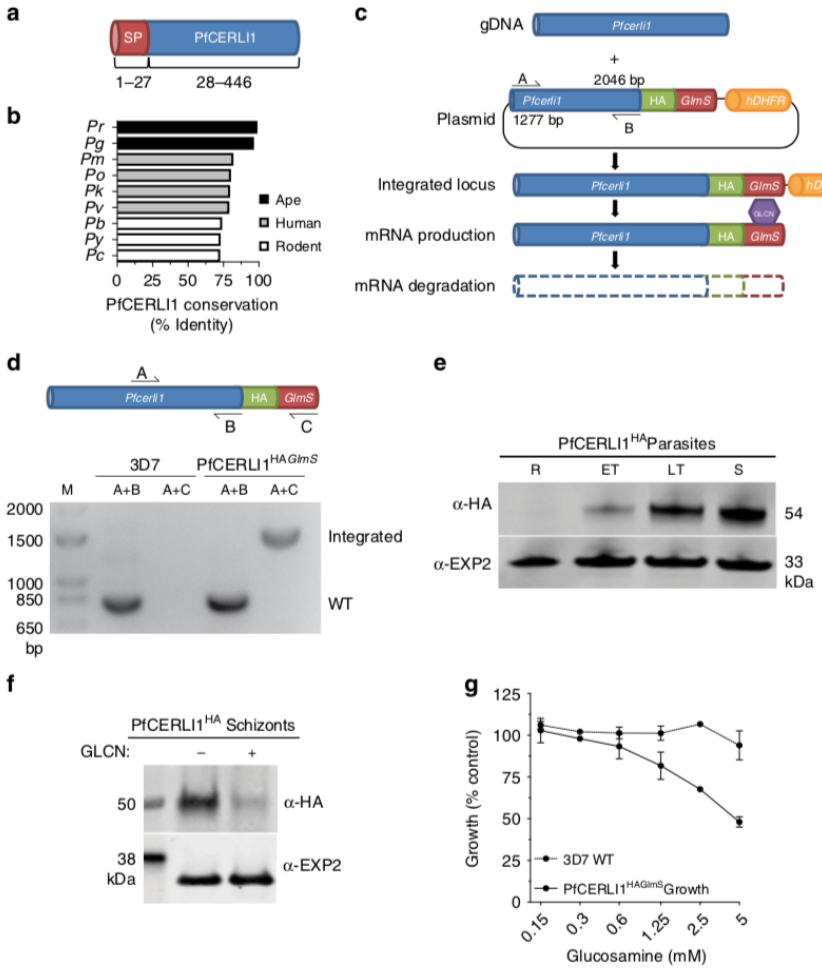

Fig. 1 Phylogeny of PfCERLI1 (Pf3D7_0210600) and development of genetic tools to investigate function. a PfCERLI1 is 446 amino acids in length and predicted to contain a signal peptide. **b** The amino acid sequence of PfCERLI1 was compared against *Plasmodium* spp. orthologues by multiple pairwise alignments. *Pr* = *P. reichenowi*, *Pg* = *P. gaboni*, *Pm* = *P. malariae*, *Po* = *P. ovale*, *Pk* = *P. knowlesi*, *Pv* = *P. vivax*, *Pb* = *P. berghei*, *Py* = *P. yoelii*, *Pc* = *P. chabaudi*. **c** Schematic representation of the HA-*GlmS* riboswitch system used to study PfCERLI1. A plasmid vector, containing a 3′ flank of the *Pfcerli1* sequence (1277bp-2046bp) with a haemagglutinin (HA) tag and under the control of a *GlmS* ribozyme was transfected into wildtype parasites by 3′ single crossover recombination. Glucosamine (GLCN) binds to the *GlmS* ribozyme, promoting *Pfcerli1* mRNA degradation. **d** Plasmid integration was confirmed by PCR using primers that amplify only WT *Pfcerli1* locus (primer A and B) or primers that amplify only integrated *Pfcerli1*^{HAGlmS} locus (primer A and C). These PCR reactions showed that the majority of parasites had integrated *Pfcerli1*^{HAGlmS} into the correct flanking region (M = size ladder). **e** Western blot of ring (R), early trophozoite (ET), late trophozoite (LT) or schizont (S) stage PfCERLI1^{HAGlmS} lysates probed with anti-HA (PfCERLI1) or anti-EXP2 (loading control) antibodies. **f** Western blot of schizont stage PfCERLI1^{HAGlmS} lysates either in the presence (+) or absence (−) of 2.5 mM GLCN, which was then probed with anti-HA (PfCERLI1) and anti-EXP2 (loading control) antibodies, showing effective knockdown of PfCERLI1 in the presence of GLCN. **g** Synchronous PfCERLI1^{HAGlmS} or 3D7 trophozoite-stage parasites were treated with increasing concentrations of GLCN for 48 h, with the number of trophozoites the following cycle measured to determine knockdown-mediated growth inhibition ($n = 3$ biological replicates. Parasite growth expressed as a % of non-inhibitory media controls, error bars = standard error of the mean (SEM). Source data are provided in source data file). X-axis presented as a log 2 scale for viewing purposes.

PfCERLI1 was expressed only at schizont stages, we limited the amount of time PfCERLI1$^{HAGlms/GFP}$ parasites were exposed to increasing concentrations of GLCN (0.125 to 5 mM) by only treating from early trophozoite stages (24 hpi) for 24 h before assessing parasite rupture and invasion. There was a dose-dependent inhibition of merozoite invasion (Fig. 2a), which was of similar magnitude to the growth inhibition recorded with longer term treatment, strongly suggesting that knockdown of PfCERLI1 restricts parasite growth by preventing invasion.

To determine whether PfCERLI1 knockdown was inhibiting invasion by interfering with merozoite production, the number of merozoites that fully developed per E64 treated PfCERLI1$^{HAGlmS/GFP}$ schizont was counted using light-microscopy of Giemsa-stained thin smears. There was no difference in the number of merozoites or stage of merozoite development evident between GLCN treated and untreated PfCERLI1$^{HAGlmS/GFP}$ parasites (Untreated 18.9 merozoites per schizont; treated 18.8 merozoites per schizont, $p = 0.5$; Fig. 2b). Furthermore, flow cytometry

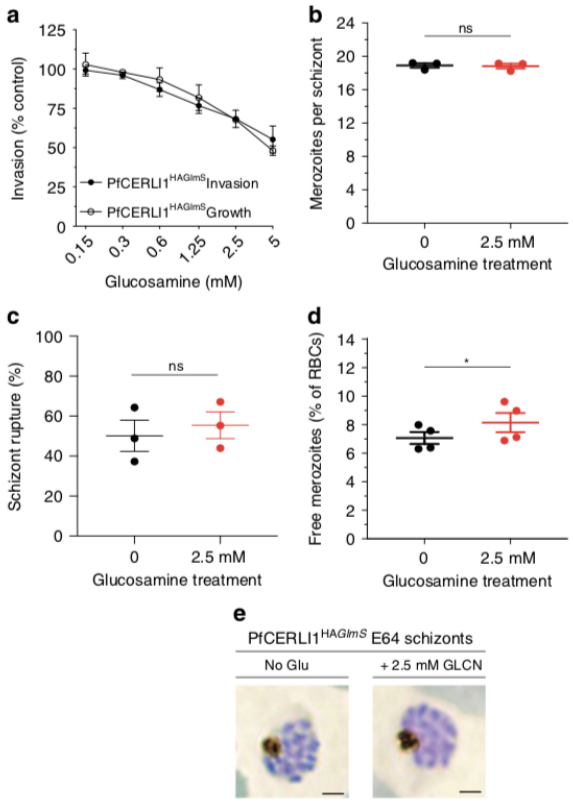

Fig. 2 PfCERLI1 knockdown does not inhibit merozoite development but does prevent merozoite invasion. a Flow cytometric detection of GFP-expressing PfCERLI1$^{HAGlmS/GFP}$ ring stage parasites after merozoite invasion indicated a direct inhibition of merozoite invasion with protein knockdown (results presented as a % of media control, $n = 4$ biological replicates). PfCERLI1^{HAGlmS} Growth is replicated from Fig. 1g for direct comparison between growth and invasion inhibition. *X*-axis presented as log 2 scale for viewing purposes (Source data are provided as a source data file). **b** Mean number of fully segmented merozoites per schizont was determined by microscopy analysis of Giemsa-stained thin blood smears. Smears were blinded and counted with each data point representing the mean number of merozoites per schizont pooled from 20 schizonts, $n = 3$ biological replicates. **c** The percentage of schizont rupture that occurred over a 6-h window either with, or without, GLCN treatment ($n = 3$ biological replicates), **d** The number of free merozoites after GLCN treatment was assessed using flow cytometry, with results presented as % of total erythrocytes ($n = 4$ biological replicates). **e** Giemsa-stained PfCERLI1^{HAGlmS} schizonts, either GLCN treated or untreated, matured normally in the presence of E64. Scale bar = 2 µm. All error bars = SEM. *$p < 0.05$, ns = $p > 0.05$ by unpaired *t*-test.

analysis also indicated that GLCN treatment did not alter schizont rupture ($p = 0.6$) (Fig. 2c).

When the number of free merozoites between GLCN and non-treated cultures was compared, there were significantly more free merozoites in the GLCN treated cultures ($p < 0.05$) (Fig. 2d). When the number of lost invasion events (lost ring stage parasitaemia) was subtracted from the number of free merozoites, there was no difference between GLCN treated and untreated parasites ($p > 0.99$, Supplementary Fig 2c), indicating that the increase of the free merozoite population was proportional to the loss in successful merozoite invasion events. In addition, GLCN treated schizonts appeared morphologically normal when Giemsa-stained (Fig. 2e), suggesting PfCERLI1 knockdown does not result in schizont developmental defects. These data indicate that knockdown of PfCERLI1 is associated with a build-up in the number of free merozoites in culture, a pattern consistent with a possible early invasion defect prior to formation of the tight-junction and engagement of the acto-myosin motor.

We also assessed whether knockdown of PfCERLI1 protein expression could lead to reduced or inhibited growth in merozoites that managed to invade a new erythrocyte. We found that there was no difference between the number of early ring stages progressing through to late trophozoite stages (36 h post-invasion) between GLCN treated and untreated cultures, indicating that PfCERLI1 knockdown merozoites that do invade do not have reduced viability (Supplementary Fig. 2b). The similarity between growth and invasion inhibition, the normal development of merozoites and the build-up of free merozoites in the culture media strongly supports a direct role for PfCERLI1 in erythrocyte invasion.

PfCERLI1 localises to the rhoptry bulb. Confocal microscopy of immuno-labelled schizonts was used to assess the spatial positioning of HA-tagged PfCERLI1 relative to the micronemal marker Cysteine-rich protective antigen (CyRPA), inner membrane complex marker glideosome-associated protein 45 (GAP45), rhoptry neck marker rhoptry neck protein 4 (RON4) and rhoptry bulb marker rhoptry-associated protein 1 (RAP1) (Fig. 3a). Using thresholded Pearson's correlation coefficient to calculate relative spatial proximity between compartments, semi-quantitative colocalisation analysis indicated that the signal of PfCERLI1 was associated most frequently with the rhoptry bulb marker RAP1 (Fig. 3b). Given the resolution limits of conventional confocal microscopy (~200 nm XY and ~500 nm Z)[24] relative to the size of the double-bulbous rhoptries[11,25], this approach was deemed unsuitable for the analysis of PfCERLI1 subcellular compartmentalisation within the rhoptries. To overcome this, we utilised Airyscan super-resolution microscopy, which revealed both PfCERLI1 and RAP1 displaying a double doughnut-shaped bulbous structure (Fig. 3c). This fluorescence pattern is analogous to the canonical structure of the rhoptry bulb and, combined with the close colocalisation between PfCERLI1 and RAP1 suggested that PfCERLI1 localises on or within the rhoptry bulb.

In order to assess whether PfCERLI1 is on the inside or the outside of the rhoptry bulb, we biochemically characterised the location of this protein in relation to the membrane of the rhoptries using a proteinase K protection assay. This assay determines the subcellular location of a protein as determined by its sensitivity to proteinase K after selective permeabilisation of non-organellar membranes with detergents. Since the rhoptry membrane is resistant to the detergent digitonin, proteins that lie inside the rhoptry are protected from proteinase K cleavage. Digitonin lysis of parasite membranes resulted in proteinase K cleavage of PfCERLI1^{HA} as detected by Western blot (Fig. 4a), indicating that PfCERLI1 lies outside the rhoptry and is exposed to the parasite cytosol. By contrast, RAP1, was not degraded significantly by proteinase K treatment, confirming that rhoptry luminal proteins are refractory to digestion. Despite the level of colocalisation between PfCERLI1 and RAP1, this difference in proteinase K sensitivity suggested that PfCERLI1 localised to the cytosolic face of the rhoptry bulb.

Having identified that PfCERLI1 lies on the cytosolic face of the rhoptry bulb membrane, we assessed how HA-tagged PfCERLI1 was bound to the rhoptry membrane through sequential, differential solubilisation of lysed parasite membranes.

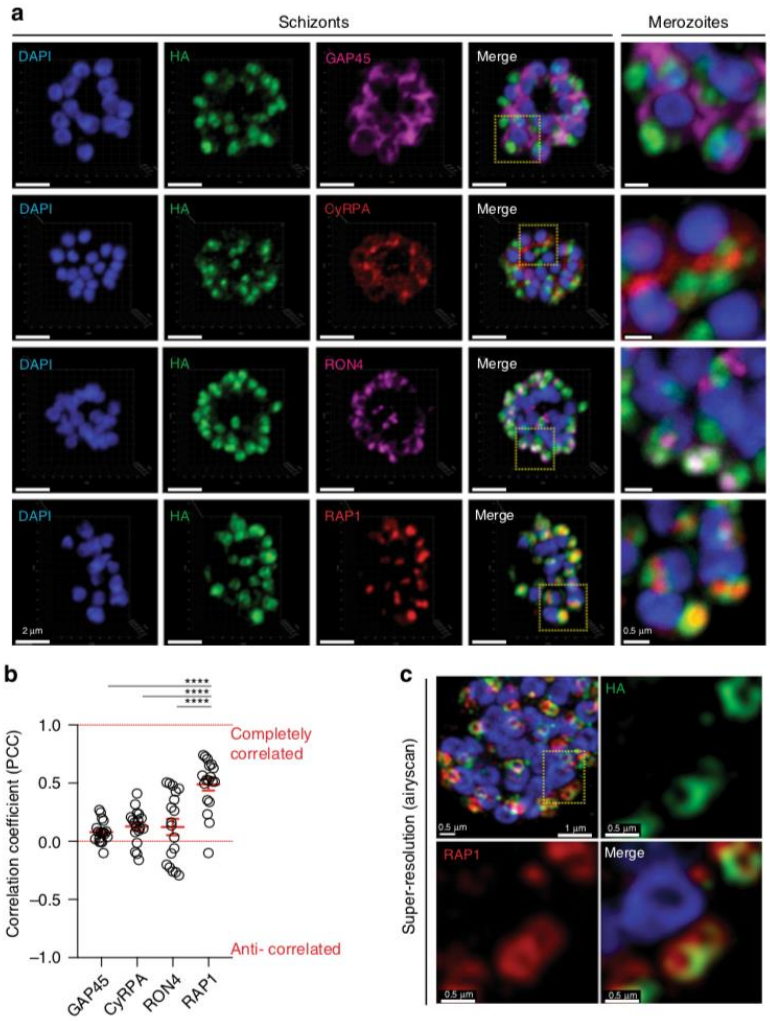

Fig. 3 PfCERLI1 localises to the rhoptry bulb of merozoites. a Immunofluorescence microscopy showing 3D reconstructed projections of confocal images with anti-HA (PfCERLI1) in green, colocalising more strongly with the rhoptry bulb marker RAP1 than with the micronemal marker CyRPA, rhoptry neck marker RON4 or the inner-membrane complex marker GAP45. **b** Quantification of the colocalisation, by Pearson's correlation coefficient when PfCERLI1 (anti-HA) staining is defined as the region of interest, with the following merozoite organelle markers: GAP45, CyRPA, RON4, and RAP1. (****$p < 0.0001$ by Analysis of variance (ANOVA), $n = 3$ biological replicates, with 6 merozoite containing schizont images taken from each, error bars = SEM). **c** Maximum intensity projections of super-resolution immunofluorescence microscopy (Airyscan) of PfCERLI1^{HAGlmS} schizonts stained with anti-HA and anti-RAP1 antibodies. Yellow box (top left panel) indicates the zoom area for the free merozoite depicted in the other three panels.

Saponin pellets from PfCERLI1^{HAGlmS} schizont-stage parasites were hypotonically lysed (to release non-membrane associated proteins), treated with sodium carbonate (Na_2CO_3; to release peripheral membrane proteins) and Triton X-100 (Tx100; to release integral membrane proteins). The supernatants containing solubilised proteins with the different treatments, as well as the final Tx100 insoluble fraction (containing covalently lipid-linked proteins[26,27]) were used in Western blots (Fig. 4b). PfCERLI1 was detected primarily in the carbonate treatment, indicating that PfCERLI1 is likely to be peripherally associated with the cytosolic face of the rhoptry bulb membrane.

PfCERLI1 is closely juxtaposed to the rhoptry bulb marker RAP1. Since biochemical analysis showed that PfCERLI1 associated with the cytosolic face of the rhoptry membrane whereas RAP1 appears confined to the rhoptry lumen, we used super-resolution microscopy to quantify the degree of physical proximity between PfCERLI1 and RAP1. To do this, we measured the radial positioning of all voxels that define the compartments of interest and plotted the signal intensities for both PfCERLI1 and RAP1 against the length of a vector drawn through the image (Fig. 4c). Using a line scan through a two-dimensional image of fluorescent objects, the distance between PfCERLI1 intensity peaks were significantly wider than that of RAP1 (Fig. 4d, e); further supporting the notion that RAP1 and PfCERLI1 are spatially segregated.

In order to assess whether PfCERLI1 is also associated with markers of the rhoptry neck that lie closer to the apical tip of the merozoite, we triple antibody-labelled schizonts that had been treated with compound 1 (C1), a Protein kinase G inhibitor that

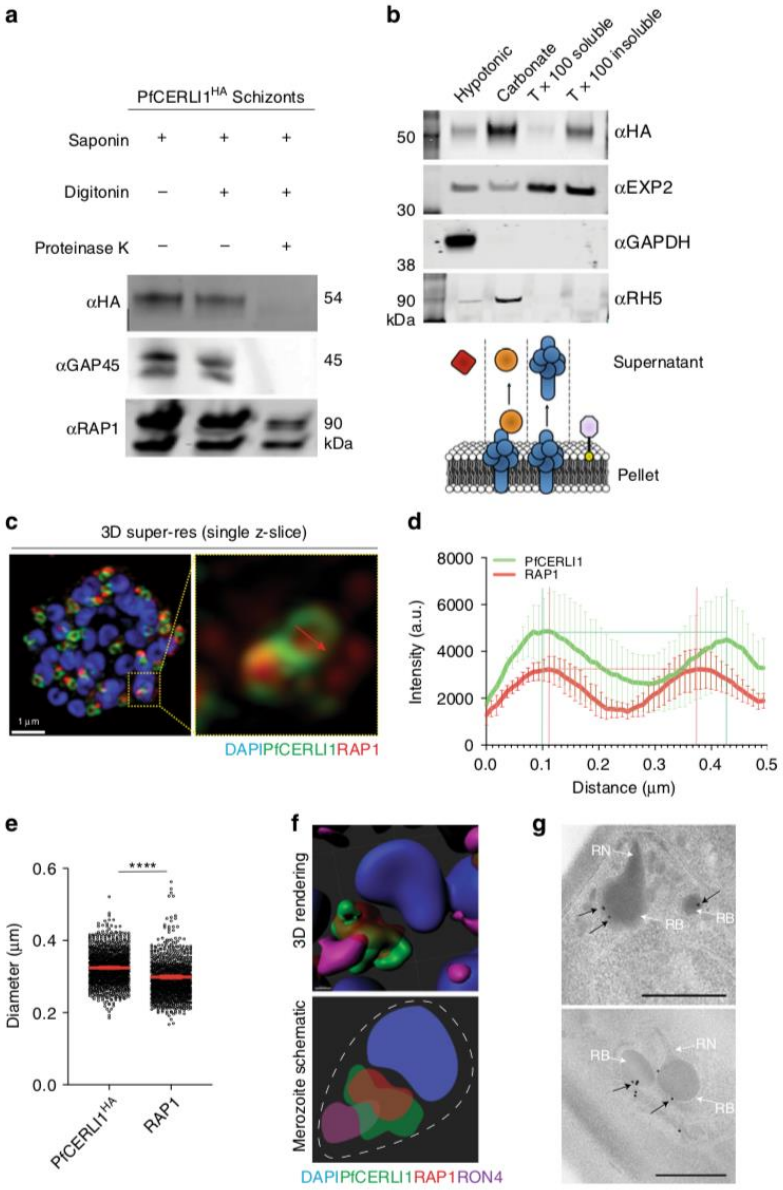

Fig. 4 PfCERLI1 is peripherally-associated with the cytosolic face of the rhoptry membrane. a PfCERLI1^{HA} schizont cultures were used for a proteinase K protection assay. Parasites were treated with either saponin alone, saponin and digitonin or saponin, digitonin and proteinase K and probed with anti-HA antibodies (PfCERLI1). GAP45 (inner-membrane complex, exposed to the cytosol) and RAP1 (rhoptry lumen) serving as positive and negative controls, respectively, for proteinase K digestion. Selected images representative of three independent experiments. **b** To determine membrane association, PfCERLI1^{HA} schizont cultures were subjected to a solubility assay. Saponin lysed parasite cultures were hypotonically lysed before being treated with sodium carbonate and then Triton-X-100 (Tx100), with supernatants and the Tx100 insoluble fraction being reserved after each treatment. Resulting samples were probed with anti-HA antibodies (PfCERLI1). The presence of a strong band in the carbonate treatment indicates release of the majority of PfCERLI1 protein into the supernatant with this treatment. Membranes were also stained with anti-EXP2 (transmembrane domain containing), anti-GAPDH (cytosolic) and anti-RH5 (peripheral) solubility controls. Selected images representative of three independent experiments. **c** A single z-slice of the double-bulbous rhoptries displaying the scheme that was used to measure the fluorescence intensity peaks (**d**) and diameter (**e**) of anti-HA and anti-RAP1 staining across the rhoptry (****$p < 0.0001$ by unpaired two-tailed t-test, $n = 5$ biological replicates, 1139 rhoptries measured for PfCERLI1^{HA} and 1040 for RAP1, Error bars = SEM). **f** 3D rendered image of a free merozoite showing the nucleus (DAPI) localising at the basal surface, PfCERLI1 (HA) wrapping around RAP1 at the rhoptry bulb and RON4 localising in the rhoptry neck at the far apical tip. **g** Representative image of Compound 1 treated PfCERLI1^{HAGlmS} schizonts that were fixed, labelled with anti-HA antibodies and probed with 18 nm colloidal gold secondary antibodies, before being imaged using transmission electron microscopy. White arrows mark rhoptry bulb (RB) and neck (RN), while black arrows mark PfCERLI1 foci. Scale bar = 500 nm.

prevents parasitophorous vacuole membrane rupture[28], with anti-HA (PfCERLI1), anti-RAP1 (rhoptry bulb), and anti-RON4 (rhoptry neck) antibodies prior to super-resolution microscopy. Enhanced spatial resolution of fully-formed merozoites revealed that RON4 is located closest to the apical tip of the merozoite (Fig. 4f), as expected. Neither PfCERLI1 nor RAP1 exhibited extensive overlap with RON4, with the RAP1 signal enclosed entirely within that of PfCERLI1. These data support that PfCERLI1 lies on the outside of the rhoptry membrane closely juxtaposed to the rhoptry bulb marker RAP1 in the rhoptry lumen, confirming that PfCERLI1 is most closely associated with the outer surface of the rhoptry bulb in mature merozoites. To confirm these findings, we performed transmission electron microscopy (TEM) of immunogold labelled PfCERLI1^{HAGlmS} C1 treated schizonts. Supporting immuno-fluorescence localisation experiments, PfCERLI1 foci localised towards the periphery of the rhoptry bulb (Fig. 4g)

PfCERLI1 contains lipid binding domains. To investigate how PfCERLI1 may be binding to the surface of the rhoptry bulb and provide insights on protein function, we used protein structural prediction software Phyre2[29], I-TASSER[30–32], and COACH[33,34]. These analyses suggested that PfCERLI1 contains a C2 domain, which are known lipid binding regions (amino acids ~50-170), a pleckstrin homology (PH) domain that typically binds calcium (amino acids ~250-360; Supplementary Fig. 3a) and an N-terminal alpha helix that is currently annotated as a SP. Outside of these domains PfCERLI1 was predicted to be partially disordered. Like most canonical C2 domains[35], the PfCERLI1 C2 domain was predicted to bind ionic calcium and phospholipids (Supplementary Fig. 3b). Of the models tested against, the PfCERLI1 C2 domain was most structurally similar to the C2 domain of human itchy homolog E3 ubiquitin protein ligase (ITCH) but the ligand(s) of this protein have not been elucidated[36]. The protein modelled to the C2 domain of PfCERLI1 with highest confidence was that of C2-domain ABA-related protein 1 (CAR1) from *Arabidopsis thaliana*, which has been shown to bind phospholipids in a calcium ion dependent manner[37,38]. The PH domain of PfCERLI1 was most structurally similar to the PH domain of Protein kinase B/Akt, and like Akt, was predicted to bind to inositol 1,3,4,5-tetrakisphosphate (IP4) (Supplementary Fig. 3c). IP4 forms the head-group of the phospholipid phosphatidylinositol (3,4,5)-trisphosphate (PIP_3), which commonly coordinates protein membrane localisation[39,40]. In addition, PfCERLI1 has previously been predicted to be palmitoylated[41]. Collectively, this suggests that PfCERLI1 contains potentially three different lipid-interacting moieties that may work cooperatively or independently to coordinate the binding of PfCERLI1 to the rhoptry bulb membrane.

PfCERLI1 residing on the cytosolic face of the rhoptry bulb membrane appeared to contrast with its predicted SP, as golgi-mediated trafficking of SP-containing proteins should place them on the luminal side of the golgi-derived rhoptries[25,42]. The putative SP displayed on PlasmoDB[43] is predicted using SignalP-3.0[44], however, the latest version of this program (SignalP-5.0[45]) no longer predicts that PfCERLI1 contains an SP (Supplementary Fig. 4a). To determine whether the putative SP is essential for rhoptry targeting by directing the protein into the secretory system, we generated a PfCERLI1 SP deletion construct (*Pfcerli1*^{NoSP}) that lacked the N-terminal 26 amino acids. *Pfcerli1*^{NoSP} was then cloned into the pArl1a vector, conjugating PfCERLI1^{NoSP} to GFP and placing *Pfcerli1*^{NoSP} under the merozoite-specific *ama1* promoter (Supplementary Fig. 4b). The overexpressed PfCERLI1^{NoSP}-GFP fusion protein, like its full-length counterpart[16], localised to the apical tip of merozoites (Supplementary Fig. 4c); suggesting that the putative SP plays no role in PfCERLI1 trafficking.

PfCERLI1 knockdown alters rhoptry architecture. Having identified PfCERLI1's confinement to the cytosolic face of the rhoptry bulb, we investigated whether PfCERLI1 may have a role in invasion ligand processing and distribution, or development of rhoptry architecture. Since a number of rhoptry antigens have been shown to be proteolytically cleaved inside the rhoptry lumen, we reasoned that if loss of PfCERLI1 function inhibited transport of rhoptry antigens to the lumen during biogenesis of the organelle, then we would be able to detect altered protein cleavage patterns in rhoptry antigens that undergo processing within this organelle. To assess this, GLCN treated and untreated PfCERLI1^{HAGlmS} schizont lysates were prepared for Western blot. PfCERLI1 knockdown did not result in any consistent changes in processing of the rhoptry bulb marker RAP1, the rhoptry neck antigen RON4, or a control protein that is a component of the inner membrane complex (GAP45) that all undergo proteolytic cleavage inside the parasite prior to invasion commencing (Supplementary Fig. 1b,c). In addition, total protein levels of both RAP1 and RON4 remained consistent following PfCERLI1 knockdown suggesting there is no relationship between PfCERLI1 and total expression levels of these rhoptry lumen antigens in the parasite.

In order to investigate whether PfCERLI1 caused changes in rhoptry architecture, we visualised rhoptries using TEM (Supplementary Fig. 5). Analysis of C1 matured schizonts failed to reveal any obvious ultrastructural differences between the rhoptries of either GLCN treated or untreated PfCERLI1^{HAGlmS} parasites. While the qualitative EM assessment indicated that PfCERLI1 knockdown was not causing clear changes in rhoptry architecture, we investigated whether there was altered rhoptry antigen distribution with PfCERLI1 knockdown using semi-quantitative super-resolution microscopy. GLCN treated and untreated PfCERLI1^{HAGlmS} (Supplementary Fig. 6a) schizonts were imaged in 3-dimensions to estimate shape (sphericity, oblate (flattened sphere), prolate (elongated sphere)), staining intensity, volume and area for the rhoptry bulb marker RAP1 (Supplementary Fig. 6b). A highly significant decrease in the intensity (50% reduction) and increase in the size of RAP1 staining with PfCERLI1 knockdown was observed. These changes were associated with a significant elongation of the RAP1 signal, but no corresponding change in the RAP1 diameter, indicating that the change in RAP1 staining intensity and size is largely due to elongation of the protein's distribution in the rhoptry (Fig. 5e). Collectively, these changes in intensity and size suggest that knockdown of PfCERLI1 alters the distribution of RAP1 within the rhoptries, and/or rhoptry shape more grossly.

To further investigate the spatial positioning of rhoptry antigens, we quantified spatial proximity between RAP1 and RON4 markers in super-resolved GLCN treated and untreated PfCERLI1^{HAGlmS} schizonts (Fig. 5a–e). We first assessed whether distribution of RON4 changes with PfCERLI1 knockdown as described for RAP1. There was a trend towards greater RON4 intensity (12% increase), probably as a result of a less elongated signal in the rhoptry neck (Supplementary Fig. 6c,d). We next investigated whether changes in RON4 and RAP1 staining altered their localisation relative to each other. Using Mander's correlation coefficient to calculate association frequency between markers, semi-quantitative colocalisation analysis indicated that the proportion of RAP1 signal that overlapped with RON4 after knockdown of PfCERLI1 was significantly reduced (Fig. 5a–d). These data indicate that PfCERLI1 knockdown causes changes in the distribution of antigens within the rhoptry, most notably for

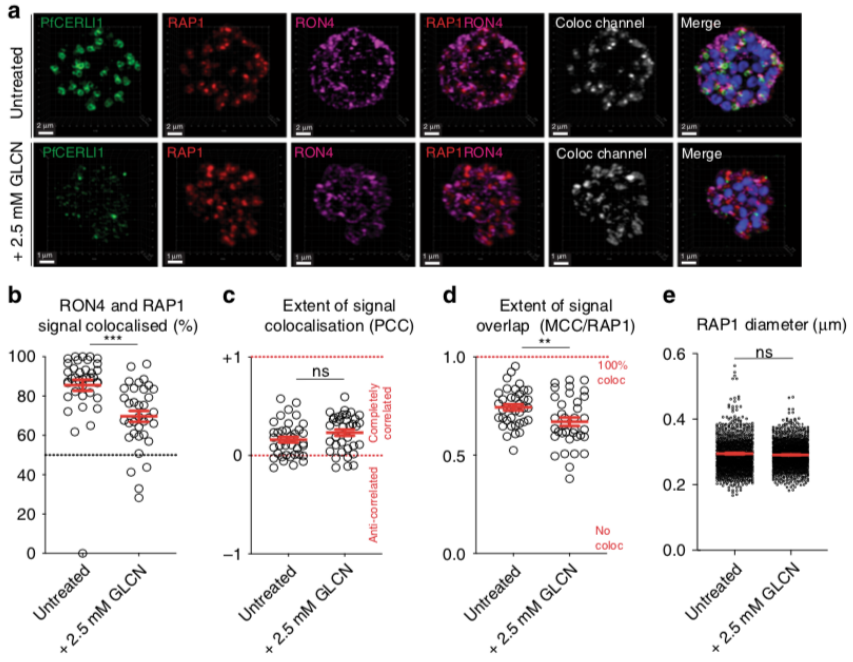

Fig. 5 PfCERLI1^{HAGlmS} knockdown alters rhoptry antigen distribution. a 3D reconstructions of super-resolution (Airyscan) micrographs for PfCERLI1^{HAGlmS} schizont cultures that were either left untreated or treated with glucosamine (+2.5 mM GLCN) before being stained with DAPI (nucleus), anti-HA (PfCERLI1), anti-RAP1 (rhoptry bulb) and anti-RON4 (rhoptry neck) antibodies. According to the image analysis pipeline detailed in Supplementary Fig. 7, the (**b**) % of RON4 that colocalised with RAP1, (**c**) Pearson's correlation coefficient (PCC) of the amount of RON4 colocalising with the RAP1 signal, and (**d**) thresholded Mander's correlation coefficient (MCC) of RON4 overlap with RAP1 signal was compared between PfCERLI1^{HAGlmS} knockdown and control parasites. Each data point represents a single schizont image ($n = 5$ biological replicates, 38 schizonts imaged for untreated and 36 for +2.5 mM GLCN schizonts). **e** Rhoptry bulb (RAP1) diameter was measured between untreated and PfCERLI1^{HAGlmS} knockdown (+2.5 mM GLCN) parasites. Each data point represents a single rhoptry ($n = 5$ biological replicates, 1220 rhoptries counted for untreated and 1217 for +2.5 mM GLCN). (ns = $p > 0.05$, $^{**}p < 0.01$, $^{***}p < 0.001$ by one-way unpaired t-test). All error bars = SEM.

RAP1, and increases the spatial segregation between rhoptry neck (RON4) and bulb (RAP1) markers.

Loss of PfCERLI1 disrupts merozoite rhoptry antigen function. After identifying that PfCERLI1 knockdown caused a significant change in the distribution of the rhoptry bulb protein RAP1, we investigated whether knockdown of PfCERLI1 changed apical organelle secretion. Ring-stage cultures were either treated with 2.5 mM GLCN or left untreated before enzymatic removal of erythrocyte surface receptors at trophozoite stages to prevent reinvasion. Schizonts were allowed to rupture, the supernatant collected, and lysates were made from saponin lysed parasite material before analysis by Western blot (Fig. 6a). Blots were probed with anti-RON4 and anti-RH4 antibodies to assess rhoptry secretion, anti-EBA175 to assess microneme secretion, anti-HA to assess PfCERLI1 knockdown and anti-ERC as a loading control. Knockdown of PfCERLI1 did not significantly alter the level of EBA175 (microneme) secretion relative to untreated controls, confirming that release of microneme contents had been triggered for both GLCN and untreated parasites (Fig. 6b). In contrast, quantitation of Western blots revealed a decrease in secreted RON4 and RH4 for PfCERLI1 knockdown parasites relative to untreated controls (Fig. 6b). In addition, RON4 was observed to be more concentrated in the GLCN treated PfCERLI1^{HAGlmS} parasite pellet relative to untreated control parasite material. These data suggest that PfCERLI1 knockdown prevents secretion of essential invasion antigens from the apical tip of the rhoptry after initiation of the invasion process, providing a probable mechanism by which PfCERLI1 knockdown inhibits invasion.

It has previously been demonstrated that RAP1 is processed by Plasmepsin IX and Subtilisin-like protease 1 (SUB1), beginning as an 84 kDa precursor and being processed to a 67 kDa product that is contained in free merozoites[46–48], with this processing likely required for function. The anti-RAP1 antibody used in this study[49] typically detects three bands, the full-length unprocessed RAP1, a 67 kDa processed RAP1 contained in merozoites, with the middle band suspected to be an intermediate cleavage product or a product of non-physiological procesing[47,48]. While we were unable to detect RAP1 in the supernatant in rhoptry secretion assays (Fig. 6a), we noticed that there was an increase in unprocessed RAP1 for PfCERLI1 knockdown treatments. We quantified the relative abundance of each of the three RAP1 bands present, relative to total RAP1 signal, for both untreated and PfCERLI1 knockdown free merozoites with PfCERLI1 knockdown causing a significant increase in the proportion of unprocessed RAP1 and a corresponding decrease in the proportion of processed RAP1 (Fig. 6c). No change in this trend was observed for 3D7 WT free merozoites in parallel assays treated with 2.5 mM GLCN, suggesting the loss in RAP1 processing is a direct result of PfCERLI1 knockdown (Supplementary Fig. 9a). In addition, RAP1 processing in C1 arrested schizonts was quantified for both PfCERLI1^{HAGlmS} and 3D7 parasites (Supplementary Fig. 9b,c). There was no change in RAP1 processing seen for C1 arrested schizonts with 2.5 mM

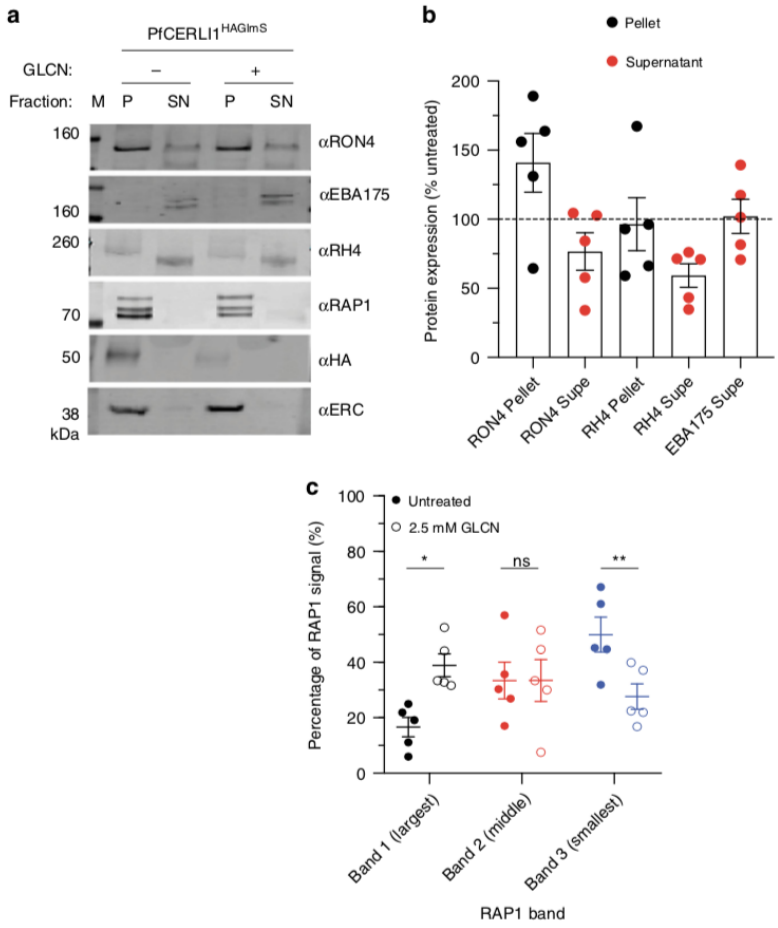

Fig. 6 PfCERLI1^{HAGlmS} knockdown alters rhoptry antigen processing and secretion. a PfCERLI1^{HAGlmS} parasites were either treated with 2.5 mM GLCN (+) or left untreated (−), with the erythrocyte surface receptors of the culture cleaved by enzyme treatment to prevent invasion but allow release of merozoite antigens. The parasite lysate (P) and culture supernatant (SN) were stained with anti-RON4 (rhoptry neck), anti-EBA175 (micronemes), anti-RH4 (rhoptry neck), anti-RAP1 (rhoptry bulb), anti-HA (PfCERLI1) and anti-ERC (loading control) antibodies and analysed by western blot. Selected blots representative of five independent experiments (M = size markers). **b** Western blots of rhoptry antigens, and secreted EBA175, were normalised to the loading control (ERC) and quantified, with data represented as +2.5 mM GLCN signal expressed as a % of the signal for the untreated control ($n = 5$ biological replicates, source data are provided as a source data file). **c** Using the parasite lysates from the rhoptry secretion experiment, each of the three individual RAP1 bands present on the western blots were quantified and presented as a percentage of the total RAP1 signal ($n = 5$ biological replicates, ns = $p > 0.05$, *$p < 0.05$, **$p < 0.01$ by two-way ANOVA). All error bars = SEM.

GLCN treatment for either PfCERLI1^{HAGlmS} or 3D7 WT parasites, suggesting the inhibition of processing occurs after release of merozoites from the schizont and possibly during the process of invasion. This observation is consistent with prior observations that this cleavage event occurs very late in schizont development or after merozoite egress[50].

Discussion

Previous studies have identified PfCERLI1 (Pf3D7_0210600) as being a potential vaccine target on the basis of its predicted SP and late schizont stage of expression, a transcription profile typical of proteins involved in merozoite invasion[17,18]. In addition, PfCERLI1 was identified as a member of the 'invadome', an interaction network of putative invasion-associated proteins, and was localised to the merozoite apical tip in this study[16]. Here we show that PfCERLI1 localises to the rhoptries and is confined to the cytosolic face on the rhoptry bulb membrane, a localisation that would prevent exposure to antibodies during the natural course of invasion. Semi-quantitative super-resolution fluorescence microscopy showed a difference between the mean diameter of PfCERLI1 and the rhoptry bulb marker RAP1 around the bulb structure, indicating they occupy distinct compartments on/within the rhoptry. PfCERLI1 was sensitive to proteinase K after selective membrane solubilisation and RAP1, which appears to lie along the luminal face of the rhoptry bulb and is protected from cleavage, was insensitive, confirming that PfCERLI1 compartmentalises to the cytosolic face of the rhoptry bulb membrane. PfCERLI1 has been shown to be palmitoylated[41], but was predominantly present in the carbonate fraction of the membrane solubility assay (Fig. 4b), suggesting that PfCERLI1 predominantly associates with the cytosolic face of the rhoptry membrane through protein-protein or protein-lipid electrostatic interactions in schizonts. PfCERLI1 was also detected in the Tx100 insoluble fraction. While the contents of this fraction are poorly understood in *Plasmodium*, they have been previously

identified as containing covalently lipid-linked (palmitoylated and myristoylated) members of the IMC[51–53]. C2 domains, as present in PfCERLI1, are predicted to bind calcium and known to form ionic bridges with lipid phosphates in membrane bilayers that are not easily disruptable[54], providing a second potential membrane binding site for PfCERLI1. The presence of two distinct moieties that are predicted to interact with membranes may explain why PfCERLI1 partially solubilises in carbonate buffer while the remainder stays in the Tx100 insoluble fraction.

Our attempts to knock-out *Pfcerli1* proved unsuccessful, confirming a previous random mutagenesis study that identified *Pfcerli1* as essential[55]. However, we successfully integrated a *GlmS*-ribozyme sequence at the 3' end of *Pfcerli1* and were able to knockdown protein expression by >80% leading to >45% inhibition of parasite growth. While we were unable to achieve complete growth inhibition, it is possible that loss of PfCERLI1 function is compensated for by other proteins with similar function or that enough PfCERLI1 remains to enable invasion of some parasites. Indeed, bioinformatic searches identified a second protein, Pf3D7_0405200 (now called PfCERLI2), with similar structure and shared predicted epitopes that has previously been implicated in merozoite invasion[56], providing a possible functional homologue that could compensate for loss of PfCERLI1.

Knockout and knockdown studies implicate PfCERLI1 as having an important role in asexual stage parasite growth and we further confirmed that loss of this protein led to a defect in invasion. Initial investigation of the PfCERLI1 knockdown parasites showed that the number and morphology of merozoites was unaffected by loss of PfCERLI1 and parasites that did invade with PfCERLI1 knockdown developed normally. We determined that PfCERLI1 knockdown led directly to a significant reduction in newly invaded ring-stage parasites and a proportional build up in free merozoites in the culture, possibly through stopping invasion at a point prior to the formation of the tight junction and engagement of the acto-myosin motor. Quantitative assessment of immunofluorescence signal revealed a significant decrease in RAP1 staining intensity with PfCERLI1 knockdown, corresponding to increases in RAP1 volume and area, indicating knockdown of PfCERLI1 changes RAP1 distribution. While changes in area and volume for RAP1 were observed, the diameter of RAP1 rhoptry bulb staining and TEM analysis indicated that there were no large morphological changes in the rhoptry bulb itself. Thus, changes in the ultrastructure of the rhoptry with PfCERLI1 knockdown appear to be minimal and the strongest indication of a modified rhoptry shape achieved to date is increase prolate staining for RAP1, which may indicate a lengthening of the rhoptries that was not noticeable in the single sections of TEM images.

To assess whether the segregation of rhoptry antigens was affected by loss of PfCERLI1, we compared the colocalisation of RAP1 (bulb) and RON4 (neck). Knockdown of PfCERLI1 led to a significant decrease in the proportion of RAP1 overlapping with RON4. Using apical organelle secretion assays, we identified that knockdown of PfCERLI1 resulted in a decrease in secretion of the rhoptry antigens RH4 and RON4 but no change in secretion of the micronemal antigen EBA175. As antigens secreted from the rhoptry neck are essential for merozoite invasion[9,57], disruption of rhoptry neck antigen secretion with PfCERLI1 knockdown points to a role for this protein in successful rhoptry antigen secretion during invasion. Furthermore, when PfCERLI1 was knocked down in free merozoites we saw a clear defect in the processing of the rhoptry bulb antigen RAP1. Given RAP1 processing occurs inside the rhoptry lumen, most likely after merozoite egress, and PfCERLI1 lies on the cytosolic face of the rhoptry bulb, we speculate that aberrant RAP1 processing is likely to be a consequence of general rhoptry dysfunction with PfCERLI1 knockdown.

A recent study by Suarez et al.,[18] reported functional analysis of a homologue of PfCERLI1, which they termed Rhoptry Apical Surface Protein 2 (RASP2), in the related Apicomplexan parasite *Toxoplasma gondii*. They identified that TgRASP2 localises to the cytosolic face of the rhoptry, is essential for tachyzoite invasion of the host cell and confirmed that the C2 domain of this protein binds to the rhoptry membrane through interactions with phospholipids. In the studies of *T. gondii*, TgRASP2 localised along the length of the tachyzoite rhoptries with foci at the rhoptry tip. Parallel studies in *P. falciparum* also identified an essential function for PfCERLI1 (PfRASP2) in invasion using a rapamycin inducible DiCre knockdown system. Although these two studies are highly complementary in the functional analysis of this protein, our quantitative analysis of the localisation of PfCERLI1 differs to that described by Suarez et al., with PfCERLI1 maintaining a clear rhoptry bulb localisation using both fluorescence and immuno-EM localisation in our study and a rhoptry tip localisation reported by Suarez et al. It is possible that PfCERLI1 and TgRASP2 have different localisations/functions, as while these organisms are related, they display markedly different host and cellular tropisms. However, further investigation will be required to tease out the specifics of these differences.

Taking all the data obtained together, we propose that PfCERLI1 has an important role in the function of the rhoptries during invasion, with PfCERLI1 knockdown leading to abnormal distribution, secretion and processing of rhoptry antigens that are likely to be essential for merozoite invasion. While further studies need to be undertaken to determine the fine detail of how PfCERLI1 knockdown causes these changes in rhoptry function, identification of PfCERLI1's direct association with release of rhoptry antigens is a key step in understanding the complex molecular events that control rhoptry secretion during invasion. By understanding how rhoptry secretion is controlled and the key proteins involved, we can identify targets for drug development that will stop merozoites invading and prevent replication of disease-causing parasites. In addition, this study makes extensive use of semi-automated quantitative immunofluorescence microscopy and highlights how this powerful tool can be used to study the process of invasion.

Methods

Bioinformatic analyses. PfCERLI1 (Pf3D7_0210600) and orthologous sequences in *P. reichenowi* (PRCDC_0209500), *P. gaboni* (PGAB01_0208200), *P. malariae* (PmUG01_04021700), *P. ovale* (PocGH01_04019500), *P. knowlesi* (PKNH_0410600), *P. vivax* (PVX_003980), *P. berghei* (PBANKA_0307500), *P. yoelii* (PY17X_0308100) and *P. chabaudi* (PCHAS_0309700) were obtained by searching within the PlasmoDB.org database[43]. Sequence similarities were determined using Geneious 9.1.3 (Biomatters) and performing multiple pairwise alignments using the global alignment with free end gaps alignment algorithm with the Blosum62 cost matrix.

Continuous culture of asexual stage *P. falciparum*. *P. falciparum* (3D7, 3D7 Δ*Pfcerli1*^{HAGlmS} and 3D7 Δ*Pfcerli1*$^{HAGlmS/GFP}$) parasites were cultured in human O^+ erythrocytes (Australian Red Cross blood service)[58]. Parasites were grown in RPMI-HEPES culture medium at pH 7.4 (Gibco) supplemented with 50 μM hypoxanthine, 25 mM $NaHCO_3$, 20 μM gentamicin and either 0.5% Albumax II (Gibco) or 0.25% w/v Albumax II, 5% v/v human serum (Australian Red Cross blood service). Parasite cultures were maintained in an atmosphere of 1% O_2, 4% CO_2 and 95% N_2 at 37 °C.

Plasmid construction and transfection. The PfCERLI1^{HAGlmS} riboswitch transfection vector was prepared from the PTEX150^{HAglmS} vector[20,59]. The final 767 base pairs of the 3' end of the *Pfcerli1* genomic sequence (excluding the stop codon) was PCR amplified using the primers *Pfcerli1* 5' F RBW (GGT**AGATCT**CATATCAAATTTGGTTCTTGAAG) and *Pfcerli1* 3' R RBW (GGT**CTGCAGC**ATCACTATAGTTGTACATATTTTTGC). The resulting PCR fragment was cloned into the PTEX150-^{HAglmS} vector using the restriction enzyme cloning sites Bgl II and Pst I (restriction enzyme sites in bold). To generate the cytosolic GFP expressing 3D7

Δ*Pfcerli1*$^{HAGlmS/GFP}$ line, the pHGBrHrBl-1/2 GFP plasmid[22] was used, without modification. For PfCERLI1 disruption, a source vector (Pf3D7_1463000 SLI-TGD) was digested with Not I and Mlu I with a 5' *Pfcerli1* flank being amplified using the primers (restriction enzyme sites in bold) *Pfcerli1* SLI-TGD F (GGT**GCGGCCGC**GATACTCACAACATATTATATCTTGG) and *Pfcerli1* SLI-TGD R (GGT**ACGCGT**CATACCTCTATGTGTACTTTGTTCTG)[19]. To construct the PfCERLI1 signal peptide deletion plasmid, *Pfcerli1* lacking the signal peptide was amplified using the forward primer *Pfcerli1* No SP F (GGT**GGTACC**ATGAGAA ACCGTGAGTTATTTC) and the reverse primer *Pfcerli1* R (GGT**CCTAGG**ATC ACTATAGTTGTACATATTTTTGC). The resulting PCR product was restriction digested using KpnI and AvrII and ligated into the pArl1a plasmid, containing the *ama1* promoter[60], to generate the *Pfcerli1*^{NoSP} pArl1a plasmid.

P. falciparum 3D7 parasites were transfected using erythrocyte loading[61]. Briefly, uninfected erythrocytes were centrifuged at 1500 rcf for 1 min, before removal of the supernatant and washing in cytomix (0.895% KCl, 0.0017% $CaCl_2$, 0.076% EGTA, 0.102% $MgCl_2$, 0.0871% K_2HPO_4, 0.068% KH_2PO_4, 0.708% HEPES). Erythrocytes were then resuspended in cytomix containing 200 µg of ethanol precipitated plasmid DNA, incubated in a 0.2 cm cuvette (Bio-Rad) on ice for 30 min and then electroporated (Bio-Rad) at 0.31 kV with a capacitance of 960 µF. Cells were washed 2× with culture media and transferred to a 10 mL dish containing magnet purified schizont stage parasites (3–5% parasitaemia). Integration of the HA-*GlmS* plasmid, or presence of the *Pfcerli1*^{NoSP} pArl1a plasmid, was selected for using 3 cycles of 5 nM WR99210 (Jacobus Pharmaceuticals) drug treatment. For generation of the Δ*Pfcerli1*$^{HAGlmS/GFP}$ line, PfCERLI1^{HAGlmS} parasites were transfected with the an episomal cytosolic GFP expressing plasmid pHGBrHrBl-1/2 and maintenance of this plasmid was selected for using 5 µg/mL blasticidin-S-deaminase HCl (Merck Millipore). Maintenance of the SLI-TGD plasmid was selected for using 5 nM WR99210, with successful integrants then selected for using 400 µg/mL G418 sulphate (geneticin, Thermo Fisher).

Parasite gDNA extraction and plasmid integration assessment. To extract parasite gDNA and confirm whether transfected constructs were stably integrated, schizont stage parasite cultures were saponin lysed. gDNA was extracted from saponin lysed parasites using the Wizard® Genomic DNA Purification Kit (Promega) according to the manufacturer's protocol. To confirm integration of *Pfcerli1*^{HAGlmS} into the parasite genome, the *Pfcerli1* locus was amplified with the forward primer *Pfcerli1* 5' F RBW (GGT**AGATCT**CATATCAAATTTGGTTCTTGAAG) and either the *Pfcerli1* 3' R RBW (GGT**CTGCAG**CATCACTATAGTTGTACATATTTTTGC) reverse primer (amplifies wildtype gDNA sequence) or the *Glms R* (GAAATCCTT ACGGCTGTGATCTG) reverse primer (amplifies DNA only upon *Pfcerli1*^{HAGlmS} integration).

Assessment of in vitro blood-stage growth and invasion. To determine the number of merozoites produced by each fully formed schizont after knockdown of PfCERLI1 protein expression, thin blood smears were made of D-(+)-Glucosamine hydrochloride (Sigma-Aldrich) (GLCN) treated and untreated schizont stage cultures matured in the presence of E64 (Sigma-Aldrich) to prevent schizont rupture. Smears were methanol fixed and stained with Giemsa (Merck Millipore) before blinded assessment of the number of merozoites by light microscopy (20 individual schizonts). All parasites assessed were fully matured, with individual segmented merozoites visible.

To assess the impact of PfCERLI1 knockdown, 3D7 Δ*Pfcerli1*^{HAGlmS} (growth) and 3D7 Δ*Pfcerli1*$^{HAGlmS/GFP}$ (invasion) parasites were synchronised to ring stages using sorbitol lysis and assays were set up in 96-well U-bottom plates at 1% parasitaemia and 1% haematocrit in a volume of 45 µL[62]. Five microlitre of 10× concentration GLCN or complete media was added to make a final volume of 50 µL. Assays were stained with 10 µg/mL ethidium bromide (Bio-Rad) in PBS before assessment of parasitaemia using flow-cytometry (BD Biosciences LSR II, 488 nm laser with FITC and PE filters). To assess merozoite development and invasion of 3D7 Δ*Pfcerli1*$^{HAGlmS/GFP}$ parasites, GLCN treated and untreated cultures were grown for 36 h, until newly invaded rings were present (0–6 h post-invasion). Flow cytometry data was analysed using FlowJo (Tree Star). The gating strategy used to identify free merozoites and ring-stage parasites is detailed in Supplementary Fig. 10.

Schizont rupture assay. To determine whether knockdown of PfCERLI1 altered the ability of schizonts to rupture, PfCERLI1^{HAGlmS} parasites were synchronised to ring-stages and set up into duplicate 96-well U-bottom plates, either in the presence or absence of GLCN, as described for growth and invasion assays. Using flow cytometry, the schizont-stage parasitaemia of both treatments was determined at an estimated pre-rupture timepoint for the first plates. After a further 6 h of incubation, the schizont-stage parasitaemia of the second (post-rupture) of the duplicate plates was determined. To determine the percentage of schizont rupture that occurred over the 6-h of incubation the following equation was used:

$$\%\ \text{schizont rupture} = \left(\frac{\text{post} - \text{rupture schizontaemia}}{\text{pre} - \text{rupture schizontaemia}}\right) \times 100$$

Saponin lysis and western blot. For protein samples, ~10 mL of high parasitaemia culture was lysed with 0.15% w/v saponin for 10 min on ice, parasite material was pelleted by centrifugation before washing once in 0.075% w/v saponin and three times in PBS. In the presence of protease inhibitors (CØmplete, Roche). Parasite lysates were resuspended in reducing sample buffer (0.125 M Tris-HCl pH 7, 4% v/v SDS, 20% v/v glycerol, 10% v/v β-mercaptoethanol (Sigma-Aldrich), 0.002% w/v bromophenol blue (Sigma-Aldrich)) and separated by size using SDS-PAGE 4-12% Bis-Tris Gels (Bolt, Invitrogen) at 130 V for 60 min. Proteins were then transferred to a nitrocellulose membrane (iBlot, Invitrogen) at 20 V for 7 min, before blocking the membrane for 1 h at room temperature in Odyssey Blocking Buffer (TBS) (LI-COR Biosciences). Primary (mouse 12CA5 anti-HA (1:4000, Roche), rabbit anti-EXP2 (1:5000,[63]), rabbit anti-GAP45 (1:10000,[64]), mouse anti-RH5 (1:5000), mouse anti-RAP1 7H8 (1:5000,[49]), rabbit anti-RON4 (1:5000), rabbit anti-EBA175 (1:5000[65]), mouse anti-RH4 2E8 (1:2500,[66]), rabbit anti-ERC (1:10000 [67])) and secondary (IRDye ® 800CW goat anti-mouse (1:4000, LI-COR Biosciences), IRDye ® 680RD goat anti-rabbit (1:4000, LI-COR Biosciences)) antibodies were incubated with membranes for 1 h at room temperature (prepared in Odyssey Blocking Buffer (TBS)), before washing in 0.05% v/v PBS Tween followed by a PBS wash after the secondary antibody incubation. Western blots were visualised using an Odyssey Infrared imaging system (LI-COR Biosciences). Western blot quantification was performed using Image Studio Lite 5.2.5 (LI-COR Biosciences). Uncropped images of all western blots can be found in Supplementary Figs. 11-13.

Proteinase K protection assay. For proteinase protection assays[13], three 5 mL aliquots of high-parasitaemia E64 treated schizonts were centrifuged at 440 rcf for 5 min before removal of supernatant and washing in 1× PBS and lysing of uninfected RBCs using saponin. The following treatments were undertaken: One tube with SOTE buffer (0.6 M sorbitol, 20 mM Tris HCl pH 7.5, 2 mM EDTA) alone. A second tube with SOTE plus 0.02% w/v digitonin (Sigma-Aldrich) incubated for 10 min at 4 °C prior to washing in SOTE buffer. A third tube with digitonin treatment followed by digestion with 0.1 µg/µL Proteinase K (Sigma-Aldrich) in SOTE for 30 min at 4 °C. Proteinase K was inactivated by adding 50 µL of 100% v/v trichloroacetic acid followed by a PBS wash. All tubes were then resuspended in 500 µL acetone before cells were pelleted, the supernatant removed, and the pellet used for Western blot analysis of proteinase K sensitivity.

Protein solubility assay. For protein solubility assays[13], Saponin-lysed pellets from 10 mL of high-parasitaemia E64 treated schizonts were resuspended in 100 µL dH_2O, snap-frozen at −80 °C four times, passed through a 26-gauge needle 5 times to disrupt the parasite membrane and then centrifuged at 15,000 rcf for 10 min with the water-soluble supernatant reserved. The pellet was washed twice in dH2O and once in 1× PBS before resuspension in 0.1 M sodium carbonate (Na_2CO_3) for 30 min at 4 °C with the supernatant reserved. Following carbonate treatment, samples were resuspended in 0.1% v/v Triton-X-100 for 30 min at 4 °C with the supernatant reserved and the resulting pellet washed and resuspended in 1× PBS. Samples were analysed by Western blotting.

Sample preparation for microscopy. Untreated and GLCN treated cultures (approximately 10 mL of 3% parasiteamia) of Compound 1 arrested PfCERLI1^{HAGlmS} late-stage schizonts were concentrated by centrifugation at 1700 rpm for 3 min, washed in PBS and fixed with 4% v/v paraformaledehyde (PFA, Sigma-Aldrich), 0.0075% v/v glutaraldehyde (pH 7.5, Electron Microscopy Sciences) solution for 30 min at room temperature with gentle shaking. Fixed parasite suspensions were adjusted to 1% haematocrit prior to adhering onto 0.01% poly-L-lysine (Sigma-Aldrich) coated #1.5 H high-precision coverslips (Carl Zeiss, Oberkochen, Germany) for 1 h at room temperature before permeabilistion with 0.1% v/v Triton-X-100 for 10 min. Coverslips were incubated with fresh blocking solution (3% w/v BSA-PBS, 0.05% v/v Tween-20) for at least 1 h. Primary antibodies (Chicken anti-HA (Abcam), mouse anti-RAP1[49], mouse anti-CyRPA 8A7[68], rabbit anti-RON4[69], rabbit anti-GAP45[64]) were diluted 1:500 in antibody diluent (1% w/v BSA-PBS, 0.05% v/v Tween-20) and added to coverslips for 1 h at room temperature or overnight at 4 °C. Cells were washed three times with PBS-Tween-20 (0.1% v/v) and incubated with goat anti-chicken/mouse/rabbit Alexa Fluor coupled secondary antibodies (488 nm, 594 nm, 647 nm) (Life Technologies) diluted 1:500 for 1 h at room temperature. After secondary antibody incubations, coverslips were washed three times with PBS-Tween-20 (0.1% v/v) then post-fixed with 4% w/v PFA for 5 min. PFA was washed off and coverslips dehydrated in ethanol at 70% v/v (3 min), 95% v/v (2 min) and 100% v/v (2 min) before being allowed to air dry and mounted on slides with ProLong® Gold antifade solution (refractive index 1.4) containing 4', 6-diamidino-2phenylindole, dihydrochloride (DAPI) (ThermoFisher Scientific). Once the mountant had cured for 24 h, cells were visualised by either conventional confocal (Olympus FV3000) or Zeiss LSM 800 Airyscan super-resolution microscopy (Carl Zeiss, Obekochen, Germany).

Confocal microscopy. Conventional confocal microscopy was performed on Olympus FV3000 fluorescent microscope (Olympus) equipped with a ×100 MPLAPON oil objective (NA 1.4) using the 405 nm, 488 nm, 561 nm, and 633 nm lasers. Z-stacks were acquired with a step size of 0.43 µm using a sequential scan (scan zoom = 10, without line averaging).

Airyscan super-resolution microscopy. Sub-diffraction microscopy was performed on a Zeiss LSM800 AxioObserver Z1 microscopy (Carl Zeiss, Obekochen, Germany) fitted with an Airyscan detector and a Plan-Apochromat ×63 (NA 1.4) M27 oil objective. TetraSpeck™ Fluorescent Microspheres (Life Technologies) were mounted on #1.5H coverslips (Carl Zeiss, Oberkochen, Germany) with a density of ~2.3×10^{10} particles/ml and used as the 200 nm bead calibration sample to correct for chromatic and spherical aberrations. The super-resolution reconstructions of multi-labelled PfCERLI1^{HAGlmS} schizonts were acquired, sequentially in four channels, as follows: channel 1 = 633 nm laser, channel 2 = 561 nm laser, channel 3 = 488 nm laser, channel 4 = 405 nm laser, with exposure times optimised from positive and negative control samples (HA blocking peptide, or omitted primary antibody) to avoid saturation. Three-dimensional (3D) Z-stacks were acquired at a pixel resolution of 0.04 µm in XY and 0.16 µm intervals in Z using piezo drive prior to being Airyscan processed in 3D using batch mode in ZEN Black (Zeiss).

Diameter measurements of super-resolved rhoptries. For further spatial exploration of the colocalised signals, 3D volumes captured with super-resolution microscopy after Airyscan processing were imported into ZEN Blue (Zeiss) for object-based colocalisation analysis. In this approach, volumetric colocalisation relies on manual identification of structures of interest and a subsequent measurement of their fluorescence intensity curves. Each rhoptry bulb immunolabelled with anti-RAP1 and anti-HA antibodies was manually quantified by a researcher blinded to experimental conditions, and the organelle diameter measured by drawing a vector through the centre of these structures and plotting the fluorescence intensities for the green and red channel against the length of the vector. Fluorescence intensity profiles of overlapping subcellular structures were then analysed in successive single sections from an image stack representing the two RAP1 and PfCERLI1^{HAGlmS} labelled structures. Fluorescence curves between the two antipodal points on the surface of the ring-like organelle were exported as.csv Excel files and plotted against the distance in nanometres. Only rhoptries with homogeneously stained ring-like structures containing no gaps in RAP1 or PfCERLI1^{HAGlmS} labelling and >100 nm in size were used for diameter measurements. Schizonts densely packed with merozoites with overlapping rhoptries were excluded from scoring. More than 800 individual organelles were scored and data from biological replicates plotted in Prism for comparison of diameters between untreated and glucosamine treated parasites.

Immunogold labelling and transmission electron microscopy. Schizont stage parasites were Percoll purified and fixed in 1% glutaraldehyde in RPMI-HEPES buffer. Samples were dehydrated in increasing concentrations of ethanol and embedded in LRGold resin. Ultrathin sections were cut and then labelled with anti-HA antibody (Mouse monoclonal clone 12CA5, Roche, diluted 1:500) and then with 18 nm Colloidal Gold (AffiniPure Goat Anti-Mouse IgG, product 115-215-166, Jackson ImmunoResearch, diluted 1:20). Sections were then post-stained with uranyl acetate and lead citrate and viewed using a Talos L120C Transmission Electron Microscope.

Rhoptry and microneme secretion assays. Apical organelle secretion assays were modified from a previous protocol[70]. Briefly, synchronous ring-stage cultures were obtained using sorbitol and either treated with 2.5 mM GLCN or left untreated and incubated in standard culture conditions for 24 h until early trophozoite stage. Cultures were then enzyme treated with neuraminidase (0.067 U/mL), chymotrypsin (1 mg/mL) and trypsin (1 mg/mL). Parasites were then allowed to rupture over the following 24 h. Following rupture, cultures were centrifuged at 13,000 rcf for 10 min in a benchtop centrifuge with some culture supernatant reserved, stored on ice, and the rest removed. The remaining pellet was then also placed on ice and saponin lysed to form a lysate containing the parasites that did not rupture and free merozoites, with this pellet and the culture supernatant analysed by Western blot.

Statistical analysis. Graphs and statistical analyses were performed using GraphPad PRISM 7 (GraphPad Software Inc.). In all figures where p-values were calculated, the corresponding statistical test is listed in the figure legend along with the number of experiments results are pooled from.

Reporting summary. Further information on research design is available in the Nature Research Reporting Summary linked to this article.

Data availability

The data that support the findings of this study are available from the corresponding author upon reasonable request. The source data underlying Figs. 1g, 2a, 6b and Supplementary Fig. 2a are provided as a source data file. Unprocessed Gel and Blot images are provided in Supplementary Fig. 11 for blots in Figs. 1d–f, 4a, b, Supplementary Fig. 12 for blots in Fig. 6a, and Supplementary Fig. 13 for blots in Supplementary Fig. 1b, 9a-c.

Received: 23 May 2019; Accepted: 15 February 2020;
Published online: 16 March 2020

References

1. World_Health_Organization. *World Malaria Report 2017*. who.int/malaria/publications/world-malaria-report-2017/en (2017).
2. Cowman, A. F., Healer, J., Marapana, D. & Marsh, K. Malaria: biology and disease. *Cell* **167**, 610–624 (2016).
3. Cowman, A. F., Tonkin, C. J., Tham, W. H. & Duraisingh, M. T. The molecular basis of erythrocyte invasion by malaria parasites. *Cell Host Microbe* **22**, 232–245 (2017).
4. Beeson, J. G. et al. Merozoite surface proteins in red blood cell invasion, immunity and vaccines against malaria. *FEMS Microbiol. Rev.* **40**, 343–372 (2016).
5. Boyle, M. J., Wilson, D. W. & Beeson, J. G. New approaches to studying Plasmodium falciparum merozoite invasion and insights into invasion biology. *Int. J. Parasitol.* **43**, 1–10 (2013).
6. Burns, A. L. et al. Targeting malaria parasite invasion of red blood cells as an antimalarial strategy. *FEMS Microbiol. Rev.* https://doi.org/10.1093/femsre/fuz005 (2019).
7. Riglar, D. T. et al. Super-resolution dissection of coordinated events during malaria parasite invasion of the human erythrocyte. *Cell Host Microbe* **9**, 9–20, https://doi.org/10.1016/j.chom.2010.12.003 (2011).
8. Counihan, N. A., Kalanon, M., Coppel, R. L. & de Koning-Ward, T. F. Plasmodium rhoptry proteins: why order is important. *Trends Parasitol.* **29**, 228–236 (2013).
9. Richard, D. et al. Interaction between Plasmodium falciparum apical membrane antigen 1 and the rhoptry neck protein complex defines a key step in the erythrocyte invasion process of malaria parasites. *J. Biol. Chem.* **285**(19), 14815–22 (2010).
10. Counihan, N. A. et al. Plasmodium falciparum parasites deploy RhopH2 into the host erythrocyte to obtain nutrients, grow and replicate. *eLife* **6**, e23217 (2017).
11. Hanssen, E. et al. Electron tomography of Plasmodium falciparum merozoites reveals core cellular events that underpin erythrocyte invasion. *Cell. Microbiol.* **15**, 1457–1472 (2013).
12. Topolska, A. E., Lidgett, A., Truman, D., Fujioka, H. & Coppel, R. L. Characterization of a Membrane-associated Rhoptry Protein of Plasmodium falciparum. *J. Biol. Chem.* **279**, 4648–4656 (2004).
13. Cabrera, A. et al. Dissection of minimal sequence requirements for rhoptry membrane targeting in the malaria parasite. *Traffic* **13**, 1335–1350 (2012).
14. Geiger, M. et al. Structural Insights Into PfARO and characterization of its interaction with PfAIP. *J. Mol. Biol.* https://doi.org/10.1016/j.jmb.2019.12.024 (2019).
15. Mueller, C. et al. Structural and functional dissection of Toxoplasma gondii armadillo repeats only protein. *J. Cell Sci.* **129**, 1031–1045 (2016).
16. Hu, G. et al. Transcriptional profiling of growth perturbations of the human malaria parasite Plasmodium falciparum. *Nat. Biotechnol.* **28**, 91 (2009).
17. Zenonos, Z. A., Rayner, J. C. & Wright, G. J. Towards a comprehensive Plasmodium falciparum merozoite cell surface and secreted recombinant protein library. *Malar. J.* **13**, 93, https://doi.org/10.1186/1475-2875-13-93 (2014).
18. Suarez, C. et al. A lipid-binding protein mediates rhoptry discharge and invasion in Plasmodium falciparum and Toxoplasma gondii parasites. *Nat. Commun.* **10**, 4041 (2019).
19. Birnbaum, J. et al. A genetic system to study Plasmodium falciparum protein function. *Nat. Methods* **14**, 450 (2017).
20. Prommana, P. et al. Inducible Knockdown of Plasmodium Gene expression using the glmS ribozyme. *PLoS ONE* **8**, e73783 (2013).
21. Lopez-Barragan, M. J. et al. Directional gene expression and antisense transcripts in sexual and asexual stages of Plasmodium falciparum. *BMC Genomics* **12**, 587 (2011).
22. Wilson, D. W., Crabb, B. S. & Beeson, J. G. Development of fluorescent Plasmodium falciparum for in vitro growth inhibition assays. *Malar. J.* **9**, 152 (2010).
23. Wilson, D. W., Langer, C., Goodman, C. D., McFadden, G. I. & Beeson, J. G. Defining the timing of action of antimalarial drugs against Plasmodium falciparum. *Antimicrobial Agents Chemother.* **57**, 1455–1467 (2013).
24. Ficz, G. & Heintzmann, R. Breaking the resolution limit in light microscopy. *Brief. Funct. Genomics* **5**, 289–301 (2006).
25. Bannister, L. H., Hopkins, J. M., Fowler, R. E., Krishna, S. & Mitchell, G. H. Ultrastructure of rhoptry development in Plasmodium falciparum erythrocytic schizonts. *Parasitology* **121**, 273–287 (2000).

26. Peskan, T., Westermann, M., Fau—Oelmuller, R. & Oelmuller, R. Identification of low-density Triton X-100-insoluble plasma membrane microdomains in higher plants. *Eur. J. Biochem.* **267**(24), 6989–95 (2000).
27. Kübler, E., Dohlman, H. G. & Lisanti, M. P. Identification of Triton X-100 insoluble membrane domains in the Yeast Saccharomyces cerevisiae: lipid requirements for targeting of heterotrimeric G-protein subunits. *J. Biol. Chem.* **271**, 32975–32980 (1996).
28. Taylor, H. M. et al. The malaria parasite cyclic GMP-dependent protein kinase plays a central role in blood-stage schizogony. *Eukaryot. Cell* **9**, 37 (2010).
29. Kelley, L. A., Mezulis, S., Yates, C. M., Wass, M. N. & Sternberg, M. J. E. The Phyre2 web portal for protein modeling, prediction and analysis. *Nat. Protoc.* **10**, 845 (2015).
30. Roy, A., Kucukural, A. & Zhang, Y. I-TASSER: a unified platform for automated protein structure and function prediction. *Nat. Protoc.* **5**, 725 (2010).
31. Yang, J. et al. The I-TASSER Suite: protein structure and function prediction. *Nat. Methods* **12**, 7 (2014).
32. Zhang, Y. I-TASSER server for protein 3D structure prediction. *BMC Bioinforma.* **9**, 40 (2008).
33. Roy, A., Yang, J. & Zhang, Y. Protein–ligand binding site recognition using complementary binding-specific substructure comparison and sequence profile alignment. *Bioinformatics* **29**, 2588–2595 (2013).
34. Yang, J., Roy, A. & Zhang, Y. BioLiP: a semi-manually curated database for biologically relevant ligand–protein interactions. *Nucleic Acids Res.* **41**, D1096–D1103 (2012).
35. Corbalan-Garcia, S. & Gómez-Fernández, J. C. Signaling through C2 domains: more than one lipid target. *Biochimica et. Biophysica Acta* **1838**, 1536–1547 (2014).
36. Liu, Y.-C. The E3 ubiquitin ligase Itch in T cell activation, differentiation, and tolerance. *Semin. Immunol.* **19**, 197–205 (2007).
37. Rodriguez, L. et al. C2-domain abscisic acid-related proteins mediate the interaction of PYR/PYL/RCAR abscisic acid receptors with the plasma membrane and regulate abscisic acid sensitivity in Arabidopsis. *Plant Cell* **26**, 4802 (2014).
38. Diaz, M. et al. Calcium-dependent oligomerization of CAR proteins at cell membrane modulates ABA signaling. *Proc. Natl Acad. Sci. USA* **113**, E396 (2016).
39. Czech, M. P. PIP2 and PIP3: complex roles at the cell surface. *Cell* **100**, 603–606 (2000).
40. Wang, X., Hills, L. B. & Huang, Y. H. Lipid and protein co-regulation of PI3K effectors Akt and Itk in lymphocytes. *Front. Immunol.* **6**, 117–117 (2015).
41. Jones, M. L., Collins, M. O., Goulding, D., Choudhary, J. S. & Rayner, J. C. Analysis of protein palmitoylation reveals a pervasive role in Plasmodium development and pathogenesis. *Cell Host Microbe* **12**, 246–258 (2012).
42. Deponte, M. et al. Wherever I may roam: protein and membrane trafficking in P. falciparum-infected red blood cells. *Mol. Biochemical Parasitol.* **186**, 95–116 (2012).
43. Aurrecoechea, C. et al. PlasmoDB: a functional genomic database for malaria parasites. *Nucleic Acids Res.* **37**, D539–D543 (2008).
44. Dyrløv Bendtsen, J., Nielsen, H., von Heijne, G. & Brunak, S. Improved prediction of signal peptides: signalP 3.0. *J. Mol. Biol.* **340**, 783–795 (2004).
45. Almagro Armenteros, J. J. et al. SignalP 5.0 improves signal peptide predictions using deep neural networks. *Nat. Biotechnol.* **37**, 420–423 (2019).
46. Silmon de Monerri, N. C. et al. Global identification of multiple substrates for Plasmodium falciparum SUB1, an essential malarial processing protease. *Infect. Immun.* **79**, 1086–1097 (2011).
47. Howard, R. F., Narum, D. L., Blackman, M. & Thurman, J. Analysis of the processing of Plasmodium falciparum rhoptry-associated protein 1 and localization of Pr86 to schizont rhoptries and p67 to free merozoites. *Mol. Biochemical Parasitol.* **92**, 111–122 (1998).
48. Nasamu, A. S. et al. Plasmepsins IX and X are essential and druggable mediators of malaria parasite egress and invasion. *Science* **358**, 518 (2017).
49. Schofield, L. et al. A rhoptry antigen of Plasmodium falciparum contains conserved and variable epitopes recognized by inhibitory monoclonal antibodies. *Mol. Biochemical Parasitol.* **18**, 183–195 (1986).
50. Bushell, G. R., Ingram, L. T., Fardoulys, C. A. & Cooper, J. A. An antigenic complex in the rhoptries of Plasmodium falciparum. *Mol. Biochemical Parasitol.* **28**, 105–112 (1988).
51. Dearnley, M. K. et al. Origin, composition, organization and function of the inner membrane complex of Plasmodium falciparum gametocytes. *J. Cell Sci.* **125**, 2053 (2012).
52. Pinder, J. C. et al. Actomyosin motor in the merozoite of the malaria parasite, Plasmodium falciparum: implications for red cell invasion. *J. Cell Sci.* **111**, 1831 (1998).
53. Parkyn Schneider, M. et al. Disrupting assembly of the inner membrane complex blocks Plasmodium falciparum sexual stage development. *PLOS Pathog.* **13**, e1006659 (2017).
54. Cho, W. & Stahelin, R. V. Membrane-protein interactions in cell signaling and membrane trafficking. *Annu. Rev. Biophy. Biomol. Struct.* **34**, 119–151 (2005).
55. Zhang, M. et al. Uncovering the essential genes of the human malaria parasite Plasmodium falciparum by saturation mutagenesis. *Science* **360**, eaap7847 (2018).
56. Gao, Y. H. et al. Identification of a vaccine candidate antigen, PfMAg-1, from Plasmodium falciparum with monoclonal antibody M26-32. *Parasitol. Res.* **105**, 1723–1732 (2009).
57. Volz, J. C. et al. Essential role of the PfRh5/PfRipr/CyRPA complex during Plasmodium falciparum Invasion of erythrocytes. *Cell Host Microbe* **20**(1), 60–71 (2016).
58. Trager, W. & Jensen, J. B. Human malaria parasites in continuous culture. *Science* **193**, 673 (1976).
59. Elsworth, B. et al. PTEX is an essential nexus for protein export in malaria parasites. *Nature* **511**, 587–591 (2014).
60. Treeck, M. et al. A conserved region in the EBL proteins is implicated in microneme targeting of the malaria parasite Plasmodium falciparum. *J. Biol. Chem.* **281**, 31995–32003 (2006).
61. Deitsch, K., Driskill, C. & Wellems, T. Transformation of malaria parasites by the spontaneous uptake and expression of DNA from human erythrocytes. *Nucleic Acids Res.* **29**, 850–853 (2001).
62. Boyle, M. J. et al. Isolation of viable Plasmodium falciparum merozoites to define erythrocyte invasion events and advance vaccine and drug development. *Proc. Natl Acad. Sci. USA* **107**, 14378 (2010).
63. Bullen, H. E. et al. Biosynthesis, localization, and macromolecular arrangement of the Plasmodium falciparum translocon of exported proteins (PTEX). *J. Biol. Chem.* **287**, 7871–7884 (2012).
64. Baum, J. et al. A conserved molecular motor drives cell invasion and gliding motility across malaria life cycle stages and other apicomplexan parasites. *J. Biol. Chem.* **281**, 5197–5208 (2006).
65. Lopaticki, S. et al. Reticulocyte and erythrocyte binding-like proteins function cooperatively in invasion of human erythrocytes by malaria parasites. *Infect. Immun.* **79**, 1107 (2011).
66. Tham, W.-H. et al. Complement receptor 1 is the host erythrocyte receptor for Plasmodium falciparum PfRh4 invasion ligand. *Proc. Natl Acad. Sci. USA* **107**, 17327 (2010).
67. Albano, F. R. et al. A homologue of Sar1p localises to a novel trafficking pathway in malaria-infected erythrocytes. *Eur. J. Cell Biol.* **78**, 453–462 (1999).
68. Chen, L. et al. Structural basis for inhibition of erythrocyte invasion by antibodies to Plasmodium falciparum protein CyRPA. *eLife* **6**, e21347 (2017).
69. Gilson, P. R. et al. MSP119 miniproteins can serve as targets for invasion inhibitory antibodies in Plasmodium falciparum provided they contain the correct domains for cell surface trafficking. *Mol. Microbiol.* **68**, 124–138 (2008).
70. Absalon, S., Robbins, J. A. & Dvorin, J. D. An essential malaria protein defines the architecture of blood-stage and transmission-stage parasites. *Nat. Commun.* **7**, 11449 (2016).

Acknowledgements

We thank the Australian Red Cross Blood Bank for the provision of human blood. We thank Prof. Alan Cowman for provision of CyRPA, RON4, EBA175 and GAP45 antibodies, Dr. Paul Gilson for EXP2 antibodies, A/Prof. Wai-Hong Tham for RH4 antibodies, and Prof. Leann Tilley for ERC and GAPDH antibodies. We also thank Dr. Paul Gilson for the PTEX150^{HAGlmS} transfection vector. Confocal microscopy was performed at Adelaide Microscopy, University of Adelaide, and super-resolution microscopy was performed at the Centre for Cancer Biology Cytometry Facility, The University of South Australia. We especially thank Dr. Jane Sibbons from Adelaide Microscopy for assistance with confocal microscopy. Electron microscopy was performed at the Bio21 Institute Advanced Microscopy Facility, The University of Melbourne (www.microscopy.unimelb.edu.au). For provision of the SLI-TGD vector, we thank Dr. Tobias Spielmann. We thank Dr. Brad Sleebs for Compound 1. We thank Arne Alder and Sarah Lemcke for help with SLI-TGD transfection and parasite culture. This work was supported by funding from the NHMRC (Project Grant APP1143974, D.W.W.), University of Adelaide Beacon Fellowship (D.W.W.), DAAD/Universities Australia joint research co-operation scheme (T. G., D.W.W., B.L.), Australian Government Research Training Program Scholarship (B. L.), South Australian Commonwealth Scholarship (B.L.).

Author contributions

Study design and planning: D.W.W., B.L., S.F., M.W.A.D., S.A.R. and T.G. Performed experiments and generated reagents: B.L., S.F., D.W.W., G.K.H., S.A.R. and B. Liu. Data analysis: S.F, B.L. and D.W.W. Manuscript writing: B.L., S.F, T.G. and D.W.W. Manuscript was drafted with input from all authors.

Competing interests

The authors declare no competing interests.

Additional information

Supplementary information is available for this paper at https://doi.org/10.1038/s41467-020-15127-w.

Correspondence and requests for materials should be addressed to D.W.W.

Peer review information *Nature Communications* thanks the anonymous reviewers for their contribution to the peer review of this work. Peer reviewer reports are available.

Reprints and permission information is available at http://www.nature.com/reprints

Publisher's note Springer Nature remains neutral with regard to jurisdictional claims in published maps and institutional affiliations.

Chapter 4 Supplementary information

Chapter 4 Supplementary methods

Ring-stage retention assay

To determine if successfully invaded PfCERLI1 KD merozoites developed and survived the following cycle, synchronous ring-stage parasites were set up in technical triplicate at 1% parasitaemia and 1% haematocrit either in the presence or absence of GLCN using duplicate 96-well U-bottom plates. 48 hours later, ring-stage parasitaemia was determined in one plate using flow-cytometry. In the duplicate plate, GLCN was either washed out or left unwashed and heparin was added to all wells to prevent further invasion events. 36 hours later, trophozoite-stage parasitaemia was determined by flow cytometry. To determine the percentage of rings that were retained from ring to trophozoite stages, the following calculation was used: $(\frac{Trophozoites\ (\%\ RBCs)}{Rings\ (\%\ RBCs)}) \times 100$. This calculation used the mean trophozoite and ring stage parasitaemias of the technical triplicates for each of the two biological replicates.

Theoretical calculation of invasion inhibition contribution to free merozoites

To calculate the build-up of free merozoites that can be detected relative to control due to invasion inhibition, the number of free merozoites was determined using flow cytometry as described above and the following equations were implemented, with the final equation applied to each experimentally determined value:

$$\frac{Parasitaemia\ fold\ change^{\#}}{Merozoites\ per\ schizont^{@}} = Prop.of\ produced\ merozoites\ that\ invade\ (mi)$$

$$\frac{5.5}{19.1} = 0.288$$

$$avg\ inv.inhib\ \times\ mi = Prop.of\ merozoites\ that\ invade\ with\ KD\ \ (msi)$$

$$0.52\ \times\ 0.288 = 0.155$$

$$mi - msi = Prop.of\ merozoites\ that\ fail\ to\ invade\ due\ to\ knockdown\ (mfi)$$

$$0.288 - 0.155 = 0.133$$

$$(1 - mfi) \times actual\ free\ merozoites = theoretical\ \ merozoites\ if\ no\ inv.inhib.$$

[#] as determined by (Reininger, Garcia et al. 2012),[@] average value from Figure 4.2b used.

Prediction of PfCERLI1 signal peptide, protein structure, and ligands

The presence of a signal peptide for both PfCERLI1 and RAP1 was predicted using SignalP-5.0 (Nielsen, Engelbrecht et al. 1997, Almagro Armenteros, Tsirigos et al. 2019). Full length PfCERLI1 protein sequence was submitted to the online protein structure prediction tools Phyre2 (Kelley, Mezulis et al. 2015) and I-TASSER (Yang, Yan et al. 2014). Residues corresponding to the predicted C2 and PH domains were then submitted to the online protein-ligand binding site prediction tool COACH (Roy, Yang et al. 2013). All predicted structures were visualised, presented and imaged using Jmol .

Transmission electron microscopy

Synchronous ring stage parasites were either treated with 2.5 mM GLCN or left untreated and incubated in standard conditions until early schizont stages before incubation with 4-[2-(4-fluorophenyl)-5-(1-methylpiperidine-4-yl)-1H-pyrrol-3-yl] pyridine (compound) 1 for 5 hours and Percoll purification of mature schizonts. Percoll purified schizonts were then fixed in 2.5 % v/v

glutaraldehyde in PBS overnight at 4°C. Cells were pre-embedded in agarose and fixed in 2% osmium tetroxide reduced in 1.5% potassium ferricyanide in 0.15 M cacodylate buffer for 1 hr at room temperature. Subsequently, the cells were dehydrated in a graded series of ethanol- H_2O mixtures, followed by progressive infiltration with EPON resin and embedding; 70 nm sections were prepared using an ultramicrotome (Leica EM UC7, Leica Microsystems). The sections were poststained with 4% uranyl acetate in water and Reynold's lead citrate. Thin sections were observed on a transmission electron microscope at 200 kV (Tecnai G2 F30, FEI).

Quantitative analysis of foci and colocalisation in super-resolved PfCERLI1^{HAGlmS} late-stage schizonts

To adapt a previous workflow on the automated measurements of colocalisation in cancer cell lines (Han, Napier et al. 2019) to malaria infected red blood cells, an advanced 3D model-based image analysis pipeline was developed in the Imaris Suite software (v9.3.0, Bitplane Inc., Switzerland) using the surface module. It accounts for significantly smaller objects, more irregular shapes and elevated levels of signal heterogeneity (e.g. 32-64 rhoptries per schizont and 0.1-0.3 µm in size depending on maturity). The approach supports quantitation of spatial positioning for a maximum four sub-cellular compartments labelled in four 3D channels (e.g. nucleus/DAPI, PfCERLI1^{HAGlmS}/488 nm, RAP1/594 nm and RON4/647 nm).

Pre-processing of three-dimensional stacks

To overcome artefacts caused by digital conversion of a light signal into an electronic signal, autofluorescence or noise, micrographs were thresholded to identify objects that are brighter than the background noise, as follows. Threshold offset was based on negative control samples (i.e. blocking peptide and/or omitted primary antibody controls) that lack cellular objects in the image. Applying a fixed threshold value [e.g. 500 for delineating RON4, 800 for RAP1 and 750 for

PfCERLI1^{HAGlmS} (0-32767)] allowed object detection in untreated conditions as well as in situations where images with reduced signals were expected (e.g. from a loss of label due to a compound treatment). Prior to object identification, the non-cellular background was computed and subtracted in each channel independently using a 3D surface fitting method. In this step, local background maxima around each pixel are computed and high frequency components supressed by subtracting the background from the original image. The main advantage of the method is that it minimizes the effect of the background correction (removal) procedure on the intensity values of the analysed objects. Next, identified objects were subjected to 3D Gaussian filtering (morphological) to remove very small speckles (e.g. single-voxel noise) from the image and to consolidate fragmented objects. Next, objects that touch the border of the image field were excluded from further analysis. Having identified optimal intensity thresholds and appropriate degree of smoothing for object identification, we next segmented objects in each channel to resolve and identify foci of interest as described below.

Three-dimensional foci detection and segmentation

For automatic detection and quantitation of PfCERLI1^{HAGlmS}, RAP1 and RON4 foci in the 488 nm, 594 nm and 647 nm channels, a series of 3D surface detection, 3D model-based segmentation, and surface filtering was performed using Imaris batch mode (v9.3.0, Bitplane Inc., Switzerland). Two methods of object identification were used prior to quantitative analyses: geometric (shape and size) and intensity (intensity peaks). The geometric method splits touching objects on the basis of shape, relying on boundary indentations to locate a line of separation. The intensity method separates touching objects using intensity peaks. This approach identifies each object with single, dominant intensity peak and uses the minimum relative height of the intensity peak (i.e. image contrast) for segmentation. Using this approach, objects were reconstructed as artificial 3D masks and their physical properties (e.g. intensity or morphology) adjusted to specified

ranges, as follows. First, selection parameters related to object's intensity were restricted to specified ranges and those objects that are too bright or too dim were excluded from further analysis. Next, object identification was limited to foci with diameter > 0.1 µm to restrict the ranges for variation in size. Lastly, area selection parameter was used to remove noise (1-2 voxel regions). To optimise object detection and eliminate false objects, coloured solid image overlays that are exactly the size and shape of each object were used for visual inspection of segmentation accuracy and to validate gating parameters. The volume statistics exported on a per cell basis included: area (μm^2), volume (μm^2), total intensity (a.u.), sphericity (a.u.) and ellipticity (a.u.).

Measuring colocalisation in three-dimensional stacks

To gain a more detailed picture of how PfCERLI1^{HAGlmS}, RAP1 and RON4 are positioned in the rhoptries we utilised Imaris Coloc Suite (v9.3.0, Bitplane Inc., Switzerland). It provides an automated quantitation of colocalisation based on correlation coefficients that measure the strength of the linear relationship between two variables, i.e. the grey values of fluorescence intensity voxels of green and red image pairs. First, the two channels (e.g. 400 nm and 594 nm) for colocalisation detection are selected and voxel distribution of the two images plotted against each other as a scatter plot. The intensity of a given voxel in the green image is used as the x-coordinate of the scatter plot and the intensity of the corresponding voxel in the red image as the y-coordinate. Pearson's correlation coefficient was then used for initial identification of diverse relationships between PfCERLI1^{HAGlmS}, RAP1, and RON4. It calculates the relationship between intensities in two images by linear regression. The slope of the fitted line provides the rate of association of two fluorophores, i.e. the PCC provides an estimate of the goodness of this approximation. Its value can range from +1 to -1, with 1 standing for complete positive correlation and -1 for negative correlation, with zero indicating no correlation. Scatterplots and PCC point to colocalization especially when it is complete; however, they rarely discriminate differences between partial

colocalization or exclusion, especially if images are noisy (e.g. in cases where signal is dispersed or reduced due to treatment). Since evaluation of colocalization using PCC alone may be ambiguous due to variations in fluorescence intensities or heterogeneous colocalization relationships throughput the sample, we next employed Mander's correlation coefficient (MCC) to study different stoichiometries of foci association. MCC is based on the PCC with average intensity values being taken out of the mathematical expression (Manders, Stap et al. 1992). This coefficient varies from 0 to 1, the former corresponding to non-overlapping images and the latter reflecting 100% colocalization between both images. Because MCC is sensitive to noise, regions of interest (i.e. masking area) was defined based on fixed intensity threshold to exclude non-cellular data from further analysis. The volume statistics exported included: number of colocalised voxels (total count of colocalised voxels), % of data set colocalised (percentage of total dataset voxels colocalised), % region of interest (ROI) colocalised (Percentage colocalization of channel A and channel B volume inside the region of interest), Pearson's coefficient (PCC) in ROI volume (PCC of channel A and channel B inside the region of interest), Original Mander's coefficient (MCC) A/B and thresholded Mander's coefficient A/B.

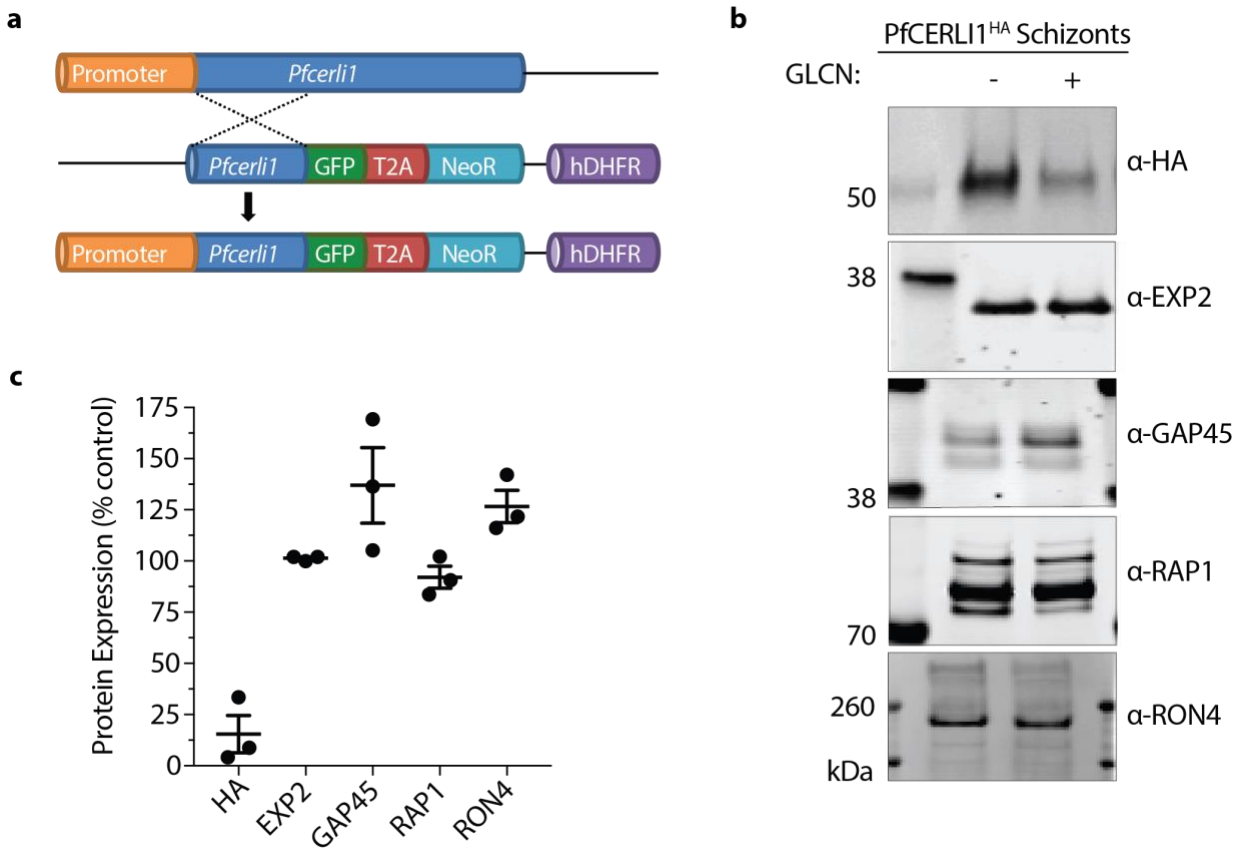

Supplementary Figure 4.1: Attempted knockout of *Pfcerli1*, Integration of PfCERLI1^{HAGlmS} into the parasite genome, and the effect of GLCN treatment on PfCERLI1 expression.

(a) *Schematic representation of the selection linked integration targeted gene disruption (SLI-TGD) system used to attempt knock-outs of Pfcerli1. A plasmid containing a Pfcerli1 flanking region, green fluorescent protein (GFP) a T2A skip peptide and neomycin resistance cassette (NeoR) was transfected into wildtype 3D7 parasites. Single cross-over integration (knock-out) is expected to be driven through selection of neomycin resistance since this can only occur when NeoR expression is driven by the endogenous Pfcerli1 promoter. Plasmid uptake was selected using the human dihydrofolate reductase (hDHFR) cassette, which confers resistance to the drug WR99210.* ***(b)*** *Synchronous PfCERLI1^{HAGlmS} ring-stage parasites were either treated with 2.5 mM GLCN (+) or left untreated (-), harvested, and saponin lysed at schizont-stage in the same cycle. Parasite lysates were then used for Western blots, probed with anti-HA (PfCERLI1), anti-EXP2 (loading control), anti-GAP45, anti-RAP1 and anti-RON4 antibodies. Representative images of 3 independent experiments.* ***(c)*** *Western blot band intensities were quantified, and results are displayed as % protein expression (band intensity) in GLCN treated samples relative to untreated samples (control). (n=3 biological replicates, error bars = SEM).*

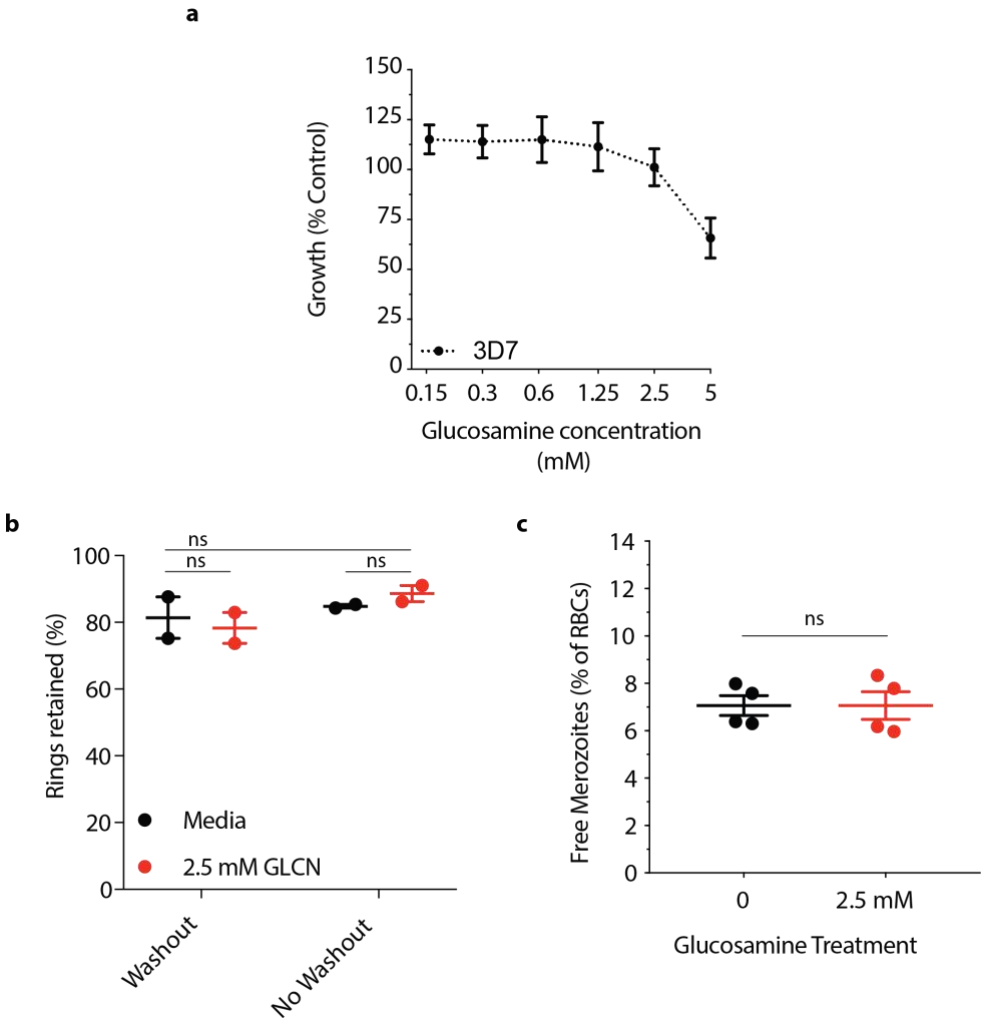

Supplementary Figure 4.2: Influence of GLCN on wildtype parasite growth, PfCERLI1 knockdown on parasite development post-invasion, and the contribution of invasion inhibition to quantified free merozoites.

(a) *3D7 wildtype parasites were treated with increasing concentrations of GLCN for 96 hours, to assess off-target growth inhibitory effects of GLCN (parasite growth expressed as a % of media control (n = 5 biological replicates).* ***(b)*** *Early PfCERLI1$^{HAGlmS/GFP}$ Ring-stage parasites were treated with glucosamine (2.5 mM GLCN) or left untreated (media). Immediately after invasion the knockdown treatment was removed (washout) or left on (no washout) and ring-stage parasitaemia was determined by flow cytometry. Schizont-stage parasitaemia was then determined 36 hours later by flow cytometry with results reported as the percentage of successfully formed rings (% rings retained) that had survived to schizont-stages (n=2 biological replicates).* ***(c)*** *Quantification of free merozoites as presented in Figure 2d, but the data points in the 2.5 mM GLCN treatment represent the number of free merozoites expected after subtraction of additional merozoites that failed to invade relative to untreated controls. (n=4 biological replicates). All error bars = SEM.*

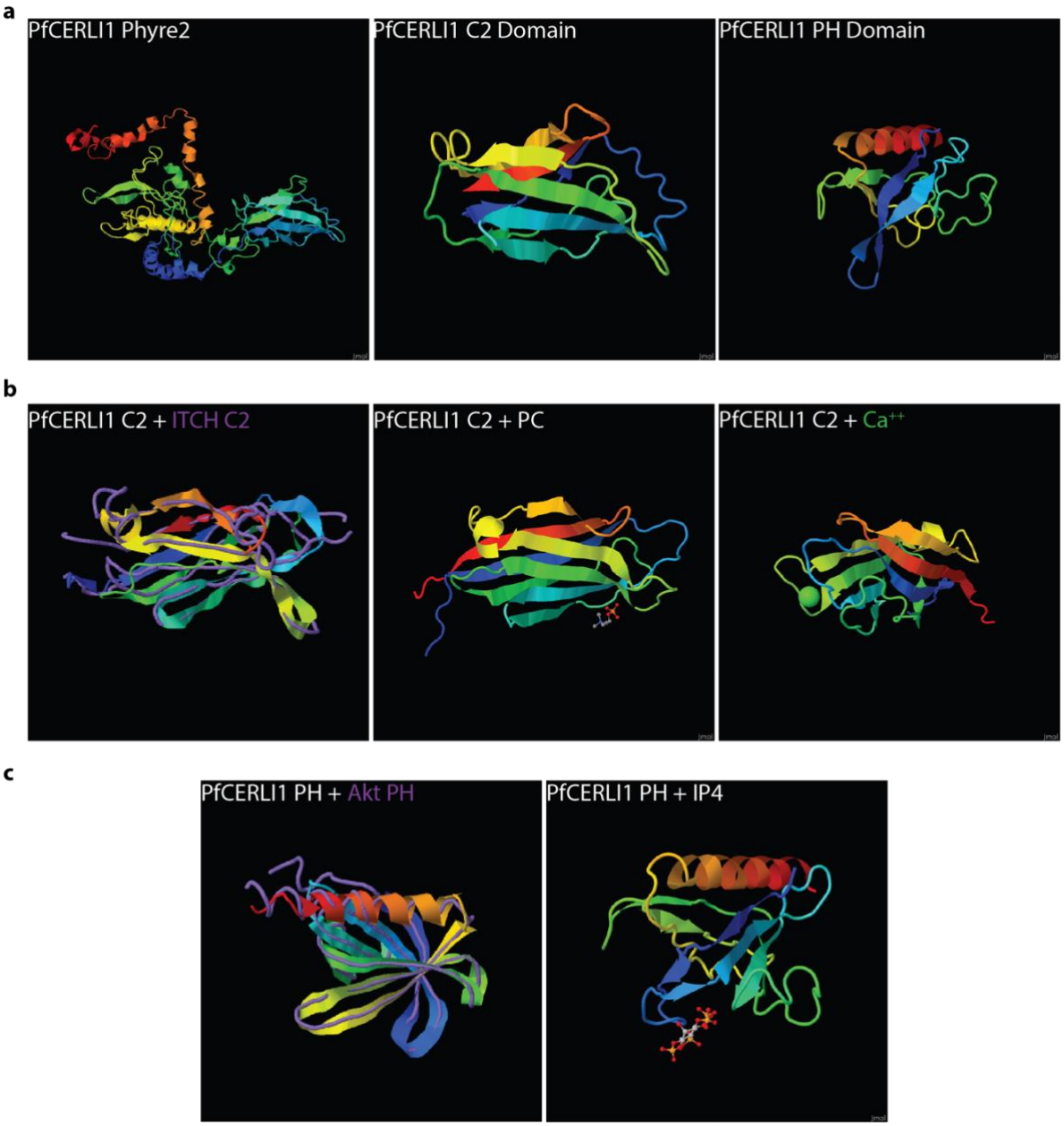

Supplementary Figure 4.3: Structural prediction of PfCERLI1.

Full length PfCERLI1 protein structure was predicted using Phyre2 ***(a)*** *and I-TASSER with both prediction software's independently identifying a C2 and pleckstrin homology (PH) domain in the PfCERLI1 protein. Ribbon diagrams of the C2 domain of human itchy homolog E3 ubiquitin protein ligase (ITCH)* ***(b)*** *and PH domain of human Protein kinase B (Akt)* ***(c)****, which were the most similar protein structures to PfCERLI1 C2 and PH domains respectively, are superimposed (purple) onto the predicted PfCERLI1 3D structures. The C2 domain of PfCERLI1 was predicted to bind both phosphocholine (PC) and a calcium ion (Ca^{++}), while the PH domain was predicted to bind to inositol 1,3,4,5- tetrakisphosphate (IP4). All structures presented are ribbon rainbow diagrams, with N-terminus to C-terminus corresponding with red to blue.*

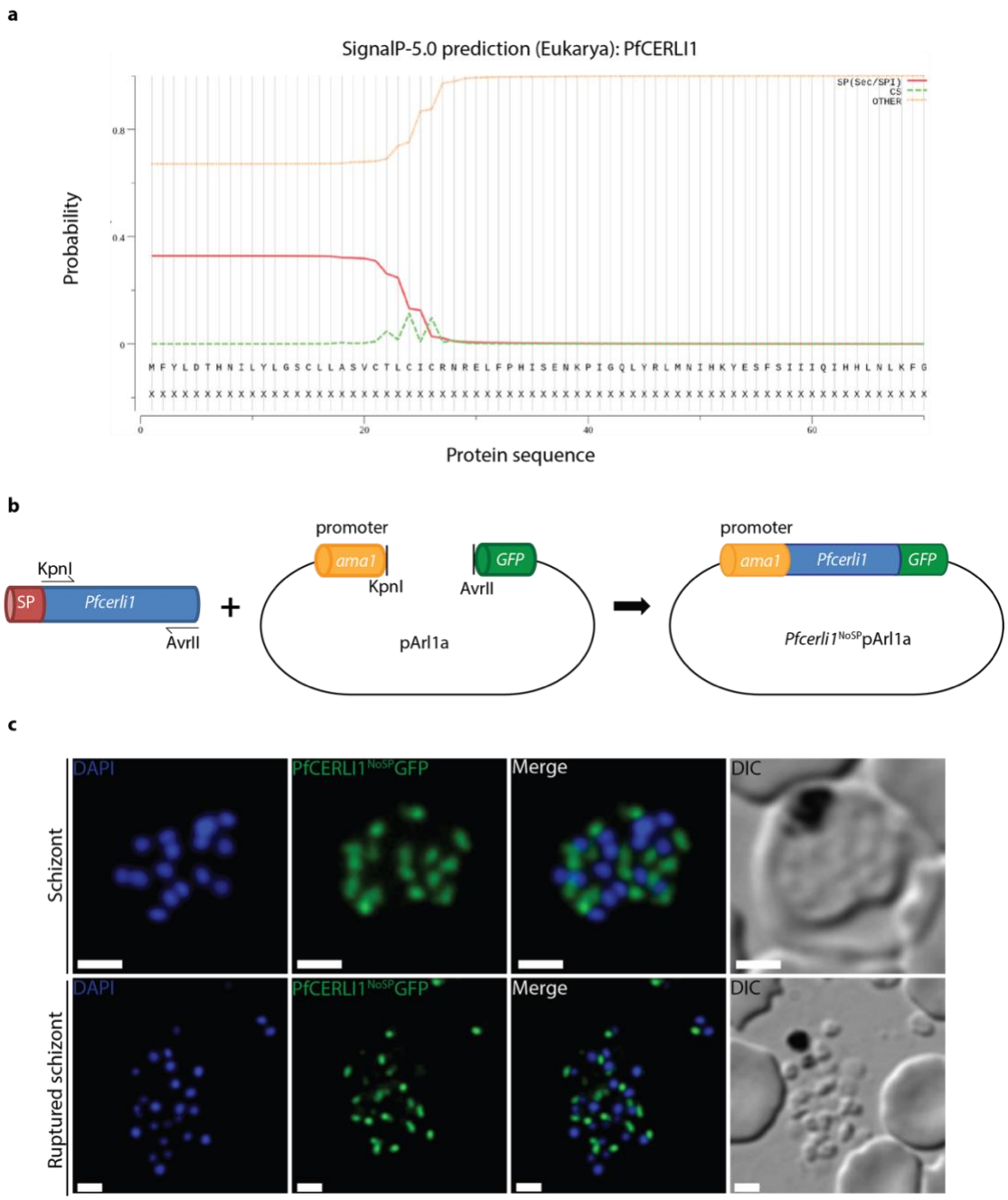

Supplementary Figure 4.4: PfCERLI1 signal peptide prediction and the generation and localisation of a PfCERLI1 deletion mutant.

*(**a**) SignalP-5.0 was used to determine whether PfCERLI1 was predicted to contain a signal peptide, with the prediction below the 0.5 probability score used to predict putative signal peptides. (**b**) The Pfcerli1 locus, lacking the putative signal peptide (1-26aa), was amplified from cDNA and cloned into the pArl1a vector, placing Pfcerli1^{NoSP} under the control of the ama1 promoter and fusing it to GFP. (**c**) Localisation of PfCERLI1^{NoSP}GFP was determined in both pre and post-rupture schizonts using live-cell widefield microscopy. Scale bar = 2 µm.*

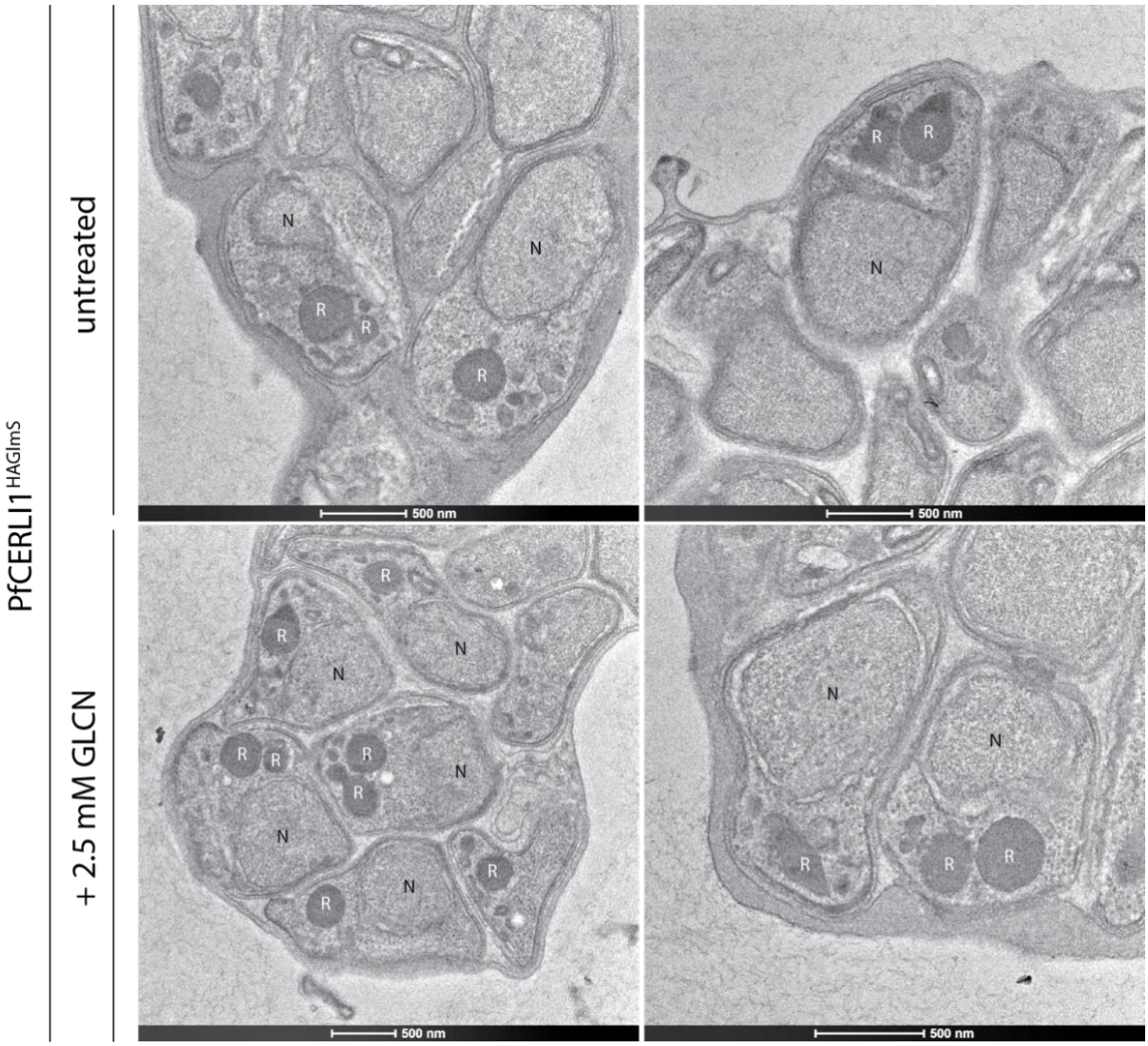

Supplementary Figure 4.5: Transmission electron microscopy of PfCERLI1^{HAGlmS} schizonts.

PfCERLI1^{HAGlmS} parasites were either treated with 2.5 mM GLCN or left untreated and schizonts were matured in the presence of compound 1 before fixation and analysis by transmission electron microscopy. R = rhoptry, N = nucleus.

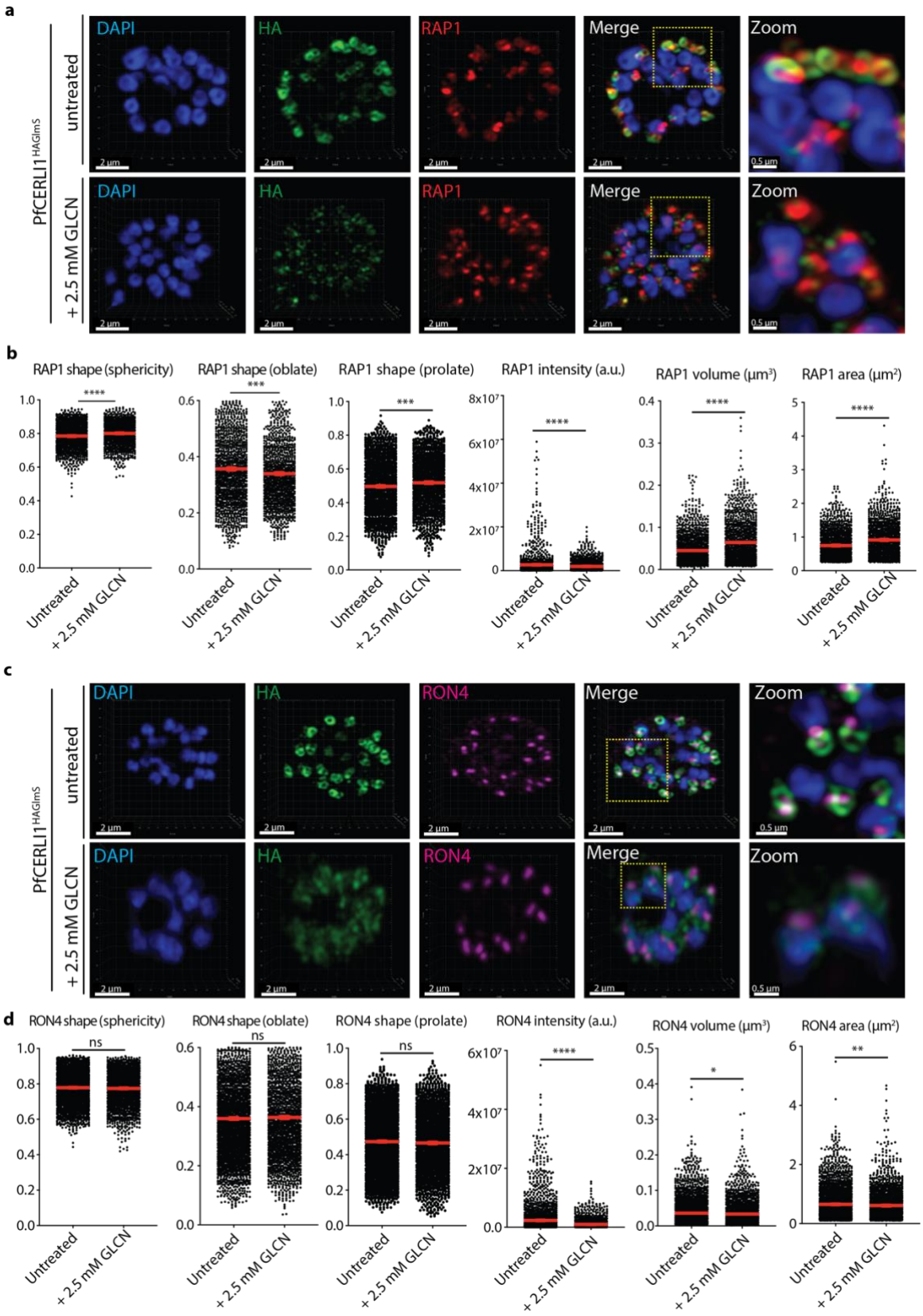
a
PfCERLI1 HAGlmS
untreated
+ 2.5 mM GLCN
DAPI
HA
RAP1
Merge
Zoom
2 µm
0.5 µm
b
RAP1 shape (sphericity)
RAP1 shape (oblate)
RAP1 shape (prolate)
RAP1 intensity (a.u.)
RAP1 volume (µm³)
RAP1 area (µm²)
****
***
Untreated
+ 2.5 mM GLCN
c
RON4
d
RON4 shape (sphericity)
RON4 shape (oblate)
RON4 shape (prolate)
RON4 intensity (a.u.)
RON4 volume (µm³)
RON4 area (µm²)
ns
*
**

Supplementary Figure 4.6: PfCERLI1HAGlmS knockdown is associated with a change in the shape of the rhoptry marker RAP1.

*PfCERLI1^{HAGlmS} ring-stage parasites were either treated with GLCN (+ 2.5 mM GLCN) or left untreated with resulting schizonts stained with DAPI, anti-HA (PfCERLI1), anti-RAP1, or anti-RON4 antibodies. Parasites were then analysed by 3D super-resolution microscopy. (a) Representative images of RAP1 stained PfCERLI1^{HAGlmS} schizonts. (b) RAP1 shape (sphericity, oblate, prolate), intensity, volume and area were quantified for GLCN treated and untreated PfCERLI1^{HAGlmS} parasites (n=5 biological replicates, 1428 RAP1 foci counted for untreated parasites and 1243 for + 2.5 mM GLCN parasites). (c) Representative images of RON4 stained PfCERLI1^{HAGlmS} schizonts. (d) RON4 shape (sphericity, oblate, prolate), intensity, volume and area were quantified for GLCN treated and untreated PfCERLI1^{HAGlmS} parasites (n=5 biological replicates, 2962 RON4 foci counted for untreated parasites and 1939 for + 2.5 mM GLCN parasites). Both datasets were quantified using the image feature extraction pipeline detailed in Supplementary Figure 4.8. (ns = p>0.05, * = p<0.05, ** = p<0.01, *** = p<0.001, **** = p<0.0001). All error bars = SEM.*

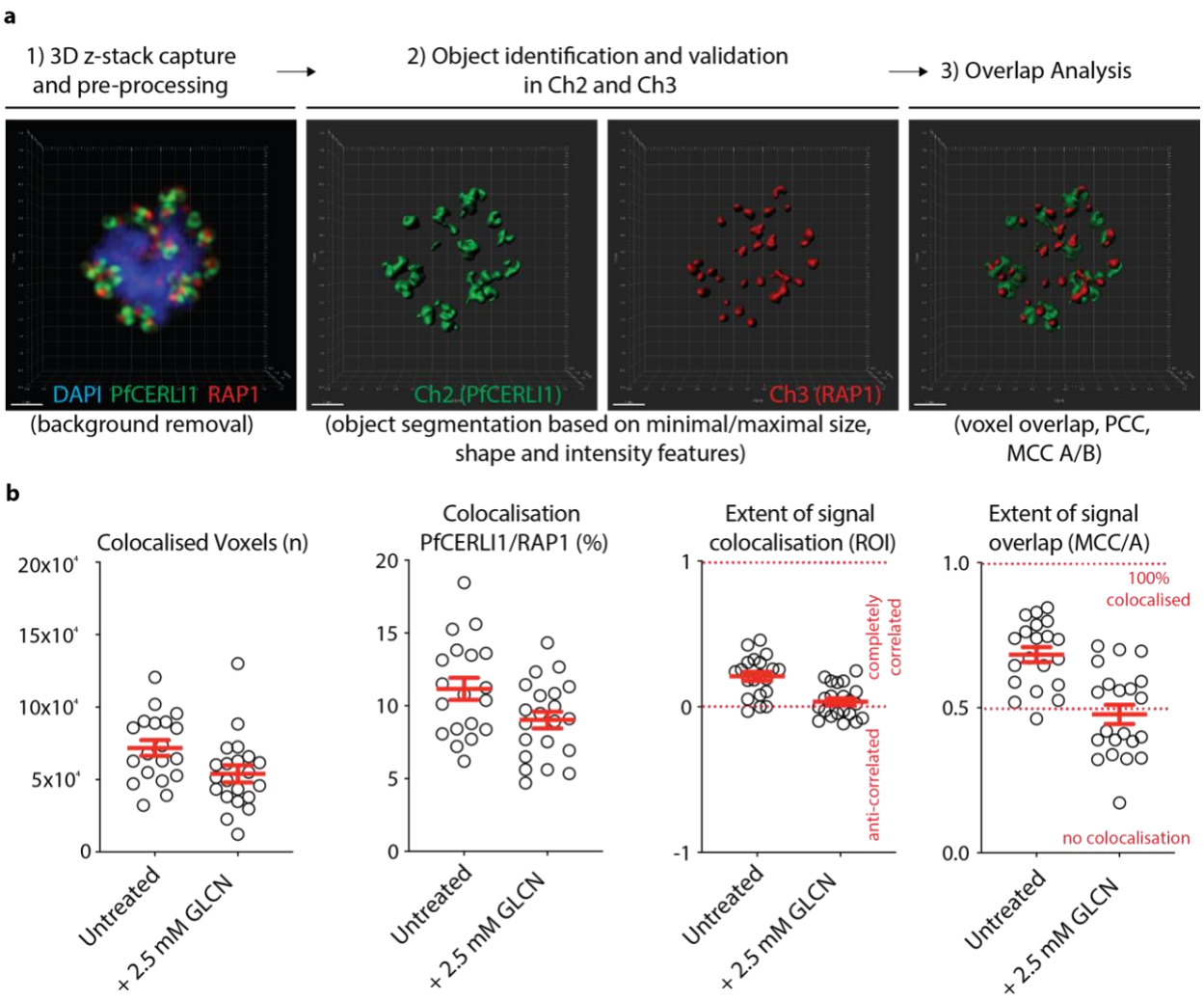

Supplementary Figure 4.7: Digital image analysis pipeline for evaluation of association frequency between two fluorescently labelled rhoptry markers.

(a) *Image processing and analysis pipeline. 3D super-resolution images were captured before pre-processing to move background noise. Signals in channels of interest were then converted to objects and segmented based on minimal/maximal size, shape and intensity. Objects in different channels were then analysed to assess their overlap and colocalisation.* ***(b)*** *Using this pipeline, the number of colocalised voxels between the channels was determined. The signal of both channels was then thresholded and one of the two channels was then designated as the region of interest (ROI). The percentage colocalisation, Pearson's correlation coefficient (PCC) and Mander's correlation coefficient (MCC) inside this designated ROI was then determined. Presented data represents a comparison with PfCERLI1 as the ROI and RAP1. n= 3 biological replicates, colocalisation was calculated for 19 untreated schizonts and 21 + 2.5 mM GLCN schizonts (error bars = SEM).*

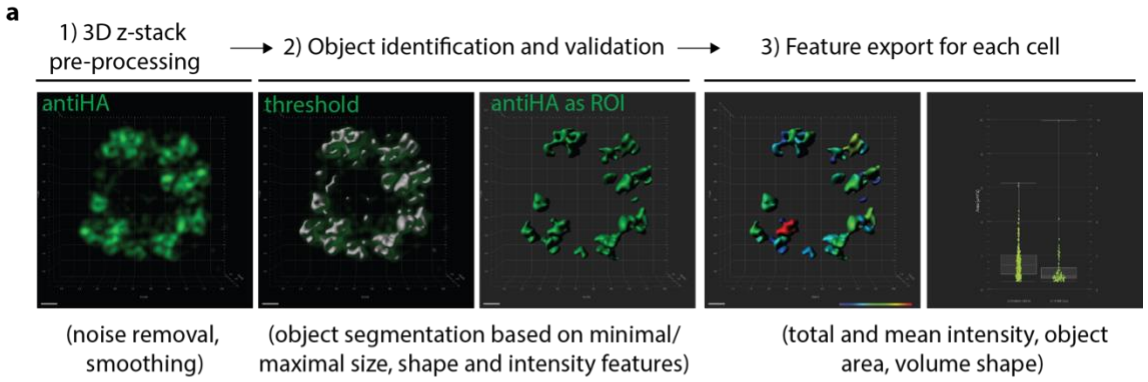
a
1) 3D z-stack pre-processing
2) Object identification and validation
3) Feature export for each cell
antiHA
threshold
antiHA as ROI
(noise removal, smoothing)
(object segmentation based on minimal/ maximal size, shape and intensity features)
(total and mean intensity, object area, volume shape)

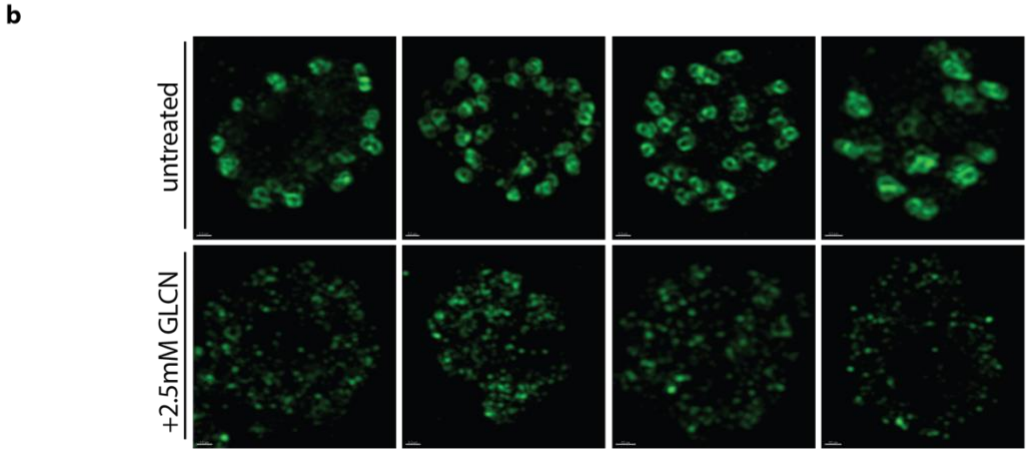
b
untreated
+2.5mM GLCN

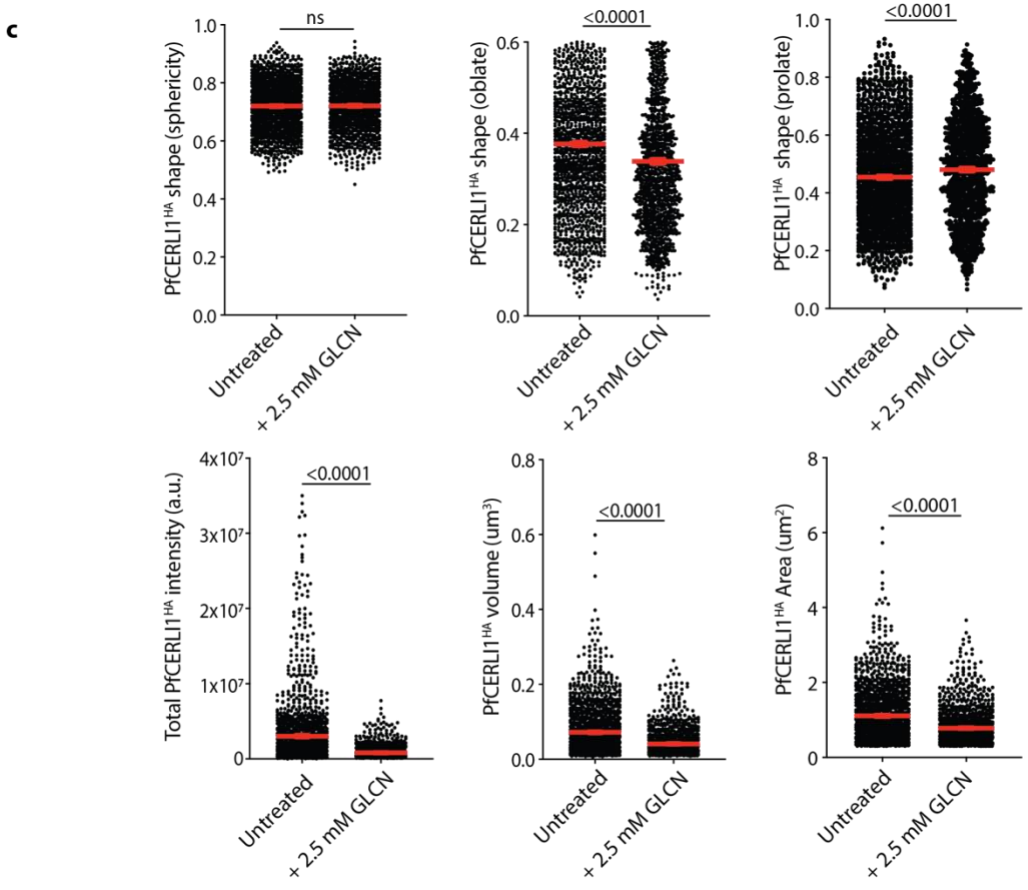
c
PfCERLI1HA shape (sphericity)
ns
PfCERLI1HA shape (oblate)
<0.0001
PfCERLI1HA shape (prolate)
<0.0001
Total PfCERLI1HA intensity (a.u.)
<0.0001
PfCERLI1HA volume (um3)
<0.0001
PfCERLI1HA Area (um2)
<0.0001
Untreated
+2.5 mM GLCN

Supplementary Figure 4.8: Digital image analysis pipeline used for 3D segmentation and analysis of merozoite organelles.

Merozoite organelles imaged by fluorescence microscopy often have indistinct outlines, and image segmentation methods must be implemented to subtract background from genuine signal. ***(a)*** *In this example, PfCERLI1 immuno-labelled with anti-HA antibodies (green) in mature schizonts have been segmented at threshold values to separate signal from noise. Signals are then converted into objects, based on minimal/maximal size, shape and signal intensity. Data can then be extracted from each of these objects, including shape (sphericity, oblate, prolate), intensity, volume, and area.* ***(b)*** *Representative super-resolution micrographs of immuno-labelled rhoptries in control (untreated) or GLCN treated (+ 2.5 mM GLCN) PfCERLI1^{HAGlmS} schizonts.* ***(c)*** *Data obtained from object analyses can then be compared between two different treatments to assess the influence of the treatment on the fluorescent marker of interest (PfCERLI1) (n = 5 biological replicates, 1489 PfCERLI1^{HA} foci counted for untreated parasites and 1197 counted for + 2.5 mM GLCN parasites) Error bars = SEM.*

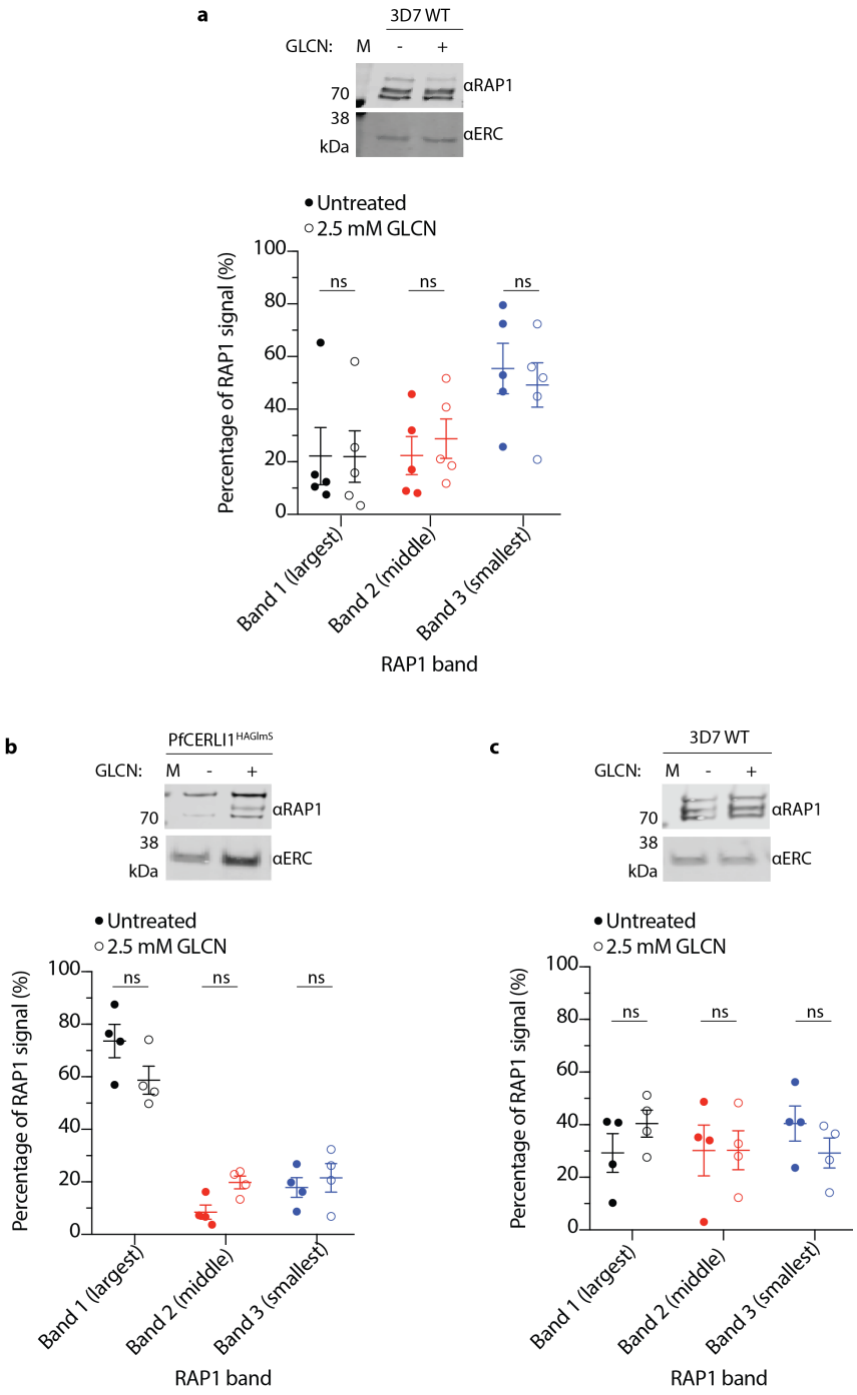

Supplementary Figure 4.9: GLCN treatment does not alter RAP1 processing**.**

(a) *Using 3D7 parasite lysates from the rhoptry secretion experiment, each of the three individual RAP1 bands present on the western blots were quantified and presented as a percentage of the total RAP1 signal (n = 5 biological replicates). Using lysates of compound 1 arrested* ***(b)*** *PfCERLI1HAGlmS or* ***(c)*** *3D7 schizonts that were either GLCN treated, or untreated, individual RAP1 bands were also quantified (n = 4 biological replicates, ns = p>0.05).*

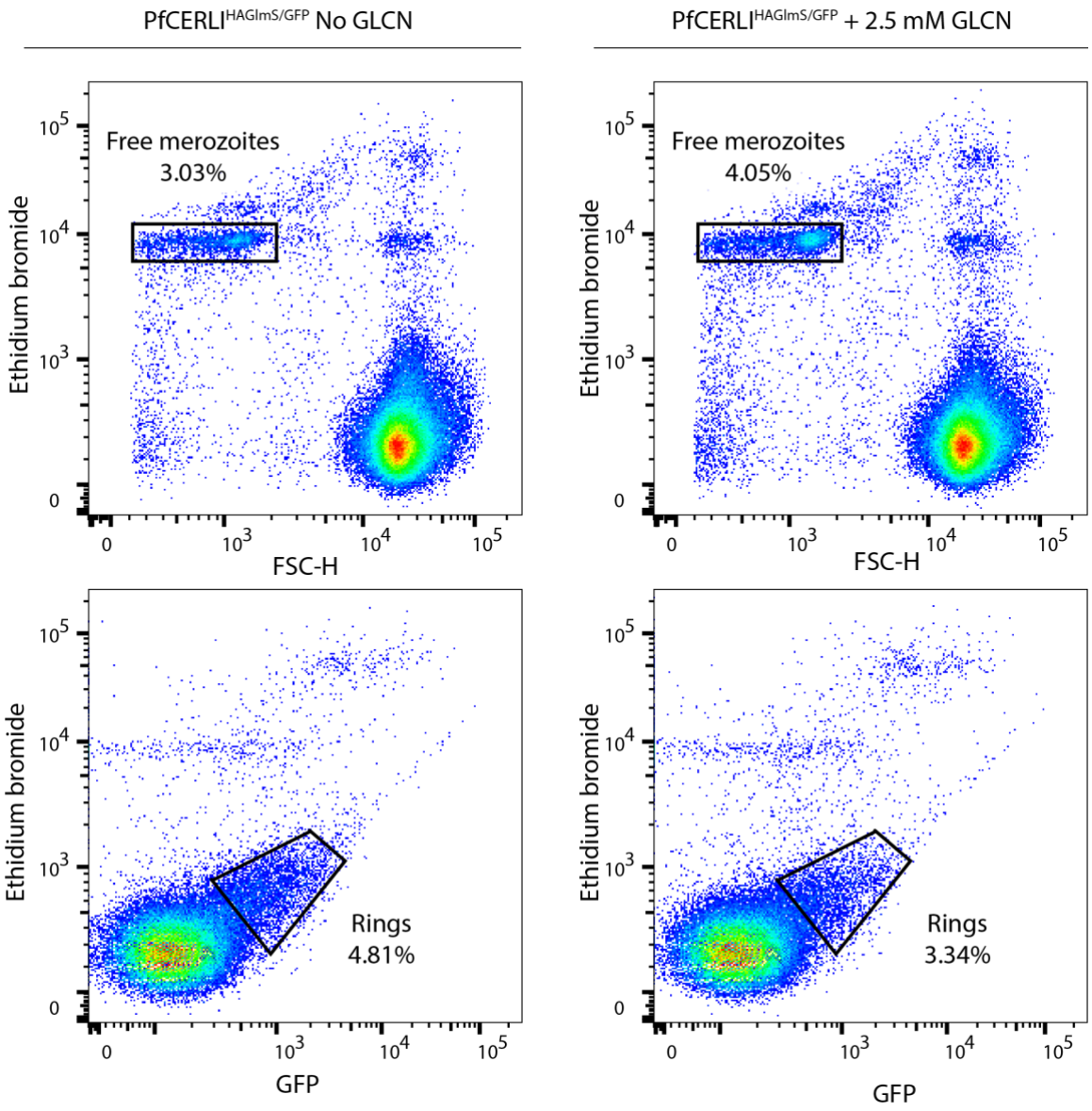

Supplementary Figure 4.10: Representative flow cytometry gating plots for invasion assays.

PfCERLI1$^{HAGlmS/GFP}$ free merozoites were gated as Ethidium bromide^{high} FSC-H^{low} events in the ungated sample. PfCERLI1$^{HAGlmS/GFP}$ ring stage parasites were gated as Ethidium bromide^{low} GFP^{high} events inside the erythrocyte gate. GLCN-mediated knockdown of PfCERLI1 inhibited merozoite invasion, leading to an increase in the free merozoite population and a decrease in the ring stage population for GLCN treated cultures.

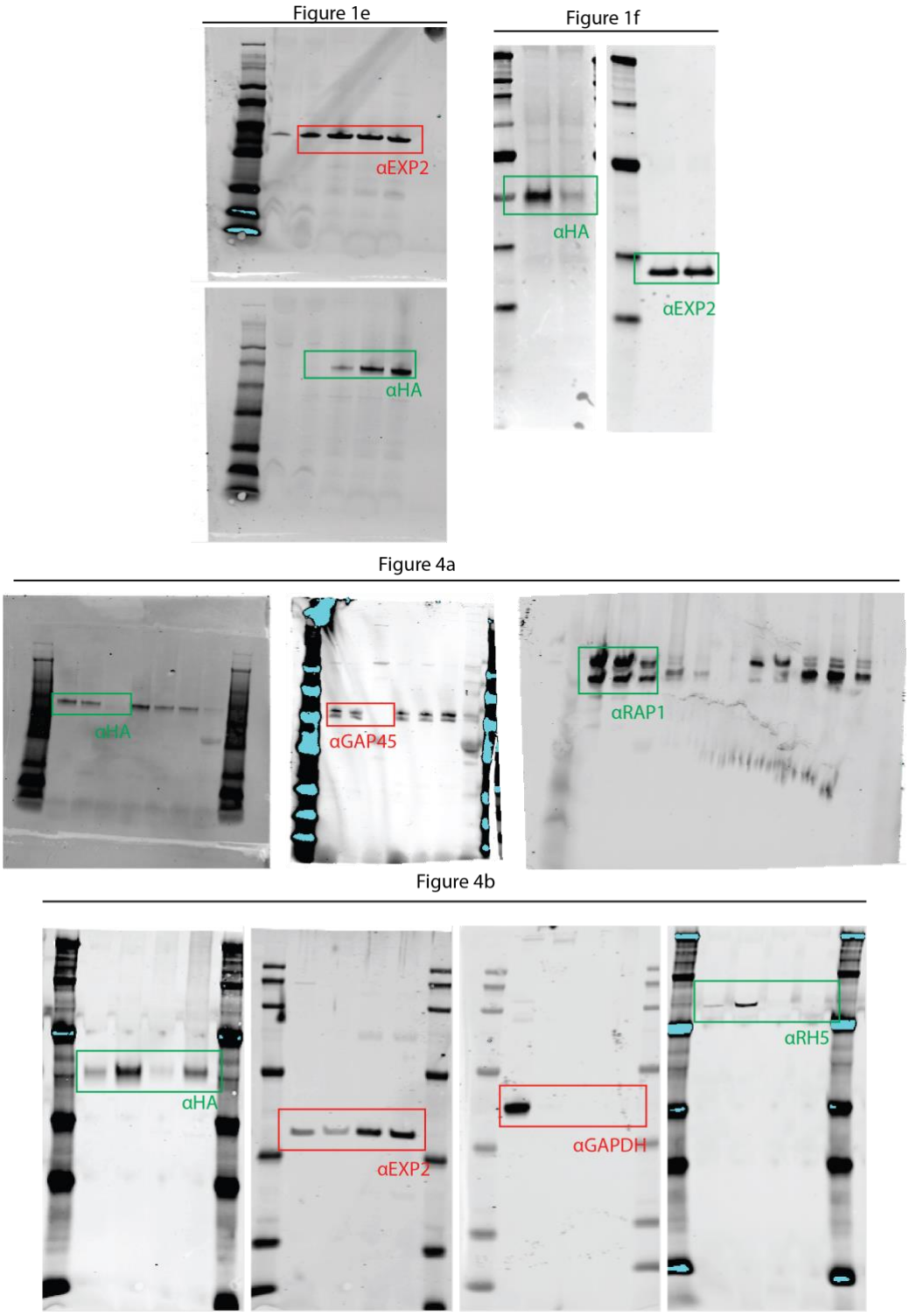

Supplementary Figure 4.11: Full length Western Blots used in Figures 1 and 4.

Corresponding Figures and antibodies used are as indicated. Bands displayed in Figures 1 and 4 are boxed. Bands indicated in green box were detected in the 800 nm channel. Bands indicated in the red box were detected in the 680 nm channel.

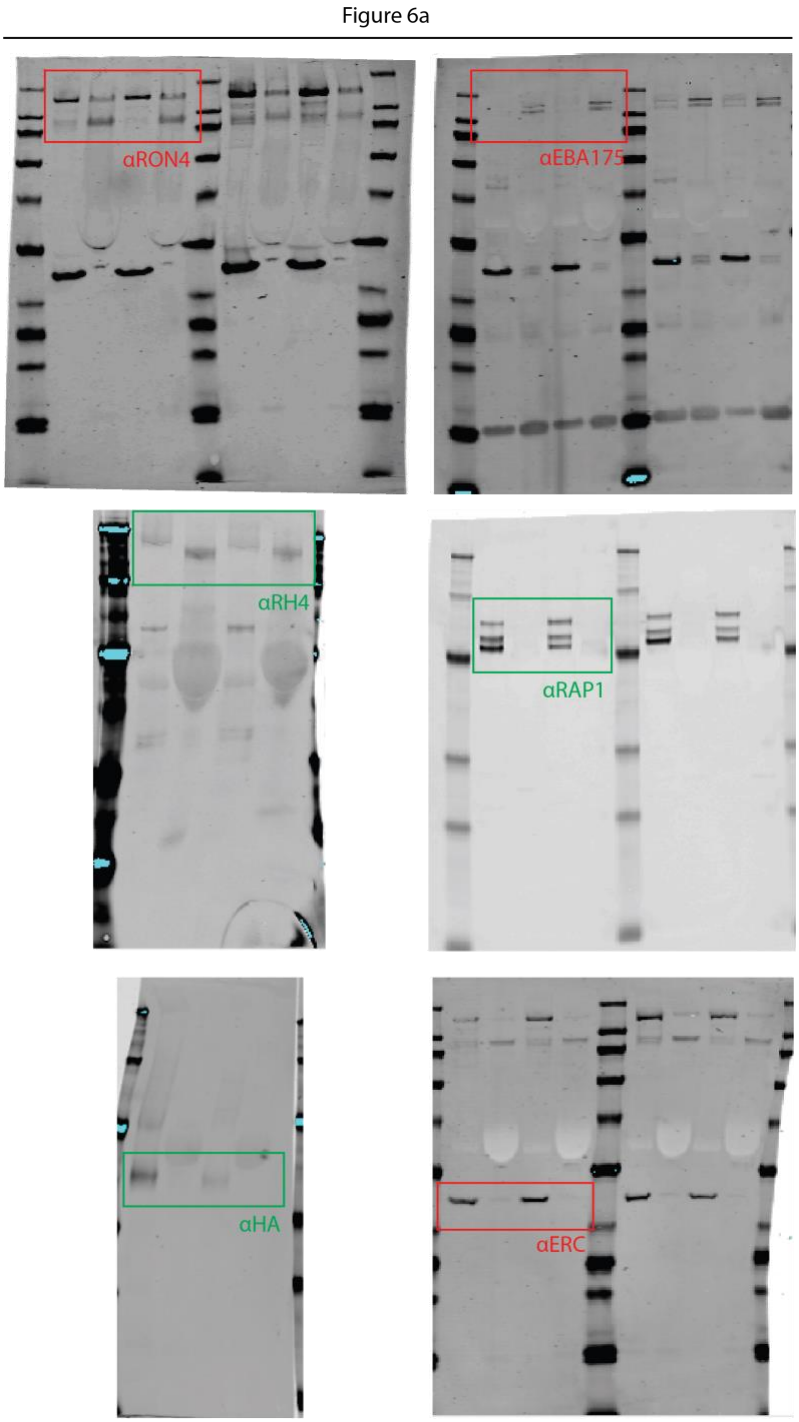

Supplementary Figure 4.12: Full length Western Blots used in Figures 6.

Corresponding Figures and antibodies used are as indicated. Bands displayed in Figure 6 are boxed. Bands indicated in green box were detected in the 800 nm channel. Bands indicated in the red box were detected in the 680 nm channel. Membranes were probed with multiple antibodies to detect several non-size overlapping proteins at once, resulting in reduced variability between specific antigen comparisons and multiple banding patterns evident with some membranes.

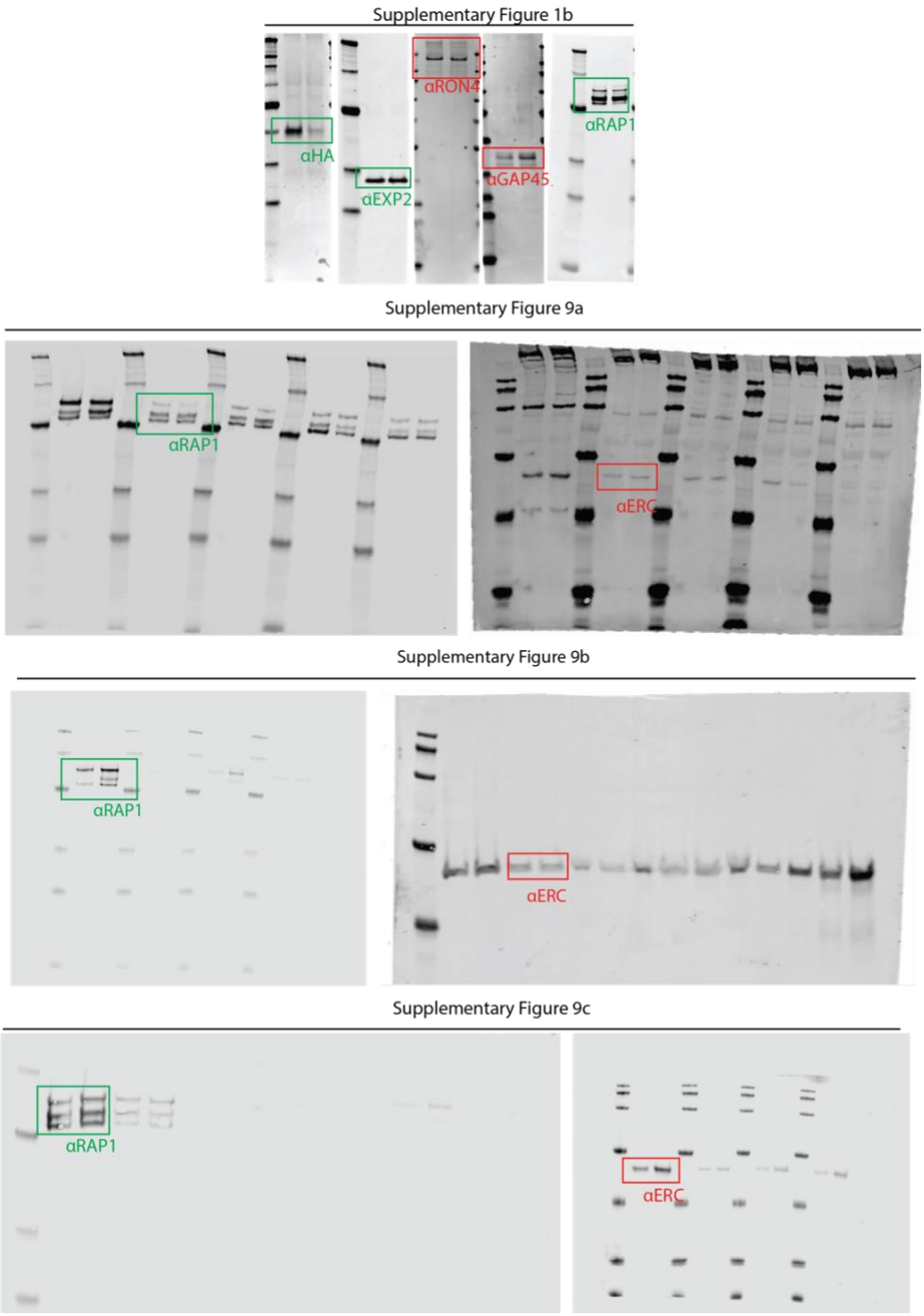

Supplementary Figure 4.13: Full length Western Blots used in Supplementary Figures 4.1 & 4.9.

Corresponding Figures and antibodies used are as indicated. Bands displayed in Supplementary Figure 4.1 and 4.9 are boxed. Bands indicated in green box were detected in the 800 nm channel. Bands indicated in the red box were detected in the 680 nm channel. Membrane 9a was probed with multiple antibodies to detect several non-size overlapping proteins at once, resulting in reduced variability between specific antigen comparisons and multiple banding patterns evident with some membranes.

Chapter 5: *Pfcerli2* arose through duplication of *Pfcerli1* and is essential for merozoite invasion by the malaria parasite *Plasmodium falciparum*.

Preface

Chapter 4 involved the functional characterisation of PfCERLI1, as well as the identification of PfCERLI2 as a protein that may share an evolutionary relationship with PfCERLI1. Chapter 5 first explores the evolutionary relationship between PfCERLI1, PfCERLI2, and their homologues in related organisms. Subsequently, PfCERLI2 is functionally characterised, showing that, like PfCERLI1, it too localises to the rhoptry bulb and its knockdown is inhibitory to merozoite invasion. Results presented in this chapter are currently unpublished but are being prepared for journal publication and so this chapter is presented in manuscript format. All experimental work presented in this chapter has been completed and so the results presented here are not subject to significant change between thesis submission, and when this work is submitted for publication.

Statement of Authorship

Title of Paper	*Pfcerli2* arose through duplication of *Pfcerli1* and is essential for merozoite invasion by the malaria parasite *Plasmodium falciparum*
Publication Status	☐ Published ☐ Accepted for Publication ☐ Submitted for Publication ☒ Unpublished and Unsubmitted work written in manuscript style
Publication Details	Liffner B, Balbin JM, Heinemann GK, Strauss J, Liu B,,Dixon MWA, Gilberger T, Wilson DW. *Pfcerli2* arose through duplication of *Pfcerli1* and is essential for merozoite invasion by the malaria parasite *Plasmodium falciparum*.

Principal Author

Name of Principal Author (Candidate)	Benjamin Liffner
Contribution to the Paper	Designed and planned the study, performed experiments and generated reagents, analysed data, wrote the manuscript.
Overall percentage (%)	40
Certification:	This paper reports on original research I conducted during the period of my Higher Degree by Research candidature and is not subject to any obligations or contractual agreements with a third party that would constrain its inclusion in this thesis. I am the primary author of this paper.
Signature	Date 02/07/20

Co-Author Contributions

By signing the Statement of Authorship, each author certifies that:

i. the candidate's stated contribution to the publication is accurate (as detailed above);
ii. permission is granted for the candidate in include the publication in the thesis; and
iii. the sum of all co-author contributions is equal to 100% less the candidate's stated contribution.

Name of Co-Author	Juan Miguel Balbin
Contribution to the Paper	Designed and planned the study, performed experiments and generated reagents, analysed data, manuscript writing. Contribution 30%
Signature	Date 3/7/20

Name of Co-Author	Gary Heinemann
Contribution to the Paper	Generated reagents. Contribution 2.5%
Signature	Date 15/07/2020

Name of Co-Author	Danny Wilson
Contribution to the Paper	Study design and planning, performed analysis and generated reagents, analysed data, manuscript writing. Contribution 15%
Signature	Date 3/7/2020

Name of Co-Author	Boyin Liu		
Contribution to the Paper	Performed transmission electron microscopy experiments Contribution 2.5%		
Signature		Date	14/07/20

Name of Co-Author	Jan Strauss		
Contribution to the Paper	Assisted with and generated phylogenetic analyses Contribution 2.5%		
Signature		Date	08/07/2020

Name of Co-Author	Matthew Dixon		
Contribution to the Paper	Study design and planning Contribution 2.5%		
Signature		Date	13/07/20

Name of Co-Author	Tim Gilberger		
Contribution to the Paper	Study design and planning, manuscript writing. Contribution 5%		
Signature		Date	7.07.2020

Pfcerli2 arose through duplication of _Pfcerli1_ and is essential for merozoite invasion by the malaria parasite _Plasmodium falciparum_.

Benjamin Liffner[1¶], Juan Miguel Balbin[1¶], Gary K. Heinemann[2], Jan Strauss[3], Boyin Liu[4], Matthew W. A. Dixon[4], Tim-Wolf Gilberger[3,5,6] Danny W. Wilson[1,7*]

[1]Research Centre for Infectious Diseases, School of Biological Sciences, University of Adelaide, Adelaide 5005, Australia.

[2]Experimental Therapeutics Laboratory, School of Pharmacy & Medical Sciences, University of South Australia Cancer Research Institute, Adelaide 5005, Australia.

[3]Centre for Structural Systems Biology, 22607 Hamburg, Germany.

[4]Department of Biochemistry and Molecular Biology, Bio21 Molecular Science and Biotechnology Institute, The University of Melbourne, Melbourne 3010, Victoria, Australia.

[5]Bernhard Nocht Institute for Tropical Medicine, 20359 Hamburg, Germany.

[6]Biology Department, University of Hamburg, 20146, Hamburg, Germany.

[7]Burnet Institute, 85 Commercial Road, Melbourne 3004, Victoria, Australia.

* Corresponding author

E-mail: Danny.wilson@adelaide.edu.au

[¶]These authors contributed equally to this work.

Abstract

Merozoite invasion of host red blood cells (RBCs) is essential for survival of the human malaria parasite *Plasmodium falciparum*. Proteins involved with RBC binding and invasion are secreted from the rhoptries, dual-club shaped organelles at the apical tip of the merozoite. Here we characterise *P. falciparum* Cytosolically Exposed Rhoptry Leaflet Interacting protein 2 (PfCERLI2), as a rhoptry bulb protein that is essential for merozoite invasion. Phylogenetic analyses show that *cerli2* arose through an ancestral gene duplication of *cerli1*, a related cytosolically exposed rhoptry bulb protein. While *cerli2* is highly conserved across most Apicomplexa, *Laverania* CERLI2 possess a unique decapeptide tandem repeat that is absent outside of this subgenus. We show that, like PfCERLI1, PfCERLI2 is essential for blood-stage growth and localises to the cytosolic face of the rhoptry bulb. Inducible knockdown of PfCERLI2 led to an inhibition of merozoite invasion following formation of the tight junction. PfCERLI2 knockdown was associated with inhibition of rhoptry antigen processing and a significant elongation of the rhoptries, suggesting that the inability of merozoites to invade is caused by aberrant rhoptry function with PfCERLI2 knockdown. These findings identify PfCERLI2 as a protein that has key roles in rhoptry biology during merozoite invasion.

Introduction

Plasmodium falciparum, a human malaria parasite, is the cause of ~400,000 deaths each year; predominantly in children under the age of five (World Health Organization 2019). *P. falciparum* is transmitted from *Anopheles* mosquitoes, its definitive host, to humans through the blood meal of an infected mosquito where invasive sporozoites are injected subcutaneously and migrate to the liver. Following invasion of liver hepatocytes, the parasite develops into thousands of daughter merozoites inside a hepatic schizont, which ruptures and releases the daughter merozoites into the blood stream where they invade red blood cells (RBCs) (Cowman, Healer et al. 2016). Over the following ~48 hours, *P. falciparum* develops inside the RBC, with each parasite forming 16-32 new daughter merozoites inside of a schizont that ruptures, releasing the merozoites that go on to infect new RBCs (Cowman, Healer et al. 2016). Replication of *P. falciparum* in this asexual blood-stage of the lifecycle is the cause of all the clinical symptoms of malaria.

RBC invasion by merozoites occurs over a period of ~30 seconds and involves the attachment of the merozoite to the RBC, which then reorients so its apical tip contacts the RBC membrane (Cowman, Tonkin et al. 2017). Specialised invasion organelles, known as the rhoptries and micronemes, then secrete their contents to form an irreversible tight junction before the merozoite pulls the RBC plasma membrane around itself; forming a parasitophorous vacuole (PV) and completing invasion (Weiss, Crabb et al. 2016). Rhoptries, which are the largest of the invasion organelles, are dual club-shaped and divided into a bulb and neck, with the neck positioned at the apical tip of the merozoite. Rhoptry neck proteins are released early in the invasion process and mediate initial attachment to the RBC and formation of the tight junction, while rhoptry bulb contents are secreted following junction formation and are typically involved in establishing the PV.

Most rhoptry proteins exclusively localise to the rhoptry bulb or neck, with minimal overlap between the two (Counihan, Kalanon et al. 2013). During the process of RBC invasion, the neck of the rhoptries fuse to the parasite plasma membrane (PPM) to allow secretion of rhoptry contents. Additionally, the dual club-shaped rhoptries fuse from neck to bulb, leaving a singular rhoptry that retains its neck and bulb structure (Hanssen, Dekiwadia et al. 2013). How compartmentalisation of rhoptry proteins occurs, along with what controls both PPM and rhoptry fusion has not been elucidated.

It is likely that both rhoptry and PPM fusion are controlled by proteins that localise to the cytosolic face of the rhoptry membrane, as they can contact both membranes to facilitate their fusion. To date, however, only three proteins in *P. falciparum* have been shown to localise to the cytosolic face of the rhoptry membrane: Armadillo repeats only (ARO) (Cabrera, Herrmann et al. 2012), ARO interacting protein (AIP) (Geiger, Brown et al. 2019), and Cytosolically exposed rhoptry leaflet interacting protein 1 (CERLI1; also known as Rhoptry apical surface protein (RASP) 2) (Suarez, Lentini et al. 2019, Liffner, Frölich et al. 2020). While all three of these proteins are essential for blood-stage growth, none have been shown to play a definitive role in either PPM or rhoptry fusion. Here we describe PfCERLI2 (Pf3D7_0405200), a paralogue of *Pfcerli1*, which localises to the cytosolic face of the rhoptry bulb membrane and is essential for merozoite invasion of RBCs.

Results

PfCERLI2 is conserved among Apicomplexa and arose from an ancestral gene duplication

Plasmodium falciparum Cytosolically Exposed Rhoptry Leaflet Interacting protein 2 (PfCERLI2) (Pf3D7_0405200) is a protein of 579 amino acids in *P. falciparum* isolate 3D7. PfCERLI2 contains a lipid-calcium binding C2 domain towards its N-terminus and possesses a decapeptide tandem repeat, with the consensus sequence QTEIkNDhi (upper case = fixed amino acid, lower case = variable amino acid) at its C-terminus, with the number of repeats varying between isolates (Figure 5.1a). PfCERLI2 shares homology (~20% amino acid identity) (Supplementary Figure 5.1) with the recently characterised protein PfCERLI1 (Suarez, Lentini et al. 2019, Liffner, Frölich et al. 2020), making them the most similar proteins to each other in the *P. falciparum* 3D7 proteome. Notably, PfCERLI1 and PfCERLI2 both possess a C2 domain towards their N-terminus as well as a short but highly conserved motif we have termed PHIS, which has the consensus sequence PHIS[-]xxP ([-] = negatively charged) in *P. falciparum*. PfCERLI2 is highly conserved amongst *Laverania* (>90% amino acid identity with *Laverania* homologues) and shares approximately 65% amino acid identity amongst more distantly related *Plasmodium* spp. (Figure 5.1b) (Supplementary Figure 5.2). Notably, PfCERLI2 shares high similarity with its homologues over the first ~420 amino acids of its sequence but this similarity decreases significantly at the C-terminal repeat region.

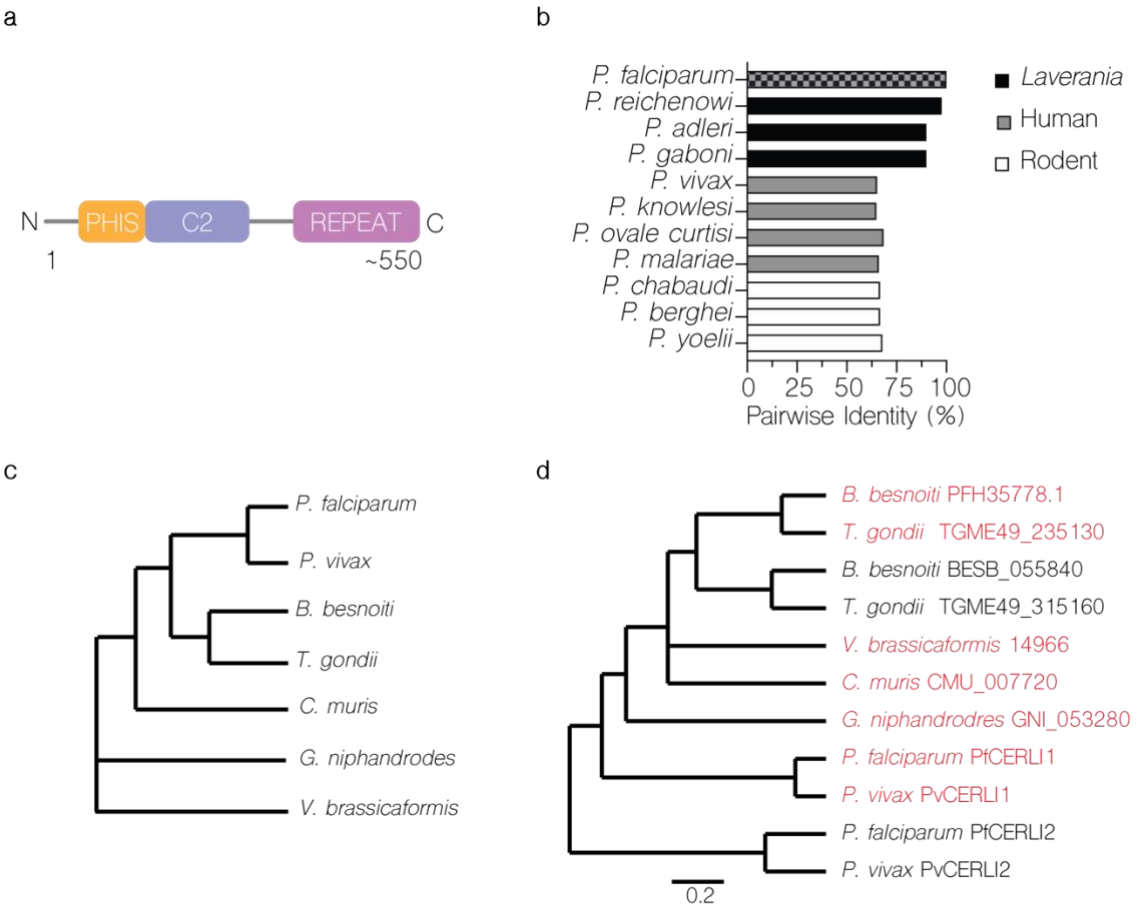
a
N
PHIS
C2
REPEAT
C
1
~550
b
P. falciparum
P. reichenowi
P. adleri
P. gaboni
P. vivax
P. knowlesi
P. ovale curtisi
P. malariae
P. chabaudi
P. berghei
P. yoelii
Laverania
Human
Rodent
0 25 50 75 100
Pairwise Identity (%)
c
P. falciparum
P. vivax
B. besnoiti
T. gondii
C. muris
G. niphandrodes
V. brassicaformis
d
B. besnoiti PFH35778.1
T. gondii TGME49_235130
B. besnoiti BESB_055840
T. gondii TGME49_315160
V. brassicaformis 14966
C. muris CMU_007720
G. niphandrodres GNI_053280
P. falciparum PfCERLI1
P. vivax PvCERLI1
P. falciparum PfCERLI2
P. vivax PvCERLI2
0.2
e
PfCERLI1
PfCERLI2
TGME49_235130
TGME49_315160
CMU_007720
Full length
C2 domain
PH Domain/
repeat

Figure 5.1: PfCERLI2 is conserved among Apicomplexa and may have evolved from an ancestral gene duplication.

(a) *PfCERLI2 is a protein of 579 amino acids in P. falciparum 3D7. Towards its N-terminus PfCERLI2 contains a motif with the consensus sequence PHIS[-]xxP we have termed PHIS, a C2 domain, and a decapeptide tandem repeat with the consensus sequence QTEIkNDhi at its C-terminus. Repeat number (10-20), and therefore PfCERLI2 amino acid length (559-659), is highly variable between P. falciparum isolates.* ***(b)*** *Amino acid sequence identity for Plasmodium spp. PfCERLI2 orthologues in Laverania, human-infecting, and rodent-infecting parasites was compared using multiple pairwise alignments.* ***(c)*** *Cladogram of evolutionary relationships between selected Apicomplexa and Chromerids.* ***(d)*** *Phylogenetic tree of PfCERLI1, PfCERLI2, and their homologues in selected Apicomplexa and Chromerids. Protein names in red are direct homologues of PfCERLI1 while those in black are direct homologues of PfCERLI2. All Accession numbers, were obtained from EuPathDB. Phylogenetic tree was constructed using unweighted pair group method with arithmetic mean (UPGMA). Branch length corresponds to amino acids substitutions per site.* ***(e)*** *Full length protein structure of PfCERLI1, PfCERLI2, their T. gondii homologues (TGME49_235130 and TGME49_315160), and their C. muris homologue (CMU_007720) was predicted using Phyre2. All proteins were predicted to have a C2 domain, and all proteins except PfCERLI2 were also predicted to contain a Pleckstrin homology (PH) domain.*

All organisms that diverged from *Plasmodium* more recently than *Cryptosporidium* contain homologues of both *Pfcerli1* and *Pfcerli2*, while earlier diverging organisms, such as *Gregarina niphandrodes* and the Chomerid *Vitrella brassicaformis*, contain only a single identifiable homologue (Figure 5.1c & d) (Supplementary Figure 5.3); suggesting that *Pfcerli1* and *Pfcerli2* are paralogues that arose from an ancestral gene duplication event. As genomic DNA (14.6 %) and amino acid (22.9 %) sequence identity is relatively low across Apicomplexa and Chromera, comparison of sequence conservation, outside of *Plasmodium*, was not able to positively identify the direct orthologues of either *Pfcerli1* or *Pfcerli2* (Supplementary Figure 5.4a). In order to identify the likely *cerli1* and *cerli2* orthologues across distantly related species, we compared gene structure of *Pfcerli1* and *Pfcerli2*, along with their homologues in Apicomplexa and Chromerids (Supplementary Table 5.1). Comparison of *cerli1* and *cerli2* orthologues across *Plasmodium spp.* indicated that *cerli1* orthologues have fewer introns and a decreased exon length than the

orthologues of *cerli2* (Supplementary Table 2). This gene structure pattern was also observed for homologues outside *Plasmodium*, allowing classification of more divergent homologues as the direct orthologue of either *Pfcerli1* or *Pfcerli2*. Using this method, we determined that the direct orthologue of *Pfcerli2* in *Toxoplasma gondii* is most likely to be TGME49_315160 (TgRASP2), which was previously reported to be the direct orthologue of *Pfcerli1* (Suarez, Lentini et al. 2019). Additionally, this classification suggests that the direct orthologue of *Pfcerli1* is TGME49_235130 (TgRASP1). As Apicomplexa and Chromerids distantly related to *P. falciparum* only possess a single homologue of *Pfcerli1* and *Pfcerli2*, we compared their gene structure to determine which gene was most likely to be the ancestral copy and which was the duplicate copy. All *Cryptosporidium spp.* homologues have an intron number and exon length similar to the *cerli1* lineage, suggesting that *cerli1* was the ancestral locus and *cerli2* the duplicated locus. There is no consistent trend in gene structure in more distantly related organisms (Gregarines or Chromerids), suggesting the gene structure may not have been conserved in more divergent organisms.

With our analysis supporting that *Pfcerli2* arose from a gene duplication event, we next assessed the selection that the *Pfcerli1* and *Pfcerli2* lineages have been under. To investigate this, we determined Ka/Ks ratios, which calculate the number of non-synonymous amino acid substitutions (Ka) relative to the number of synonymous substitutions (Ks). *Pfcerli1* and *Pfcerli2* across *Plasmodium* spp. had Ka/Ks of 0.091 and 0.29 respectively, indicating strong negative selection (favouring low sequence diversity), which is consistent with their essentiality for *P. falciparum* (Zhang, Wang et al. 2018, Suarez, Lentini et al. 2019, Liffner, Frölich et al. 2020) and *P. berghei* (Bushell, Gomes et al. 2017) blood-stage survival. This negative selection in both lineages may be indicative of subfunctionalisation in Apicomplexa, where both paralogues have maintained a subset of the function of the ancestral gene.

Interestingly, homologues of PfCERLI2 in *Plasmodium* no longer have the predicted Pleckstrin homology (PH) domain that is possessed by other homologues of PfCERLI1 and PfCERLI2 (Figure 5.1e) and has been shown to be involved in rhoptry localisation and secretion for TgRASP2(Suarez, Lentini et al. 2019). Analysis of predicted structures of PfCERLI1 and PfCERLI2 homologues outside of *Plasmodium* show that this PH domain is typically predicted to contain two sets of anti-parallel beta-sheets separated by a short alpha-helix, followed by a C-terminal helix (Supplementary Figure 5.5). By contrast, *Plasmodium* homologues of CERLI2 are predicted to possess an expanded helix between the beta-sheets that disrupts their interaction (Supplementary Figure 5.5). Additionally, PfCERLI2 is predicted to contain a much shorter C-terminal helix and a large disordered region between the beta-sheets (Supplementary Figure 5.5). Disruption of the interaction between the two sets of anti-parallel beta-sheets likely indicates that CERLI2 homologues in *Plasmodium* have a degenerated and therefore non-functional PH domain.

While the overall sequence identity between PfCERLI1, PfCERLI2, and their homologues is low, all contain the highly conserved PHIS motif, which has the consensus sequence PHPSECxP when comparing all apicomplexan/chromerid homologues (Supplementary Figure 5.4b) and PHIS[-]xxP within *P. falciparum* (Supplementary Figure 5.6). Notably, the first proline is 100% conserved, and the histidine residue is mutated only in *Gregarina niphandrodes*. Such high sequence conservation across highly divergent organisms suggests this motif is likely to be critical to the functions of PfCERLI1, PfCERLI2 and their homologues. While the function of this motif is unknown, similar motifs exist in other *P. falciparum* proteins; including the ring-expressed surface antigens (RESA, RESA2, RESA3, and RESA-like), Iron superoxide dismutase (FeSoD) and ATP-dependent Clp protease proteolytic subunit (ClpR) (Supplementary Table 5.3) (Supplementary Figure 5.6). Although the PHIS motif is a signature of PfCERLI1 and PfCERLI2,

and their apicomplexan homologues, nothing is currently known about the function of this motif or whether it has a related role in the other *P. falciparum* PHIS-containing proteins.

PfCERLI2 contains a variable copy number decapeptide tandem repeat

All PfCERLI2 homologues in *Laverania* contain a C-terminal decapeptide tandem repeat, with the consensus sequence QTIEIkNDhi in *P. falciparum*, which is not present in any homologues outside the subgenus (Supplementary Table 5.4) (Gao, Li et al. 2009). The repeat number is variable both between *P. falciparum* isolates (e.g. 10 repeats in isolate 7G8 and 20 repeats in isolate Dd2), and also between *Laverania* (9 repeats in *P. praefalciparum* and 4 repeats in *P. adleri*). It is not clear what the function of this repeat is, or what drives changes in its number. However, we noticed that all sequenced *P. falciparum* isolates have a higher number of repeats than other *Laverania*, with organisms more closely related to *P. falciparum* also displaying higher repeat numbers than those more distantly related (Supplementary Figure 5.7) (Supplementary Table 5.4). When comparing the amino acid sequences of PfCERLI2 and its Laveranian homologues without the repeat region, their identity parallels the evolutionary relatedness of different *Laverania* (Supplementary Figure 5.7). The full sequence of *Pfcerli2* is under strong negative selection across *Laverania*, with a Ka/Ks ratio of 0.3. By contrast, the repeat region of *Pfcerli2* when comparing across *Laverania* has a Ka/Ks ratio of 1.43 indicating that positive selection (favouring sequence diversity) is occurring in the decapeptide repeat region of PfCERLI2 and Laveranian homologues.

PfCERLI2 is essential for blood-stage growth.

PfCERLI2 has previously been suggested to be essential by a saturation mutagenesis screen (Zhang, Wang et al. 2018), and its homologue in *P. berghei* has also been shown to be essential for

blood-stage growth (Bushell, Gomes et al. 2017). To confirm this, we attempted to knockout *Pfcerli2* using selection linked integration targeted gene disruption (SLI-TGD) (Birnbaum, Flemming et al. 2017) but were unsuccessful, suggesting that *Pfcerli2* is indispensable for blood-stage growth (Figure 5.2a). As *Pfcerli2* was essential, we placed it under control of the glucosamine (GLCN) inducible *GlmS* ribozyme, whereby addition of GLCN leads to specific degradation of *Pfcerli2* mRNA (Figure 5.2 b&c). Additionally, we introduced a haemaglutinnin (HA) tag onto the C-terminus of PfCERLI2, allowing detection using anti-HA antibodies. Using these PfCERLI2^{HAGlmS} parasites, we harvested cultures at either ring, trophozoite or schizont stages and probed for PfCERLI2 by Western blot (Figure 5.2d). Concordant with previously published transcriptomic data (Lopez-Barragan, Lemieux J Fau - Quinones et al. 2011), PfCERLI2 was most highly expressed in schizonts. When PfCERLI2^{HAGlmS} parasites were treated from ring stages to schizonts with 2.5 mM GLCN, we saw a reduction in PfCERLI2 expression of 72% relative to untreated controls (Figure 5.2e), showing that PfCERLI2 is efficiently knocked down using the *GlmS* system.

To determine whether knockdown of PfCERLI2 altered parasite growth, we treated ring-stage PfCERLI2^{HAGlmS} and 3D7 WT parasites with increasing concentrations of GLCN and measured trophozoite-stage parasitaemia by flow cytometry 72 hours later (Figure 5.2f). At 5 mM GLCN there was ~77% decrease in the growth of PfCERLI2^{HAGlmS} parasites. However, at this high concentration of GLCN growth of 3D7 WT parasites was also affected. At a concentration of 2.5 mM GLCN, growth of PfCERLI2^{HAGlmS} parasites was inhibited by ~53%, with 3D7 WT parasites showing negligible off-target growth defects.

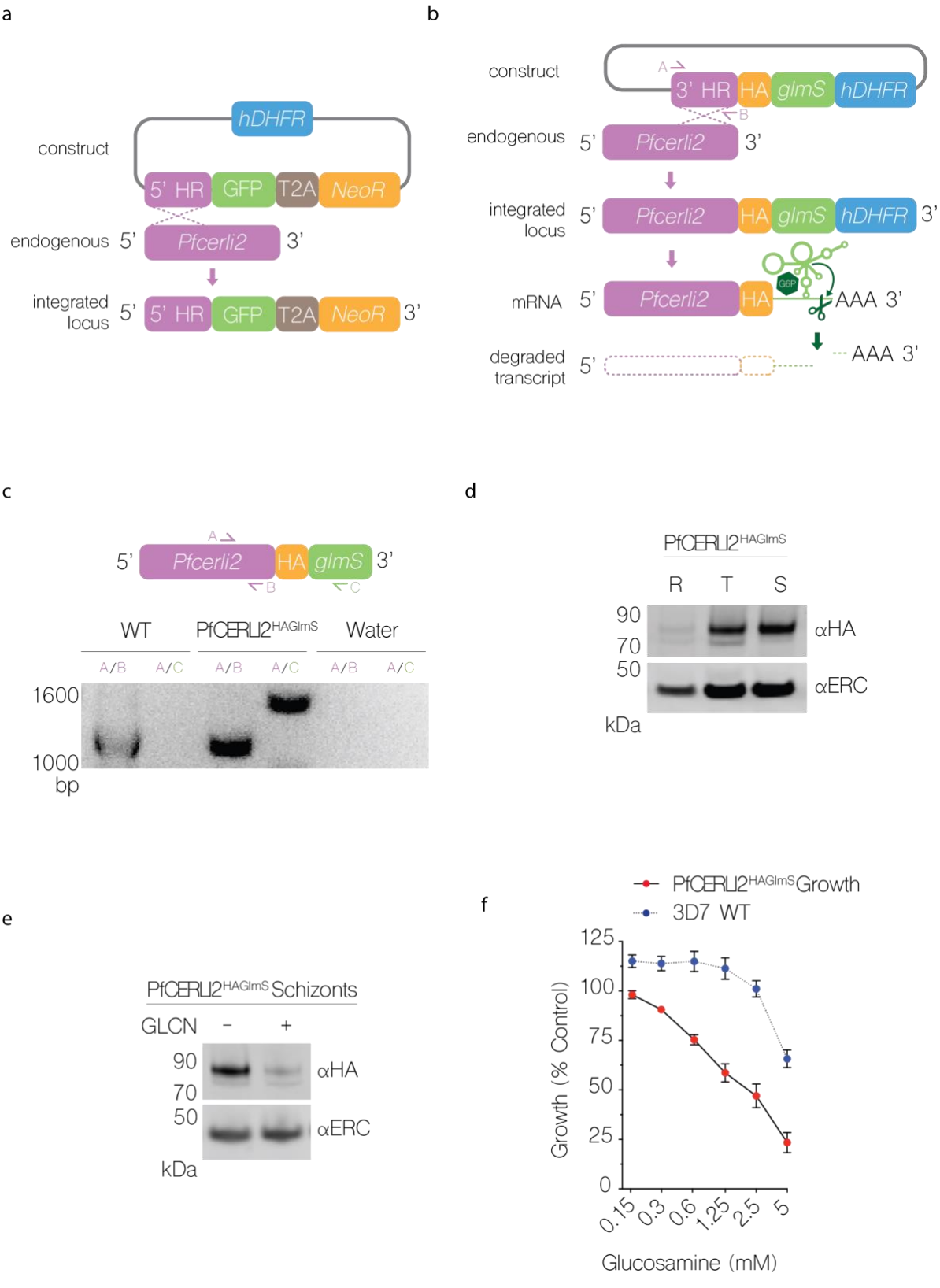
a
construct
hDHFR
5' HR
GFP
T2A
NeoR
endogenous 5'
Pfcerli2
3'
integrated locus 5'
5' HR
GFP
T2A
NeoR
3'
b
construct
A
3' HR
HA
glmS
hDHFR
B
endogenous 5'
Pfcerli2
3'
integrated locus 5'
Pfcerli2
HA
glmS
hDHFR
3'
mRNA 5'
Pfcerli2
HA
GFP
AAA 3'
degraded transcript 5'
AAA 3'
c
5'
Pfcerli2
HA
glmS
3'
A
B
C
WT
PfCERLI2HAGlmS
Water
A/B
A/C
A/B
A/C
A/B
A/C
1600
1000
bp
d
PfCERLI2HAGlmS
R
T
S
90
70
50
αHA
αERC
kDa
e
PfCERLI2HAGlmS Schizonts
GLCN
–
+
90
70
50
αHA
αERC
kDa
f
PfCERLI2HAGlmS Growth
3D7 WT
Growth (% Control)
125
100
75
50
25
0
0.15
0.3
0.6
1.25
2.5
5
Glucosamine (mM)

Figure 5.2: PfCERLI2 is essential for blood-stage growth.

(a) *Schematic representation of the selection linked integration targeted gene disruption (SLI-TGD) system used for the attempted gene knockout of Pfcerli2, which failed follwing 8 transfections.* ***(b)*** *Schematic representation of the haemaglutinnin (HA) tag, and GlmS ribozyme system used to identify and knockdown PfCERLI2. A plasmid that contained a 3' Pfcerli2 flank (2154bp-2912bp) with an HA-tag and GlmS ribyzome was transfected into 3D7 parasites by single crossover recombination. Following mRNA production, glucosamine-6-phosphate (G6P) binds to the GlmS ribozyme, leading to the cleavage of Pfcerli2 mRNA and subsequent protein knockdown.* ***(c)*** *To confirm integration of the Pfcerli2^{HAGlmS} plasmid, gDNA was harvested from transfected parasites. A Pfcerli2 specific forward primer, A, with either a Pfcerli2 specific, B (WT), or GlmS specific, C (integrated), reverse primer was used to confirm WT DNA sequence or integration of the Pfcerli2^{HAGlmS} plasmid.* ***(d)*** *Western blot of ring, trophozoite, or schizont stage PfCERLI2^{HAGlmS} lysates probed with either anti-HA (PfCERLI2) or anti-ERC (loading control) antibodies.* ***(e)*** *Western blot of PfCERLI2^{HAGlmS} schizont lysates either GLCN treated (+) or untreated (-) and probed with anti-HA (PfCERLI2) or anti-ERC (loading control) antibodies.* ***(f)*** *PfCERLI2^{HAGlmS} or 3D7 WT parasites were treated with increasing concentrations of GLCN for 72 hours, with the trophozoite-stage parasitaemia determined by flow cytometry. Growth is expressed as a percentage of an untreated media control. n=4, error bars = SEM. X-axis presented as a log 2 scale for viewing purposes.*

PfCERLI2 knockdown inhibits merozoite invasion

As PfCERLI2 was most highly expressed at schizont-stages, and its knockdown inhibited growth, we hypothesised that PfCERLI2 could be involved in schizont development, rupture, or merozoite invasion. To test this using flow cytometry, we transfected PfCERLI2^{HAGlmS} parasites with a plasmid that expresses cytosolic GFP (PfCERLI2$^{HAGlmS/GFP}$), which allows detection of newly invaded ring stages by flow cytometry. Treating PfCERLI2$^{HAGlmS/GFP}$ parasites with increasing concentrations of GLCN from trophozoite-stages for 24 hours until early ring-stages the following cycle, we saw that PfCERLI2 knockdown inhibited invasion in a dose-dependent manner (Figure 5.3a). The extent of invasion inhibition caused by PfCERLI2 knockdown was lower than growth inhibition over 72 hours, however, it is likely that this difference is caused by the shorter GLCN treatment time used for assessing inhibition of invasion.

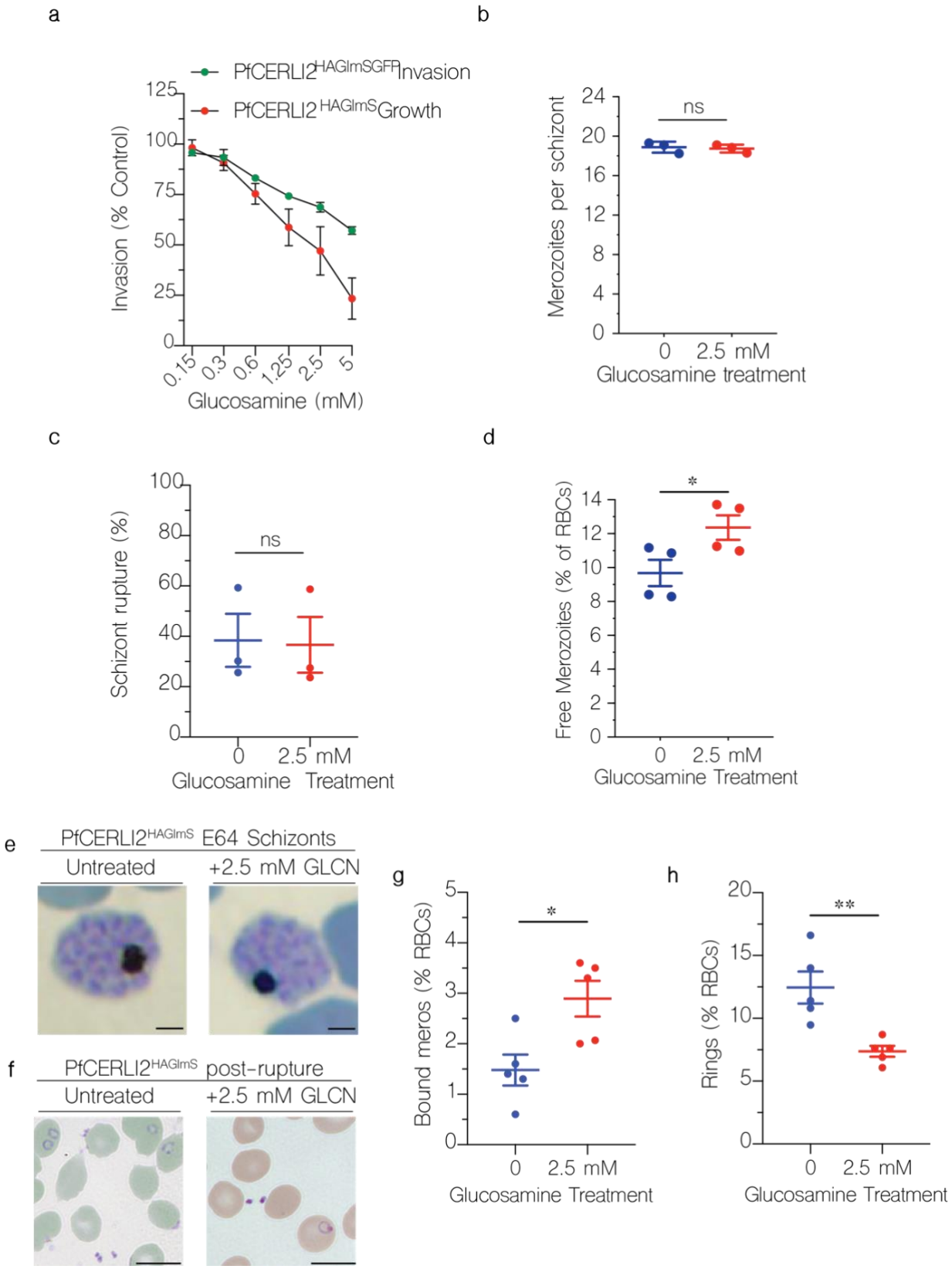
a
PfCERLI2HAGlmSGFPInvasion
PfCERLI2HAGlmSGrowth
Invasion (% Control)
125
100
75
50
25
0
0.15
0.3
0.6
1.25
2.5
5
Glucosamine (mM)
b
Merozoites per schizont
24
20
16
12
8
4
0
ns
0
2.5 mM
Glucosamine treatment
c
Schizont rupture (%)
100
80
60
40
20
0
ns
0
2.5 mM
Glucosamine Treatment
d
Free Merozoites (% of RBCs)
14
12
10
8
6
4
2
0
*
0
2.5 mM
Glucosamine Treatment
e
PfCERLI2HAGlmS E64 Schizonts
Untreated
+2.5 mM GLCN
f
PfCERLI2HAGlmS post-rupture
Untreated
+2.5 mM GLCN
g
Bound meros (% RBCs)
5
4
3
2
1
0
*
0
2.5 mM
Glucosamine Treatment
h
Rings (% RBCs)
20
15
10
5
0
**
0
2.5 mM
Glucosamine Treatment

Figure 5.3: PfCERLI2 knockdown inhibits merozoite invasion.

(a) *GFP-expressing PfCERLI2$^{HAGlmS/GFP}$ parasites were treated with increasing concentrations of GLCN from early trophozoite stages until early rings the following cycle (~24 hours), with invasion assessed by flow cytometry as the number of newly invaded rings as a percentage of an untreated media control. n=4, error bars = SEM. PfCERLI2^{HAGlmS} growth (~72 hours) is replicated from Figure 5.2f for direct comparison between growth and invasion inhibition. X-axis presented as log 2 scale for viewing purposes.* ***(b)*** *Early schizonts were treated with the egress inhibitor E64 for ~5 hours. Following treatment, cultures were smeared and the number of merozoites per schizont was determined by blinded microscopy analysis of Giemsa-stained blood smears. Each data point represents the mean number of merozoites per schizont from 20 schizonts. n=3, error bars = SEM, ns=p>0.05.* ***(c)*** *Percentage of schizonts that ruptured over a 6-hour window in either the presence or absence of GLCN, as determined by flow cytometry. n=3, error bars = SEM, ns=p>0.05.* ***(d)*** *During the invasion assay described in 3a, the number of free merozoites was also quantified by flow cytometry, with results presented as % of total RBCs. n=4, error bars = SEM, *=p<0.05 by unpaired t-test.* ***(e)*** *PfCERLI2^{HAGlmS} schizonts, either in the presence or absence of GLCN, were matured in the presence of the schizont rupture inhibitor E64 being fixed, Giemsa-stained and imaged by light microscopy. Scale bar = 2 µm. PfCERLI2^{HAGlmS} parasites were treated with 2.5 mM GLCN or left untreated, with giemsa smears made following schizont rupture* ***(f)*** *and the number of merozoites bound to RBCs* ***(g)*** *and newly-invaded rings* ***(h)*** *quantified. Scale bar = 5 µm, n=5, error bars =SEM, *=p<0.05, **=p<0.01.*

To determine if this invasion inhibition was specifically due to a defect in merozoite development, PfCERLI2^{HAGlmS} schizonts either GLCN treated or untreated, were matured in the presence of the schizont egress inhibitor E64. Knockdown of PfCERLI2 did not result in a change in the number of fully formed merozoites per schizont (Figure 5.3b) and the merozoites within the schizonts appeared morphologically normal (Figure 5.3e). To determine whether PfCERLI2 knockdown altered the ability of schizonts to rupture, the ability of both GLCN treated and untreated PfCERLI2^{HAGlmS} synchronised schizonts to rupture over a period of 6 hours was measured using flow cytometry. PfCERLI2 knockdown had no influence on the rate of schizont rupture (Figure 5.3c), suggesting knockdown has no influence on schizont development or egress. To test if PfCERLI2 knockdown directly inhibited the invasion of merozoites, we measured the number of free merozoites in the culture supernatant following invasion in both GLCN treated and untreated PfCERLI2$^{HAGlmS/GFP}$ parasites. PfCERLI2 knockdown lead to an increase in the number

of free merozoites, suggesting that a direct defect in the ability of merozoites to invade is the cause PfCERLI2 knockdown-mediated growth inhibition. From this flow cytometry based assay, it could not be determined whether these free merozoites were being inhibited prior to or after tight-junction formation and so to determine this, we made thin smears of GLCN treated and untreated PfCERLI2^{HAGlmS} ring-stage parasites and quantified the with the number of bound merozoites quantified following schizont rupture (Figure 5.3 f&g). PfCERLI2 knockdown led to a 49% increase in the percentage of merozoites bound to RBCs, suggesting that knockdown inhibits invasion following tight-junction formation. Newly invaded ring-stage parasites (Figure 5.3h) were also quantified, with GLCN treatment leading to a 41% reduction in newly invaded ring stages. These data indicate that the GLCN inducible knockdown PfCERLI2 inhibits merozoite invasion at and prior to formation of the tight-junction.

PfCERLI2 localises to the rhoptry bulb

Having determined PfCERLI2 knockdown inhibits merozoite invasion, we wanted to determine where PfCERLI2 localises in merozoites. To overcome the low peak expression level of *Pfcerli2* (Lopez-Barragan, Lemieux J Fau - Quinones et al. 2011) limiting sensitivity of traditional antibody-based immunofluorescence microscopy, we used a high affinity anti-HA biotin system (Yao, Zhang et al. 1995) that enabled reliable detection of PfCERLI2 signal in schizonts. Despite its peak transcription late in schizont development, we observed that PfCERLI2 foci were strongest in early schizonts (~44 hrs post invasion) (Figure 5.4a), but largely absent in fully mature E64-treated schizonts (~48 hrs post invasion) (Supplementary Figure 5.9). Harvesting exclusively early schizonts (~44hr post invasion), we colocalised PfCERLI2 against the markers RAP1 (rhoptry bulb), RON4 (rhoptry neck), AMA1 (micronemes) and MSP1-19 (merozoite surface) (Figure 5.4 a&b). In early schizonts, PfCERLI2 showed the strongest colocalisation with the rhoptry bulb

marker RAP1, suggesting PfCERLI2 likely localises to the rhoptry bulb (Figure 5.4a&b). For a more precise localisation of PfCERLI2, we used the super-resolution microscopy platform Airyscan, which showed that PfCERLI2 forms the donut shape characteristic of rhoptry bulb proteins (Figure 5.4c).

Repeat immunofluorescence experiments consistently showed that mature schizonts had little PfCERLI2 staining. Parallel western blots, however, showed no significant decrease in PfCERLI2 detection between early and late schizonts (Supplementary Figure 5.10). Given the lack of change in detectability by Western blot, it is likely that the HA epitope is masked or PfCERLI2 is proteolytically processed at its C-terminus late in schizont development and therefore undetectable using anti-HA antibodies.

PfCERLI2 is peripherally associated with the cytosolic face of the rhoptry bulb membrane.

To determine whether PfCERLI2 was located within the lumen of the rhoptries, or is exposed to the cytosol, we subjected PfCERLI2^{HAGlmS} schizont lysates to a proteinase protection assay. Following lysis with saponin and digitonin, which lyse the RBC membrane, PVM, and PPM, but not organellar membranes, PfCERLI2 was sensitive to proteinase K degradation (Figure 5.5a); suggesting it is exposed to the cytosol. To assess membrane association of PfCERLI2, we performed a solubility assay using lysates from PfCERLI2^{HAGlmS} schizonts (Figure 5.5b), whereby proteins are solubilised into cytosolic (hypotonic lysis), peripheral membrane (carbonate treatment), integral membrane (triton-x-100 soluble), or covalently lipid-linked (triton-x-100 insoluble) fractions. PfCERLI2 predominantly solubilised in the carbonate fraction, suggesting it is a peripheral membrane protein. Combining the localisation results with the proteinase protection and solubility assays suggest that PfCERLI2 localises to the cytosolic face of the rhoptry bulb membrane, a localisation that mirrors that of PfCERLI1 (Liffner, Frölich et al. 2020).

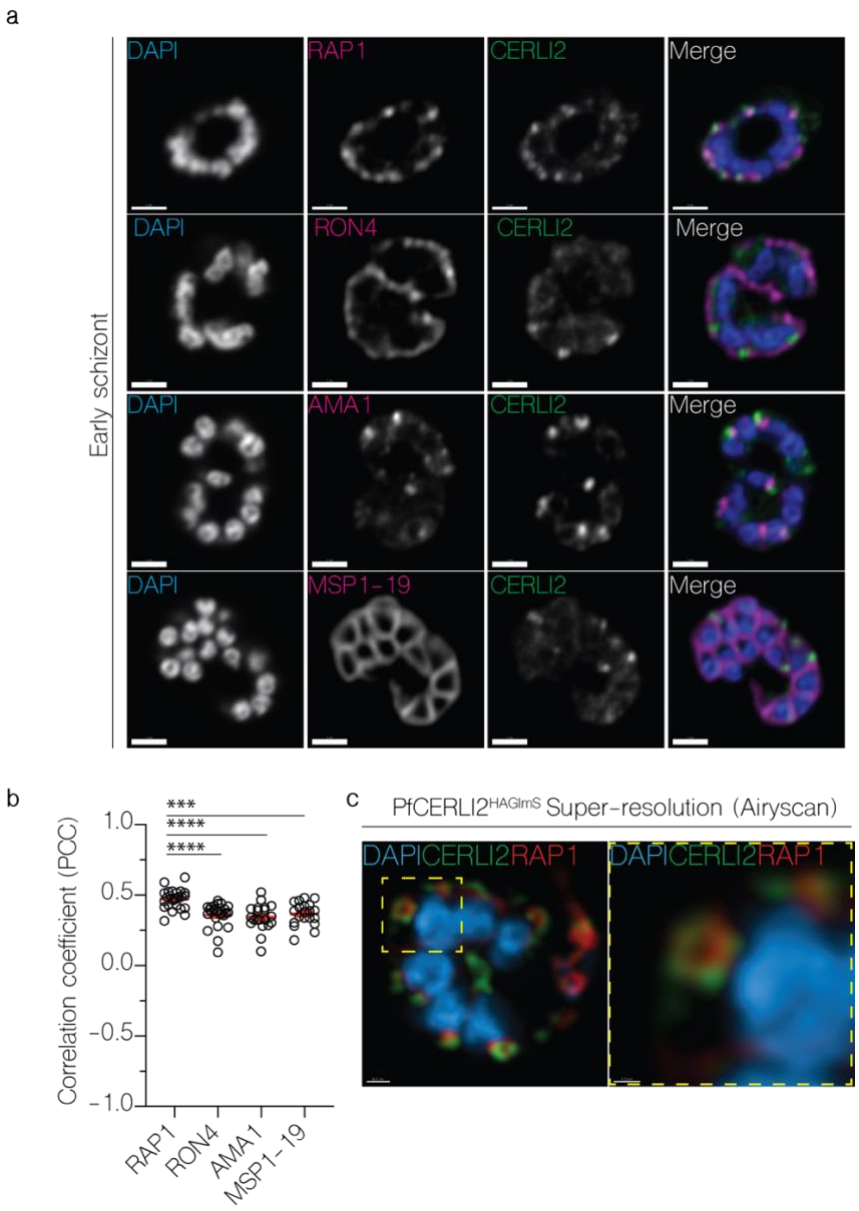

Figure 5.4: PfCERLI2 localises to the rhoptry bulb.

(a) *Immunofluorescence microscopy of early PfCERLI2^{HAGlmS} schizonts stained with DAPI (nucleus) and anti-HA (PfCERLI2) antibodies, along with antibodies to either RAP1 (rhoptry bulb), RON4 (rhoptry neck), AMA1 (micronemes), or MSP1-19 (merozoite surface). Scale bar = 2 µm* ***(b)*** *Quantification of colocalisation between PfCERLI2 and the merozoite organelle markers RAP1, RON4, AMA1 and MSP1-19. Colocalisation quantified as Pearson's correlation coefficient (PCC) when the PfCERLI2 signal was defined as the region of interest. n= 3 biological replicates, 6 schizonts per replicate. Error bars = SEM, *** = p<0.001, **** = p<0.0001.* ***(c)*** *Representative image of PfCERLI2^{HAGlmS} parasites stained with antibodies to RAP1 (rhoptry bulb) and HA (CERLI2) and imaged using the super-resolution microscopy platform Airyscan. Yellow box indicates the zoom area for the right-hand panel.*

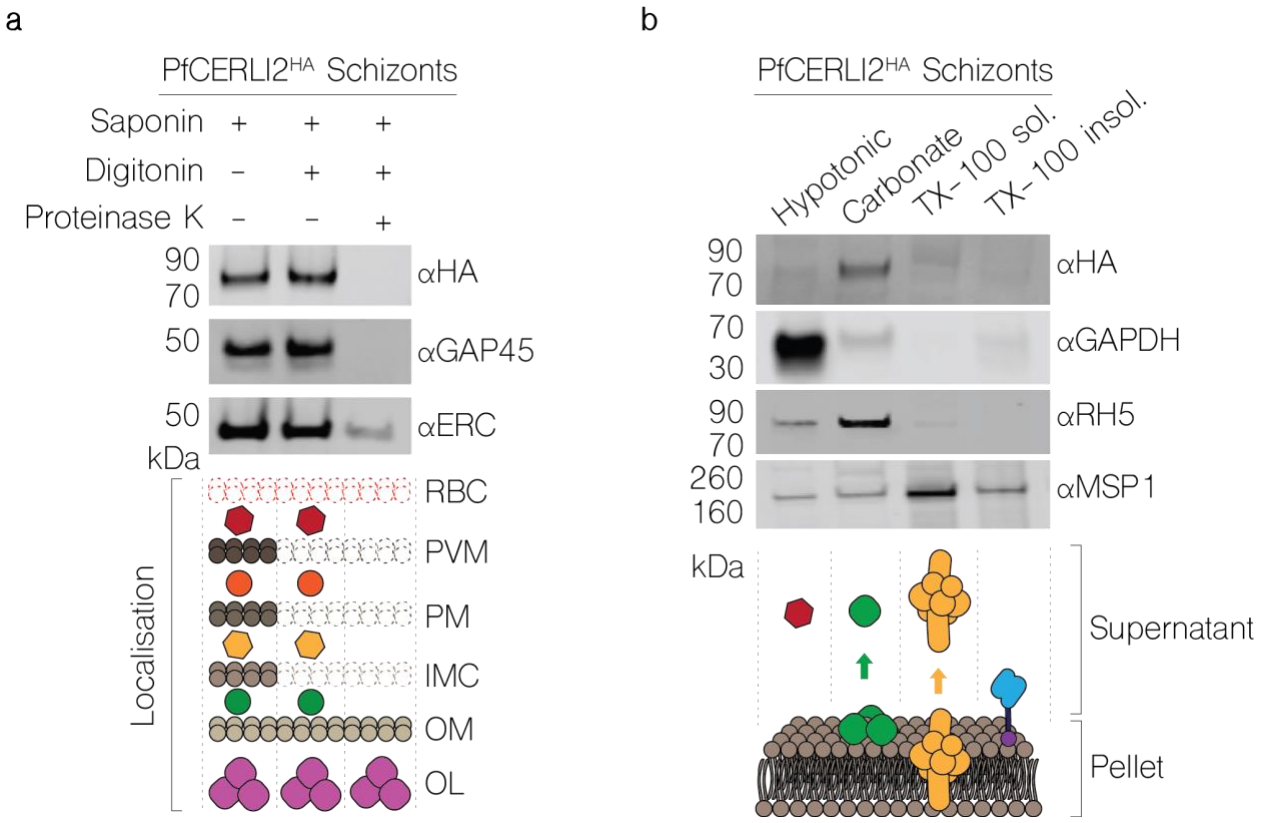

Figure 5.5: PfCERLI2 is peripherally associated with the cytosolic face of the rhoptry bulb membrane.

(a) *PfCERLI2^{HAGlmS} Schizont lysates were treated with either saponin alone, saponin and digitonin, or saponin, digitonin, and proteinase K. Saponin lyses the RBC membrane and PVM, while digitonin lyses the parasite plasma membrane but leaves the membrane of internal organelles intact. Treated lysates were then probed with anti-HA (PfCERLI2), anti-ERC (endoplasmic reticulum internal protein), or anti-GAP45 (inner-membrane complex, exposed to cytosol) antibodies with ERC and GAP45 serving as negative and positive controls, respectively, for proteinase K digestion. Images representative of 3 independent experiments. RBC = RBC membrane, PVM = PV membrane, PM = parasite plasma membrane, IMC = inner-membrane complex, OM= organellar membrane, OL = organelle lumen.* ***(b)*** *PfCERLI2^{HAGlmS} schizont lysates were subjected to differential lysis and sequential solubilisation to determine the membrane solubility of PfCERLI2. Lysates were first hypotonically lysed (cytosolic proteins), before being treated sequentially with sodium carbonate (peripheral membrane proteins) and triton-x-100 (integral membrane proteins). The supernatant was collected following each treatment, along with a final triton-x-100 insoluble fraction (covalently lipid linked proteins). Each fraction was then probed with anti-HA (PfCERLI2), anti-GAPDH (cytosolic),anti-RH5 (peripheral) and anti-MSP1 (transmembrane domain containing) antibodies. Images representative of 3 independent experiments.*

PfCERLI2 knockdown inhibits rhoptry bulb antigen processing but not secretion of rhoptry neck proteins

PfCERLI1 has previously been shown to be involved with rhoptry secretion (Suarez, Lentini et al. 2019, Liffner, Frölich et al. 2020), and given the similarities between PfCERLI1 and PfCERLI2 we wanted to determine whether PfCERLI2 was also involved in rhoptry secretion. To test the effect of PfCERLI2 knockdown on rhoptry secretion, ring-stage PfCERLI2^{HAGlmS} parasites were treated with 2.5 mM GLCN or left untreated, and treated with trypsin, chymotrypsin, and neuraminidase to prevent reinvasion. Parasites were cultured until schizont rupture when the supernatant was collected (containing secreted proteins) and a parasite lysate (containing unruptured schizonts and merozoites) were prepared for Western blot (Figure 5.6a). PfCERLI2 knockdown did not result in a defect in the secretion of the rhoptry neck antigens reticulocyte binding homologue 4 (RH4) and rhoptry neck protein 4 (RON4), or the micronemal antigen erythrocyte binding antigen 175 (EBA-175) (Figure 5.6b).

Parasite lysates from the secretion assay, containing free merozoites, were also probed with the antibodies to rhoptry bulb antigen rhoptry associated protein 1 (RAP1) (Figure 5.6a), which has previously been shown to be processed by Plasmepsin IX and subtilisin-like protease 1 (SUB1) from an 84 kDa precursor in intact schizonts into a 67 kDa mature product in free merozoites (Howard, Narum et al. 1998, Silmon de Monerri, Flynn et al. 2011, Nasamu, Glushakova et al. 2017, Favuzza, de Lera Ruiz et al. 2020). When PfCERLI2 was knocked down RAP1 processing was inhibited, leading to a substantial reduction in the mature RAP1 product and a corresponding increase in the unprocessed form (Figure 5.6c). When PfCERLI2^{HAGlmS} schizonts either with, or without, 2.5 mM GLCN were arrested prior to parasitophorous vacuole membrane (PVM) rupture with the protein kinase G inhibitor compound 1 (C1) (Taylor, McRobert et al. 2010) and probed for RAP1 (Supplementary Figure 5.11a), PfCERLI2 knockdown no longer lead to an alteration in

RAP1 processing (Supplementary Figure 5.11b). Collectively, this suggests that knockdown of PfCERLI2 inhibits the processing of RAP1 between PVM rupture and merozoite invasion, a phenotype previously demonstrated for PfCERLI1 knockdown, but not for GLCN treated 3D7 WT parasites (Liffner, Frölich et al. 2020).

PfCERLI2 knockdown alters rhoptry morphology.

While PfCERLI2 knockdown schizonts showed no gross morphological defects, we wanted to determine if PfCERLI2 knockdown altered the morphology or biogenesis of internal organelles. We matured GLCN treated or untreated 3D7 WT and PfCERLI2^{HAGlmS} schizonts in the presence C1 and subsequently fixed and imaged these mature schizonts using thin-section transmission electron microscopy (TEM) (Figure 5.6d). PfCERLI2^{HAGlmS} schizonts that had not been treated with GLCN were morphologically indistinguishable to both GLCN treated and untreated 3D7 WT parasites. By contrast, GLCN treated PfCERLI2^{HAGlmS} parasites appeared to contain noticeably elongated rhoptry necks. When rhoptry length was quantified, rhoptries of GLCN treated PfCERLI2^{HAGlmS} parasites were on average ~90 nm, and up to >400 nm, longer than those in untreated parasites (Figure 5.6e). Thus, PfCERLI2 knockdown alters rhoptry morphology and is associated with incomplete processing of the rhoptry bulb protein RAP1, suggesting that PfCERLI2 plays key roles in rhoptry biology.

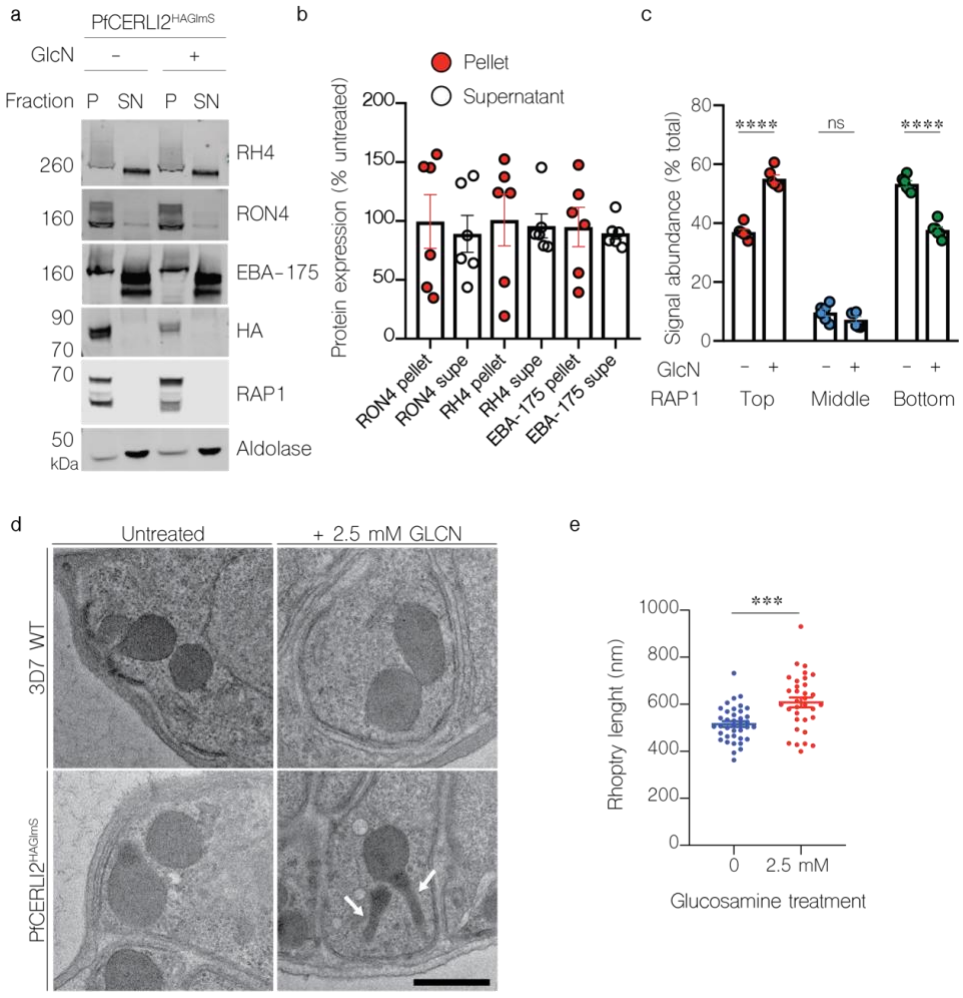

Figure 5.6: Knockdown of PfCERLI2 inhibits rhoptry antigen processing, but not secretion, and is associated with rhoptry malformation.

(a) *PfCERLI2^{HAGlmS} ring-stage parasites were GLCN treated (+) or left untreated (-), before enzyme treatment of RBCs to prevent reinvasion. Lysates (P) and culture supernatants (SN) were harvested following schizont rupture and probed with anti-RH4, anti-RON4 (rhoptry neck), anti-EBA-175 (microneme), anti-HA (PfCERLI2), anti-RAP1 (rhoptry bulb), or anti-aldolase (loading control) antibodies. Representative blots of 5 biological replicates shown.* ***(b)*** *Western blots were normalised to the loading control, aldolase, and quantified, with results displayed as protein expression in GLCN treated sample as a percentage of the untreated signal. n=5 biological replicates.* ***(c)*** *Quantification of individiual band intensities, as a percentage of the total signal, from RAP1 signals using the parasite lysates from the secretion assay. n=5 biological replicates.* ***(d)*** *Transmission electron microscopy of C1 schizont arrested PfCERLI2 and 3D7 WT parasites, either in the presence or absence of GLCN. Representative images from 3 biological replicates.* ***(e)*** *Quantification of rhoptry length from PfCERLI2^{HAGlmS} TEM images. n=3 biological replicates. ns= p>0.05, *** = p<0.001, **** = p<0.0001 by two-way ANOVA. Error bars = SEM.*

To further investigate the elongation of the rhoptries we observed by electron microscopy we performed Airyscan immunofluorescence microscopy on either untreated or 2.5 mM GLCN treated PfCERLI2^{HAGlmS} parasites, with rhoptry bulb and neck markers RAP1 and RON4. We then measured the distance between the basal end of the nucleus and the centre of the RAP1 (Figure 5.7a) or RON4 (Figure 5.7b) focus, with the hypothesis that elongated rhoptries would bring these foci closer to the nucleus. In GLCN treated parasites, we consistently observed a shorter distance between the nucleus and both RAP1 (Figure 5.7c) and RON4 (Figure 5.7d) foci, supporting the observation of rhoptry elongation following PfCERLI2 knockdown.

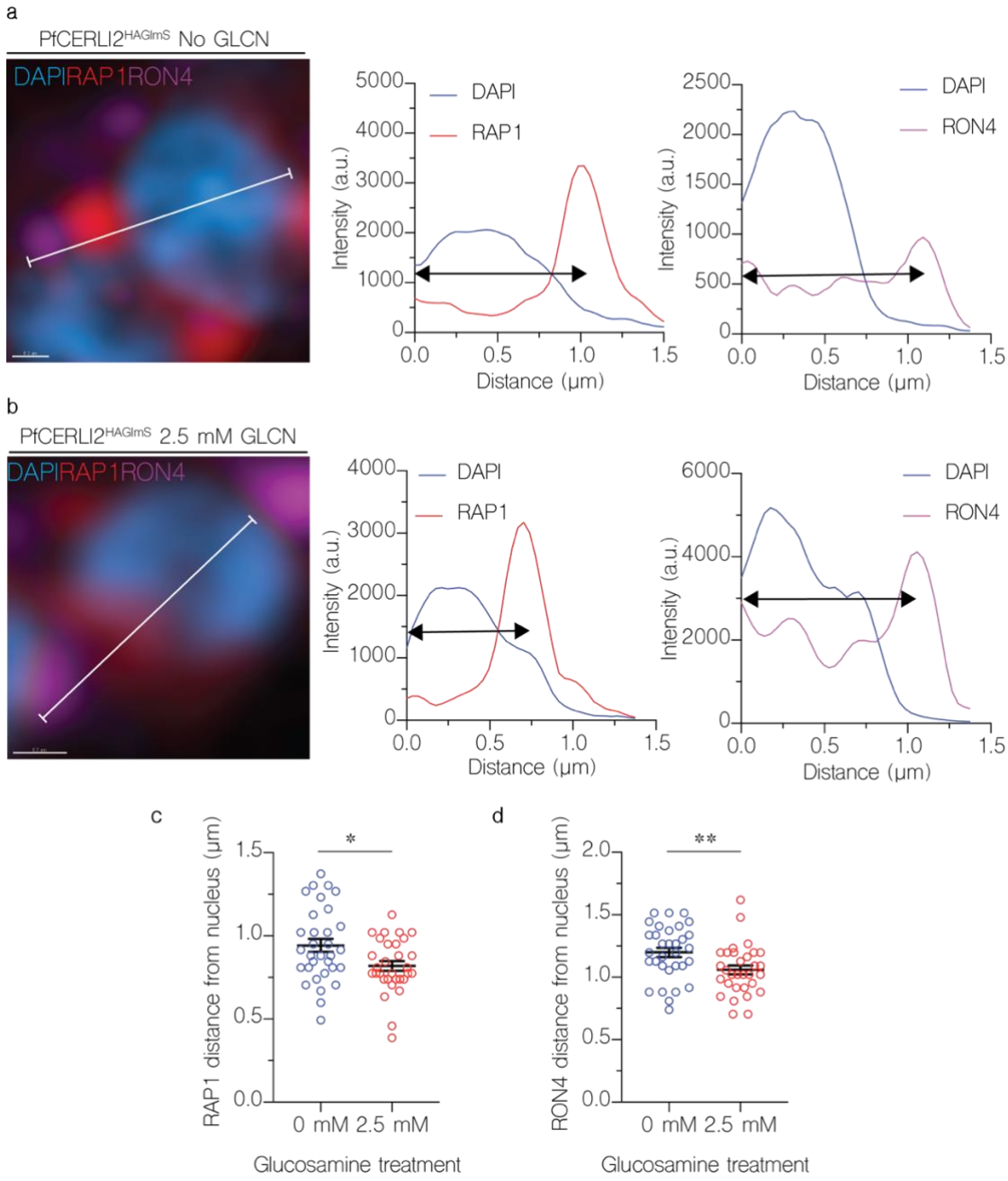

Figure 5.7: Knockdown of PfCERLI2 alters rhoptry antigen positioning

*PfCERLI2^{HAGlmS} schizonts were matured in the presence of E64, stained with antibodies against RAP1 (rhoptry bulb) and RON4 (rhoptry neck), and imaged by Airyscan super-resolution microscopy. The flourescence intensity of RAP1 and RON4 signals was then measured from the basal end of the nucleus and plotted against merozoite length for parasites that were either left untreated **(a)** or treated with 2.5 mM GLCN **(b)**. These distances were then plotted for both RAP1 **(c)** and RON4 **(d)**. * = p<0.05, ** = p<0.01 by two-tailed t-test. 32 merozoites for untreated and 31 merozoites for 2.5 mM GLCN treated were measured from a total of 12 schizont images across three biological replicates. Error bars = SEM.*

Discussion

We, along with others, had previously identified the rhoptry bulb protein PfCERLI1 and determined that it played an essential role in merozoite invasion and rhoptry secretion (Suarez, Lentini et al. 2019, Liffner, Frölich et al. 2020). Bioinformatic searches identified PfCERLI2 as a protein potentially related to PfCERLI1 based on their amino acid sequence homology. Here, we have shown that *cerli2* likely arose through ancestral gene duplication of *cerli1*. Furthermore, we have shown that like PfCERLI1, PfCERLI2 also localises to the cytosolic face of the rhoptry bulb, is essential for merozoite invasion and has important functions in rhoptry biology.

A previous study identified a growth inhibitory monoclonal antibody, known as M26-32, which was suggested to bind to PfCERLI2 and was reported to localise this protein to the merozoite surface (Gao, Li et al. 2009). However, it had also been shown that MG26-32 reacted with multiple *P. falciparum* proteins, and that the peptide it recognised was contained in many proteins (Cheng, Jones et al. 1991). Our results indicate, using endogenous tagging of PfCERLI2, that it localises to the rhoptry bulb of developing schizonts. This implicates PfCERLI2 in rhoptry function rather than having a role on the merozoite surface.

PfCERLI2 solubilised overwhelmingly in the carbonate treatment, suggesting it is perhipherally associated with the rhoptry bulb membrane. PfCERLI1 was present in both the carbonate and triton-x100 insoluble fractions, which we hypothesised may be a result of strong cooperative membrane association through its C2 domain, PH domain, and palmitoylation site (Liffner, Frölich et al. 2020). By contrast, PfCERLI2 appears to lack a functional PH domain and the palmitoylation site possessed by PfCERLI1. In the *Toxoplasma gondii* homologue of PfCERLI2 (TGME49_315160, also known as TgRASP2), the PH domain (degenerated in PfCERLI2) is involved in, but not essential for, rhoptry localisation and secretion (Suarez, Lentini et al. 2019). Based on evidence from its *T.* gondii homologue and the lack of a functional PH

domain and palmitoylation site, we suggest that PfCERLI2 localises to the cytosolic face of the rhoptry bulb membrane predominantly through lipid interactions with its C2 domain.

Knockdown of PfCERLI2 led to reduced parasite growth and merozoite invasion. Following PfCERLI2 knockdown, merozoite containing schizonts appeared morphologically normal, and displayed no defect in schizont rupture. Using flow cytometry, we observed a significant increase in the number of free merozoites, indicating that loss of PfCERLI2 inhibited merozoite invasion directly. The fact that we were able to measure an increase in free merozoites suggests that some of the PfCERLI2 deficient merozoites were unable to form the tight-junction or remain attached to the RBC after invasion was stopped. By assessing Giemsa stained thin smears, we found that PfCERLI2 knockdown also causes a significant increase in the number of merozoites that bind to RBCs and fail to invade. The increase in RBC bound merozoites following PfCERLI2 knockdown suggests that rhoptry neck and micronemal protein contents were secreted for PfCERLI2 deficient merozoites, and the tight junction formed for some of these, but these merozoites were then unable to proceed with invasion. The fact that we saw no reduction in secretion of the rhoptry neck proteins RON4 and RH4 following CERLI2 knockdown supports the idea that in many cases PfCERLI2 knockdown parasites can secrete enough protein to form the tight junction, but these merozoites fail to invade due to a later-occurring defect.

The presence of a prominent decapeptide repeat region at the C-terminus of PfCERLI2 is a differentiating feature compared to PfCERLI1. Based on its differential evolution relative to the rest of the PfCERLI2 protein, and its exclusive presence in *Laverania*, we hypothesise that the decapeptide tandem repeat number may be under positive selection, whereas amino acids outside the repeat region are under negative selection. It has previously been reported that the decapeptide tandem repeat contains highly immunogenic antigens that bind malaria-exposed serum antibodies (Gao, Li et al. 2009). A potential mechanism for the positive selection of the PfCERLI2 repeat

could therefore be classical antibody selection. However, our data using endogenously tagged PfCERLI2 shows that the protein localises to the cytosolic face of the rhoptry bulb membrane and has a role in the function of this organelle, making it unlikely that PfCERLI2 is significantly exposed to the host immune system and antibody selection. We therefore suggest that the PfCERLI2 repeat may have an as yet unidentified function in *P. falciparum* whose evolution is under positive selection based on its Ka/Ks value of 1.43 across *Laverania*. Amongst *P. falciparum* isolates, repeat number varies and it is currently unclear whether the same occurs among different isolates of all *Laverania*, or whether this is a unique property of PfCERLI2. Given the conservation of the repeat sequence in *P. falciparum*, but the variation in repeat number, we can speculate that this variation in repeat number has an important role in this protein's function between isolates.

Due to the presence of two paralogous genes in all coccidians and haematozoa, it is likely that *cerli1* was duplicated in the most recent common ancestor of these related parasite lineages. By contrast, all more divergent Apicomplexans and Chromerids contain only a single *cerli* gene and it is therefore likely that the most recent common ancestor of the Apicomplexa and Chromerids also only possessed a single *cerli* gene, making it likely that there was originally only a single *cerli* gene in the more distant ancestors of coccidia and haematozoa. *Cryptosporidium* is more divergent than coccidia and haematozoa and contain only a single CERLI homologue. As the gene structure of the *Cryptosporidium cerli* homologue is highly similar to that of *cerli1* across other Apicomplexa, we suggest that *cerli1* was the ancestral gene and *cerli2* the duplicated gene. From studies of both PfCERLI1 and PfCERLI2, it is clear that both proteins have functional similarities due to their stage of expression and localisation, along with their knockout and knockdown phenotypes (Zhang, Wang et al. 2018, Suarez, Lentini et al. 2019, Liffner, Frölich et al. 2020). Additionally, in *Toxoplasma gondii* it has been reported that TgRASP1 and TgRASP2 form a complex (Suarez, Lentini et al. 2019), but it not clear if this occurs in other Apicomplexa. For the

coccidia and haematozoa containing *cerli* paralogues, it is likely that the duplicated *cerli2* locus contributed to the function of the ancestral CERLI protein, through subfunctionalisation. This is supported by shared characteristics of PfCERLI1 and PfCERLI2, along with the strong negative selection CERLI2 has been under across Apicomplexa. A potential mechanism for this subfunctionalisation may have been the direct binding of CERLI1 to CERLI2, which could constrain CERLI2 sequence variation.

CERLI2 homologues in coccidia and haematozoa possess a PH domain towards their C-terminus that is under negative selection. The exception to this is the genus *Plasmodium*, where CERLI homologues instead contain a degenerated and likely non-functional PH domain. Additionally, PfCERLI2 homologues in the *Laverania* subgenus of *Plasmodium* also have a decapeptide tandem repeat that is under positive selection. While it is not clear what the function of this repeat region is, the likely absence of the PH domain's lipid-binding function (Suarez, Lentini et al. 2019) and presence of the decapeptide repeat region may indicate that CERLI2 in *Laverania* has undergone neosubfunctionalisation, where following subfunctionalisation one paralogue adopts a new function. We can therefore speculate that CERLI2 homologues in *Laverania* may have modified functions or different protein-protein/protein-lipid interactions compared to homologues outside this subgenus.

Methods

Bioinformatic analyses

PfCERLI2 (Pf3D7_0405200), PfCERLI1 (Pf3D7_0210600) and orthologous sequences used for comparison *of Pfcerli1* and *Pfcerli2* gene structure from *Babesia bigemina* (BBBOND_0209090, BBBOND_0311360), *B. bovis* (BBOV_IV005720, BBOV_III003780), *Cryptosporidium andersoni* (cand_006180) *C. hominis* (Chro.60252), *C. muris* (CMU_007720), *C. parvum* (cgd6_2143), *C. tyzzeri* (CTYZ_00001395), *C. ubiquitum* (cubi_02338), *Chromera Velia* (Cvel_21914), *Cyclospora Cayetanensis* (cyc_01372), *Cystoisopora Suis* (CSUI_005102), *Cytauxzoon Felis* (CF002482, CF003293), *Eimeria brunetti* (EBH_0041390), *G. niphandrodes* (GNI_053280), *N. caninum* (NCLIV_057920, NCLIV_049720), *P. reichenow*i (PRCDC_0402800, PRCDC_0209500), *P. malariae* (PmUG01_03015300, PmUG01_04021700), *P. ovale* (PocGH01_03012700, PocGH01_04019500), *P. knowlesi* (PKNH_0303300, PKNH_0410600), *P. vivax* (PVP01_0304600, PVP01_0414300), *P. berghei* (PBANKA_1002900, PBANKA_0307500), *P. yoelii* (PY17X_1004300, PY17X_0308100) and *P. chabaudi* (PCHAS_1003800, PCHAS_0309700), *S. neurona* (SN3_01800355, SN3_00600405), *T. annulata* (TA21020, TA12010), *T. equi* (BEWA_030720, BEWA_019330), *T. gondii* (TGME49_315160, TGME49_235130), *T. orientalis* (TOT_010000334, TOT_020000207), *V. brassicaformis* (Vbra_14966) were obtained by searching within the EuPathDB.org database (Aurrecoechea, Barreto et al. 2016). Additionally, homologues of PfCERLI2 from the Laveranian parasites *P. adleri* (PADL01_0404800), *P. billcollinsi* (PBILCG01_0404100), *P. blacklocki* (PBLACG01_0402700), *P. gaboni* (PGABG01_0403400), *and P. praefalciparum* (PFRFG01_0404700) were obtained by searching within the PlasmoDB.org database (Aurrecoechea, Brestelli J Fau - Brunk et al. 2008).

Both pairwise and multiple sequence alignments were generated using Geneious 9.1.3 (Biomatters) using a Geneious global alignment with free end gaps (gap open penalty = 12, gap extension penalty = 3) algorithm with the Blosum62 cost matrix. All phylogenetic trees were constructed using the Jukes-Cantor genetic distance model and were built using the unweighted pair group method with arithmetic mean (UPGMA) tree build method.

To identify *P. falciparum* proteins that contained a PHIS, or PHIS-like motif, the PHIS sequence from PfCERLI1, PfCERLI2, or the consensus sequence generated from their Apicomplexan homologues was used in a BLASTp search against the *P. falciparum* 3D7 proteome.

Ka/Ks ratios were calculated using the online Ka/Ks Calculation tool (http://services.cbu.uib.no/tools/kaks) (Liberles 2001, Siltberg and Liberles 2002) using the maximum likelihood tree method, discrete_Grantham submatrix, and a LI rate of moderate. Where Ka/Ks ratios are reported, they were generated using the same coding sequences as the corresponding phylogenetic tree.

Protein structure prediction

The protein structure of PfCERLI1, PfCERLI2, along with their homologues in *T. gondii* (TGME49_235130, TGME49_31516) and *C. muris* (CMU_007720) was predicted using the online protein structure prediction tool Phyre2 on intensive mode (Kelley, Mezulis et al. 2015). All predicted structures were visualised, presented and imaged using either Jmol or EzMol (Jmol , Reynolds, Islam et al. 2018).

Continuous culture of asexual stage *P. falciparum*

P. falciparum 3D7 parasites were cultured in O^+ red blood cells (Red Cross Blood Service Australia) as previously described (Trager and Jensen 1976). Parasites were grown in RPMI-

HEPES media (Sigma-Aldrich) supplemented with 0.5% v/v Albumax (Gibco), 52 μM gentamycin (Gibco), 367 μM hypoxanthine (Sigma-Aldrich), 2 mM L-Glutamax (Gibco) and 2 mM sodium bicarbonate (Thermo Fisher Scientific), adjusted to a pH of 7.4. Cultures were maintained at 37ºC in sealed acrylic boxes with the following gas composition: 1% O2, 5% CO2 and 94% N2.

Plasmid construction and transfection

List of genetic constructs in this study: *Pfcerli2*^{HAGlmS}, *Pfcerli2*$^{HAGlmS/GFP}$, *Pfcerli2*$^{SLI\text{-}TGD}$.

Pfcerli2^{HAGlmS} riboswitch transfection vectors were prepared from a PTEX150^{HAGlmS} plasmid backbone (Elsworth, Matthews et al. 2014). A 758 base pair homology region of *Pfcerli2* was PCR amplified from the 3' end of the genomic sequence of 3D7 gDNA using the primers *Pfcerli2* 5' F RBW (GGT**AGATCT**GAAGGAATCTTTTGGAGATGAGC) and *Pfcerli2* 3' R RBW (GGT**CTGCAGC**TATATTTTGTATGGTATTTTCTAATTGTGC). Each of the resulting PCR products were digested with the restriction enzymes BglII and PstI (indicated in bold in primer sequence) and cloned into the PTEX150^{HAGlmS} vector.

To generate the *Pfcerli2*$^{HAGlmS/GFP}$ parasite line, which expresses cytosolic GFP, the pHGBrHrBl-1/2 GFP plasmid was used, without modification (Wilson, Crabb et al. 2010).

For disruption of *Pfcerli2* using selection linked integration – targeted gene disruption (SLI-TGD) system, a source SLI-TGD vector (Pf3D7_1463000 SLI-TGD) was used (Birnbaum, Flemming et al. 2017). A 772 bp homology region of *Pfcerli2* was PCR amplified using the primers *Pfcerli2* SLI-TGD F (GGT**GCGGCCGCT**CCACATATAAGTGATTTCGAGCC) and *Pfcerli2* SLI-TGD R (GGT**ACGCGT**CCTTGCACACTTCTTGTCC). Both PCR products, and the SLI-TGD vector were then digested with NotI and MluI (restriction sites in bold) and ligated together.

P. falciparum 3D7 parasites were transfected by RBC loading (Deitsch, Driskill et al. 2001) (*Pfcerli2*^{HAGlmS}, *Pfcerli2*$^{HAGlmS/GFP}$) or schizont loading (Moon, Hall et al. 2013) (*Pfcerli2*$^{SLI\text{-}TGD}$). For RBC loading, uninfected RBCs were centrifuged at 440 rcf for 1 min, washed in culture media and then washed in cytomix (0.895% KCl, 0.0017% $CaCl_2$, 0.076% EGTA, 0.102% $MgCl_2$, 0.0871% K_2HPO_4, 0.068% KH_2PO_4, 0.708% HEPES). Washed RBCs were then resuspended in cytomix containing 200 μg of the plasmid of interest. The combined RBCs and DNA were transferred to a 0.2 cm cuvette (Bio-Rad) to be electroporated (Bio-Rad) at 0.31 kV with a capacitance of 960 uF. Electroporated RBCs were rinsed from the cuvette with culture media, centrifuged at 440 rcf for 1 min, and washed twice before being introduced to cultures of gelatin-purified schizont stage parasites. Alternatively for schizont loading, 3-5 % parasitaemia 40 hr schizont parasitaemia cultures were Percoll-purified and replaced in culture treated with 2 μM 4-[2-(fluorophenyl)-5-(1-methylpiperidine-4-yl)-1H-pyrrol-3-yl] pyridine (Compound 1, C1) (Taylor, McRobert et al. 2010) for 2 hr in order to allow schizonts to fully develop their merozoites but arrest egress. Once developed, cultures were then centrifuged at 440 rcf for 5 min and washed in culture media to remove C1 before being transferred to 1.5 mL tubes and shaken at 37 ^oC for 20 min. After shaking, schizonts were resuspended in P3 primary cell solution containing 50 μg of the plasmid of interest, and electroporated using a 4D Nucleofector (Lonza) on program FP158. Electroporated parasites were placed into 1.5 mL tubes with culture media and 200 μL uninfected RBCs and shaken at 37^oC for 20 min to promote merozoites to invade, before being placed back into culture. To generate *Pfcerli2*^{HAGlmS}, 5 nM WR99210 (Jacobus Pharmaceuticals) drug treatment was used to select for integration of the HA-*GlmS* construct over 3 cycles. For *Pfcerli2*$^{HAGlmS/GFP}$, the HA-*GlmS* line was transfected with the pHGBrHrBl-1/2 construct in order to episomally express cytosolic GFP then selected for using 5 μg/mL blasticidin-S-deaminase HCl (Merck Millipore). To generate *Pfcerli2*$^{SLI\text{-}TGD}$, maintenance of the SLI-TGD construct was selected using

4 nM WR99210 and integrants were selected using 400 μg/mL G418 (geneticin, Thermo Fisher). *Pfcerli2*$^{SLI\text{-}TGD}$ plasmids were transfected into eight independent cultures, which all grew on WR99210 and were selected with G418 for eight weeks.

Assessment of *in vitro* blood stage growth and invasion

To investigate the effects of *Pfcerli2* knockdown on parasite growth 3D7 and *Pfcerli2*^{HAGlmS} cultures were synchronised to ring-stages using sorbitol lysis and adjusted to 1% parasitaemia at 1% haematocrit in 96 well U-bottom plates (Corning) as previously described (Wilson, Langer et al. 2013).From this adjusted culture, 45 μL was then suspended in 5 μL of a 10 x stock of D-(+)-glucosamine hydrochloride (hereby referred to as GLCN, Sigma-Aldrich) or media to a final volume of 50 μL. Plates were then incubated in standard culture conditions for 72 hours, until trophozoite stages the following cycle. Completed assays were then stained in 10 μg/mL ethidium bromide (Bio-Rad) in PBS and the final parasitaemia was assessed using the BD Accuri^{TM} C6 Plus flow cytometer (PE-H, FSC-H filters for growth, PE-H, FITC-H for invasion to visualise GFP-fluorescent ring stages). All flow cytometry files were analysed using FlowJo Version 10 (Tree Star).

To investigate the effect of *Pfcerli2* knockdown on invasion, *Pfcerli2*^{HAGlmS} cultures were synchronised to early trophozoite stages using sorbitol lysis and adjusted to 1% parasitaemia at 1% haematocrit and placed in 96 well U-bottom plates and set up as described for growth assays. Plates were subsequently incubated in standard culture conditions for 24 hours, until early ring stages the following cycle. Completed assays were stained with ethidium bromide and analysed by flow cytometry as described for growth assays.

To observe whether PfCERLI2 knockdown had an impact on merozoite quantity per schizont or merozoite morphology, *Pfcerli2*^{HAGlmS} parasites were treated with or without 2.5 mM

GLCN at ring stages until matured into 40 hr schizonts. To ensure full merozoite development, schizonts were arrested with E64 for 4 hrs to prevent rupture and then smeared as a thin blood film. Smears were fixed in 100% v/v methanol and stained in 10% v/v Giemsa (Merck Millipore) in water and then blindly assessed by light microscopy (n = 20 individual schizonts). To count free merozoites, *Pfcerli2*$^{HAGlmS/GFP}$ schizonts +/- 2.5 mM GLCN without E64 were permitted to incubate until rupture and gated for merozoites by flow cytometry as described above.

Schizont rupture assay

To observe whether PfCERLI2 knockdown affected schizont rupture and merozoite egress, synchronous *Pfcerli2*^{HAGlmS} ring stages were treated in duplicate with or without 2.5 mM GLCN in 96-well U bottom plates as described above. Parasites were permitted to grow into schizonts prior to rupture and the parasitaemia was recorded by flow cytometry. Plates were then incubated for an additional 6 hrs to allow for schizont rupture followed by a second round of parasitaemia measurement by flow cytometry. To calculate the percentage of schizont rupture within this time window, the following equation was used:

$$\% \text{ schizont rupture} = \left(\frac{post-rupture\ schizontaemia}{pre-rupture\ schizontaemia}\right) \times 100$$

Bound merozoite assay

To determine whether PfCERLI2 knockdown inhibited merozoite invasion prior to, or following, tight junction formation PfCERLI2^{HAGlmS} ring-stage parasites were either treated with 2.5 mM GLCN or left untreated and incubated until schizont rupture. Following schizont rupture, Giemsa-stained smears were made of these cultures without washing or removing the culture

medium and were blinded and counted to determine the number of bound merozoites and newly invaded rings in each treatment. For each treatment >1000 RBCs were counted per replicate.

Saponin lysis and Western blot

To prepare protein samples, high parasitaemia cultures were lysed in 0.15% w/v saponin (ThermoFisher Scientific) on ice for 10 min, centrifuged at 16000 rcf, washed once in 0.075% w/v saponin and twice in PBS. All lysis reagents included protease inhibitors (CØmplete, Roche). Parasite lysates were DNase I treated (Qiagen) for 5 min at room temperature before being resuspended in reducing sample buffer (0.125 M Tris-HCl pH 7, 20% v/v glycerol, 4% v/v SDS, 10% v/v β-mercaptoethanol (Sigma-Aldrich), 0.002% w/v bromophenol blue (Sigma-Aldrich)). Protein lysates were separated by size on SDS-PAGE 4-12% Bis-tris Gels (Bolt, Invitrogen) at 110 V for 80 min then transferred onto a nitrocellulose membrane (iBlot, Invitrogen) at 20 V for 7 min. Membranes were blocked in 1% w/v skim milk 0.05% v/v Tween20 (Sigma-Aldrich) in PBS (hereby referred to as 1% milk PBS-T) for 1 hr at room temperature. Primary (mouse 12CA5 anti-HA (1:5000 Roche), rabbit anti-aldolase (1:5000 abcam), rabbit anti-GAP45 (Baum, Richard et al. 2006) (1:5000), mouse anti-RAP1(Schofield, Bushell et al. 1986) (1:10000), rabbit anti-RON4 (Richard, MacRaild et al. 2010) (1:5000), rabbit anti-Rh4 (Tham, Wilson et al. 2010) (1:5000), rabbit anti-EBA175 (Lopaticki, Maier et al. 2011) (1:10000) and secondary (IRDye ® 800CW goat anti-mouse (1:4000, LI-COR Biosciences), IRDye® 680RD goat anti-rabbit (1:4000, LI-COR Biosciences) antibodies were prepared in 1% milk PBS-T and incubated on the membranes for 1 hr each at room temperature while rocking. Primary antibodies were washed three times in 0.05% v/v PBS-Tween20 (hereby referred to as PBS-T), while secondary antibodies were washed twice in PBS-T and once in PBS. Completed blots were dried on filter paper (Whatman) and visualised

on the Odyssey Infrared Imaging System (LI-COR Biosciences). All band quantification was performed in Image Studio Lite 5.2.5 (LI-COR Biosciences).

Proteinase K protection assay

To determine whether PfCERLI2 was cytosolically exposed or compartmentalised in an organelle, a proteinase K protection assay modified from a previous study was performed (Liffner, Frölich et al. 2020). Three 10 mL aliquots of high schizontaemia cultures were centrifuged at 440 rcf for 5 min, supernatant removed and lysed in 0.15% w/v saponin as described above. One set of schizonts were treated in SOTE (0.6 M sorbitol, 20 mM Tris HCl pH 7.5, 2 mM EDTA) alone, the second treated in SOTE with 0.02% w/v digitonin (Sigma-Aldrich) left incubating for 10 min at 4ºC before being washed in SOTE, and the third digested with 0.1 μg/μL Proteinase K (Sigma-Aldrich) in SOTE for 30 min at 4ºC following the aforementioned digitonin treatment. Proteinase K was inactivated with 50 μL 100% v/v trichloroacetic acid followed by PBS. All samples were resuspended in 500 μL acetone to ensure full Proteinase K deactivation, centrifuged then washed twice in 500 μL MilliQ H_2O. The final pellets were used for Western blot analysis of PfCERLI2's sensitivity to Proteinase K.

Protein solubility assay

To biochemically determine whether PfCERLI2 was membrane-associated and by what mechanism of association, a protein solubility assay was performed as previously described (Liffner, Frölich et al. 2020). Briefly, a high schizontaemia culture was saponin-lysed as described above, resuspended in 100 μL MilliQ H_2O, snap-frozen in dry ice four times, passed through a 29 gauge needle 5 times to disrupt parasite membranes, centrifuged at 16000 rcf for 10 min before reserving the water-soluble fraction containing cytosolic proteins. The remaining pellet was

washed twice in MilliQ H_2O and once in PBS before being resuspended in 100 μL 0.1 M Na_2CO_3 for 30 min at 4°C, centrifuged before reserving the carbonate-soluble fraction containing peripherally-associated proteins. The pellet was washed in the same manner above before being resuspended in 0.1% v/v Triton X-100 for 30 min at 4°C, centrifuged and the final supernatant reserved containing integral proteins. The remaining pellet was washed twice in PBS and was used to represent Triton X-100-insoluble proteins. All fractions were analysed by Western blot to determine PfCERLI2's membrane solubility profile.

Sample preparation for fixed-cell immunofluorescence microscopy

Pfcerli2^{HAGlmS} cultures of 3% E64 arrested schizonts were centrifuged at 440 rcf for 3 min, washed in PBS and resuspended in fixative (4% v/v paraformaldehyde (PFA, Sigma-Aldrich), 0.0075% v/v glutaraldehyde (Electron Microscopy Sciences), pH 7.4) and was left gently rocking for 30 min at room temperature. Samples were centrifuged at 440 rcf, fixative removed, washed twice in PBS, then adjusted to 1% haematocrit in PBS. #1.5H high-precision coverslips (Carl Zeiss, Oberkochen, Germany) were soaked in methanol, airdried, coated in 0.01% v/v poly-L-lysine (Sigma-Aldrich) for 30 min at room temperature then washed in MilliQ H_2O. Fixed cells were then laid on top at room temperature for 30 min, with non-adherent cells being gently aspirated off. Cells were permeabilised with 0.1% v/v Triton X-100 for 10 minutes then incubated in 3% bovine serum albumin (BSA) in PBS-T for 1 hr. Primary antibodies (anti-HA biotin conjugate 1:1000 (Roche), mouse anti-RAP1(Schofield, Bushell et al. 1986) 1:500, mouse anti-AMA1 (Coley, Parisi et al. 2006)1:500, rabbit anti-RON4 (Richard, MacRaild et al. 2010) 1:500, rabbit anti-MSP1(O'Donnell, Saul et al. 2000) 1:500) were diluted in 1% w/v BSA in PBS-T as specified above and applied to the coverslips overnight at 4°C. The next day, coverslips were washed three times in PBS-T, before being incubated with Alexa Fluor-conjugated secondary

antibodies (streptavidin 488 nm, mouse 594 nm, rabbit 647 nm, Life Technologies) for 1 hour in the dark at room temperature. Coverslips were again washed three times in PBS-T before being dehydrated in ethanol (70% v/v 3 min, 90% v/v 3 min, 100 v/v 3 min), air dried and then mounted on glass slides with 20 μL Prolong® Gold antifade solution (refractive index 1.4) with 4', 6-diamidino-2-phenylindole dihydrochloride (DAPI, Thermofisher Scientific). The mountant was allowed to cure overnight and coverslips were analysed on an Olympus FV3000 confocal microscope.

Confocal microscopy and colocalisation analysis

Confocal microscopy was performed using a Olympus FV3000 fluorescent microscope (Olympus) equipped with a ×100 MPLAPON oil objective (NA 1.4) using the 405 nm, 488 nm, 561 nm, and 633 nm lasers. Colocalisation analysis was performed using Imaris Coloc Suite (v9.5.0, Bitplane Inc., Switzerland) as described in detail previously (Liffner, Frölich et al. 2020). Briefly, images were exported from the Olympus FV3000 in .oir format, before conversion into .ims format. Following conversion, colocalisation analysis was performed whereby the image dataset was masked to the thresholded PfCERLI2 (anti-HA, 488nm laser) signal, defining the PfCERLI2 signal as the region of interest. Subsequently the other thresholded channels, corresponding to either RAP1, RON4, AMA1, or MSP1-19, were colocalised with the PfCERLI2 signal. Colocalisation statistics reported in this study are Pearson's correlation coefficient between the PfCERLI2 signal and the signal of the corresponding organelle marker, when PfCERLI2 is defined as the region of interest. Colocalisation analyses were performed over three biological replicates. For each of these biological replicates, threshold values were determined for each of the channels used in the colocalisation analysis to differentiate between true signal and background. Threshold values were fixed across all channels for each image in that biological replicate.

Rhoptry and microneme ligand secretion assay

Secretion assays were modified from a previous protocol (Liffner, Frölich et al. 2020). Briefly, *Pfcerli2*^{HAGlmS} synchronous ring stages at 15% haematocrit were grown in 6-well plates (Corning) with or without 2.5 mM GLCN for 24 hrs. Once trophozoite stages had formed, cultures were centrifuged at 440 rcf, supernatant removed and resuspended in an enzyme mix (0.067 U/mL neuraminidase (Sigma-Aldrich), 1 mg/mL chymotrypsin (Worthington Biochemical Corporation), 1 mg/mL trypsin (Sigma-Aldrich)) to be incubated at 37^{o}C for 45 minutes to cleave RBC surface receptors. Parasites were then washed twice in culture media and returned to culture for a further 24 hrs until schizont rupture. Once ruptured, cultures were centrifuged at 16000 rcf for 10 min at 4^{o}C to pellet uninvaded merozoites. Supernatants containing secreted protein was collected and kept on ice, and the pellet subject to saponin lysis to represent non-secreted protein. Each fraction was analysed by Western blot and quantified in Image Studio Lite 5.2.5 (LI-COR Biosciences).

Transmission electron microscopy

Pfcerli2^{HAGlmS} synchronous ring stage cultures were treated with or without 2.5 mM GLCN and grown until early schizonts had formed before being treated with 2 μM C1 for 4 hrs. Late schizonts were then enriched using Percoll then fixed in 2.5% v/v glutaraldehyde (Electron Microscopy Sciences) in PBS overnight at 4^{o}C. Fixed schizonts were then embedded in agarose and stained in 2% osmium tetroxide reduced in 1.5% w/v potassium ferricyanide in 0.15 M cacodylate buffer for 1 hr at room temperature. Cells were then dehydrated in increasing concentrations of ethanol-H_2O and finally embedded in EPON™ resin. 70 nm sections were prepared using the Leica EM UC7 ultramicrotome (Leica Microsystems) and were post-stained in 4% uranyl acetate and lead citrate. Sections were then imaged on the Tecnai G2 F30 transmission electron microscope (Field Electron and Ion Company, FEI).

Quantitative analysis of rhoptry length in thin-section schizonts

Rhoptry length was quantified from transmission electron micrographs for rhoptries where necks could be seen contacting the merozoite plasma membrane and the bottom of the bulb could be clearly discerned. Using blinded assessment, a vector was drawn from the tip of the necks to the end of the rhoptry bulbs in ImageJ to provide a length in nm. Micrographs where the rhoptries had been cut sideways such that it removed part of the neck or bulb were excluded from this analysis.

Airyscan microscopy and merozoite measurement

Airyscan microscopy was performed using a Zeiss LSM800 AxioObserver Z1 microscope (Carl Zeiss, Oberkochen, Germany) that had an Airyscan detector and a Plan-Apochromat 63x M27 oil objective (NA 1.4). Z-stacks were acquired using a 0.04 µm XY and 0.16 µm Z pixel resolution. Images were acquired sequentially as follows: Channel 1 (RON4) – 633 nm laser, channel 2 (RAP1) – 594 nm laser, channel 3 (HA) – 488 nm laser, channel 4 (DAPI) – 405 nm laser.

The distance between the basal end of the nucleus (DAPI signal) and the RAP1 or RON4 foci was measured as described previously (Ebrahimzadeh, Mukherjee et al. 2019). Images were first blinded and then using the Plot Profile plugin on FIJI, a line was drawn from the basal extremity of the DAPI signal through the RAP1 and RON4 foci to generate intensity profiles for the three markers as a function of distance of the line. Data generated from these intensity plots was then exported, and graphed using GraphPad PRISM 7, with the distance corresponding to the highest RAP1 or RON4 signal intensity representing the distance of that signal from the basal end of the DAPI signal.

Statistical analysis

All graphs and statistical analyses were completed in Graphpad PRISM 7 (GraphPad Software Inc.). All figure legends note the type of statistical test, the definition of significance for various p-values, and the number of biological replicates (n) for each experiment.

Acknowledgements

We thank Prof. Alan Cowman for provision of RON4, EBA175 and GAP45 antibodies, A/Prof. Wai-Hong Tham for RH4 antibodies, and Prof. Leann Tilley for ERC and GAPDH antibodies. We also thank Dr. Paul Gilson for the PTEX150^{HAGlmS} transfection vector. Electron microscopy was performed at the Bio21 Institute Advanced Microscopy Facility, The University of Melbourne (www.microscopy.unimelb.edu.au). For provision of the SLI-TGD vector, we thank Dr. Tobias Spielmann. We thank Dr. Brad Sleebs for Compound 1.

This work was supported by funding from the NHMRC (Project Grant APP1143974, DW), University of Adelaide Beacon Fellowship (DW), DAAD/Universities Australia joint research co-operation scheme (TG, DW, BL), Australian Government Research Training Program Scholarship (BL, JB), South Australian Commonwealth Scholarship (BL).

Author contributions

Study design and planning: D.W.W., B.L., J.B., M.W.A.D., and T.G. Performed experiments and generated reagents: B.L., J.B., D.W.W., J.S., G.K.H., and B.L. Data analysis: B.L., J.B., and D.W.W. Manuscript writing: B.L, J.B., and D.W.W. Manuscript was drafted with input from all authors.

Competing interests

The authors declare no competing interests.

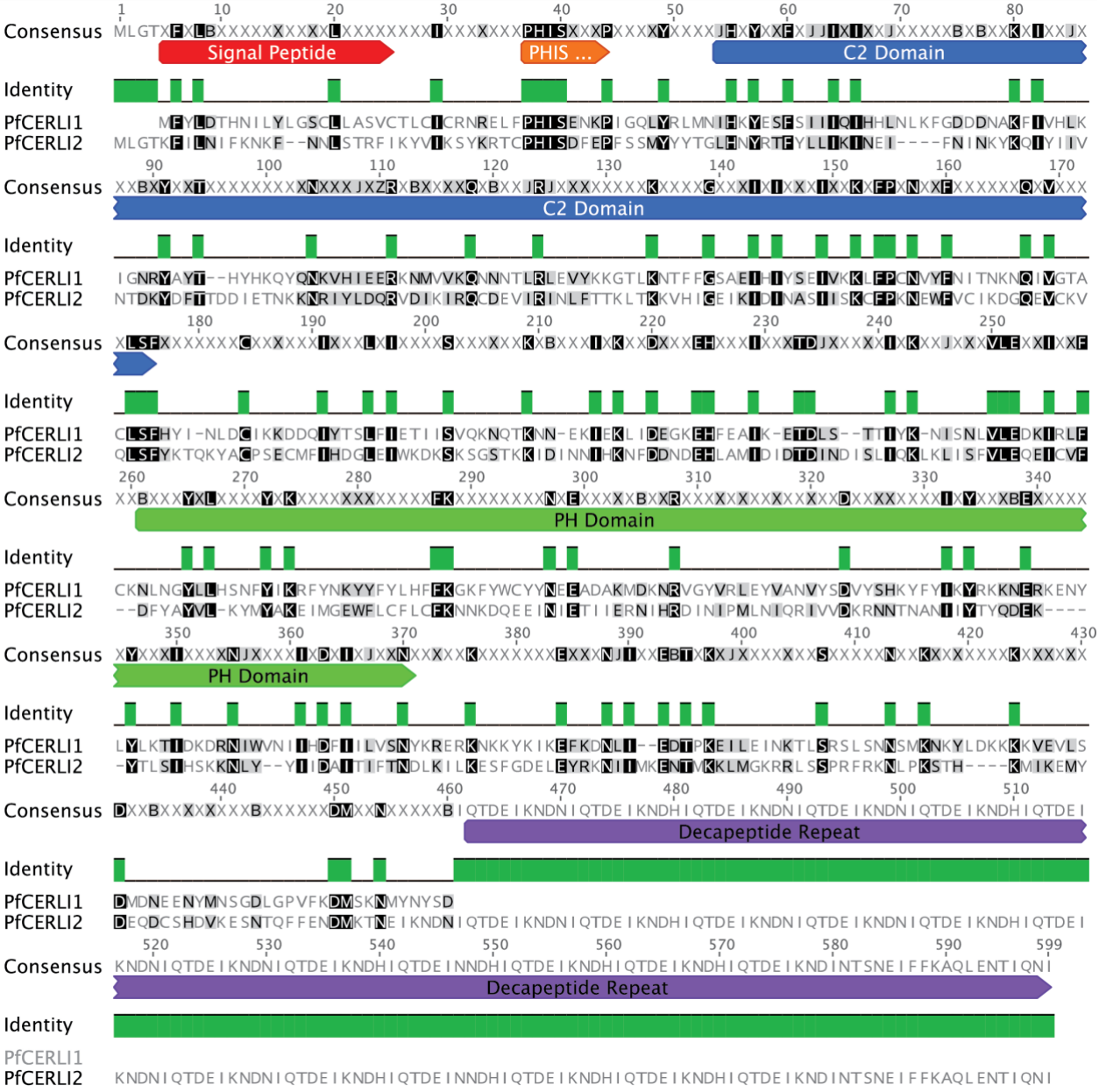

Supplementary Figure 5.1: Alignment of PfCERLI1 and PfCERLI2.

Geneious global alignment with free-end gaps between the amino acid sequences of PfCERLI1 (Pf3D7_0210600) and PfCERLI2 (Pf3D7_0405200).

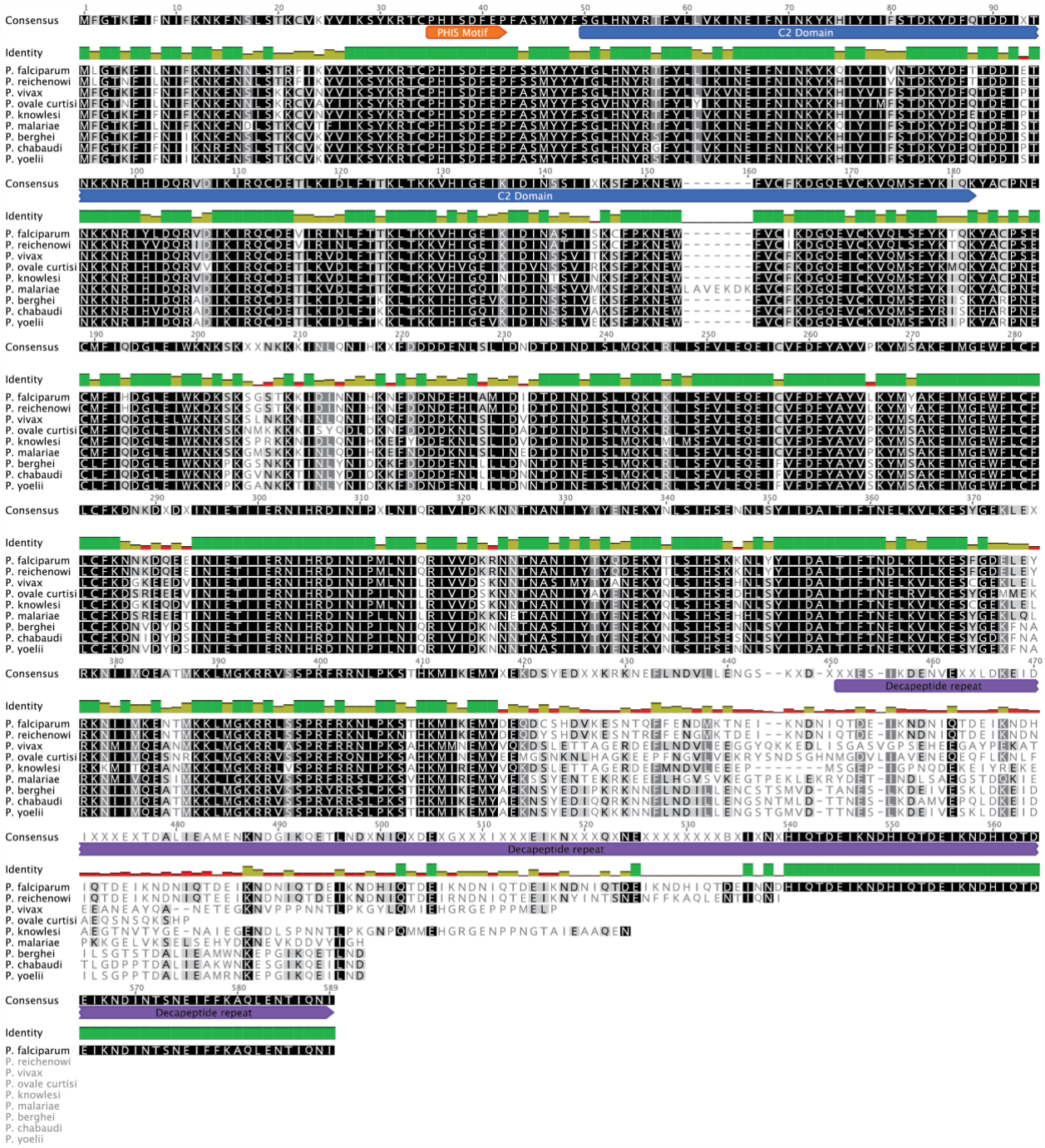

Supplementary Figure 5.2: Alignment of PfCERLI2 and its *Plasmodium* homologues.

Geneious global alignment with free-end gaps between the amino acid sequences of PfCERLI2 (Pf3D7_0405200) and its homologues in P. reichenowi (PRCDC_0402800), P. vivax (PVP01_0304600), P. ovale curtisi (PocGH01_030212700), P. knowlesi (PKNH_0303300) , P. malariae (PmUG01_03015300), P. berghei (PBANKA_1002900), P. chabaudi (PCHAS_1003800) , and P. yoelii (PY17X_1004300).

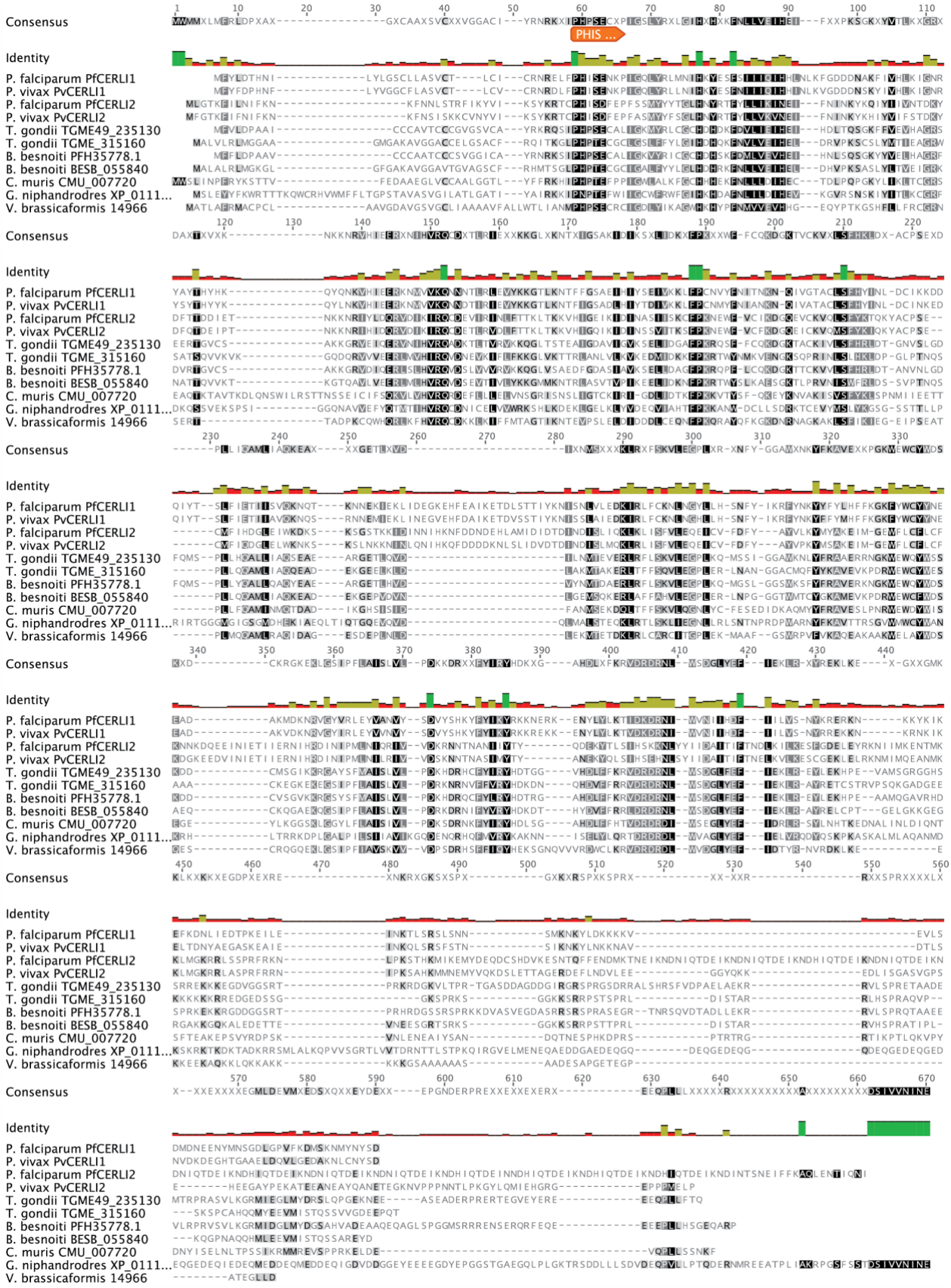
Consensus
PHIS ...
Identity
P. falciparum PfCERLI1
P. vivax PvCERLI1
P. falciparum PfCERLI2
P. vivax PvCERLI2
T. gondii TGME49_235130
T. gondii TGME_315160
B. besnoiti PFH35778.1
B. besnoiti BESB_055840
C. muris CMU_007720
G. niphandrodres XP_0111...
V. brassicaformis 14966

Supplementary Figure 5.3: Alignment of PfCERLI1, PfCERLI2, and their Apicomplexan homologues.

Geneious global alignment with free-end gaps between the amino acid sequences of PfCERLI1 (Pf3D7_0210600), PfCERLI2 (Pf3D7_0405200) and their homologues in P. vivax (PVP01_0414300 & PVP01_0304600), Toxoplasma gondii (TGME49_235130 & TGME49_315160), Besnoitia besnoiti (PFH35778.1 & BESB_055840), Cryptosporidium muris (CMU_007720) , Gregarina niphandrodes (XP_011129839.1), and Vitrella brassicaformis (14966).

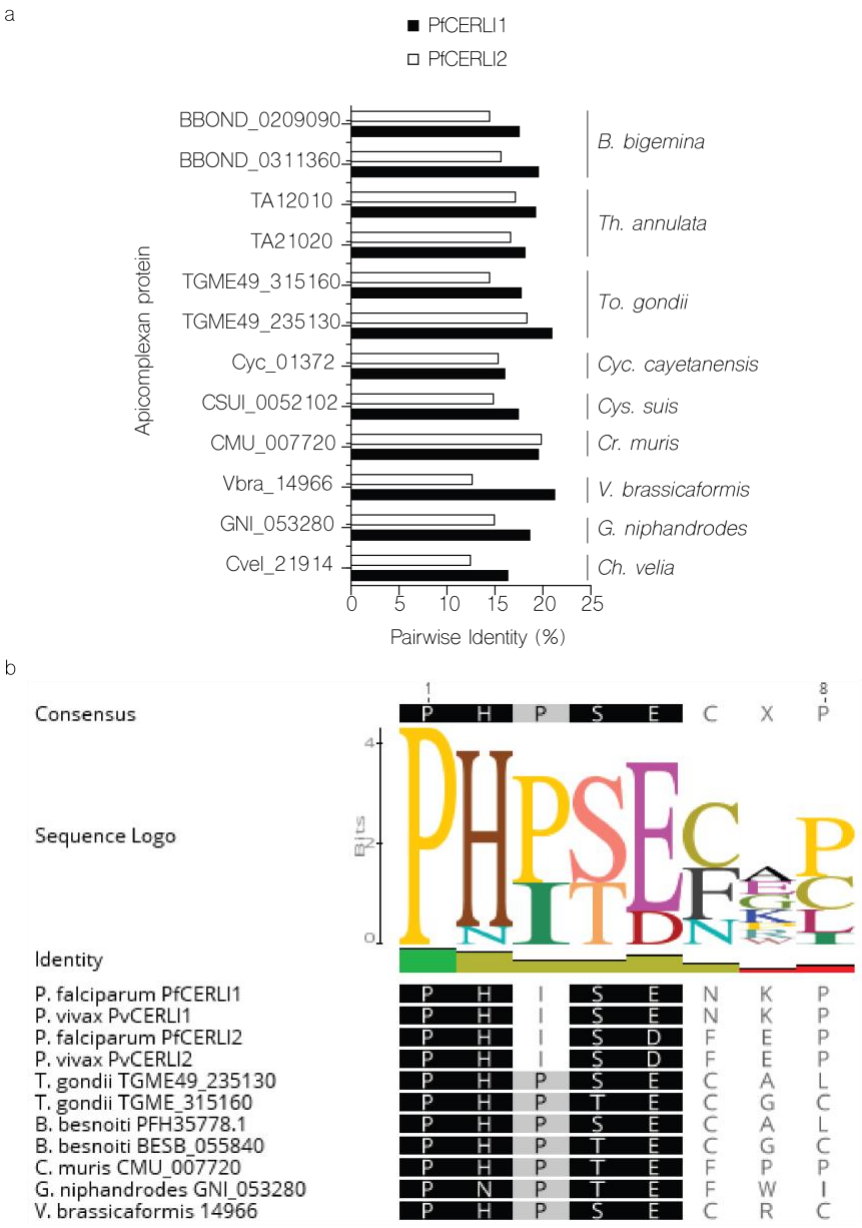

Supplementary Figure 5.4: Pairwise identity of PfCERLI1, PfCERLI2, and their Apicomplexan homologues.

(a) *Pairwise identities, as determined by Geneious global alignment with free-end gaps, of the amino acid sequence for either PfCERLI1 or PfCERLI2 and their homologues in Babesia bigemina (BBOND_0209090 & BBOND_0311360), Theileria annulata (TA12010 & TA21020), Toxoplasma gondii (TGME49_235130 & TGME49_315160), Cyclospora cayetanensis (Cyc_01372), Cystoisospora suis (CSUI_0052102), Cryptosporidium muris (CMU_007720), Vitrella brassicaformis (Vbra_14966), Gregarina niphandrodes (GNI_053280), and Chromera velia (Cvel_21914).* ***(b)*** *Consensus sequence and conservation of the PHIS motif in PfCERLI1, PfCERLI2, and their apicomplexan homologues.*

EuPathDB identifier	Chromosome	Organism	*Cerli* lineage	Gene length (bp)	mRNA length (bp)	Intron length (bp)	Protein length (aa)	Introns	Exons	Avg. intron length (bp)	Avg. exon length (bp)	Avg. UTR length (bp)
GNI_053280	NA	*G. niphandrodes*	*Cerli1*	1755	1755	0	584	0	1	0	1755	0
Cvel_21914	NA	*Ch. Velia*	*Cerli1*	8609	1656	6953	321	8	9	869.1	184	690
Chro.60252	NA	*C. hominis*	*Cerli1*	789	789	0	262	0	1	0	789	0
Vbra_14966	NA	*V. brassicaformis*	*Cerli1*	2407	1354	1053	393	11	12	95.7	112.8	172
Pf3D7_0210600	2	*P. falciparum*	*Cerli1*	2046	1341	705	446	4	5	176.2	268.2	0
PBANKA_0307500	3	*P. berghei*	*Cerli1*	1948	1341	607	446	4	5	151.7	268.2	0
PCHAS_0309700	3	*P. chabaudi*	*Cerli1*	1857	1341	516	446	4	5	129	268.2	0
PKNH_0410600	4	*P. knowlesi*	*Cerli1*	2109	1341	768	446	4	5	192	268.2	0
PRCDC_0209500	2	*P. reichenowi*	*Cerli1*	2064	1332	732	443	4	5	183	266.4	0
PVP01_0414300	4	*P. vivax*	*Cerli1*	2176	1341	835	446	4	5	208.7	268.2	0
PY17X_0308100	3	*P. yoelii*	*Cerli1*	2036	1341	695	446	4	5	173.7	268.2	0
PocGH01_04019500	4	*P. ovale curtisi*	*Cerli1*	1952	1341	611	446	4	5	152.7	268.2	0
PmUG01_04021700	4	*P. malariae*	*Cerli1*	2713	1344	1369	447	4	5	342.2	268.8	0
TGME49_235130	10	*T. gondii*	*Cerli1*	8309	5982	2327	487	3	4	775.7	1495.5	4518
CSUI_005102	NA	*Cys. Suis*	*Cerli1*	7465	4631	2834	601	3	4	944.7	1157.7	2825
EBH_0041390	NA	*E. brunetti*	*Cerli1*	2677	1404	1273	467	3	4	424.3	351	0
cyc_01372	NA	*Cyc. Cayetanensis*	*Cerli1*	2469	1101	1368	366	4	5	342	220.2	0
NCLIV_049720	10	*N. caninum*	*Cerli1*	3882	1464	2418	487	3	4	806	366	0
SN3_00600405	NA	*S. neurona*	*Cerli1*	10552	6246	4306	463	3	4	1435.3	1561.5	4854
cgd6_2143	6	*C. parvum*	*Cerli1*	1536	1371	165	451	3	4	55	342.7	15
cubi_02338	NA	*C. ubiquitum*	*Cerli1*	1523	1386	137	461	3	4	45.7	346.5	0
CTYZ_00001395	6	*C. tyzzeri*	*Cerli1*	1520	1356	164	451	3	4	54.7	339	0
TA12010	2	*T. annulata*	*Cerli1*	1728	1290	438	429	4	5	109.5	258	0
CF003293	NA	*Cyt. Felis*	*Cerli1*	2051	1446	605	481	5	6	121	241	0
BBOV_III003780	3	*B. bovis*	*Cerli1*	1714	1309	405	398	4	5	101.2	261.8	112
BBBOND_0311360	3	*B. bigemina*	*Cerli1*	1745	1242	503	413	4	5	125.7	248.4	0
cand_006180	NA	*C. andersoni*	*Cerli1*	1580	1404	176	467	3	4	58.7	351	0

EuPathDB identifier	Chromosome	Organism	*Cerli* lineage	Gene length (bp)	mRNA length (bp)	Intron length (bp)	Protein length (aa)	Introns	Exons	Avg. intron length (bp)	Avg. exon length (bp)	Avg. UTR length (bp)
CMU_007720	NA	*C. muris*	*Cerli1*	1581	1404	177	467	3	4	59	351	0
TOT_020000207	2	*T. orientalis*	*Cerli1*	1600	1266	334	421	4	5	83.5	253.2	0
BEWA_019330	1	*T. equi*	*Cerli1*	1067	954	113	317	3	4	37.7	238.5	0
Pf3D7_0405200	4	*P. falciparum*	*Cerli2*	2912	1740	1172	579	8	9	146.5	193.3	0
PBANKA_1002900	10	*P. berghei*	*Cerli2*	2748	1470	1278	489	8	9	159.7	163.3	0
PCHAS_1003800	10	*P. chabaudi*	*Cerli2*	2740	1470	1270	489	8	9	158.7	163.3	0
PKNH_0303300	3	*P. knowlesi*	*Cerli2*	2904	1527	1377	508	8	9	172.1	169.7	0
PRCDC_0402800	4	*P. reichenowi*	*Cerli2*	2820	1590	1230	529	8	9	153.7	176.7	0
PVP01_0304600	3	*P. vivax*	*Cerli2*	2780	1527	1253	508	8	9	156.6	169.7	0
PY17X_1004300	10	*P. yoelii*	*Cerli2*	2744	1470	1274	489	8	9	159.2	163.3	0
PmUG01_03015300	3	*P. malariae*	*Cerli2*	3116	1494	1622	497	8	9	202.7	166	0
PocGH01_03012700	3	*P. ovale curtisi*	*Cerli2*	2736	1425	1311	474	8	9	163.9	158.3	0
TGME49_315160	11	*T. gondii*	*Cerli2*	11204	3875	7329	437	8	9	916.1	430.5	2561
NCLIV_057920	11	*N. caninum*	*Cerli2*	7617	1392	6225	463	9	10	691.7	139.2	0
SN3_01800355	NA	*S. neurona*	*Cerli2*	20733	8583	12150	471	8	9	1518.7	953.7	7167
BEWA_030720	1	*T. equi*	*Cerli2*	1291	1035	256	344	7	8	36.6	129.4	0
TOT_010000334	1	*T. orientalis*	*Cerli2*	1314	1038	276	345	7	8	39.42	129.7	0
TA21020	1	*T. annulata*	*Cerli2*	1357	1038	319	345	7	8	45.6	129.7	0
CF002482	NA	*Cyt. Felis*	*Cerli2*	1638	1035	603	344	7	8	86.14	129.4	0
BBBOND_0209090	2	*B. bigemina*	*Cerli2*	1385	1035	350	344	6	7	58.3	147.8	0
BBOV_IV005720	NA	*B. bovis*	*Cerli2*	1273	1002	271	333	5	6	54.2	167	0

Supplementary Table 5.1: Gene structure of *cerli1*, *cerli2* and their homologues in Apicomplexa and Chromerids.

All data collected from EuPathDB (Aurrecoechea, Barreto et al. 2016) or derived from EuPathDB predictions. mRNA length is inclusive of any predicted untranslated regions (UTRs). Intron length = total combined length of all introns in gene, avg. intron/exon length = mean length of introns/exons in gene.

***Cerli* lineage**	**Gene length (bp)**	**mRNA length (bp)**	**Intron length (bp)**	**Protein length (aa)**	**Intron number**	**Exon number**	**Avg. intron length (bp)**	**Avg. exon length (bp)**	**UTR length (bp)**
Cerli1	2765.4	1820	945.4	447.6	3.6	4.6	280.3	415.2	2464.8
Cerli2	4072.9	1874.8	2198.1	443.8	7.5	8.55	273.3	215.6	4864

Supplementary Table 5.2: Average Gene structure of *cerli1* and *cerli2* lineage genes.

Average values from gene structure characteristics of genes identified as being members of either the cerli1 or cerli2 lineage

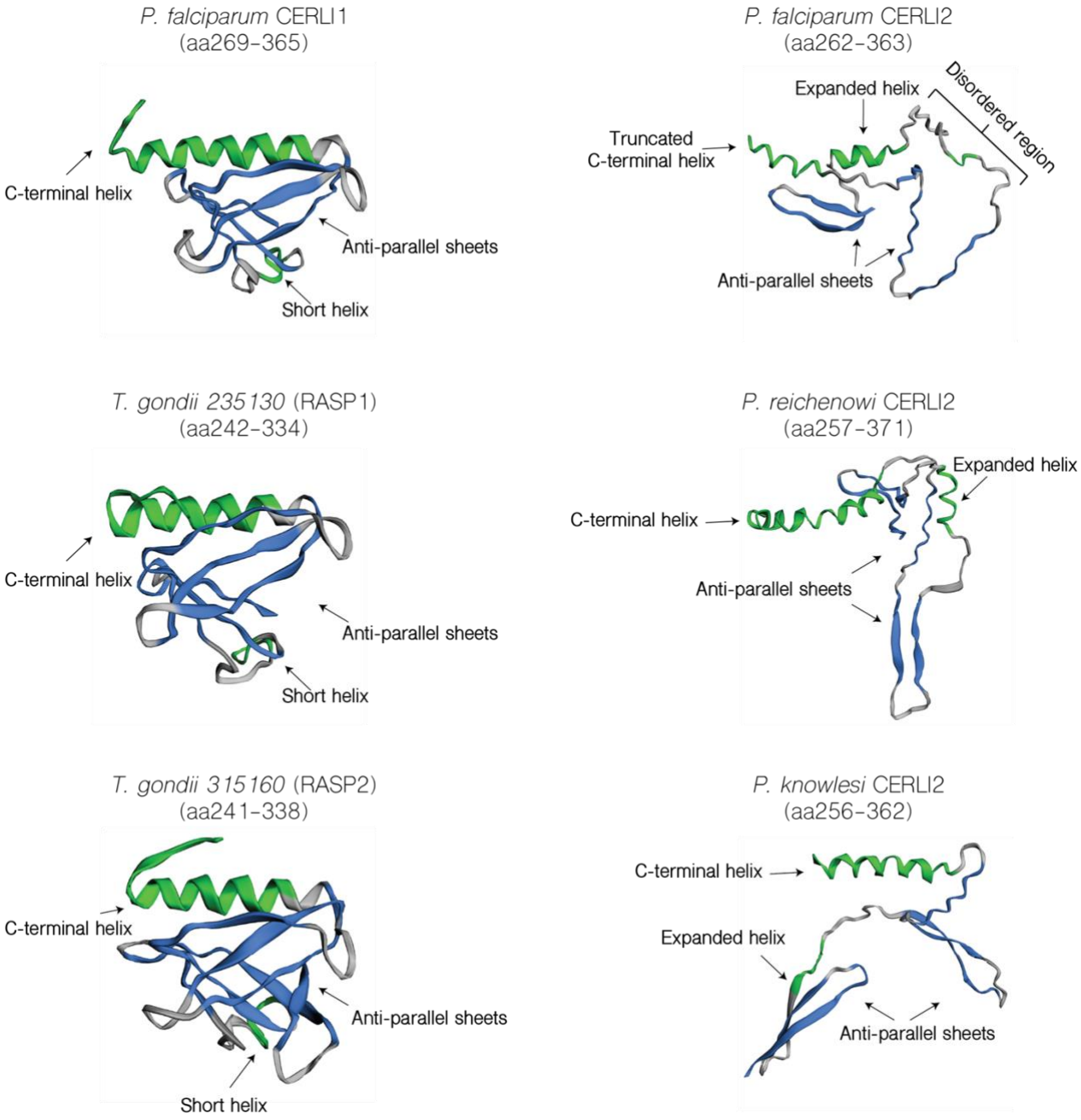

Supplementary Figure 5.5: Predicted structure of the PH domain region of PfCERLI2, PfCERLI1 and their homologues.

Full length protein sequences for PfCERLI1, PfCERLI2, along with both their homologues in Toxoplasma gondii, and the homologues of CERLI2 in Plasmodium reichenowi and Plasmodium knowlesi, were predicted using Phyre2. The PH domain region of those structures was visualised using EzMol. Region of each protein depicted are shown in brackets. Green = alpha-helix, blue = beta-strand, grey = coil.

PlasmoDB ID	Name	PlasmoDB annotation	Sequence	Peak expression	PiggyBac Dispensibility?
PF3D7_0210600	PfCERLI1	PfCERLI1	PHISENKP	Schizonts	Essential
PF3D7_0405200	PfCERLI2	PfCERLI2	PHISDFEP	Schizonts	Essential
PF3D7_0102200	RESA	Ring-infected erythrocyte surface antigen	PHISEFNP	Rings	Dispensible
PF3D7_1149500	RESA2	Ring-infected erythrocyte surface antigen 2	PHVKEFKP	Rings	Dispensible
PF3D7_1149200	RESA3	Ring-infected erythrocyte surface antigen 3	PHTREFNP	Rings	Dispensible
PF3D7_1038800	N/A	RESA-like protein with PHIST and DnaJ domains	PYVKKYNP	Rings	Dispensible
PF3D7_0814900	FeSOD	Iron superoxide dismutase	PHISEETL	Trophs/ gams	Essential
PF3D7_1436800	ClpR	ATP-dependent Clp protease proteolytic subunit	PHISEQII	Trophs/ gams	Essential
PF3D7_1024400	N/A	Conserved Plasmodium protein, unknown function	PHISKNKN	Schizonts	Essential

Supplementary Table 5.3: Summary of PHIS containing proteins in *P. falciparum*.

Summary of all PHIS motif containing proteins in the P. falciparum 3D7 proteome, as determined by BLASTp search using the PHIS sequence of either PfCERLI1 or PfCERLI2. Expression data obtained from (Lopez-Barragan, Lemieux J Fau - Quinones et al. 2011) Dispensability data obtained from previously published resources (Zhang, Wang et al. 2018).

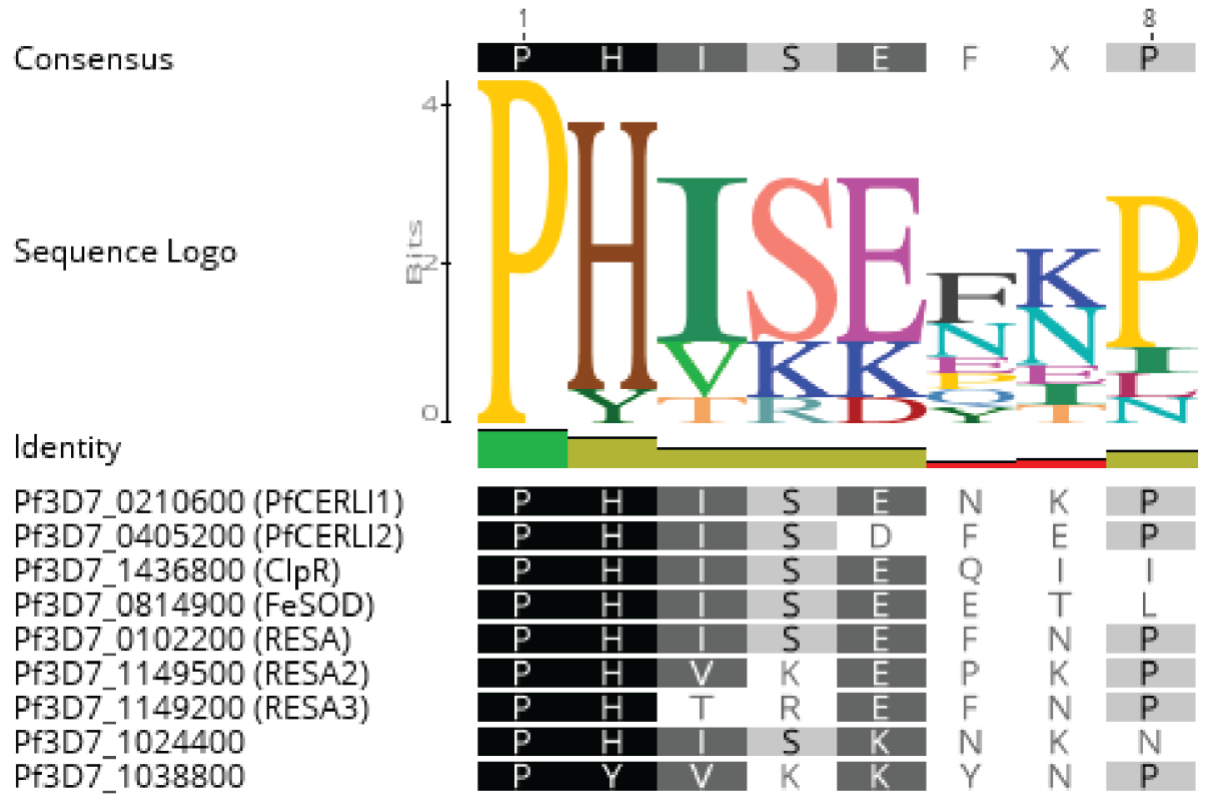

Supplementary Figure 5.6: PHIS consensus sequence of *P. falciparum* PHIS-containing proteins.

Consensus sequence and conservation of the PHIS motif for PHIS-containing proteins of P. falciparum.

***Plasmodium* Species**	**Strain**	**Genome size(Mb)**	**Host**	**Exons**	**Repeat seq.**	**Repeat number**	**aa length**
falciparum	3D7	23.3	Human	9	QTDEIkNDhi	12	579
falciparum	7G8	22.7	Human	9	QTdEikNDhi	10	559
falciparum	CD01	23.5	Human	9	QTdEikNDhi	20	659
falciparum	GB4	23.4	Human	9	QTdEikNDni	18	639
falciparum	HB3	22.7	Human	9	QTdEikNDhi	15	609
falciparum	IT	23.1	Human	9	QTdEikNDhi	17	629
falciparum	Dd2	22.6	Human	9	QTdEikNDhi	17	629
praefalciparum	G01	26	Gorilla	9	QTdEikNDhi	9	549
reichenowi	CDC	24.5	Chimp	9	QTdEIkNdni	7	529
reichenowi	G01	24.1	Chimp	9	qTdEIKNdni	6	509
adleri	GO1	22.2	Gorilla	9	tEElKNdni?	4	490
billcollinsi	G01	23.1	Chimp	9	tEevkndnin	8	528
blacklocki	G01	22	Gorilla	9	NIkkEEIkNd	8	534
gaboni	G01	21.8	Chimp	9	teEiKNdnin	6	509

Supplementary Table 5.4: Summary of CERLI2 repeat structures in *Laverania*.

Summary of the characteristics of PfCERLI2 in multiple P. falciparum isolates and their homologues in Laverania. Repeat sequences represent the consensus sequence of all repeats in that protein. Upper case letters = amino acid position fixed across repeats, lower case letters = amino acid position variable across repeats,? = no obvious pattern across repeats.

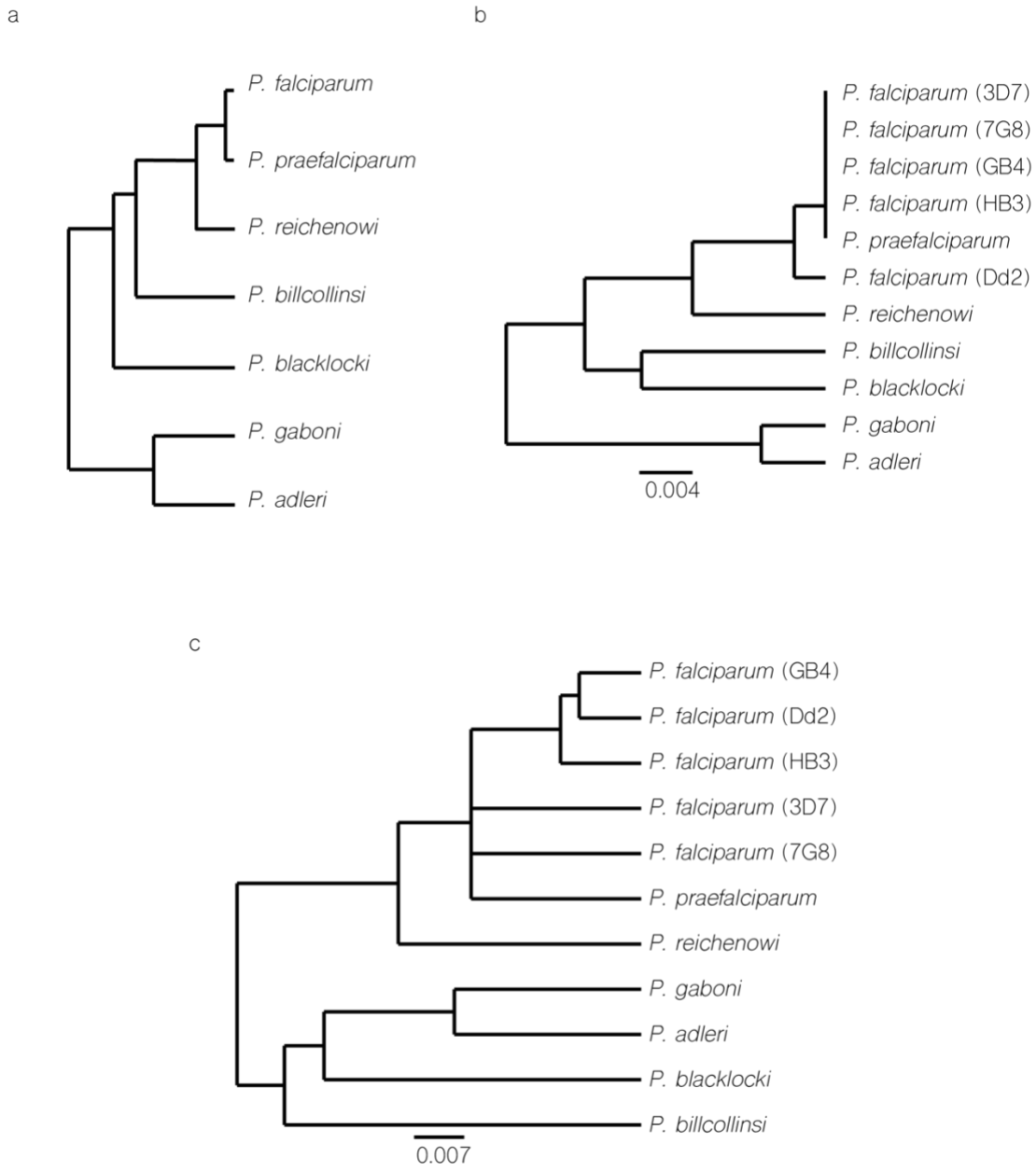

Supplementary Figure 5.7: The decapeptide repeat of PfCERLI2 is under differential selection in *Laverania*.

(a) *Cladogram of relationships between Laverania as determined by Otto et al., Nat. Microb. 2018.* ***(b)*** *Phylogenetic tree of PfCERLI2 and its homologues in Laverania and multiple P. falciparum isolates when the decapeptide repeat region of each protein has been removed.* ***(c)*** *Phylogenetic tree of full length PfCERLI2 and its homologues in Laverania and multiple P. falciparum. Scale bars = amino acid substitutions per site. Phylogenetic trees constructed using unweighted pair group method with arithmetic mean (UPGMA). Branch length corresponds to amino acids substitutions per site.*

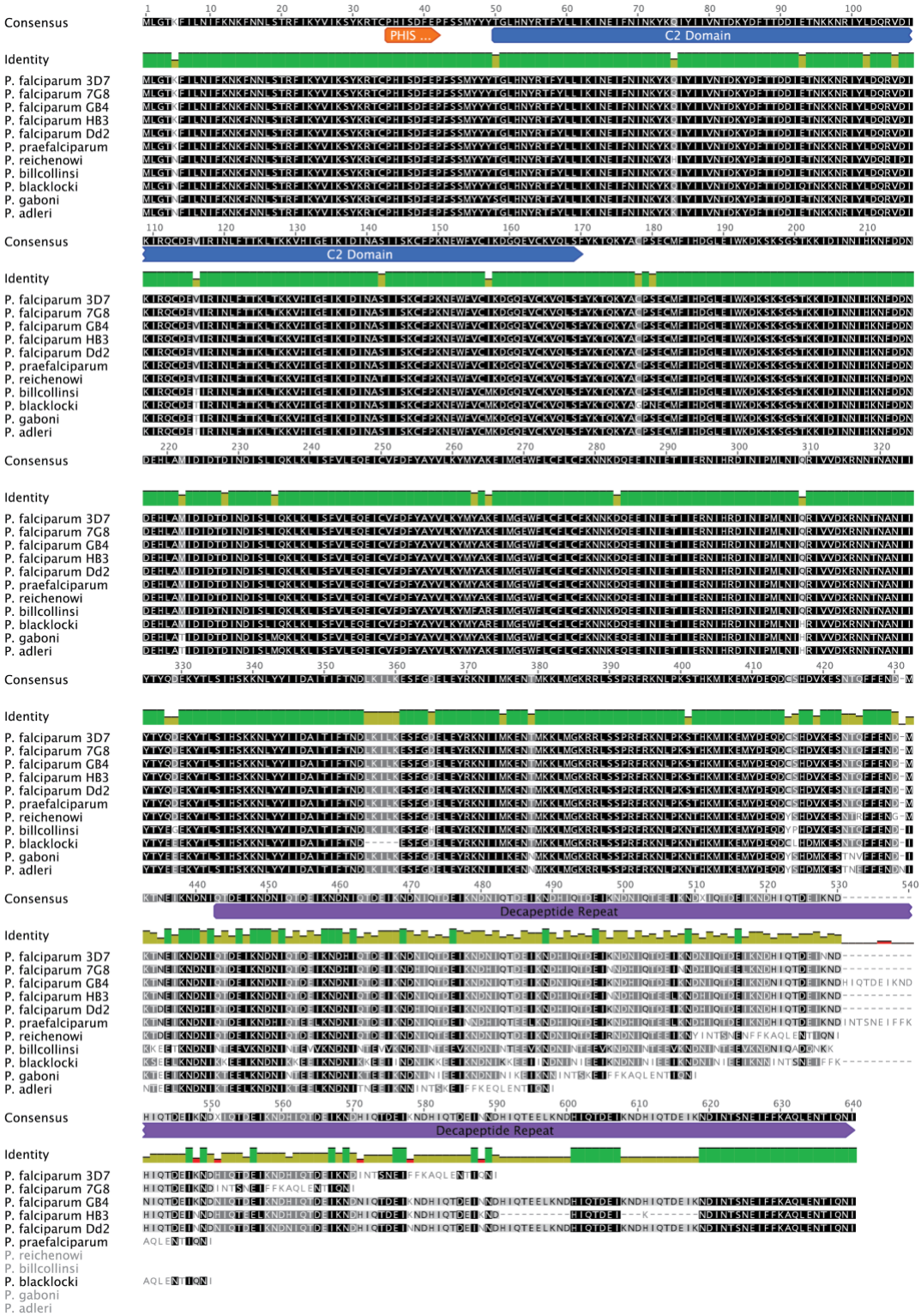

Supplementary Figure 5.8: Alignment of PfCERLI2 and its homologues in Laverania.

Geneious global alignment with free-end gaps between full length PfCERLI2 in Laverania and multiple P. falciparum isolates.

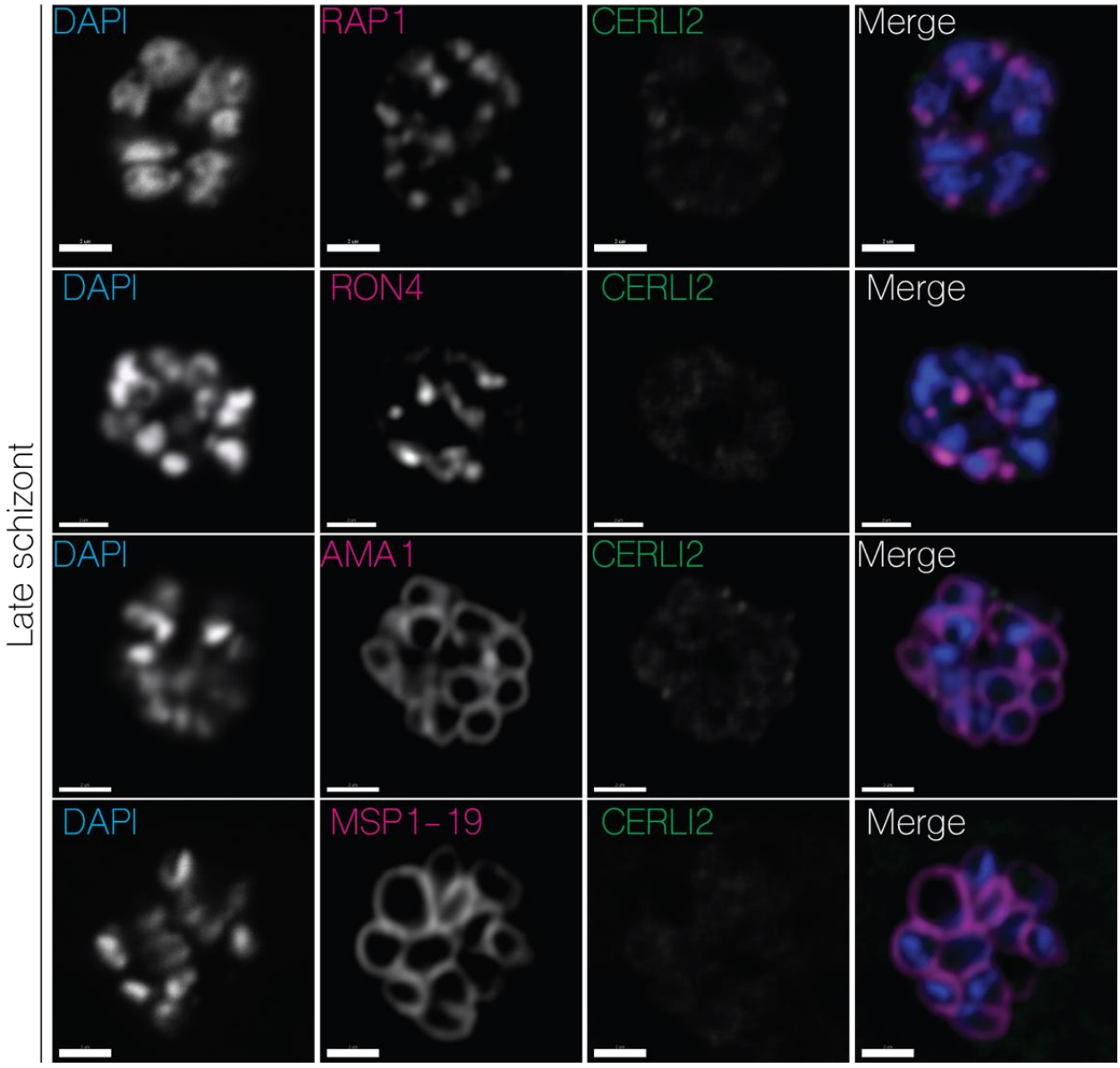

Supplementary Figure 5.9: Colocalisation of PfCERLI2 in late schizonts shows reduced CERLI2 signal.

Immunofluorescence microscopy of either late PfCERLI2^{HAGlmS} schizonts stained with DAPI (nucleus) and anti-HA (PfCERLI2) antibodies, along with antibodies to either RAP1 (rhoptry bulb, RON4 (rhoptry neck), AMA1 (micronemes), or MSP1-19 (merozoite surface). Scale bar = 2 µm

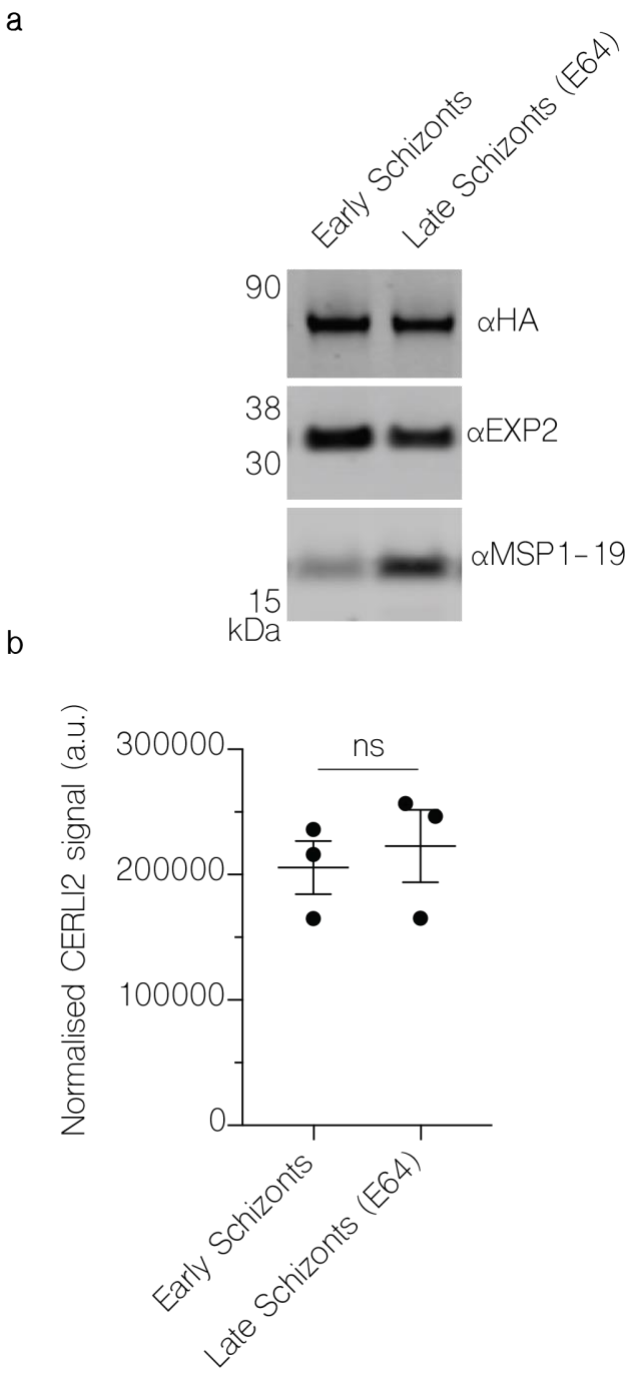

Supplementary Figure 5.10: Western blot of early and late PfCERLI2^{HAGlmS} Schizonts.

(a) *PfCERLI2^{HAGlmS} parasite lysates were either harvested for Western blot as early schizonts (~44 hours post invasion), or matured in the presence of E64 and harvested as late schizonts (~48). Lysates were probed with either anti-HA (PfCERLI2), anti-EXP2 (loading control), or anti-MSP1-19 (schizont maturity control) antibodies. Image representative of 3 biological replicates.* ***(b)*** *Quantification of PfCERLI2 signal, normalised to EXP2, for both early and late schizonts. n=3, ns=p>0.05 by unpaired t-test. Error bars = SEM.*

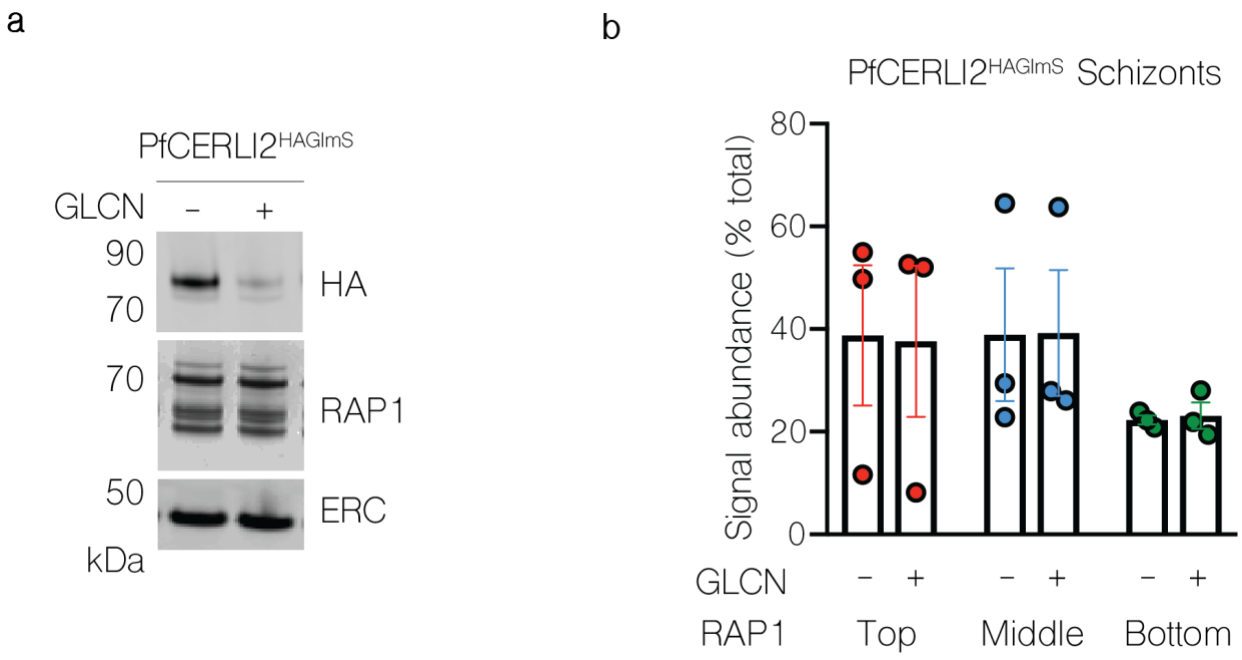

Supplementary Figure 5.11: PfCERLI2 knockdown does not alter RAP1 processing in C1 arrested schizonts.

(a) *PfCERLI2^{HAGlmS} parasites were either treated with 2.5 mM GLCN or left untreated, before being matured in the presence of C1 to prevent PVM rupture. Parasite lysates were then prepared and probed with anti-HA (PfCERLI2), anti-RAP1 (rhoptry bulb), and anti-ERC (loading control) antibodies. Images representative of 3 biological replicates.* ***(b)*** *Quantification of individiual band intensities, as a percentage of the total signal, from RAP1 signals using the parasite lysates from the secretion assay. n=3 biological replicates. Error bars = SEM.*

Chapter 6: Final Discussion

Preface

The aims of the research presented in this thesis was to determine the subcellular localisations of PfCERLI1 and PfCERLI2 and characterise the functions of these proteins by assessing the phenotype of knockdown parasites. Results presented in this thesis have shown that both PfCERLI1 and PfCERLI2 localise to the cytosolic face of the rhoptry bulb. Additionally, it was shown that knockdown of either PfCERLI1 or PfCERLI2 is inhibitory to merozoite invasion. Further, these data show that PfCERLI1 is involved in rhoptry secretion, that PfCERLI2 is involved in rhoptry morphology, and loss of either of these proteins interferes with rhoptry bulb antigen processing. Another aim of the research presented in this thesis was to conduct a bioinformatic analysis of PfCERLI1, PfCERLI2, and their homologues in related organisms to determine if an evolutionary relationship exists between these two proteins. These studies showed that *Pfcerli1* and *Pfcerli2* are paralogous genes that are derived from an ancestral gene duplication event that likely occurred in the most recent common ancestor of all haematozoa and coccidia. Analysis of gene structure also suggests that *cerli1* is likely to be the ancestral locus and *cerli2* the duplicated locus. These analyses shed insight on how paralogues may be under differential selection in closely related organisms.

Both Chapters 4 and 5 were presented in manuscript format, each with their own discussion sections. Due to the significant overlap between the two chapters, however, this chapter will consist of a single unified discussion of the results presented in both Chapters 4 and 5.

PfCERLI1 and PfCERLI2 as vaccine candidates

Prior to the work presented in this thesis, PfCERLI1 and PfCERLI2 were investigated as potential merozoite vaccine candidates (Gao, Li et al. 2009, Hu, Cabrera et al. 2009, Zenonos, Rayner et al. 2014). Promise for their vaccine candidacy was based predominantly on their stage of expression, the presence of a predicted signal peptide suggesting export of PfCERLI1 to the merozoite surface, merozoite surface localisation suggested for PfCERLI2 from immunofluorescence assays, and reported susceptibility to invasion inhibitory antibodies that were thought to target PfCERLI2 (Gao, Li et al. 2009, Hu, Cabrera et al. 2009). Additionally, they are lowly polymorphic between *P. falciparum* isolates, and are relatively lowly expressed (Lopez-Barragan, Lemieux J Fau - Quinones et al. 2011); two characteristics they share with the leading blood stage vaccine candidate RH5 (Zenonos, Rayner et al. 2014).

The work undertaken in this thesis demonstrates that PfCERLI1 and PfCERLI2 are not likely to be exported to the merozoite surface such that they can be targeted by protective antibody responses. Sensitivity of both PfCERLI1 and PfCERLI2 to proteinase K, following treatment with saponin and digitonin, suggests that both are exposed to the merozoite cytoplasm and are therefore unlikely to be secreted. Moreover, secreted PfCERLI1 and PfCERLI2 could not be detected by Western blot in rhoptry and microneme secretion assays, and both proteins were conclusively localised to the rhoptry bulb by immunofluorescence microscopy. Further support for the observation that PfCERLI1 and PfCERLI2 are intracellular proteins is the recently reported cytosolic localisation of their homologues in *T. gondii* (Suarez, Lentini et al. 2019). Given the evidence that PfCERLI1 and PfCERLI2 are internal parasite proteins, it is unlikely that they will form the basis of highly effective blood stage vaccines. Antibodies directed against both PfCERLI1 and PfCERLI2 have been reported in sera from people living in malaria endemic areas (Zenonos, Rayner et al. 2014, Dent, Nakajima et al. 2015), but as neither could be found secreted from or

present on the merozoite surface, it is unlikely that these antibodies are protective. Antibodies targeting PfCERLI1 and PfCERLI2 in human sera are therefore more likely to be the result of phagocytosis of free merozoites. It is also possible that antibodies reported to be reactive against PfCERLI1 or PfCERLI2 could have been derived from sporozoites (Zanghì, Vembar et al. 2018, Hoo, Bruske et al. 2019), or due to antibody cross-reactivity; as previously seen with the monoclonal antibody M26-32 that was reported to target PfCERLI2 (Cheng, Jones et al. 1991). Despite their importance for the survival of blood stage parasites, these results suggest PfCERLI1 and PfCERLI2 are not promising vaccine candidates; contrary to initial hypotheses presented in the literature (Gao, Li et al. 2009, Zenonos, Rayner et al. 2014).

Functions of PfCERLI1 and PfCERLI2

Comparison between PfCERLI1, PfCERLI2 and their *Toxoplasma gondii* homologues

A recent publication extensively characterised the *T. gondii* homologues of PfCERLI1 and PfCERLI2, which they termed rhoptry apical surface protein (RASP) 1 and 2 (Suarez, Lentini et al. 2019). After initially characterising TgRASP1 and TgRASP2, and identifying that they are paralogous genes, the authors characterised PfCERLI1 in the blood-stages of *P. falciparum*, with the hypothesis that it was the direct orthologue of TgRASP2 (Suarez, Lentini et al. 2019). Our classification of the apicomplexan homologues into *cerli1* and *cerli2* lineages, however, suggests that PfCERLI2 is the direct orthologue of TgRASP2, and PfCERLI1 the direct orthologue of TgRASP1. For this reason, this discussion will continue to call the *P. falciparum* orthologus PfCERLI1 and PfCERLI2. This study also identified a protein the authors termed TgRASP3, which localised to the rhoptries and was reported to interact with TgRASP2 by immunoprecipitation and yeast two-hybrid (Suarez, Lentini et al. 2019). TgRASP3 is not evolutionarily related to TgRASP1

or TgRASP2 and lacks a homologue outside of Coccidia, and so will not be discussed further in this thesis (Suarez, Lentini et al. 2019).

While this study by Suarez et al., was largely complementary to the results presented in this thesis, there are some key differences between the findings of each study. Both TgRASP2 and PfCERLI1 were shown to be essential for host cell invasion, with knockdown specifically causing a defect in rhoptry secretion (Suarez, Lentini et al. 2019). In contrast to our inability to disrupt either *Pfcerli1* or *Pfcerli2*, TgRASP1 was found to be dispensable for growth, with knockouts demonstrated to have no noticeable loss in fitness (Suarez, Lentini et al. 2019). Moreover, *Tgrasp1* knockouts did not display a compensatory increase in TgRASP2 expression by Western blot (Suarez, Lentini et al. 2019), indicating that the loss of TgRASP1 is not compensated for through increased expression of TgRASP2. Therefore, it is yet to be determined why PfCERLI1 is essential for *P. falciparum* growth while its orthologue PfRASP1 is dispensable for *T. gondii* growth. However, it should be noted that *P. falciparum* and *T. gondii* have very different rhoptry structures and host cell tropisms that could impact on the importance of one RASP protein in a particular cell type.

Our analysis suggests that TgRASP2 is not the direct orthologue of PfCERLI1, and so it is prudent to not infer the functions of PfCERLI1 from observations regarding TgRASP2 without supporting evidence. Differences were observed in localisation of PfCERLI1 between the study by Suarez et al. and the results presented in this thesis. Our quantitative immunofluorescence colocalisation showed convincingly that PfCERLI1 localises to the rhoptry bulb, however Suarez et al. reported PfCERLI1 instead localising to the rhoptry neck (Suarez, Lentini et al. 2019). Localisation analysis of TgRASP2 showed that it, like PfCERLI1 and PfCERLI2, localised to the cytosolic face of the rhoptries. However, unlike PfCERLI1 or PfCERLI2, TgRASP2 also appeared to localise across both the bulb and neck of the rhoptries using both immuno-electron microscopy

and immunofluorescence microscopy (Suarez, Lentini et al. 2019). Based on these localisation results, and the observation that both PfCERLI1 and TgRASP2 were involved in rhoptry secretion, the authors inferred that both PfCERLI1 and TgRASP2 coordinate fusion between the rhoptry neck and PPM right at the apical tip of the host-cell invading merozoite an tachyzoite respectively (Suarez, Lentini et al. 2019). While this may be the case for TgRASP2, our comprehensive localisation of PfCERLI1 as a rhoptry bulb protein suggests that this is unlikely to be the case for PfCERLI1.

As our analysis shows that TgRASP2 is the direct orthologue of PfCERLI2, it is reasonable to hypothesise that PfCERLI2 is more likely to be involved in fusion of the rhoptry neck and PPM membranes based on the reported function of TgRASP2. Like PfCERLI1, however, our quantitative localisation showed that PfCERLI2 also localises to the rhoptry bulb and therefore is unlikely to be involved in fusion between the rhoptry neck and PPM unless it was to translocate there between schizont rupture and merozoite invasion. Moreover, we found that knockdown of PfCERLI2 did not lead to a defect in the secretion of rhoptry neck contents. Instead, we saw an increase in the merozoites that had failed to invade and remained bound to the RBC, consistent with rhoptry neck antigens being secreted and leading to formation of the tight-junction in PfCERLI2 deficient merozoites that failed to invade.

For PfCERLI1 knockdown, we found that there was evidence for reduced secretion of rhoptry neck antigens and that this was associated with a build-up in free merozoites of comparable number to lost invasion events. This indicates that PfCERLI1 deficient parasites are less able to secrete rhoptry neck antigens that are required for tight junction formation. Suarez et al., reported an apical tip localisation for PfCERLI1, differing from our bulb localisation in free merozoites and reduced secretion of rhoptry bulb antigens following conditional knockout of this protein (Suarez, Lentini et al. 2019). However, the apical tip localisation was not quantitatively assessed and the

authors also reported widespread binding of merozoites to the RBC surface following PfCERLI1 knockdown (Suarez, Lentini et al. 2019). These bound merozoites are an indication that the tight junction has formed, but this would not occur frequently if fusion between the rhoptry neck and the PPM is prevented. This is because as secretion of rhoptry neck proteins, essential for the formation of the tight junction, would be blocked if the rhoptry neck and the PPM fail to fuse.

Our analyses does not yet support that PfCERLI1 nor PfCERLI2 are likely to mediate the fusion between the rhoptry neck and PPM in *P. falciparum* based on their localisation in schizonts and the increase of RBC bound merozoites seen following PfCERLI2 knockdown. While our quantitative imaging studies indicate that PfCERLI1 and PfCERLI2 localise to the rhoptry bulb of merozoites, that analysis was performed using merozoites inside mature schizonts. By contrast, the rhoptry neck localisation reported by Suarez et al. for PfCERLI1 is indicated from representative immunofluorescence images of free merozoites (Suarez, Lentini et al. 2019). This discrepancy could possibly be explained by a translocation of PfCERLI1 from rhoptry bulb to neck between schizont rupture and merozoite invasion. Whether this translocation occurs would need to be determined using a fluorescent endogenously tagged PfCERLI1 with live cell imaging of schizont rupture and merozoite invasion. Initial attempts to create this line failed and the generation of these parasites will be undertaken in follow up studies to address this possibility in live parasites. Currently, we leave open the possibility that PfCERLI1 and PfCERLI2 translocate to the apical tip from the rhoptry bulb between schizont rupture and merozoite invasion to facilitate rhoptry neck fusion to the PPM. However, since dynamic changes in rhoptry structure during invasion are thought to start at the rhoptry neck and then work their way towards the bulb, it is difficult to see how translocation of PfCERLI1 and PfCERLI2 in the opposite direction over the same short timescale would be an efficient mechanism to mediate fusion between the PPM and rhoptry neck.

It is important to reiterate that rhoptry structure differs drastically between *P. falciparum* merozoites and *T. gondii* tachyzoites, and thus it cannot be assumed that the role of these proteins is absolutely shared between the two. Therefore, future studies will need to be undertaken to investigate changes in PfCERLI1 and PfCERLI2 localisation between egress and merozoite invasion, along with comparative studies to understand the similarities and differences between the functions of these proteins in *Plasmodium* and *Toxoplasma*.

Evidence and potential mechanisms for involvement of PfCERLI1 and PfCERLI2 in dynamic rhoptry biology

Our current understanding of the mechanisms that control rhoptry fusion, rhoptry secretion, and rhoptry/PPM fusion during apicomplexan invasion is extremely limited. We have characterised PfCERLI1 and PfCERLI2 as cytosolic rhoptry interacting proteins (C-RIPs), a group of proteins whose localisation highlight them as putative candidates for involvement in the dynamic functions of the rhoptry.

Defining the function of PfCERLI1 in rhoptry biology

We have shown that PfCERLI1 knockdown inhibits secretion of rhoptry neck antigens and processing of rhoptry bulb antigens, while Suarez et al. showed that knockdown of PfCERLI1 inhibits rhoptry bulb secretion (Suarez, Lentini et al. 2019). The molecular mechanism of how PfCERLI1 knockdown inhibits rhoptry secretion and RAP1 processing, along with the significance of inhibited RAP1 processing, are currently unclear. While we were unable to see a clear change in rhoptry morphology with PfCERLI1 knockdown by TEM, we did quantitatively identify changes in distribution of the rhoptry neck maker RON4 and the rhoptry bulb marker RAP1 by immunofluorescence microscopy. We hypothesise that these changes in antigen distribution

indicate that normal rhoptry biology is disturbed with PfCERLI1 knockdown and this is likely to contribute to reduced rhoptry antigen secretion.

It has been suggested previously that RAP1 is proteolytically processed by the proteases Plasmepsin IX, which localises to the rhoptry bulb, and SUB1 (Silmon de Monerri, Flynn et al. 2011, Nasamu, Glushakova et al. 2017, Pino, Caldelari et al. 2017, Favuzza, de Lera Ruiz et al. 2020). Notably, Plasmepsin IX knockdown results in a similar phenotype of invasion inhibition to PfCERLI1 knockdown, whereby RAP1 processing is inhibited and merozoites are released but fail to invade (Nasamu, Glushakova et al. 2017, Pino, Caldelari et al. 2017). By contrast, it is currently unclear what influence SUB1 has on invasion, as it also processes SERA5 and this processing event is essential for egress (Silmon de Monerri, Flynn et al. 2011). Considering that both PfCERLI1 and Plasmepsin IX localise to the rhoptry bulb, and their knockdown inhibits RAP1 processing and merozoite invasion, it is possible that given their close proximity, knockdown of one protein may impact on the other. As PfCERLI1 lies on the cytosolic face of the rhoptry and Plasmepsin IX the rhoptry lumen, the most likely explanations for reduced RAP1 cleavage are that PfCERLI1 knockdown either leads to reduced transport of Plasmepsin IX into the rhoptry. Alternatively, changes in rhoptry biology with PfCERLI1 knockdown, as evidenced by changes in rhoptry antigen distribution, may inhibit normal rhoptry bulb function and activation of Plasmepsin IX.

Defining the timing of PfCERLI1 function in rhoptry biology

When PfCERLI1 was knocked down, we observed an increase in free merozoites but detected no noticeable change in the number of merozoites that remained bound to RBCs but failed to invade, indicating these PfCERLI1 deficient merozoites failed to form the tight junction. The inability to form the tight junction is a likely consequence of reduced rhoptry neck protein secretion that we observed following PfCERLI1 knockdown. By contrast, Suarez *et al.*, observed an increase in RBC bound merozoites following PfCERLI1 knockdown, leading them to suggest that

PfCERLI1 knockdown inhibited invasion following tight junction formation (Suarez, Lentini et al. 2019). It is possible that this difference is due to the difference in knockdown system used to study PfCERLI1 function. We utilised the *GlmS* ribozyme system (Prommana, Uthaipibull et al. 2013), while Suarez *et al.*, used a DiCre-mediated conditional knockout system (Knuepfer, Napiorkowska et al. 2017, Suarez, Lentini et al. 2019). With the *GlmS* system (Prommana, Uthaipibull et al. 2013), PfCERLI1 is knocked down in nearly all cells but protein expression is reduced to a low level rather than removed completely. Using the DiCre conditional knockout system, however, *Pfcerli1* is excised from the parasite genome (Knuepfer, Napiorkowska et al. 2017), leaving little to no functional PfCERLI1 during merozoite invasion (Suarez, Lentini et al. 2019). It is possible that this variation in knockdown efficiency may influence whether merozoites form the tight junction or not following PfCERLI1 knockdown. However, we would expect that the DiCre system, with more efficient knockdown, would cause the greatest impact on rhoptry protein secretion and block invasion prior to the formation of the tight junction. Regardless, based on the loss of rhoptry neck antigen secretion following PfCERLI1 knockdown, we hypothesise that PfCERLI1 has a role in rhoptry antigen secretion required for tight junction formation.

Defining the function of PfCERLI2 in rhoptry biology

Knockdown of PfCERLI2 also inhibits rhoptry processing and merozoite invasion, similar to knockdown of PfCERLI1, but key differences in the knockdown phenotypes of these proteins means that they may not have completely overlapping functions. PfCERLI2 knockdown led to a lengthening of the rhoptry that could be quantified by TEM and immunofluorescence microscopy, but did not influence the secretion of rhoptry neck antigens. It should be noted that the secretion of rhoptry bulb antigens could not be measured using the secretion assay that was performed. Rhoptry bulb antigens are secreted directly into the RBC cytosol (Riglar, Richard et al. 2011) and therefore

cannot be detected in the culture supernatant. It is therefore possible that PfCERLI2 knockdown could also lead to a defect in the secretion of rhoptry bulb antigens, but this is yet to be determined.

Defining the timing of PfCERLI2 function in rhoptry biology

It appears that PfCERLI2 knockdown causes a defect during rhoptry biogenesis that causes a significant lengthening of this organelle, but we observe no defect in rhoptry neck antigen secretion following PfCERLI2 knockdown. These data indicate that following PfCERLI2 knockdown, PfCERLI2 deficient merozoites are able to secrete their rhoptry neck antigens and form the tight junction, but then fail to progress invasion further. As there is no rhoptry neck antigen secretion defect, this likely indicates PfCERLI2 knockdown causes a defect in rhoptry bulb secretion or function following tight junction formation. By contrast to PfCERLI2, our results indicate that PfCERLI1 knockdown inhibits the secretion of rhoptry neck antigens, which is supported by the observation that PfCERLI1 deficient merozoites fail to form the tight junction and are not found bound to RBCs in non-GLCN treated cultures. Whether this reflects that PfCERLI2 has a more significant role post tight junction formation than PfCERLI1, or if this difference is a consequence of the different levels of GLCN-induced knockdown will be elucidated in future studies aimed at further defining the timing of PfCERLI1 and PfCERLI2 function.

One potential mechanism for the inhibition of rhoptry bulb secretion following PfCERLI2 knockdown is that the significant rhoptry structural defects, where rhoptries are aberrantly elongated, somehow interferes with fusion between the two rhoptry bulbs. It has previously been suggested that the secretion of rhoptry bulb contents occurs as the two rhoptries fuse together (Hanssen, Dekiwadia et al. 2013), and it is possible that the alteration to rhoptry morphology caused by PfCERLI2 knockdown inhibits this fusion and therefore rhoptry bulb secretion. TgRASP2, the direct orthologue of PfCERLI2, has been shown to interact with TgFormin 1 (Suarez, Lentini et al. 2019), a protein that regulates actin polymerisation and localises to the tight junction during

tachyzoite invasion (Daher, Plattner et al. 2010, Ignatev, Bhargav et al. 2012). Furthermore, PfFormin 1 has been shown to be essential for blood stage growth, and localises between the rhoptry bulb and IMC membranes (Baum, Tonkin et al. 2008). It is not known whether PfCERLI2 interacts with PfFormin 1 but rhoptry fusion and rhoptry bulb secretion are both likely to involve interaction with cytoskeletal elements, and this interaction could therefore provide a platform for this interaction to occur. One hypothesis could be that PfCERLI2 interacts with PfFormin 1 during rhoptry biogenesis, that this interaction controls correct rhoptry morphology, and that when this interaction is inhibited it prevents normal rhoptry fusion and subsequently rhoptry bulb secretion.

PfCERLI1 and PfCERLI2 in other lifecycle stages

Many proteins in *Plasmodium* have been shown to have different function across multiple lifecycle stages (Dearnley, Yeoman et al. 2012, Parkyn Schneider, Liu et al. 2017).Transcriptomic data suggests that PfCERLI1 is expressed more highly in both gametocytes and ookinetes (Aurrecoechea, Brestelli J Fau - Brunk et al. 2008, Lopez-Barragan, Lemieux J Fau - Quinones et al. 2011) than schizonts. Given that both gametocytes and ookinetes lack rhoptries, the localisation and function(s) of PfCERLI1 in these lifecycle stages is difficult to infer. As rhoptries are Golgi-derived, one hypothesis may be that PfCERLI1 localises to different Golgi-derived vesicles/organelles in lifecycle stages lacking rhoptries. It is currently unknown whether PfCERLI1 disruption or knockdown influences these lifecycle stages. Transcriptomic studies of *P. falciparum* suggest that PfCERLI1 is expressed considerably lower in sporozoites than asexual parasites (Zanghì, Vembar et al. 2018, Hoo, Bruske et al. 2019) and PfCERLI1 has not been detected in previous sporozoite proteomic studies. Typically, merozoite rhoptry proteins share overlapping localisations with sporozoite rhoptry proteins (Tokunaga, Nozaki et al. 2019) and so it is likely that if indeed PfCERLI1 is functional in sporozoites that it has a similar function to merozoites. By

contrast to PfCERLI1, transcriptomic studies suggest PfCERLI2 is expressed much lower in ookinetes and gametocytes than asexual parasites (Lopez-Barragan, Lemieux J Fau - Quinones et al. 2011, Delves, Ruecker et al. 2013). Additionally, many PfCERLI2 peptides have been identified in sporozoite proteomic studies (Lindner, Swearingen et al. 2013), suggesting PfCERLI2 is indeed expressed in sporozoites. Like PfCERLI1, PfCERLI2 has not been functionally characterised outside the asexual blood stage of the *P. falciparum* lifecycle.

Evolutionary relationships between CERLI proteins

Emergence and evolution of *cerli* paralogues

CERLI homologues can be found in all Apicomplexa and Chromerida whose genomes are present on the eukaryotic pathogen database (EuPathDB) (Aurrecoechea, Barreto et al. 2017). Chromerida lack true rhoptries and given that the most recent common ancestor of Apicomplexa and Chromerida is thought to have been photosynthetic (Moore, Oborník et al. 2008, Oborník, Modrý et al. 2012, Pontarotti 2017), the ancestral CERLI must have had a function outside of rhoptry secretion. CERLI paralogues have only been characterised in the invasive stages of *P. falciparum* and *T. gondii* with PfCERLI1, PfCERLI2, TgRASP2 all having reported roles in rhoptry biology (Suarez, Lentini et al. 2019). Due to the lack of a growth defect in TgRASP1 knockout parasites, it has not been determined whether it has a role in rhoptry secretion (Suarez, Lentini et al. 2019). As Chromerida, along with *P. falciparum* ookinetes and gametocytes, lack true rhoptries it is possible that CERLI expressed in these organisms, or at these stages of the lifecycle, may more closely mirror the function(s) of the ancestral CERLI (Pontarotti 2017). With the evolutionary origins of rhoptries likely being highly divergent endosomes (Ngô, Yang et al. 2004, Gubbels and Duraisingh 2012, Klinger, Nisbet et al. 2013), it is possible that the CERLI ancestor

mediated endosomal fusion or similar processes analogous to rhoptry biology in modern Apicomplexa. Indeed, formins, which TgRASP2 is thought to interact with, have been shown to be involved in the delivery of secretory vesicles (Evangelista, Zigmond et al. 2003).

Mechanism of *cerli* duplication and subsequent selection

As the presence of two CERLI homologues is highly conserved amongst Apicomplexa, with the exception of *Cryptosporidium* and *Gregarina*, it is likely that following duplication both proteins performed either important or essential functions. This is evidence by the conservation of the PHIS motif across all CERLI homologues, and the conservation of both C2 and PH domains in all CERLI homologues, with the exception of the PH domains of *Plasmodium* CERLI2 homologues. Following on from gene duplication, one of three outcomes are likely to occur. If, following duplication, both the duplicated and ancestral loci retain part of the ancestral function, known as subfunctionalisation, neither gene can be lost or accumulate nonsense mutations, as they both perform non-redundant functions (MacCarthy and Bergman 2007, Sandve, Rohlfs et al. 2018). If a newly duplicated gene has either neutral or negative influence on the fitness of the cell, it is likely to either be deleted, or accumulate significant mutations including nonsense mutations that lead to premature gene termination (Emanuel and Shaikh 2001). In the case where a duplicated gene is functionally redundant, it can accumulate mutations without altering fitness of the cell and these mutations can lead to the emergence of new functions; known as neofunctionalisation (Lynch 2007, Conant and Wolfe 2008).

Given the difficulty in determining whether a *cerli* gene in one organism is the orthologue or paralogue of a *cerli* gene in another organism, because of no clear DNA or amino acid signatures that differentiate the two genes, it is most likely that following gene duplication the *cerli* loci underwent subfunctionalisation. Had they undergone neofunctionalisation, it is likely that clear

cerli1 and *cerli2* orthologues would be evident based on the inheritance of shared DNA or amino acid sequence signatures as each lineage would be adapted to take on significantly different roles. Further support for subfunctionalisation is that both CERLI1 and CERLI2 have retained their rhoptry localisation and rhoptry-associated function, at least across *Plasmodium* and *Toxoplasma*. Had either paralogue undergone neofunctionalisation, there is the potential that this may have also resulted in a change in localisation or function away from the rhoptries.

Functional significance of the decapeptide repeat in *Laverania* CERLI2

Conservation of the C2 and PH domains, along with similar functions across Apicomplexa provide strong evidence for subfunctionalisation of CERLI1 and CERLI2 following duplication. Complicating this, however, is the observation that CERLI2 homologues in *Plasmodium* contain a degenerated PH domain. Furthermore, CERLI2 homologues in the *Plasmodium* subgenus *Laverania* possess a decapeptide repeat towards the C-terminus of the protein. All other CERLI homologues, even in organisms that have only a single CERLI, contain a C2 domain at their N-terminus, a PH domain towards their C-terminus, and lack this decapeptide repeat region. While it is not entirely clear what the functions of these domains are, their conserved presence in all other CERLI homologues across hundreds of millions of years of evolution implicates them as having an important function. By contrast, we showed that the decapeptide repeat region of *Laverania* CERLI2 homologues are undergoing positive selection, suggesting that diversification of this region may be beneficial to parasite fitness.

Decapeptide tandem repeats are extremely poorly characterised in other proteins, with the most well studied example being *Mytilus edulis* foot protein 1 (mfp-1) (Kanyalkar, Srivastava et al. 2002, Lin, Gourdon et al. 2007). Mfp-1 is a large protein that is produced by mussels and is involved in adhesion between mussels and the surfaces that they grow on (Kanyalkar, Srivastava

et al. 2002, Lin, Gourdon et al. 2007). It is not entirely understood how mfp-1 allows adherence to surfaces, but it has been shown to be dependent on 3,4-dihydroxyphenyl-L-alaine (DOPA) post-translational modifications in its repeat region (Kanyalkar, Srivastava et al. 2002, Lin, Gourdon et al. 2007). DOPA modifications, however, involve the modification of tyrosine residues (Lim, Kim et al. 2011), which are not present in the repeats of *Laverania* CERLI2. It is therefore unclear functionally, what the significance of these decapeptide repeats may be, or how these repeats expand.

Following the emergence of the CERLI2 decapeptide repeat, it is not clear whether repeat number changes confer a selective advantage. It is difficult to infer trends across the CERLI2 repeats in *Laverania*, however, it is clear that species more closely related to *P. falciparum* both have more repeats and the amino acids that make their repeat are more well defined. It is therefore possible that the influence of repeat number and structure differs across *Laverania*. It was hypothesised that tolerance of repeats, or the mechanism driving their expansion, may differ across *Laverania* independently of PfCERLI2, whereby repeats either occur more frequently or are more well tolerated in some species rather than others. As a surrogate for the tolerance or frequency of repeat expansion, the genome size of *Laverania* was assessed, but no association between genome size and CERLI2 repeat number was observed. This likely means that changes in repeat number are specific to CERLI2 and based on the positive selection in this region, may have an adaptive function.

Broadly, tandem repeats with highly consistent amino acid sequences are predicted to have expanded more recently than those with less consistent amino acid sequences (Mendes, Lobo et al. 2013). CERLI2 repeats in *P. falciparum* and the most closely related *Laverania*, *P. praefalciparum* and *P. reichenowi*, have a greater number and more consistent repeat sequences compared to more distantly related parasites, such as *P. adleri* and *P. gaboni*. This suggests that the most recent

common ancestor of all *Laverania* may have had a small number of repeats but that these repeats underwent an expansion in the most recent common ancestor of *P. falciparum*, *P. praefalciparum*, and *P. reichenowi*. The large diversity in repeat number between *P. falciparum* isolates and the increased number compared to *P. praefalciparum* and *P. reichenowi* suggests that the CERLI2 repeat expansion has accelerated and recently undergone further changes between *P. falciparum* isolates. A key driver of repeat expansion can be through unequal crossing over during meiosis, with the subsequent expansion of conserved repeats increasing the likelihood of further unequal crossing over and repeat expansion (Gemayel, Vinces et al. 2010, Davies, Nofal et al. 2017). Under this scenario, selection for repeat expansion does not have to be driven directly by function. Furthermore, it can be difficult to infer what, if any, functional changes this may cause to the protein.

Tandem repeats are typically disordered (Davies, Nofal et al. 2017), as is the case for the CERLI2 repeat, but these sequences are not always devoid of function. It has been shown that repeat copy number changes can alter the adhesive and hydrophobicity properties of *Saccharomyces cerevisiae* (Fidalgo, Barrales et al. 2006, Davies, Nofal et al. 2017). Moreover, while tandem repeats are typically disordered, they often form an ordered structure upon binding of a protein interacting partner as is the case for binding between a the repetitive C-terminal domain of RNA polymerase II and proteins of the mediator complex (Lunde, Reichow et al. 2010, Davies, Nofal et al. 2017). Alternatively, if repeat expansion is beneficial, it can be selected for. It is difficult to infer, therefore, if changes to repeat number in CERLI2 are adaptive and functional, neutral, or fitness decreasing.

The repeat region is present in all *Laverania* CERLI2 homologues, which may indicate that it performs an important function. Contrarily, the positive selection occurring in this repeat region, compared to the negative selection occurring across the remainder of the protein, indicates

that the repeat region is tolerant of amino acid changes and expansion. Due to the lack of high-quality genomes for multiple different isolates of *Laverania* spp., it is difficult to infer how variable repeat number is. It is clear, however, that repeat number varies dramatically in *P. falciparum,* with isolate 7G8 containing 10 repeats and isolate CD01 containing 20. For all *P. falciparum* isolates currently available on PlasmoDB (Aurrecoechea, Brestelli J Fau - Brunk et al. 2008) the repeat number is greater than any *Laverania* CERLI2 homologue. If repeat expansion was deleterious to parasite fitness, it is unlikely that it would be tolerated, and we would therefore be unlikely to see multiple parasite isolates with repeat numbers higher than other *Laverania.* We hypothesise that repeat expansion in *P. falciparum* is either neutral, or beneficial, for parasite fitness but there is currently insufficient evidence to suggest whether this is also the case for other *Laverania.*

CERLI1 and CERLI2 as therapeutic targets

Merozoite invasion has previously been suggested as an attractive drug target as it is essential for parasite survival, proteins required for host-cell invasion are often not present in mammalian cells, and essential proteins shared between related parasites represent potential pan-Apicomplexa drug targets (Burns, Balbin et al. 2019, Dans, Weiss et al. 2020). Moreover, no clinically used antimalarials specifically inhibit invasion, therefore existing antimalarial resistance mechanisms are unlikely to influence susceptibility to invasion inhibitory antimalarials. Given their essentiality for blood stage growth, CERLI1 and CERLI2 could represent targets for the development of invasion inhibitory antimalarials. Chloroquine and artemisinins, historically the two most widely used classes of antimalarials, are generally thought to inhibit haeme catabolism (Padmanaban and Rangarajan 2000) and the proteasome (Tilley, Straimer et al. 2016), respectively. Other drugs, such as pyrimethamine and atovaquone work by targeting enzymatic activity (Robertson 2005). Most FDA approved drugs are either antagonists or agonists of G-protein

coupled receptors (Lundstrom 2009), and while similar receptors exist in *Plasmodium* (Madeira, Galante et al. 2008), no currently licensed antimalarials target them. Compounds currently being studied that inhibit merozoite invasion include inhibitors of Plasmepsin IX and X (enzyme inhibitors) (Favuzza, de Lera Ruiz et al. 2020), SUB1 inhibitors (enzyme inhibitors) (Brogi, Giovani et al. 2016), inhibitors of AMA1-RON2 interaction (protein-protein interaction (PPI) inhibitors) (Harris, Casey et al. 2005), and MSP1 inhibitors (glycan mimetics) (Chandramohanadas, Basappa et al. 2014). Given CERLI1's and CERLI2's limited predicted structural complexity, it is likely that drugs designed to inhibit these proteins' functions would need to be drugs that inhibit their interactions with other proteins; known as PPI inhibitors. No currently licensed antimalarials are known PPI inhibitors, however, they are a rapidly emerging class of drugs, particularly in oncology (Zinzalla and Thurston 2009, Scott, Bayly et al. 2016).

It is likely that PfCERLI1 and PfCERLI2 undergo protein-protein interactions that are essential for their function, and by extension merozoite invasion. It has been shown that TgRASP1 and TgRASP2, along with a third protein not present in *Plasmodium* form a tripartite complex (Suarez, Lentini et al. 2019). It is not clear if this complex forms in part in *P. falciparum*, however, it is possible that prevention of complex formation would be inhibitory to merozoite invasion. As mentioned previously, TgRASP2 has been shown to interact with TgFormin 1 (Suarez, Lentini et al. 2019) and this may be important for rhoptry morphology and fusion. If this interaction were to also occur between PfCERLI2 and PfFormin 1, it is possible that this could be developed as a target of PPI inhibitors. Therefore, future identification of PfCERLI1 and PfCERLI2 interacting partners may enable development of PPI inhibitors that block merozoite invasion of the RBC.

In order to identify drug targetable PfCERLI1 and PfCERLI2 protein-protein interactions, pull down assays or proximity ligation assays would need to be undertaken with proteomic identification of interacting partners. Once these interactions have been confirmed experimentally,

PfCERLI1 and PfCERLI2 PPI inhibitors can be identified broadly in one of four ways. High-throughput screening for *in vitro* activity (Wadsworth, Folorunso et al. 2019), fragment-based drug discovery (E., T. et al. 2011), rational design (Rognan 2015), and *in silico* approaches (Kuenemann, Sperandio et al. 2015). It is difficult to predict which of these methods is most likely to identify inhibitors, as this is dependent on the nature of the PPI and how much is known about the structure(s) of the interacting partners. Potential obstacles for these kinds of approaches include recombinant protein production and purification, and protein structure determination; which are necessary for at least one protein in the aforementioned methods. Promisingly, inhibitors of either PPIs and protein-lipid interactions for C2 and PH domains that are effective both *in vitro* and *in vivo* have been identified using rational design (Nicolaes, Kulharia et al. 2014), high-throughput screening (Miao, Skidan et al. 2010), and *in silico* (Segers, Sperandio et al. 2007, Mahadevan, Powis et al. 2008, Chen, Du-Cuny et al. 2015) approaches. Considering the relative rarity of clinically used PPI inhibitors, and relative difficulty of identifying these kinds of inhibitors, it may prove very challenging to develop antimalarials that target PfCERLI1 or PfCERLI2 interactions. If potent inhibitors are identified, however, they would represent very promising antimalarial drug targets due to the uniqueness and importance of the function of these proteins, along with potential to have functions in other lifecycle stages of parasite biology.

Future directions

The studies presented in this thesis, along with other recent studies (Suarez, Lentini et al. 2019), have significantly enhanced our understanding of PfCERLI1 and PfCERLI2 and their role in rhoptry biology. Despite this, much more work is required in future to fully elucidate their functions during merozoite invasion and other stages of the parasite lifecycle, identify their interacting partners and determine the significance of their evolutionary relationship.

Characterisation of PfCERLI1 and PfCERLI2 in other lifecycle stages

PfCERLI1 and PfCERLI2 have not been characterised at all outside of the blood stage of *P. falciparum*. The PfCERLI1^{HAGlmS} and PfCERLI2^{HAGlmS} parasites generated in this study serve as useful tools for studying the blood stage functions of these proteins, but are not readily applicable to the study of other lifecycle stages. Both PfCERLI1^{HAGlmS} and PfCERLI2^{HAGlmS} were transfected into a 3D7 parental line, and while 3D7 likely has the most well characterised blood stage of *P. falciparum* isolates, it is not the most suitable isolate to make viable gametocytes that produce viable offspring in the mosquito. Therefore, in order to characterise the functions of PfCERLI1 and PfCERLI2 during gametocytogenesis and gamete fusion, the HA*GlmS* construct could be transfected into the NF54 isolate, whose PfCERLI1 and PfCERLI2 sequences are identical to 3D7 and are much more suitable for producing viable gametocytes. Using these parasites, thorough studies into the localisations of PfCERLI1 and PfCERLI2 in gametocytes could be performed, along with assessment of the influence of knockdown on gametocytogenesis and gamete fusion. Additionally, these parasites, or *Pfcerli1* and *Pfcerli2* DiCre knockdown parasites, could be taken up by mosquitoes and used to produce sporozoites. This would allow the study of PfCERLI1 and PfCERLI2 localisation in sporozoites and enable assessment of the effect of knockdown of PfCERLI1 or PfCERLI2 on sporozoite invasion.

Identification and characterisation of CERLI1 and CERLI2 interacting partners

PfCERLI1 and PfCERLI2 have key functions in the dynamic biology of rhoptries and it is likely that they both have a number of protein interacting partners that enable these functions. To date, however, no thorough characterisation of the interacting partners of PfCERLI1 or PfCERLI2 has been performed. Many methods for detecting protein interacting partners are routinely employed. However, in addition to understanding the direct interacting partners of PfCERLI1 and

PfCERLI2, which could be achieved using a traditional HA-tagged affinity chromatography experiment, it would be of particular interest to understand the changes in protein-protein interactions during rhoptry biogenesis, as rhoptry function proceeds during invasion and during rhoptry disassembly post invasion. Therefore, proximity ligation-based methods, followed by proteomics will likely be the best approach for both identifying PfCERLI1 and PfCERLI2 interacting partners and enhancing our understanding of nearby and rhoptry protein-protein interactions.

Recently published are two techniques, dimerization-inducible quantitative BioID (DiQ-BioID) (Geiger, Brown et al. 2019, Birnbaum, Scharf et al. 2020) and TurboID (Branon, Bosch et al. 2018), which could be applied to the study of PfCERLI1 an PfCERLI2. DiQ-BioID is a system recently developed for *P. falciparum* whereby the endogenous gene locus expresses the gene of interest conjugated to an FK506 binding protein (FKBP) domain and GFP. Transfected at the same time is an episomal plasmid that expresses the *Escherichia coli* biotin ligase BirA conjugated to an FKPB-rapamycin-binding (FRB) domain and mCherry (Geiger, Brown et al. 2019, Birnbaum, Scharf et al. 2020). Upon addition of rapalog (a structural analogue of rapamycin), the FKBP and FRB domain dimerise, bringing BirA into contact with the gene of interest and then biotinylating it, along with nearby proteins, in a proximity dependent manner (Geiger, Brown et al. 2019, Birnbaum, Scharf et al. 2020). Biotinylated proteins can then be purified using streptavidin and measured quantitatively using mass spectrometry (Geiger, Brown et al. 2019, Birnbaum, Scharf et al. 2020). Biotinylation, however, occurs on a scale of hours (Geiger, Brown et al. 2019, Birnbaum, Scharf et al. 2020) and so attempts to identify PfCERLI1 and PfCERLI2 interacting partners using this method would give little temporal resolution. By contrast, the recently developed TurboID uses a BirA that has undergone directed evolution, which results in efficient biotinylation in under 10 minutes (Branon, Bosch et al. 2018). By replacing the BirA of DiQ-BioID with TurboID,

PfCERLI1 and PfCERLI2 interacting partners could be studied temporally across rhoptry biogenesis, immediately pre-invasion, during invasion, and post invasion. While technically challenging, these experiments would provide a time course of physiologically relevant interactions, with some of these interactions likely being essential for PfCERLI1 and PfCERLI2 function. Following the identification of binding partners using the aforementioned methods, reciprocal experiments would need to be performed to validate these observations. Such an approach would significantly enhance our understanding of PfCERLI1, PfCERLI2, along with other cytosolic rhoptry interacting proteins (C-RIPs), and the dynamic biology of rhoptries during merozoite invasion.

Structural characterisation of PfCERLI1 and PfCERLI2

Resolution of protein structures can provide extremely detailed insights into the functions of a protein, particularly in regard to its interacting partners. Determination of the structure of PfCERLI1 or PfCERLI2 by X-ray crystallography, small angle x-ray scattering (SAXS), or cryo-EM, would therefore be invaluable for further characterisation of these proteins. To date, the structure of relatively few merozoite proteins have been resolved, mostly owing to their large size, extensive proteolytic processing, and disordered regions. ARO was the first *P. falciparum* rhoptry protein, and therefore the first C-RIP, to have its structure determined by X-ray crystallography (Geiger, Brown et al. 2019). This structure provided detailed insights into its potential interactions with AIP and identified sites that are likely involved with other protein-protein interactions (Geiger, Brown et al. 2019). Despite this, it may prove technically difficult to resolve the crystal structure of full-length PfCERLI1 or PfCERLI2. While there are two defined domains in PfCERLI1 and one in PfCERLI2, outside of these domains the proteins are almost entirely intrinsically disordered. Intrinsically disordered proteins typically do not form stable conformations and therefore their

structures are often difficult to determine by X-ray crystallography (Na, Lee et al. 2018). Whether this will be the case with PfCERLI1 and PfCERLI2 is yet to be determined and will have to be addressed by attempting crystallisation experimentally. Promisingly, many C2 and PH domains have been crystallised and had their structure resolved (Dhe-Paganon, Ottinger et al. 1999, Thomas, Dowler et al. 2001, Liu, Song et al. 2006, Zhang, Shen et al. 2013). Therefore, if the full length PfCERLI1 or PfCERLI2 proteins cannot be crystallised, it is likely that these individual domains could be, and structural information could be derived from them. Additionally, intrinsically disordered proteins can either interact with themselves to form a higher order structure or interact with other proteins to adopt a stable conformation, which may allow crystallisation and structure resolution (Dyson and Wright 2005). If PfCERLI1 and PfCERLI2 are produced and remain as monomers, it is possible that interaction with one, or multiple, of their interacting partners may stabilise their structures. After the determination of PfCERLI1 and PfCERLI2 interacting partners, it may therefore be possible to perform co-crystallisation studies to resolve the structures of PfCERLI1 or PfCERLI2, and their protein interacting partners in complex. If the crystal structure of PfCERLI1, PfCERLI2, or either protein in complex with an interacting partner, were to be resolved it would provide a platform from which PPI inhibitors could be developed as previously described. If a crystal structure cannot be determined, it is possible that the structure of PfCERLI1 or PfCERLI2 could be determined using SAXS or cryo-EM. Currently, the resolution range that these techniques routinely cover is significantly lower than X-ray crystallography (Smyth and Martin 2000, Korasick and Tanner 2018, Murata and Wolf 2018) and so the quality of structural information may be limited by this. If PfCERLI1 or PfCERLI2 are found to be members of a larger protein complex, however, these techniques may offer a much more robust analysis of the structure of the complex. Recent analysis of the Rh5-CyRPA-Ripr complex by cryo-EM provided significant insights into the interprotein interactions and behavior of this complex that could not have been

achieved otherwise (Wong, Huang et al. 2019). Moreover, recent structures determined using cryo-EM have resolutions approaching that of X-ray crystallography (Herzik, Wu et al. 2019, Parey, Haapanen et al. 2019, Grinzato, Kandiah et al. 2020) and so it is possible that the usefulness of this technique for studying smaller proteins may be much greater in the near future.

Functional characterisation of CERLI protein features

C2 and PH domains are well studied in other organisms and their range of functions are relatively well understood. By contrast, the PHIS motif is highly conserved in CERLI proteins and is present in other *P. falciparum* proteins including RESA, but to the best of our knowledge have not previously been identified or characterised in other organisms. Additionally, decapeptide tandem repeats, like those possessed by *Laverania* CERLI2 proteins, are extremely poorly understood. Characterisation of these regions in CERLI proteins would reveal not only their functional significance for *P. falciparum* blood stages but may also shed light on their role in CERLI proteins of other Apicomplexans or for similar motifs in diverse organisms.

Functional characterisation of the CERLI PHIS motif

It is entirely unclear what the function of the PHIS motif might be, however its extremely high conservation over hundreds of millions of years of apicomplexan evolution, in both CERLI lineages, suggests it is likely crucial for the function of CERLI proteins. Of particular interest are the proline in the first position of the motif, which is 100 % conserved across all Apicomplexa and Chromerids. Additionally, the histidine at the second position of the motif, the proline at the third position (translocated to the 8th position in *Plasmodium*), and the presence of a negatively charged amino acid (D/E) at the fifth position of the motif are highly conserved across Apicomplexa and Chromerida.

We noted that similar motifs exist in *P. falciparum* proteins including the iron superoxide dismutase, ClpR, RESA and RESA-like proteins. Interestingly, four out of seven PHIS-like motifs from these non-CERLI proteins in *P. falciparum* possess an isoleucine at the third position and a proline at the eight position of the motif, similar to PfCERLI1 and PfCERLI2. In all CERLI homologues outside *Plasmodium*, however, the third position is a proline rather than an isoleucine, and the eight position is flexible. Such a difference between the PHIS motifs in *Plasmodium* and other closely related organisms may indicate phylum specificity in the function(s) of this motif; if indeed they do share a common function. Moreover, the fact that all CERLI homologues across Apicomplexa and Chromera, along with six out of seven non-CERLI *P. falciparum* PHIS-containing proteins contain two proline residues may indicate that two proline residues are important for the function of this motif.

In order to comprehensively understand the contribution of the PHIS region to CERLI function, regional or site-directed mutagenesis studies should be undertaken. Obvious candidates for the function of the PHIS motif are to direct localisation or coordinate a protein-protein interaction. To determine if the PHIS region directs localisation for either PfCERLI1 or PfCERLI2, episomal GFP fusion proteins could be made that lack the PHIS region. Localisation of PHIS-negative PfCERLI1 and PfCERLI2 could then be determined by GFP localisation and compared to the localisation of full-length PfCERLI1 and PfCERLI2. To first determine if the PHIS region is essential for either PfCERLI1 or PfCERLI2, it could be deleted using CRISPR-Cas9 gene editing. If the PHIS-negative parasites are viable, they could be compared to both wildtype and PfCERLI1^{HAGlmS}/PfCERLI2^{HAGlmS} knockdown parasite growth to determine if their fitness is compromised by deletion of this domain. If the PHIS-negative parasites are not viable, point mutations could be made in the PHIS motifs to determine the residues that are crucial for its essential function. Logical candidates would be mutation of the proline in the first position to an

alanine or mutation of the conserved histidine or negatively charged residues. An additional candidate would be to mutate the isoleucine present only in *Plasmodium* to the proline present in all other CERLI proteins. If indeed this amino acid is involved in a *Plasmodium* specific recognition, or function, its mutation is likely to be deleterious to the functions of PfCERLI1 and PfCERLI2. Functional characterisation of this motif would enhance understanding of this conserved motif and may enhance our understanding of similar motifs in otherwise unrelated *P. falciparum* proteins.

Functional characterisation of the *Laverania* CERLI2 decapeptide tandem repeat

Like the PHIS motif, our understanding of the function of the decapeptide tandem repeat of CERLI in *Laverania* is extremely poor. While decapeptide repeats have been studied in a limited capacity previously, they have largely been studied in the context of a post-translational modification that does not occur in the CERLI2 repeat (Kanyalkar, Srivastava et al. 2002, Lin, Gourdon et al. 2007). Therefore, little information from other proteins can be applied specifically to the repeat of CERLI2. One broad question that is yet to be elucidated is whether repeat expansions offer a fitness advantage, or indeed if the repeat region is at all essential for CERLI2 function. Conveniently, the entire decapeptide repeat region is contained within the final exon of *cerli2*. To study whether the repeat region is essential for merozoite invasion, and CERLI2 function, the aforementioned DiCre inducible knockout system could be applied in such a way that it inducibly excises only the final exon, and thus repeat, of *cerli2*. Localisation of PfCERLI2^{NoRepeat} could then be determined to see if the repeat region influences rhoptry targeting of PfCERLI2. Additionally, growth assays could be performed to determine if loss of the repeat region influences blood stage growth or merozoite invasion. If the repeat region is important for merozoite invasion, it is possible that alterations to the repeat number confer changes to parasite fitness. To determine the influence of repeat copy number change on the function of PfCERLI2, CRISPR-Cas9 gene

editing could be used to replace the endogenous 3D7 repeat with either the longer repeat of Dd2, or the shorter repeat of *P. praefalciparum*. Additionally, to determine if repeat structure, rather than copy number, is important for PfCERLI2 function, the 3D7 repeat could be replaced with the degenerated repeats of *P. adleri*. If these modifications to the repeat region produced viable parasites, it could be subsequently determined whether these modifications influence PfCERLI2 localisation or merozoite invasion. These kinds of variable copy number tandem repeats are poorly understood but are common, especially in *P. falciparum* (Davies, Nofal et al. 2017). Thorough characterisation of the PfCERLI2 repeat region would provide evolutionary insights into CERLI2 of *Laverania* and may provide insights into many other repetitive proteins in both *P. falciparum* and other systems.

Characterisation of PfCERLI1 and PfCERLI2 using live cell microscopy

All work presented in this thesis studied PfCERLI1 and PfCERLI2 using either antibodies for protein detection, or episomal overexpression vectors. To get a more thorough understanding of the localisation of these proteins during merozoite invasion, they need to be studied using endogenous fluorescent tagging and live cell microscopy. Our quantitative microscopy analysis, particularly of PfCERLI1, provided very useful information in regard to the interaction of CERLIs with other rhoptry proteins. What this kind of analysis does not address, however, is the dynamic and rapid nature of merozoite invasion. One currently unanswered question that arises from the difference in PfCERLI1 localisation presented in this study and determined by Suarez et al., is whether the localisation of PfCERLI1 changes between schizont rupture and merozoite invasion. To determine this, PfCERLI1^{HAGlmS} parasites could be arrested using compound 1 (prior to PVM rupture) and E64 (prior to RBC membrane rupture). Additionally, purified free merozoites could be produced and arrested with either R1 peptide (prior to tight junction formation) or cytochalasin

D (after tight junction formation). These four treatments could then be fixed and the localisation of PfCERLI1 could be quantitatively determined by comparison with rhoptry neck and rhoptry bulb markers. This would both determine if PfCERLI1 translocation occurs and give some temporal indication of when this occurs.

Analysis of merozoite invasion following knockdown of PfCERLI1 or PfCERLI2 would allow a deeper characterisation of when inhibition occurs during the process of merozoite invasion. Invasion efficiency during live filming, however, is lower than in standard *in vitro* culture conditions and so it is possible that these experiments could not be performed using the *GlmS* system, where knockdown in invasion is limited to around 50% of the merozoite population, that is already established. For live-filming of invasion inhibitory drugs, the drugs are routinely tested at 2 or 4 x IC_{90}, a level of inhibition to maximise the number of clear failed invasion events, which is far beyond what we achieved using the *GlmS* system. A more effective knockdown system, such as DiCre-mediated inducible knockout, is likely to achieve a much greater level of merozoite invasion inhibition and therefore this system may need to be used in order to quantify defects to merozoite invasion.

Concluding remarks

The results presented in this thesis represent a significant advance in our understanding of the molecular biology of invasion by apicomplexan parasites. They have shown that *Pfcerli1* and *Pfcerli2* are paralogues and arose through a gene duplication event that occurred following the divergence of *Cryptosporidium* and all other Apicomplexa. Additionally, they have shown that PfCERLI1 and PfCERLI2 both localise to the cytosolic face of the rhoptry bulb membrane, making them C-RIPs, and that this localisation is likely dependent on the conserved C2 and PH domains for PfCERLI1 and the C2 domain for PfCERLI2. Furthermore, this work has shown that PfCERLI1 and PfCERLI2 are both essential for merozoite invasion and that these proteins are involved in coordinating rhoptry antigen processing and secretion. Despite these advances in our understanding of PfCERLI1 and PfCERLI2, C-RIPs remain poorly characterised. There are many gaps in our understanding of the dynamic protein biology that must direct rhoptry function, and many key questions remain around the functions of PfCERLI1 and PfCERLI2 and their currently unknown interacting partners. PfCERLI1 and PfCERLI2 now stand out as relatively well characterised C-RIPs that will no doubt be the subject of significant number of further studies in the future.

References

Abeku, T. A. (2007). "Response to malaria epidemics in Africa." Emerging infectious diseases **13**(5): 681-686.

Absalon, S., K. Blomqvist, R. M. Rudlaff, T. J. DeLano, M. P. Pollastri and J. D. Dvorin (2018). "Calcium-Dependent Protein Kinase 5 Is Required for Release of Egress-Specific Organelles in *Plasmodium falciparum*." mBio **9**(1): e00130-00118.

Absalon, S., J. A. Robbins and J. D. Dvorin (2016). "An essential malaria protein defines the architecture of blood-stage and transmission-stage parasites." Nature Communications **7**: 11449.

Adams, J. H., B. K. Sim, S. A. Dolan, X. Fang, D. C. Kaslow and L. H. Miller (1992). "A family of erythrocyte binding proteins of malaria parasites." Proceedings of the National Academy of Sciences of the United States of America **89**(15): 7085-7089.

Aikawa, M., M. Torii, A. Sjölander, K. Berzins, P. Perlmann and L. H. Miller (1990). "Pf155/RESA antigen is localized in dense granules of *Plasmodium falciparum* merozoites." Experimental Parasitology **71**(3): 326-329.

Alanine, D. G. W., D. Quinkert, R. Kumarasingha, S. Mehmood, F. R. Donnellan, N. K. Minkah, B. Dadonaite, A. Diouf, F. Galaway, S. E. Silk, A. Jamwal, J. M. Marshall, K. Miura, L. Foquet, S. C. Elias, G. M. Labbé, A. D. Douglas, J. Jin, R. O. Payne, J. J. Illingworth, D. J. Pattinson, D. Pulido, B. G. Williams, W. A. de Jongh, G. J. Wright, S. H. I. Kappe, C. V. Robinson, C. A. Long, B. S. Crabb, P. R. Gilson, M. K. Higgins and S. J. Draper (2019). "Human Antibodies that Slow Erythrocyte Invasion Potentiate Malaria-Neutralizing Antibodies." Cell **178**(1): 216-228.e221.

Albano, F. R., A. Berman, N. La Greca, A. R. Hibbs, M. Wickham, M. Foley and L. Tilley (1999). "A homologue of Sar1p localises to a novel trafficking pathway in malaria-infected erythrocytes." European Journal of Cell Biology **78**(7): 453-462.

Alexander, D., S. Arastu-Kapur, J.-F. Dubremetz and J. C. Boothroyd (2006). "*Plasmodium falciparum* AMA1 binds a rhoptry beck protein homologous to TgRON4, a component of the moving junction in *Toxoplasma gondii*." Eukaryotic Cell **5**: 4.

Almagro Armenteros, J. J., K. D. Tsirigos, C. K. Sonderby, T. N. Petersen, O. Winther, S. Brunak, G. von Heijne and H. Nielsen (2019). "SignalP 5.0 improves signal peptide predictions using deep neural networks." Nat Biotechnol **37**(4): 420-423.

Anders, R. F. (1986). "Multiple cross-reactivities amongst antigens of *Plasmodium falciparum* impair the development of protective immunity against malaria." Parasite Immunol **8**(6): 529-539.

Aniweh, Y., J. Suurbaar, C. M. Morang'a, P. B. Nyarko, K. E. Wright, K. A. Kusi, F. Ansah, E. Kyei-Baafour, E. Quansah, J. Asante, L. G. Thiam, M. K. Higgins and G. A. Awandare (2020). "Analysis of *Plasmodium falciparum* Rh2b deletion polymorphism across different transmission areas." Scientific Reports **10**(1): 1498.

Aurrecoechea, C., A. Barreto, E. Y. Basenko, J. Brestelli, B. P. Brunk, S. Cade, K. Crouch, R. Doherty, D. Falke, S. Fischer, B. Gajria, O. S. Harb, M. Heiges, C. Hertz-Fowler, S. Hu, J. Iodice, J. C. Kissinger, C. Lawrence, W. Li, D. F. Pinney, J. A. Pulman, D. S. Roos, A. Shanmugasundram, F. Silva-Franco, S. Steinbiss, C. J. Stoeckert, Jr., D. Spruill, H. Wang, S. Warrenfeltz and J. Zheng (2017). "EuPathDB: the eukaryotic pathogen genomics database resource." Nucleic Acids Res **45**(D1): D581-d591.

Aurrecoechea, C., A. Barreto, E. Y. Basenko, J. Brestelli, B. P. Brunk, S. Cade, K. Crouch, R. Doherty, D. Falke, S. Fischer, B. Gajria, O. S. Harb, M. Heiges, C. Hertz-Fowler, S. Hu, J. Iodice, J. C. Kissinger, C. Lawrence, W. Li, D. F. Pinney, J. A. Pulman, D. S. Roos, A. Shanmugasundram, F. Silva-Franco, S. A.-O. h. o. o. Steinbiss, C. J. Stoeckert, Jr., D. Spruill, H. Wang, S. Warrenfeltz and J. Zheng (2016). "EuPathDB: the eukaryotic pathogen genomics database resource." Nucleic Acids Research(1362-4962 (Electronic)).

Aurrecoechea, C., B. P. Brestelli J Fau - Brunk, J. Brunk Bp Fau - Dommer, S. Dommer J Fau - Fischer, B. Fischer S Fau - Gajria, X. Gajria B Fau - Gao, A. Gao X Fau - Gingle, G. Gingle A Fau - Grant, O. S. Grant G Fau - Harb, M. Harb Os Fau - Heiges, F. Heiges M Fau - Innamorato, J. Innamorato F Fau - Iodice, J. C. Iodice J Fau - Kissinger, E. Kissinger Jc Fau - Kraemer, W. Kraemer E Fau - Li, J. A. Li W Fau - Miller, V. Miller Ja Fau - Nayak, C. Nayak V Fau - Pennington, D. F. Pennington C Fau - Pinney, D. S. Pinney Df Fau - Roos, C. Roos Ds Fau - Ross, C. J. Ross C Fau - Stoeckert, Jr., C. Stoeckert Cj Jr Fau - Treatman, H. Treatman C Fau - Wang and H. Wang (2008). "PlasmoDB: a functional genomic database for malaria parasites." Nucleic Acids Research(1362-4962 (Electronic)).

Baldi, D. L., K. T. Andrews, R. F. Waller, D. S. Roos, R. F. Howard, B. S. Crabb and A. F. Cowman (2000). "RAP1 controls rhoptry targeting of RAP2 in the malaria parasite *Plasmodium falciparum*." The EMBO journal **19**(11): 2435-2443.

Baldi, D. L., R. Good, M. T. Duraisingh, B. S. Crabb and A. F. Cowman (2002). "Identification and disruption of the gene encoding the third member of the low-

molecular-mass rhoptry complex in *Plasmodium falciparum*." Infection and immunity **70**(9): 5236-5245.

Bannister, L. H., J. M. Hopkins, R. E. Fowler, S. Krishna and G. H. Mitchell (2000). "Ultrastructure of rhoptry development in *Plasmodium falciparum* erythrocytic schizonts." Parasitology **121**(3): 273-287.

Baum, J., D. Richard, J. Healer, M. Rug, Z. Krnajski, T.-W. Gilberger, J. L. Green, A. A. Holder and A. F. Cowman (2006). "A Conserved Molecular Motor Drives Cell Invasion and Gliding Motility across Malaria Life Cycle Stages and Other Apicomplexan Parasites." Journal of Biological Chemistry **281**(8): 5197-5208.

Baum, J., C. J. Tonkin, A. S. Paul, M. Rug, B. J. Smith, S. B. Gould, D. Richard, T. D. Pollard and A. F. Cowman (2008). "A Malaria Parasite Formin Regulates Actin Polymerization and Localizes to the Parasite-Erythrocyte Moving Junction during Invasion." Cell Host & Microbe **3**(3): 188-198.

Beck, J. R., C. Fung, K. W. Straub, I. Coppens, A. A. Vashisht, J. A. Wohlschlegel and P. J. Bradley (2013). "A *Toxoplasma* Palmitoyl Acyl Transferase and the Palmitoylated Armadillo Repeat Protein TgARO Govern Apical Rhoptry Tethering and Reveal a Critical Role for the Rhoptries in Host Cell Invasion but Not Egress." PLOS Pathogens **9**(2): e1003162.

Beeson, J. G., D. R. Drew, M. J. Boyle, G. Feng, F. J. I. Fowkes and J. S. Richards (2016). "Merozoite surface proteins in red blood cell invasion, immunity and vaccines against malaria." FEMS Microbiology Reviews **40**(3): 343-372.

Berhane, A., K. Anderson, S. Mihreteab, K. Gresty, E. Rogier, S. Mohamed, F. Hagos, G. Embaye, A. Chinorumba, A. Zehaie, S. Dowd, N. C. Waters, M. L. Gatton, V. Udhayakumar, Q. Cheng and J. Cunningham (2018). "Major Threat to Malaria Control Programs by *Plasmodium falciparum* Lacking Histidine-Rich Protein 2, Eritrea." Emerging infectious diseases **24**(3): 462-470.

Betuela, I., S. Maraga, M. W. Hetzel, T. Tandrapah, A. Sie, S. Yala, J. Kundi, P. Siba, J. C. Reeder and I. Mueller (2012). "Epidemiology of malaria in the Papua New Guinean highlands." Tropical Medicine & International Health **17**(10): 1181-1191.

Birnbaum, J., S. Flemming, N. Reichard, A. B. Soares, P. Mesén-Ramírez, E. Jonscher, B. Bergmann and T. Spielmann (2017). "A genetic system to study *Plasmodium falciparum* protein function." Nature Methods **14**: 450.

Birnbaum, J., S. Scharf, S. Schmidt, E. Jonscher, W. A. M. Hoeijmakers, S. Flemming, C. G. Toenhake, M. Schmitt, R. Sabitzki, B. Bergmann, U. Fröhlke, P. Mesén-Ramírez, A. Blancke Soares, H. Herrmann, R. Bártfai and T. Spielmann (2020). "A Kelch13-defined endocytosis pathway mediates artemisinin resistance in malaria parasites." Science **367**(6473): 51-59.

Boddey, J. A., M. T. O'Neill, S. Lopaticki, T. G. Carvalho, A. N. Hodder, T. Nebl, S. Wawra, P. van West, Z. Ebrahimzadeh, D. Richard, S. Flemming, T. Spielmann, J. Przyborski, J. J. Babon and A. F. Cowman (2016). "Export of malaria proteins requires co-translational processing of the PEXEL motif independent of phosphatidylinositol-3-phosphate binding." Nature Communications **7**(1): 10470.

Boothroyd, J. C. and J.-F. Dubremetz (2008). "Kiss and spit: the dual roles of *Toxoplasma* rhoptries." Nature Reviews Microbiology **6**(1): 79-88.

Boyle, M. J., D. W. Wilson, J. S. Richards, D. T. Riglar, K. K. A. Tetteh, D. J. Conway, S. A. Ralph, J. Baum and J. G. Beeson (2010). "Isolation of viable *Plasmodium falciparum* merozoites to define erythrocyte invasion events and advance vaccine and drug development." Proceedings of the National Academy of Sciences **107**(32): 14378.

Branon, T. C., J. A. Bosch, A. D. Sanchez, N. D. Udeshi, T. Svinkina, S. A. Carr, J. L. Feldman, N. Perrimon and A. Y. Ting (2018). "Efficient proximity labeling in living cells and organisms with TurboID." Nature Biotechnology **36**(9): 880-887.

Brasil, P., M. G. Zalis, A. de Pina-Costa, A. M. Siqueira, C. B. Júnior, S. Silva, A. L. L. Areas, M. Pelajo-Machado, D. A. M. de Alvarenga, A. C. F. da Silva Santelli, H. G. Albuquerque, P. Cravo, F. V. Santos de Abreu, C. L. Peterka, G. M. Zanini, M. C. Suárez Mutis, A. Pissinatti, R. Lourenço-de-Oliveira, C. F. A. de Brito, M. de Fátima Ferreira-da-Cruz, R. Culleton and C. T. Daniel-Ribeiro (2017). "Outbreak of human malaria caused by *Plasmodium simium* in the Atlantic Forest in Rio de Janeiro: a molecular epidemiological investigation." The Lancet Global Health **5**(10): e1038-e1046.

Brogi, S., S. Giovani, M. Brindisi, S. Gemma, E. Novellino, G. Campiani, M. J. Blackman and S. Butini (2016). "*In silico* study of subtilisin-like protease 1 (SUB1) from different *Plasmodium* species in complex with peptidyl-difluorostatones and characterization of potent pan-SUB1 inhibitors." Journal of Molecular Graphics and Modelling **64**: 121-130.

Bullen, H. E., S. C. Charnaud, M. Kalanon, D. T. Riglar, C. Dekiwadia, N. Kangwanrangsan, M. Torii, T. Tsuboi, J. Baum, S. A. Ralph, A. F. Cowman, T. F. de Koning-Ward, B. S. Crabb and P. R. Gilson (2012). "Biosynthesis, Localization, and Macromolecular Arrangement of the *Plasmodium falciparum* Translocon of Exported Proteins (PTEX)." Journal of Biological Chemistry **287**(11): 7871-7884.

Burns, A. L., J. M. Balbin, D. W. Wilson, P. R. Gilson, M. G. Dans, J. G. Beeson, M. J. Boyle and T. F de Koning-Ward (2019). "Targeting malaria parasite invasion of red blood cells as an antimalarial strategy." FEMS Microbiology Reviews.

Bushell, E., A. R. Gomes, T. Sanderson, B. Anar, G. Girling, C. Herd, T. Metcalf, K. Modrzynska, F. Schwach, R. E. Martin, M. W. Mather, G. I. McFadden, L. Parts, G. G. Rutledge, A. B. Vaidya, K. Wengelnik, J. C. Rayner and O. Billker (2017).

"Functional Profiling of a *Plasmodium* Genome Reveals an Abundance of Essential Genes." Cell **170**(2): 260-272.e268.

Bushell, G. R., L. T. Ingram, C. A. Fardoulys and J. A. Cooper (1988). "An antigenic complex in the rhoptries of *Plasmodium falciparum*." Molecular and Biochemical Parasitology **28**(2): 105-112.

Cabrera, A., S. Herrmann, D. Warszta, J. M. Santos, A. T. John Peter, M. Kono, S. Debrouver, T. Jacobs, T. Spielmann, C. Ungermann, D. Soldati-Favre and T. W. Gilberger (2012). "Dissection of minimal sequence requirements for rhoptry membrane targeting in the malaria parasite." Traffic **13**(10): 1335-1350.

Caminade, C., S. Kovats, J. Rocklov, A. M. Tompkins, A. P. Morse, F. J. Colón-González, H. Stenlund, P. Martens and S. J. Lloyd (2014). "Impact of climate change on global malaria distribution." Proceedings of the National Academy of Sciences **111**(9): 3286-3291.

Cao, J., O. Kaneko, A. Thongkukiatkul, M. Tachibana, H. Otsuki, Q. Gao, T. Tsuboi and M. Torii (2009). "Rhoptry neck protein RON2 forms a complex with microneme protein AMA1 in *Plasmodium falciparum* merozoites." Parasitology International **58**(1): 29-35.

Cappellini, M. D. and G. Fiorelli (2008). "Glucose-6-phosphate dehydrogenase deficiency." The Lancet **371**(9606): 64-74.

Casanova, J. L. (2015). "Human genetic basis of interindividual variability in the course of infection." Proc Natl Acad Sci U S A **112**(51): E7118-7127.

Centers for Disease Control and Prevention. (2018). "Elimination of Malaria in the United States (1947-1951)." 2020, from https://www.cdc.gov/malaria/about/history/elimination_us.html.

Centers for Disease Control and Prevention. (2018). "The History of Malaria, an Ancient DIsease." Retrieved 21/05/2020, 2020, from https://www.cdc.gov/malaria/about/history/.

Chandramohanadas, R., Basappa, B. Russell, K. Liew, Y. H. Yau, A. Chong, M. Liu, K. Gunalan, R. Raman, L. Renia, F. Nosten, S. G. Shochat, M. Dao, R. Sasisekharan, S. Suresh and P. Preiser (2014). "Small molecule targeting malaria merozoite surface protein-1 (MSP-1) prevents host invasion of divergent plasmodial species." J Infect Dis **210**(10): 1616-1626.

Chardin, P. and F. McCormick (1999). "Brefeldin A: The Advantage of Being Uncompetitive." Cell **97**(2): 153-155.

Chaumeau, V., L. Kajeechiwa, B. Fustec, J. Landier, S. Naw Nyo, S. Nay Hsel, P. Phatharakokordbun, P. Kittiphanakun, S. Nosten, M. M. Thwin, S. Win Tun, J. Wiladphaingern, G. Cottrell, D. M. Parker, M. C. Minh, N. Kwansomboon, S.

Metaane, C. Montazeau, K. Kunjanwong, S. Sawasdichai, C. Andolina, C. Ling, W. Haohankhunnatham, P. Christiensen, S. Wanyatip, K. Konghahong, D. Cerqueira, M. Imwong, A. M. Dondorp, T. Chareonviriyaphap, N. J. White, F. H. Nosten and V. Corbel (2019). "Contribution of Asymptomatic *Plasmodium* Infections to the Transmission of Malaria in Kayin State, Myanmar." The Journal of infectious diseases **219**(9): 1499-1509.

Chen, L., L. Du-Cuny, S. Moses, S. Dumas, Z. Song, A. H. Rezaeian, H.-K. Lin, E. J. Meuillet and S. Zhang (2015). "Novel Inhibitors Induce Large Conformational Changes of GAB1 Pleckstrin Homology Domain and Kill Breast Cancer Cells." PLOS Computational Biology **11**(1): e1004021.

Chen, L., Y. Xu, J. Healer, J. K. Thompson, B. J. Smith, M. C. Lawrence and A. F. Cowman (2014). "Crystal structure of PfRh5, an essential *P. falciparum* ligand for invasion of human erythrocytes." eLife **3**: e04187.

Chen, L., Y. Xu, W. Wong, J. K. Thompson, J. Healer, E. D. Goddard-Borger, M. C. Lawrence and A. F. Cowman (2017). "Structural basis for inhibition of erythrocyte invasion by antibodies to *Plasmodium falciparum* protein CyRPA." eLife **6**: e21347.

Cheng, Q., G. Jones, E. X. Liu, C. Kidson and A. Saul (1991). "Identification of a common *Plasmodium* epitope (CPE) recognised by a pan-specific inhibitory monoclonal antibody." Mol Biochem Parasitol **49**(1): 73-82.

Childs, R. A., J. Miao, C. Gowda and L. Cui (2013). "An alternative protocol for *Plasmodium falciparum* culture synchronization and a new method for synchrony confirmation." Malar J **12**: 386.

Chisholm, S. A., E. McHugh, R. Lundie, M. W. A. Dixon, S. Ghosh, M. O'Keefe, L. Tilley, M. Kalanon and T. F. de Koning-Ward (2016). "Contrasting Inducible Knockdown of the Auxiliary PTEX Component PTEX88 in *P. falciparum* and *P. berghei* Unmasks a Role in Parasite Virulence." PLOS ONE **11**(2): e0149296.

Chotivanich, K. T., R. Udomsangpetch, B. Pipitaporn, B. Angus, Y. Suputtamongkol, S. Pukrittayakamee and N. J. White (1998). "Rosetting characteristics of uninfected erythrocytes from healthy individuals and malaria patients." Ann Trop Med Parasitol **92**(1): 45-56.

Cibulskis, R. E., P. Alonso, J. Aponte, M. Aregawi, A. Barrette, L. Bergeron, C. A. Fergus, T. Knox, M. Lynch, E. Patouillard, S. Schwarte, S. Stewart and R. Williams (2016). "Malaria: Global progress 2000 - 2015 and future challenges." Infectious diseases of poverty **5**(1): 61-61.

Coats, D. W. (1999). "Parasitic Life Styles of Marine Dinoflagellates 1." Journal of Eukaryotic Microbiology **46**(4): 402-409.

Cohen, S., G. I. Mc and S. Carrington (1961). "Gamma-globulin and acquired immunity to human malaria." Nature **192**: 733-737.

Coleman, B. I., S. Saha, S. Sato, K. Engelberg, D. J. P. Ferguson, I. Coppens, M. B. Lodoen and M.-J. Gubbels (2018). "A Member of the Ferlin Calcium Sensor Family Is Essential for *Toxoplasma gondii* Rhoptry Secretion." mBio **9**(5): e01510-01518.

Coley, A. M., K. Parisi, R. Masciantonio, J. Hoeck, J. L. Casey, V. J. Murphy, K. S. Harris, A. H. Batchelor, R. F. Anders and M. Foley (2006). "The most polymorphic residue on Plasmodium falciparum apical membrane antigen 1 determines binding of an invasion-inhibitory antibody." Infection and immunity **74**(5): 2628-2636.

Collins, C. R., F. Hackett, J. Atid, M. S. Y. Tan and M. J. Blackman (2017). "The *Plasmodium falciparum* pseudoprotease SERA5 regulates the kinetics and efficiency of malaria parasite egress from host erythrocytes." PLoS pathogens **13**(7): e1006453-e1006453.

Collins, C. R., F. Hackett, M. Strath, M. Penzo, C. Withers-Martinez, D. A. Baker and M. J. Blackman (2013). "Malaria Parasite cGMP-dependent Protein Kinase Regulates Blood Stage Merozoite Secretory Organelle Discharge and Egress." PLOS Pathogens **9**(5): e1003344.

Collins, E., N. M. Vaselli, M. Sylla, A. H. Beavogui, J. Orsborne, G. Lawrence, R. E. Wiegand, S. R. Irish, T. Walker and L. A. Messenger (2019). "The relationship between insecticide resistance, mosquito age and malaria prevalence in *Anopheles gambiae* s.l. from Guinea." Scientific Reports **9**(1): 8846.

Comeaux, C. A., B. I. Coleman, A. K. Bei, N. Whitehurst and M. T. Duraisingh (2011). "Functional analysis of epigenetic regulation of tandem RhopH1/clag genes reveals a role in *Plasmodium falciparum* growth." Molecular Microbiology **80**(2): 378-390.

Conant, G. C. and K. H. Wolfe (2008). "Turning a hobby into a job: How duplicated genes find new functions." Nature Reviews Genetics **9**(12): 938-950.

Cooper, J. A., L. T. Ingram, G. R. Bushell, C. A. Fardoulys, D. Stenzel, L. Schofield and A. J. Saul (1988). "The 140/130/105 kilodalton protein complex in the rhoptries of *Plasmodium falciparum* consists of discrete polypeptides." Molecular and Biochemical Parasitology **29**(2): 251-260.

Coronado, L. M., C. T. Nadovich and C. Spadafora (2014). "Malarial hemozoin: from target to tool." Biochimica et biophysica acta **1840**(6): 2032-2041.

Counihan, N. A., S. A. Chisholm, H. E. Bullen, A. Srivastava, P. R. Sanders, T. K. Jonsdottir, G. E. Weiss, S. Ghosh, B. S. Crabb, D. J. Creek, P. R. Gilson and T. F.

de Koning-Ward (2017). "*Plasmodium falciparum* parasites deploy RhopH2 into the host erythrocyte to obtain nutrients, grow and replicate." eLife **6**: e23217.

Counihan, N. A., M. Kalanon, R. L. Coppel and T. F. de Koning-Ward (2013). "*Plasmodium* rhoptry proteins: why order is important." Trends in Parasitology **29**(5): 228-236.

Cowman, A. F., D. L. Baldi, J. Healer, K. E. Mills, R. A. O'Donnell, M. B. Reed, T. Triglia, M. E. Wickham and B. S. Crabb (2000). "Functional analysis of proteins involved in *Plasmodium falciparum* merozoite invasion of red blood cells." FEBS Letters **476**(1-2): 84-88.

Cowman, A. F. and B. S. Crabb (2006). "Invasion of Red Blood Cells by Malaria Parasites." Cell **124**(4): 755-766.

Cowman, A. F., J. Healer, D. Marapana and K. Marsh (2016). "Malaria: Biology and Disease." Cell **167**(3): 610-624.

Cowman, A. F., C. J. Tonkin, W. H. Tham and M. T. Duraisingh (2017). "The Molecular Basis of Erythrocyte Invasion by Malaria Parasites." Cell Host and Microbe **22**(2): 232-245.

Crabb, B. S., M. Rug, T.-W. Gilberger, J. K. Thompson, T. Triglia, A. G. Maier and A. F. Cowman (2004). Transfection of the Human Malaria Parasite *Plasmodium falciparum*. Parasite Genomics Protocols. S. E. Melville. Totowa, NJ, Humana Press**:** 263-276.

Crosnier, C., L. Y. Bustamante, S. J. Bartholdson, A. K. Bei, M. Theron, M. Uchikawa, S. Mboup, O. Ndir, D. P. Kwiatkowski, M. T. Duraisingh, J. C. Rayner and G. J. Wright (2011). "Basigin is a receptor essential for erythrocyte invasion by *Plasmodium falciparum*." Nature **480**(7378): 534-537.

Cunningham, J., S. Jones, M. L. Gatton, J. W. Barnwell, Q. Cheng, P. L. Chiodini, J. Glenn, S. Incardona, C. Kosack, J. Luchavez, D. Menard, S. Nhem, W. Oyibo, R. R. Rees-Channer, I. Gonzalez and D. Bell (2019). "A review of the WHO malaria rapid diagnostic test product testing programme (2008–2018): performance, procurement and policy." Malaria Journal **18**(1): 387.

Curtidor, H., L. C. Patiño, G. Arévalo-Pinzón, M. E. Patarroyo and M. A. Patarroyo (2011). "Identification of the *Plasmodium falciparum* rhoptry neck protein 5 (PfRON5)." Gene **474**(1): 22-28.

Curtidor, H., L. C. Patiño, G. Arévalo-Pinzón, M. Vanegas, M. E. Patarroyo and M. A. Patarroyo (2014). "*Plasmodium falciparum* rhoptry neck protein 5 peptides bind to human red blood cells and inhibit parasite invasion." Peptides **53**: 210-217.

Cutts, J. C., P. A. Agius, L. Zaw, R. Powell, K. Moore, B. Draper, J. A. Simpson and F. J. I. Fowkes (2020). "Pregnancy-specific malarial immunity and risk of malaria in

pregnancy and adverse birth outcomes: a systematic review." BMC Medicine **18**(1): 14.

Daher, W., F. Plattner, M.-F. Carlier and D. Soldati-Favre (2010). "Concerted Action of Two Formins in Gliding Motility and Host Cell Invasion by *Toxoplasma gondii*." PLOS Pathogens **6**(10): e1001132.

Dans, M. G., G. E. Weiss, D. W. Wilson, B. E. Sleebs, B. S. Crabb, T. F. de Koning-Ward and P. R. Gilson (2020). "Screening the Medicines for Malaria Venture Pathogen Box for invasion and egress inhibitors of the blood stage of *Plasmodium falciparum* reveals several inhibitory compounds." International Journal for Parasitology **50**(3): 235-252.

Das, B. S. (2008). "Renal failure in malaria." J Vector Borne Dis **45**(2): 83-97.

Das, S., B. Saha, A. K. Hati and S. Roy (2018). "Evidence of Artemisinin-Resistant *Plasmodium falciparum* Malaria in Eastern India." New England Journal of Medicine **379**(20): 1962-1964.

Davies, H. M., S. D. Nofal, E. J. McLaughlin and A. R. Osborne (2017). "Repetitive sequences in malaria parasite proteins." FEMS microbiology reviews **41**(6): 923-940.

Dawn, A., S. Singh, K. R. More, F. A. Siddiqui, N. Pachikara, G. Ramdani, G. Langsley and C. E. Chitnis (2014). "The Central Role of cAMP in Regulating *Plasmodium falciparum* Merozoite Invasion of Human Erythrocytes." PLOS Pathogens **10**(12): e1004520.

de Koning-Ward, T. F., P. R. Gilson, J. A. Boddey, M. Rug, B. J. Smith, A. T. Papenfuss, P. R. Sanders, R. J. Lundie, A. G. Maier, A. F. Cowman and B. S. Crabb (2009). "A newly discovered protein export machine in malaria parasites." Nature **459**(7249): 945-949.

Dearnley, M. K., J. A. Yeoman, E. Hanssen, S. Kenny, L. Turnbull, C. B. Whitchurch, L. Tilley and M. W. A. Dixon (2012). "Origin, composition, organization and function of the inner membrane complex of *Plasmodium falciparum* gametocytes." Journal of Cell Science **125**(8): 2053.

Deitsch, K., C. Driskill and T. Wellems (2001). "Transformation of malaria parasites by the spontaneous uptake and expression of DNA from human erythrocytes." Nucleic acids research **29**(3): 850-853.

Delemarre, B. J. and H. J. van der Kaay (1979). "[Tropical malaria contracted the natural way in the Netherlands]." Ned Tijdschr Geneeskd **123**(46): 1981-1982.

Delgadillo, R. F., M. L. Parker, M. Lebrun, M. J. Boulanger and D. Douguet (2016). "Stability of the *Plasmodium falciparum* AMA1-RON2 Complex Is Governed by the Domain II (DII) Loop." PLoS One **11**(1): e0144764.

Delves, M. J., A. Ruecker, U. Straschil, J. Lelièvre, S. Marques, M. J. López-Barragán, E. Herreros and R. E. Sinden (2013). "Male and Female *Plasmodium falciparum* Mature Gametocytes Show Different Responses to Antimalarial Drugs." Antimicrobial Agents and Chemotherapy **57**(7): 3268-3274.

Dent, A. E., R. Nakajima, L. Liang, E. Baum, A. M. Moormann, P. O. Sumba, J. Vulule, D. Babineau, A. Randall, D. H. Davies, P. L. Felgner and J. W. Kazura (2015). "*Plasmodium falciparum* Protein Microarray Antibody Profiles Correlate With Protection From Symptomatic Malaria in Kenya." J Infect Dis **212**(9): 1429-1438.

Deponte, M., H. C. Hoppe, M. C. S. Lee, A. G. Maier, D. Richard, M. Rug, T. Spielmann and J. M. Przyborski (2012). "Wherever I may roam: Protein and membrane trafficking in *P. falciparum*-infected red blood cells." Molecular and Biochemical Parasitology **186**(2): 95-116.

Dhe-Paganon, S., E. A. Ottinger, R. T. Nolte, M. J. Eck and S. E. Shoelson (1999). "Crystal structure of the pleckstrin homology-phosphotyrosine binding (PH-PTB) targeting region of insulin receptor substrate 1." Proceedings of the National Academy of Sciences **96**(15): 8378-8383.

Dobbs, K. R. and A. E. Dent (2016). "*Plasmodium* malaria and antimalarial antibodies in the first year of life." Parasitology **143**(2): 129-138.

Dondorp, A. M. (2005). "Pathophysiology, clinical presentation and treatment of cerebral malaria." Nerology Asia **10**.

Dondorp, A. M., F. Nosten, P. Yi, D. Das, A. P. Phyo, J. Tarning, K. M. Lwin, F. Ariey, W. Hanpithakpong, S. J. Lee, P. Ringwald, K. Silamut, M. Imwong, K. Chotivanich, P. Lim, T. Herdman, S. S. An, S. Yeung, P. Singhasivanon, N. P. J. Day, N. Lindegardh, D. Socheat and N. J. White (2009). "Artemisinin Resistance in *Plasmodium falciparum* Malaria." New England Journal of Medicine **361**(5): 455-467.

Doolan, D. L., C. Dobaño and J. K. Baird (2009). "Acquired immunity to malaria." Clinical microbiology reviews **22**(1): 13-36.

Dowse, T. J., K. Koussis, M. J. Blackman and D. Soldati-Favre (2008). Roles of Proteases during Invasion and Egress by *Plasmodium* and *Toxoplasma*. Molecular Mechanisms of Parasite Invasion: Subcellular Biochemistry. B. A. Burleigh and D. Soldati-Favre. New York, NY, Springer New York**:** 121-139.

Dvorin, J. D., A. K. Bei, B. I. Coleman and M. T. Duraisingh (2010). "Functional diversification between two related *Plasmodium falciparum* merozoite invasion ligands is determined by changes in the cytoplasmic domain." Molecular Microbiology **75**(4): 990-1006.

Dvorin, J. D., D. C. Martyn, S. D. Patel, J. S. Grimley, C. R. Collins, C. S. Hopp, A. T. Bright, S. Westenberger, E. Winzeler, M. J. Blackman, D. A. Baker, T. J.

Wandless and M. T. Duraisingh (2010). "A Plant-Like Kinase in *Plasmodium falciparum* Regulates Parasite Egress from Erythrocytes." Science **328**(5980): 910-912.

Dyrløv Bendtsen, J., H. Nielsen, G. von Heijne and S. Brunak (2004). "Improved Prediction of Signal Peptides: SignalP 3.0." Journal of Molecular Biology **340**(4): 783-795.

Dyson, H. J. and P. E. Wright (2005). "Intrinsically unstructured proteins and their functions." Nature Reviews Molecular Cell Biology **6**(3): 197-208.

E., V., S. T., M. M., G. S. and H. M. (2011). Targeting Protein-Protein Interactions and Fragment-Based Drug Discovery. Fragment-Based Drug Discovery and X-Ray Crystallography. Berlin, Germany, Springer.

Ebrahimzadeh, Z., A. Mukherjee, M.-È. Crochetière, A. Sergerie, S. Amiar, L. A. Thompson, D. Gagnon, D. Gaumond, R. V. Stahelin, J. B. Dacks and D. Richard (2019). "A pan-apicomplexan phosphoinositide-binding protein acts in malarial microneme exocytosis." EMBO reports **20**(6): e47102.

Ekland, Eric H., Myles H. Akabas and David A. Fidock (2011). "Taking Charge: Feeding Malaria via Anion Channels." Cell **145**(5): 645-647.

Elsworth, B., K. Matthews, C. Q. Nie, M. Kalanon, S. C. Charnaud, P. R. Sanders, S. A. Chisholm, N. A. Counihan, P. J. Shaw, P. Pino, J. A. Chan, M. F. Azevedo, S. J. Rogerson, J. G. Beeson, B. S. Crabb, P. R. Gilson and T. F. de Koning-Ward (2014). "PTEX is an essential nexus for protein export in malaria parasites." Nature **511**(7511): 587-591.

Emanuel, B. S. and T. H. Shaikh (2001). "Segmental duplications: an 'expanding' role in genomic instability and disease." Nat Rev Genet **2**(10): 791-800.

English, M., R. Sauerwein, C. Waruiru, M. Mosobo, J. Obiero, B. Lowe and K. Marsh (1997). "Acidosis in severe childhood malaria." Quarterly Journal of Medicine **90**: 7.

Evangelista, M., S. Zigmond and C. Boone (2003). "Formins: signaling effectors for assembly and polarization of actin filaments." Journal of Cell Science **116**(13): 2603-2611.

Favuzza, P., M. de Lera Ruiz, J. K. Thompson, T. Triglia, A. Ngo, R. W. J. Steel, M. Vavrek, J. Christensen, J. Healer, C. Boyce, Z. Guo, M. Hu, T. Khan, N. Murgolo, L. Zhao, J. S. Penington, K. Reaksudsan, K. Jarman, M. H. Dietrich, L. Richardson, K.-Y. Guo, S. Lopaticki, W.-H. Tham, M. Rottmann, T. Papenfuss, J. A. Robbins, J. A. Boddey, B. E. Sleebs, H. J. Sabroux, J. A. McCauley, D. B. Olsen and A. F. Cowman (2020). "Dual Plasmepsin-Targeting Antimalarial Agents Disrupt Multiple Stages of the Malaria Parasite Life Cycle." Cell Host & Microbe.

Fidalgo, M., R. R. Barrales, J. I. Ibeas and J. Jimenez (2006). "Adaptive evolution by mutations in the FLO11 gene." Proceedings of the National Academy of Sciences **103**(30): 11228-11233.

Fluckiger, F. and D. Hanburg (1874). Pharmacographia: A history of the principal drugs of vegtable origin met with in Great Britain and British India. London, United Kingdom, Macmillan and Co.

Foley, M., L. Tilley, W. H. Sawyer and R. F. Anders (1991). "The ring-infected erythrocyte surface antigen of *Plasmodium falciparum* associates with spectrin in the erythrocyte membrane." Mol Biochem Parasitol **46**(1): 137-147.

Food and Agriculture Organisation of the United Nations and World Organisation for Animal Health. (2011). "Joint FAO/OIE Committee on Global Rinderpest Eradication." Retrieved 14/05/2020, 2020, from https://www.oie.int/doc/ged/D10943.PDF.

Foth, B. J., M. C. Goedecke and D. Soldati (2006). "New insights into myosin evolution and classification." Proceedings of the National Academy of Sciences of the United States of America **103**(10): 3681-3686.

Galaway, F., L. G. Drought, M. Fala, N. Cross, A. C. Kemp, J. C. Rayner and G. J. Wright (2017). "P113 is a merozoite surface protein that binds the N terminus of *Plasmodium falciparum* RH5." Nature Communications **8**(1): 14333.

Galaway, F., R. Yu, A. Constantinou, F. Prugnolle and G. J. Wright (2019). "Resurrection of the ancestral RH5 invasion ligand provides a molecular explanation for the origin of *P. falciparum* malaria in humans." PLOS Biology **17**(10): e3000490.

Gao, X., K. Gunalan, S. S. L. Yap and P. R. Preiser (2013). "Triggers of key calcium signals during erythrocyte invasion by *Plasmodium falciparum*." Nat Commun **4**.

Gao, Y. H., H. L. Li, Y. Lu, F. M. Gao, Y. H. Lin, H. C. Zhou, L. H. Zhang and H. Wang (2009). "Identification of a vaccine candidate antigen, PfMAg-1, from *Plasmodium falciparum* with monoclonal antibody M26-32." Parasitol Res **105**(6): 1723-1732.

Garnham, P. (1980). "Relapses in malaria." Cahiers ORSTOM, Entomologie Medicale et Parasitologie **18**(2): 103-106.

Gates, B. (2007). "Malaria Forum Keynote Address." Retrieved 08/05/2020, 2020, from https://www.gatesfoundation.org/Media-Center/Speeches/2007/10/Bill-Gates-Malaria-Forum.

Gates, M. F. (2007). "Malaria Forum Keynote Address." Retrieved 08/05/2020, 2020, from https://www.gatesfoundation.org/media-center/speeches/2007/10/melinda-french-gates-malaria-forum.

GBD 2015 Mortality and Causes of Death Collaborators (2016). "Global, regional, and national life expectancy, all-cause mortality, and cause-specific mortality for 249 causes of death, 1980-2015: a systematic analysis for the Global Burden of Disease Study 2015." Lancet (London, England) **388**(10053): 1459-1544.

Geiger, M., C. Brown, J. S. Wichers, J. Strauss, A. Lill, R. Thuenauer, B. Liffner, L. Wilcke, S. Lemcke, D. Heincke, S. Pazicky, A. Bachmann, C. Löw, D. W. Wilson, M. Filarsky, P.-C. Burda, K. Zhang, M. Junop and T. W. Gilberger (2019). "Structural Insights Into PfARO and Characterization of its Interaction With PfAIP." Journal of Molecular Biology.

Gemayel, R., M. D. Vinces, M. Legendre and K. J. Verstrepen (2010). "Variable tandem repeats accelerate evolution of coding and regulatory sequences." Annu Rev Genet **44**: 445-477.

Genton, B., I. Betuela, I. Felger, F. Al-Yaman, R. F. Anders, A. Saul, L. Rare, M. Baisor, K. Lorry, G. V. Brown, D. Pye, D. O. Irving, T. A. Smith, H. P. Beck and M. P. Alpers (2002). "A recombinant blood-stage malaria vaccine reduces *Plasmodium falciparum* density and exerts selective pressure on parasite populations in a phase 1-2b trial in Papua New Guinea." J Infect Dis **185**(6): 820-827.

Georgieff, M. K. (2011). "Long-term brain and behavioral consequences of early iron deficiency." Nutrition reviews **69 Suppl 1**(Suppl 1): S43-S48.

Gerald, N., B. Mahajan and S. Kumar (2011). "Mitosis in the human malaria parasite *Plasmodium falciparum*." Eukaryotic cell **10**(4): 474-482.

Ghoneim, M. A. (2013). "Trafficking of Plasmodium falciparum chimeric rhoptry protein with Brefeldin A." Folia Parasitologica **60**(1): 75-78.

Ghosh, A. K. and M. Jacobs-Lorena (2009). "Plasmodium sporozoite invasion of the mosquito salivary gland." Current opinion in microbiology **12**(4): 394-400.

Ghosh, S., K. Kennedy, P. Sanders, K. Matthews, S. A. Ralph, N. A. Counihan and T. F. de Koning-Ward (2017). "The Plasmodium rhoptry associated protein complex is important for parasitophorous vacuole membrane structure and intraerythrocytic parasite growth." Cellular Microbiology **19**(8): e12733.

Gilberger, T. W., J. K. Thompson, T. Triglia, R. T. Good, M. T. Duraisingh and A. F. Cowman (2003). "A novel erythrocyte binding antigen-175 paralogue from Plasmodium falciparum defines a new trypsin-resistant receptor on human erythrocytes." J Biol Chem **278**(16): 14480-14486.

Gosling, R. and L. von Seidlein (2016). "The Future of the RTS,S/AS01 Malaria Vaccine: An Alternative Development Plan." PLoS medicine **13**(4): e1001994-e1001994.

Grinzato, A., E. Kandiah, C. Lico, C. Betti, S. Baschieri and G. Zanotti (2020). "Atomic structure of potato virus X, the prototype of the Alphaflexiviridae family." Nature Chemical Biology **16**(5): 564-569.

Gubbels, M.-J. and M. T. Duraisingh (2012). "Evolution of apicomplexan secretory organelles." International journal for parasitology **42**(12): 1071-1081.

Gunasekaran, K., S. S. Sahu and P. Jambulingam (2014). "Estimation of vectorial capacity of *Anopheles minimus* Theobald & *An. fluviatilis* James (Diptera: Culicidae) in a malaria endemic area of Odisha State, India." The Indian journal of medical research **140**(5): 653-659.

Guttery, D. S., A. A. Holder and R. Tewari (2012). "Sexual development in *Plasmodium*: lessons from functional analyses." PLoS pathogens **8**(1): e1002404-e1002404.

Håkansson, S., A. J. Charron and L. D. Sibley (2001). "*Toxoplasma* evacuoles: a two-step process of secretion and fusion forms the parasitophorous vacuole." The EMBO journal **20**(12): 3132-3144.

Hallée, S., J. A. Boddey, A. F. Cowman and D. Richard (2018). "Evidence that the *Plasmodium falciparum* Protein Sortilin Potentially Acts as an Escorter for the Trafficking of the Rhoptry-Associated Membrane Antigen to the Rhoptries." mSphere **3**(1).

Han, M., C. E. Napier, S. Frolich, E. Teber, T. Wong, J. R. Noble, E. H. Y. Choi, R. D. Everett, A. J. Cesare and R. R. Reddel (2019). "Synthetic lethality of cytolytic HSV-1 in cancer cells with ATRX and PML deficiency." J Cell Sci **132**(5).

Hanoune, J. and N. Defer (2001). "Regulation and Role of Adenylyl Cyclase Isoforms." Annual Review of Pharmacology and Toxicology **41**(1): 145-174.

Hanssen, E., C. Dekiwadia, D. T. Riglar, M. Rug, L. Lemgruber, A. F. Cowman, M. Cyrklaff, M. Kudryashev, F. Frischknecht, J. Baum and S. A. Ralph (2013). "Electron tomography of *Plasmodium falciparum* merozoites reveals core cellular events that underpin erythrocyte invasion." Cellular Microbiology **15**(9): 1457-1472.

Harris, K. S., J. L. Casey, A. M. Coley, R. Masciantonio, J. K. Sabo, D. W. Keizer, E. F. Lee, A. McMahon, R. S. Norton, R. F. Anders and M. Foley (2005). "Binding hot spot for invasion inhibitory molecules on *Plasmodium falciparum* apical membrane antigen 1." Infect Immun **73**(10): 6981-6989.

Hartmeyer, G. N., C. R. Stensvold, T. Fabricius, E. S. Marmolin, S. V. Hoegh, H. V. Nielsen, M. Kemp and L. S. Vestergaard (2019). "*Plasmodium cynomolgi* as Cause of Malaria in Tourist to Southeast Asia, 2018." Emerg Infect Dis **25**(10): 1936-1939.

Herzik, M. A., M. Wu and G. C. Lander (2019). "High-resolution structure determination of sub-100 kDa complexes using conventional cryo-EM." Nature Communications **10**(1): 1032.

Ho, C.-M., J. R. Beck, M. Lai, Y. Cui, D. E. Goldberg, P. F. Egea and Z. H. Zhou (2018). "Malaria parasite translocon structure and mechanism of effector export." Nature **561**(7721): 70-75.

Hodder, A. N., P. E. Crewther, M. L. Matthew, G. E. Reid, R. L. Moritz, R. J. Simpson and R. F. Anders (1996). "The disulfide bond structure of *Plasmodium* apical membrane antigen-1." J Biol Chem **271**(46): 29446-29452.

Holt, D. C., D. L. Gardiner, E. A. Thomas, M. Mayo, P. F. Bourke, C. J. Sutherland, R. Carter, G. Myers, D. J. Kemp and K. R. Trenholme (1999). "The cytoadherence linked asexual gene family of *Plasmodium falciparum*: are there roles other than cytoadherence?" International Journal for Parasitology **29**(6): 939-944.

Hoo, R., E. Bruske, S. Dimonte, L. Zhu, B. Mordmüller, B. K. L. Sim, P. G. Kremsner, S. L. Hoffman, Z. Bozdech, M. Frank and P. R. Preiser (2019). "Transcriptome profiling reveals functional variation in *Plasmodium falciparum* parasites from controlled human malaria infection studies." EBioMedicine **48**: 442-452.

Howard, R. F., D. L. Narum, M. Blackman and J. Thurman (1998). "Analysis of the processing of *Plasmodium falciparum* rhoptry-associated protein 1 and localization of Pr86 to schizont rhoptries and p67 to free merozoites." Molecular and Biochemical Parasitology **92**(1): 111-122.

Howard, R. F. and C. M. Schmidt (1995). "The secretory pathway of *Plasmodium falciparum* regulates transport of p82/RAP-1 to the rhoptries." Molecular and Biochemical Parasitology **74**(1): 43-54.

Hu, G., A. Cabrera, M. Kono, S. Mok, B. K. Chaal, S. Haase, K. Engelberg, S. Cheemadan, T. Spielmann, P. R. Preiser, T.-W. Gilberger and Z. Bozdech (2009). "Transcriptional profiling of growth perturbations of the human malaria parasite *Plasmodium falciparum*." Nature Biotechnology **28**: 91.

Hulden, L. and L. Hulden (2011). "Activation of the hypnozoite: a part of *Plasmodium vivax* life cycle and survival." Malaria journal **10**: 90-90.

Ignatev, A., S. P. Bhargav, J. Vahokoski, P. Kursula and I. Kursula (2012). "The Lasso Segment Is Required for Functional Dimerization of the *Plasmodium* Formin 1 FH2 Domain." PLOS ONE **7**(3): e33586.

Ingham, V. A., A. Anthousi, V. Douris, N. J. Harding, G. Lycett, M. Morris, J. Vontas and H. Ranson (2020). "A sensory appendage protein protects malaria vectors from pyrethroids." Nature **577**(7790): 376-380.

Ito, D., E.-T. Han, S. Takeo, A. Thongkukiatkul, H. Otsuki, M. Torii and T. Tsuboi (2011). "Plasmodial ortholog of *Toxoplasma gondii* rhoptry neck protein 3 is localized to the rhoptry body." Parasitology International **60**(2): 132-138.

Ito, D., E. Takashima, T. Yamasaki, S. Hatano, T. Hasegawa, K. Miura, M. Morita, A. Thongkukiatkul, M. Diakite, C. A. Long, J. Sattabongkot, R. Udomsangpetch, H. Iriko, T. Ishino and T. Tsuboi (2019). "Antibodies against a *Plasmodium falciparum* RON12 inhibit merozoite invasion into erythrocytes." Parasitology International **68**(1): 87-91.

Jacot, D., W. Daher and D. Soldati-Favre (2013). "*Toxoplasma gondii* myosin F, an essential motor for centrosomes positioning and apicoplast inheritance." The EMBO Journal **32**(12): 1702-1716.

Jmol. "Jmol: an open-source Java viewer for chemical structures in 3D." 2019, from http://www.jmol.org.

Kaneko, O., B. Y. S. Y. Lim, H. Iriko, I. T. Ling, H. Otsuki, M. Grainger, T. Tsuboi, J. H. Adams, D. Mattei, A. A. Holder and M. Torii (2005). "Apical expression of three RhopH1/Clag proteins as components of the *Plasmodium falciparum* RhopH complex." Molecular and Biochemical Parasitology **143**(1): 20-28.

Kanyalkar, M., S. Srivastava and E. Coutinho (2002). "Conformation of a model peptide of the tandem repeat decapeptide in mussel adhesive protein by NMR and MD simulations." Biomaterials **23**(2): 389-396.

Kawai, S., I. Igarashi, A. Abgaandorjiin, K. Miyazawa, H. Ikadai, H. Nagasawa, K. Fujisaki, T. Mikami, N. Suzuki and H. Matsuda (1999). "Ultrastructural characteristics of *Babesia caballi* in equine erythrocytes *in vitro*." Parasitol Res **85**(10): 794-799.

Keeley, A. and D. Soldati (2004). "The glideosome: a molecular machine powering motility and host-cell invasion by Apicomplexa." Trends Cell Biol **14**(10): 528-532.

Kelley, L. A., S. Mezulis, C. M. Yates, M. N. Wass and M. J. E. Sternberg (2015). "The Phyre2 web portal for protein modeling, prediction and analysis." Nature Protocols **10**: 845.

Klaus, H. and H. Norbert (2010). "Ultrastructural and functional aspects of static and motile systems in two taxa of the Alveolata: Dinoflagellata and Ciliata." Protistology **6**(3).

Klinger, C. M., R. E. Nisbet, D. T. Ouologuem, D. S. Roos and J. B. Dacks (2013). "Cryptic organelle homology in apicomplexan parasites: insights from evolutionary cell biology." Current opinion in microbiology **16**(4): 424-431.

Knuepfer, E., M. Napiorkowska, C. van Ooij and A. A. Holder (2017). "Generating conditional gene knockouts in Plasmodium - a toolkit to produce stable DiCre recombinase-expressing parasite lines using CRISPR/Cas9." Sci Rep **7**(1): 3881.

Knuepfer, E., O. Suleyman, A. R. Dluzewski, U. Straschil, A. H. O'Keeffe, S. A. Ogun, J. L. Green, M. Grainger, R. Tewari and A. A. Holder (2014). "RON12, a novel *Plasmodium*-specific rhoptry neck protein important for parasite proliferation." Cellular Microbiology **16**(5): 657-672.

Koch, M., K. E. Wright, O. Otto, M. Herbig, N. D. Salinas, N. H. Tolia, T. J. Satchwell, J. Guck, N. J. Brooks and J. Baum (2017). "*Plasmodium falciparum* erythrocyte-binding antigen 175 triggers a biophysical change in the red blood cell that facilitates invasion." Proceedings of the National Academy of Sciences **114**(16): 4225-4230.

Kojin, B. B. and Z. N. Adelman (2019). "The Sporozoite's Journey Through the Mosquito: A Critical Examination of Host and Parasite Factors Required for Salivary Gland Invasion." Frontiers in Ecology and Evolution **7**(284).

Korasick, D. A. and J. J. Tanner (2018). "Determination of protein oligomeric structure from small-angle X-ray scattering." Protein Sci **27**(4): 814-824.

Krishnan, A. and D. R. Karnad (2003). "Severe falciparum malaria: an important cause of multiple organ failure in Indian intensive care unit patients." Crit Care Med **31**(9): 2278-2284.

Kuenemann, M. A., O. Sperandio, C. M. Labbé, D. Lagorce, M. A. Miteva and B. O. Villoutreix (2015). "*In silico* design of low molecular weight protein–protein interaction inhibitors: Overall concept and recent advances." Progress in Biophysics and Molecular Biology **119**(1): 20-32.

Kurup, S. P., N. S. Butler and J. T. Harty (2019). "T cell-mediated immunity to malaria." Nat Rev Immunol **19**(7): 457-471.

Lambros, C. and J. P. Vanderberg (1979). "Synchronization of *Plasmodium falciparum* erythrocytic stages in culture." J Parasitol **65**(3): 418-420.

Leahy, R. (2015). Exploring the functions of poorly characterised *Plasmodium falciparum* merozoite vaccine candidates Pf3D7_0405200 & Pf3D7_0210600. Bachelor of Science (Honours), University of Adelaide.

Lee, C. F., G. C. Melkani and S. I. Bernstein (2014). Chapter Four - The UNC-45 Myosin Chaperone: From Worms to Flies to Vertebrates. International Review of Cell and Molecular Biology. K. W. Jeon, Academic Press. **313:** 103-144.

Lek, A., F. J. Evesson, R. B. Sutton, K. N. North and S. T. Cooper (2012). "Ferlins: Regulators of Vesicle Fusion for Auditory Neurotransmission, Receptor Trafficking and Membrane Repair." Traffic **13**(2): 185-194.

Liberles, D. A. (2001). "Evaluation of Methods for Determination of a Reconstructed History of Gene Sequence Evolution." Molecular Biology and Evolution **18**(11): 2040-2047.

Liffner, B. (2016). Functional characterisation of malaria blood-stage vaccine candidates Pf3D7_0405200 & Pf3D7_0210600. Bachelor of Science (Honours), University of Adelaide.

Liffner, B., S. Frölich, G. K. Heinemann, B. Liu, S. A. Ralph, M. W. A. Dixon, T.-W. Gilberger and D. W. Wilson (2020). "PfCERLI1 is a conserved rhoptry associated protein essential for Plasmodium falciparum merozoite invasion of erythrocytes." Nature Communications **11**(1): 1411.

Lim, S., K. R. Kim, Y. S. Choi, D. K. Kim, D. Hwang and H. J. Cha (2011). "*In vivo* post-translational modifications of recombinant mussel adhesive protein in insect cells." Biotechnol Prog **27**(5): 1390-1396.

Lin, Q., D. Gourdon, C. Sun, N. Holten-Andersen, T. H. Anderson, J. H. Waite and J. N. Israelachvili (2007). "Adhesion mechanisms of the mussel foot proteins mfp-1 and mfp-3." Proceedings of the National Academy of Sciences **104**(10): 3782-3786.

Linder, J. U. and J. E. Schultz (2003). "The class III adenylyl cyclases: multi-purpose signalling modules." Cell Signal **15**(12): 1081-1089.

Lindner, S. E., K. E. Swearingen, A. Harupa, A. M. Vaughan, P. Sinnis, R. L. Moritz and S. H. I. Kappe (2013). "Total and putative surface proteomics of malaria parasite salivary gland sporozoites." Molecular & cellular proteomics : MCP **12**(5): 1127-1143.

Ling, I. T., L. Florens, A. R. Dluzewski, O. Kaneko, M. Grainger, B. Y. Yim Lim, T. Tsuboi, J. M. Hopkins, J. R. Johnson, M. Torii, L. H. Bannister, J. R. Yates, 3rd, A. A. Holder and D. Mattei (2004). "The *Plasmodium falciparum* clag9 gene encodes a rhoptry protein that is transferred to the host erythrocyte upon invasion." Mol Microbiol **52**(1): 107-118.

Liu, L., X. Song, D. He, C. Komma, A. Kita, J. V. Virbasius, G. Huang, H. D. Bellamy, K. Miki, M. P. Czech and G. W. Zhou (2006). "Crystal Structure of the C2 Domain of Class II Phosphatidylinositide 3-Kinase C2α." Journal of Biological Chemistry **281**(7): 4254-4260.

Loevinsohn, M. E. (1994). "Climatic warming and increased malaria incidence in Rwanda." Lancet **343**(8899): 714-718.

Lopaticki, S., A. G. Maier, J. Thompson, D. W. Wilson, W.-H. Tham, T. Triglia, A. Gout, T. P. Speed, J. G. Beeson, J. Healer and A. F. Cowman (2011). "Reticulocyte and Erythrocyte Binding-Like Proteins Function Cooperatively in

Invasion of Human Erythrocytes by Malaria Parasites." Infection and Immunity **79**(3): 1107.

Lopez-Barragan, M. J., M. Lemieux J Fau - Quinones, K. C. Quinones M Fau - Williamson, A. Williamson Kc Fau - Molina-Cruz, K. Molina-Cruz A Fau - Cui, C. Cui K Fau - Barillas-Mury, K. Barillas-Mury C Fau - Zhao, X.-z. Zhao K Fau - Su and X. Z. Su (2011). "Directional gene expression and antisense transcripts in sexual and asexual stages of *Plasmodium falciparum*." BMC Genomics(1471-2164 (Electronic)).

Lozoff, B., J. Beard, J. Connor, F. Barbara, M. Georgieff and T. Schallert (2006). "Long-lasting neural and behavioral effects of iron deficiency in infancy." Nutrition reviews **64**(5 Pt 2): S34-S91.

Lunde, B. M., S. L. Reichow, M. Kim, H. Suh, T. C. Leeper, F. Yang, H. Mutschler, S. Buratowski, A. Meinhart and G. Varani (2010). "Cooperative interaction of transcription termination factors with the RNA polymerase II C-terminal domain." Nat Struct Mol Biol **17**(10): 1195-1201.

Lundstrom, K. (2009). An Overview on GPCRs and Drug Discovery: Structure-Based Drug Design and Structural Biology on GPCRs. G Protein-Coupled Receptors in Drug Discovery. W. R. Leifert. Totowa, NJ, Humana Press**:** 51-66.

Lynch, V. J. (2007). "Inventing an arsenal: adaptive evolution and neofunctionalization of snake venom phospholipase A2 genes." BMC Evolutionary Biology **7**(1): 2.

MacCarthy, T. and A. Bergman (2007). "The limits of subfunctionalization." BMC Evolutionary Biology **7**(1): 213.

Madeira, L., P. A. F. Galante, A. Budu, M. F. Azevedo, B. Malnic and C. R. S. Garcia (2008). "Genome-Wide Detection of Serpentine Receptor-Like Proteins in Malaria Parasites." PLOS ONE **3**(3): e1889.

Mahadevan, D., G. Powis, E. A. Mash, B. George, V. M. Gokhale, S. Zhang, K. Shakalya, L. Du-Cuny, M. Berggren, M. A. Ali, U. Jana, N. Ihle, S. Moses, C. Franklin, S. Narayan, N. Shirahatti and E. J. Meuillet (2008). "Discovery of a novel class of AKT pleckstrin homology domain inhibitors." Molecular cancer therapeutics **7**(9): 2621-2632.

Mahmoudi, S. and H. Keshavarz (2017). "Efficacy of phase 3 trial of RTS, S/AS01 malaria vaccine: The need for an alternative development plan." Human vaccines & immunotherapeutics **13**(9): 2098-2101.

Maier, A. G., J. Baum, B. Smith, D. J. Conway and A. F. Cowman (2009). "Polymorphisms in Erythrocyte Binding Antigens 140 and 181 Affect Function and Binding but Not Receptor Specificity in *Plasmodium falciparum*." Infection and Immunity **77**(4): 1689-1699.

Maier, A. G., M. T. Duraisingh, J. C. Reeder, S. S. Patel, J. W. Kazura, P. A. Zimmerman and A. F. Cowman (2003). "Plasmodium falciparum erythrocyte invasion through glycophorin C and selection for Gerbich negativity in human populations." Nature medicine **9**(1): 87-92.

Manders, E. M., J. Stap, G. J. Brakenhoff, R. van Driel and J. A. Aten (1992). "Dynamics of three-dimensional replication patterns during the S-phase, analysed by double labelling of DNA and confocal microscopy." J Cell Sci **103 (Pt 3)**: 857-862.

Marsh, K., D. Forster, C. Waruiru, I. Mwangi, M. Winstanley, V. Marsh, C. Newton, P. Winstanley, P. Warn, N. Peshu, G. Pasvol and R. Snow (1995). "Indicators of Life-Threatening Malaria in African Children." New England Journal of Medicine **332**(21): 1399-1404.

Martens, S. (2010). "Role of C2 domain proteins during synaptic vesicle exocytosis." Biochemical Society Transactions **38**(1): 213-216.

Mathieu, L. C., H. Cox, A. M. Early, S. Mok, Y. Lazrek, J.-C. Paquet, M.-P. Ade, N. W. Lucchi, Q. Grant, V. Udhayakumar, J. S. F. Alexandre, M. Demar, P. Ringwald, D. E. Neafsey, D. A. Fidock and L. Musset (2020). "Local emergence in Amazonia of *Plasmodium falciparum* k13 C580Y mutants associated with *in vitro* artemisinin resistance." eLife **9**: e51015.

Matthews, H., C. W. Duffy and C. J. Merrick (2018). "Checks and balances? DNA replication and the cell cycle in *Plasmodium*." Parasites & Vectors **11**(1): 216.

Mayer, D. C. G., J. Cofie, L. Jiang, D. L. Hartl, E. Tracy, J. Kabat, L. H. Mendoza and L. H. Miller (2009). "Glycophorin B is the erythrocyte receptor of *Plasmodium falciparum* erythrocyte-binding ligand, EBL-1." Proceedings of the National Academy of Sciences of the United States of America **106**(13): 5348-5352.

Mayer, D. C. G., J.-B. Mu, O. Kaneko, J. Duan, X.-z. Su and L. H. Miller (2004). "Polymorphism in the *Plasmodium falciparum* erythrocyte-binding ligand JESEBL/EBA-181 alters its receptor specificity." Proceedings of the National Academy of Sciences of the United States of America **101**(8): 2518-2523.

Mendes, T. A., F. P. Lobo, T. S. Rodrigues, G. F. Rodrigues-Luiz, W. D. daRocha, R. T. Fujiwara, S. M. Teixeira and D. C. Bartholomeu (2013). "Repeat-enriched proteins are related to host cell invasion and immune evasion in parasitic protozoa." Mol Biol Evol **30**(4): 951-963.

Miao, B., I. Skidan, J. Yang, A. Lugovskoy, M. Reibarkh, K. Long, T. Brazell, K. A. Durugkar, J. Maki, C. V. Ramana, B. Schaffhausen, G. Wagner, V. Torchilin, J. Yuan and A. Degterev (2010). "Small molecule inhibition of phosphatidylinositol-3,4,5-triphosphate (PIP3) binding to pleckstrin homology domains." Proceedings of the National Academy of Sciences **107**(46): 20126-20131.

Mills, J. P., M. Diez-Silva, D. J. Quinn, M. Dao, M. J. Lang, K. S. W. Tan, C. T. Lim, G. Milon, P. H. David, O. Mercereau-Puijalon, S. Bonnefoy and S. Suresh (2007). "Effect of plasmodial RESA protein on deformability of human red blood cells harboring *Plasmodium falciparum*." Proceedings of the National Academy of Sciences **104**(22): 9213-9217.

Milton, M. E. and S. W. Nelson (2016). "Replication and maintenance of the *Plasmodium falciparum* apicoplast genome." Mol Biochem Parasitol **208**(2): 56-64.

Miotto, O., M. Sekihara, S.-I. Tachibana, M. Yamauchi, R. D. Pearson, R. Amato, S. Gonçalves, S. Mehra, R. Noviyanti, J. Marfurt, S. Auburn, R. N. Price, I. Mueller, M. Ikeda, T. Mori, M. Hirai, L. Tavul, M. Hetzel, M. Laman, A. Barry, P. Ringwald, J. Ohashi, F. Hombhanje, D. P. Kwiatkowski and T. Mita (2020). "Emergence of artemisinin-resistant *Plasmodium falciparum* with kelch13 C580Y mutations on the island of New Guinea." bioRxiv: 621813.

Mohan, A., S. K. Sharma and S. Bollineni (2008). "Acute lung injury and acute respiratory distress syndrome in malaria." J Vector Borne Dis **45**(3): 179-193.

Moody, A. (2002). "Rapid Diagnostic Tests for Malaria Parasites." Clinical Microbiology Reviews **15**(1): 66-78.

Moon, R. W., J. Hall, F. Rangkuti, Y. S. Ho, N. Almond, G. H. Mitchell, A. Pain, A. A. Holder and M. J. Blackman (2013). "Adaptation of the genetically tractable malaria pathogen Plasmodium knowlesi to continuous culture in human erythrocytes." Proceedings of the National Academy of Sciences of the United States of America **110**(2): 531-536.

Moore, R. B., M. Oborník, J. Janouškovec, T. Chrudimský, M. Vancová, D. H. Green, S. W. Wright, N. W. Davies, C. J. S. Bolch, K. Heimann, J. Šlapeta, O. Hoegh-Guldberg, J. M. Logsdon and D. A. Carter (2008). "A photosynthetic alveolate closely related to apicomplexan parasites." Nature **451**(7181): 959-963.

Moraes Barros, R. R., T. J. Gibson, W. A. Kite, J. M. Sá and T. E. Wellems (2017). "Comparison of two methods for transformation of *Plasmodium knowlesi*: Direct schizont electroporation and spontaneous plasmid uptake from plasmid-loaded red blood cells." Molecular and biochemical parasitology **218**: 16-22.

Morahan, B. J., G. B. Sallmann, R. Huestis, V. Dubljevic and K. L. Waller (2009). "*Plasmodium falciparum*: Genetic and immunogenic characterisation of the rhoptry neck protein PfRON4." Experimental Parasitology **122**(4): 280-288.

Morita, M., H. Nagaoka, E. H. Ntege, B. N. Kanoi, D. Ito, T. Nakata, J.-W. Lee, K. Tokunaga, T. Iimura, M. Torii, T. Tsuboi and E. Takashima (2018). "PV1, a novel *Plasmodium falciparum* merozoite dense granule protein, interacts with exported protein in infected erythrocytes." Scientific Reports **8**(1): 3696.

Mueller, C., N. Klages, D. Jacot, Joana M. Santos, A. Cabrera, Tim W. Gilberger, J.-F. Dubremetz and D. Soldati-Favre (2013). "The *Toxoplasma* Protein ARO Mediates the Apical Positioning of Rhoptry Organelles, a Prerequisite for Host Cell Invasion." Cell Host & Microbe **13**(3): 289-301.

Mueller, C., A. Samoo, P.-M. Hammoudi, N. Klages, J. P. Kallio, I. Kursula and D. Soldati-Favre (2016). "Structural and functional dissection of *Toxoplasma gondii* armadillo repeats only protein." Journal of Cell Science **129**(5): 1031-1045.

Murata, K. and M. Wolf (2018). "Cryo-electron microscopy for structural analysis of dynamic biological macromolecules." Biochimica et Biophysica Acta (BBA) - General Subjects **1862**(2): 324-334.

Na, J.-H., W.-K. Lee and Y. G. Yu (2018). "How Do We Study the Dynamic Structure of Unstructured Proteins: A Case Study on Nopp140 as an Example of a Large, Intrinsically Disordered Protein." International journal of molecular sciences **19**(2): 381.

Nájera, J. A., M. González-Silva and P. L. Alonso (2011). "Some lessons for the future from the Global Malaria Eradication Programme (1955-1969)." PLoS medicine **8**(1): e1000412-e1000412.

Narum, D. L. and A. W. Thomas (1994). "Differential localization of full-length and processed forms of PF83/AMA-1 an apical membrane antigen of *Plasmodium falciparum* merozoites." Molecular and Biochemical Parasitology **67**(1): 59-68.

Nasamu, A. S., S. Glushakova, I. Russo, B. Vaupel, A. Oksman, A. S. Kim, D. H. Fremont, N. Tolia, J. R. Beck, M. J. Meyers, J. C. Niles, J. Zimmerberg and D. E. Goldberg (2017). "Plasmepsins IX and X are essential and druggable mediators of malaria parasite egress and invasion." Science **358**(6362): 518.

Ngô, H. M., M. Yang and K. Joiner (2004). "Are rhoptries in Apicomplexan parasites secretory granules or secretory lysosomal granules?" Molecular Microbiology **52**(6).

Ngotho, P., A. B. Soares, F. Hentzschel, F. Achcar, L. Bertuccini and M. Marti (2019). "Revisiting gametocyte biology in malaria parasites." FEMS Microbiology Reviews **43**(4): 401-414.

Nicolaes, G. A. F., M. Kulharia, J. Voorberg, P. H. Kaijen, A. Wroblewska, S. Wielders, R. Schrijver, O. Sperandio and B. O. Villoutreix (2014). "Rational design of small molecules targeting the C2 domain of coagulation factor VIII." Blood **123**(1): 113-120.

Nielsen, H., J. Engelbrecht, S. Brunak and G. von Heijne (1997). "Identification of prokaryotic and eukaryotic signal peptides and prediction of their cleavage sites." Protein Eng **10**(1): 1-6.

Niikura, M., S. I. Inoue, T. Fukutomi, J. Yamagishi, H. Asahi and F. Kobayashi (2018). "Comparative genomics and proteomic analyses between lethal and nonlethal strains of *Plasmodium berghei*." Exp Parasitol **185**: 1-9.

O'Donnell, R. A., A. Saul, A. F. Cowman and B. S. Crabb (2000). "Functional conservation of the malaria vaccine antigen MSP-119across distantly related Plasmodium species." Nat Med **6**(1): 91-95.

Oborník, M., D. Modrý, M. Lukeš, E. Černotíková-Stříbrná, J. Cihlář, M. Tesařová, E. Kotabová, M. Vancová, O. Prášil and J. Lukeš (2012). "Morphology, Ultrastructure and Life Cycle of *Vitrella brassicaformis* n. sp., n. gen., a Novel Chromerid from the Great Barrier Reef." Protist **163**(2): 306-323.

Ocampo, M., L. E. Rodríguez, H. Curtidor, A. Puentes, R. Vera, J. J. Valbuena, R. López, J. E. García, L. E. Ramírez, E. Torres, J. Cortes, D. Tovar, Y. López, M. A. Patarroyo and M. E. Patarroyo (2005). "Identifying Plasmodium falciparum cytoadherence-linked asexual protein 3 (CLAG 3) sequences that specifically bind to C32 cells and erythrocytes." Protein Sci **14**(2): 504-513.

Padmanaban, G. and P. N. Rangarajan (2000). "Heme Metabolism of *Plasmodium* Is a Major Antimalarial Target." Biochemical and Biophysical Research Communications **268**(3): 665-668.

Paing, M. M., N. D. Salinas, Y. Adams, A. Oksman, A. T. R. Jensen, D. E. Goldberg and N. H. Tolia (2018). "Shed EBA-175 mediates red blood cell clustering that enhances malaria parasite growth and enables immune evasion." eLife **7**: e43224.

Parey, K., O. Haapanen, V. Sharma, H. Köfeler, T. Züllig, S. Prinz, K. Siegmund, I. Wittig, D. J. Mills, J. Vonck, W. Kühlbrandt and V. Zickermann (2019). "High-resolution cryo-EM structures of respiratory complex I: Mechanism, assembly, and disease." Science Advances **5**(12): eaax9484.

Parkyn Schneider, M., B. Liu, P. Glock, A. Suttie, E. McHugh, D. Andrew, S. Batinovic, N. Williamson, E. Hanssen, P. McMillan, M. Hliscs, L. Tilley and M. W. A. Dixon (2017). "Disrupting assembly of the inner membrane complex blocks *Plasmodium falciparum* sexual stage development." PLOS Pathogens **13**(10): e1006659.

Patel, A., A. J. Perrin, H. R. Flynn, C. Bisson, C. Withers-Martinez, M. Treeck, C. Flueck, G. Nicastro, S. R. Martin, A. Ramos, T. W. Gilberger, A. P. Snijders, M. J. Blackman and D. A. Baker (2019). "Cyclic AMP signalling controls key components of malaria parasite host cell invasion machinery." PLOS Biology **17**(5): e3000264.

Paul, F., S. Roath, D. Melville, D. C. Warhurst and J. O. S. Osisanya (1981). "Separation of malaria-infected erythrocytes from whole blood: use of a selective high-gradient magnetic separation technique." The Lancet **318**(8237): 70-71.

Payne, R. O., S. E. Silk, S. C. Elias, K. Miura, A. Diouf, F. Galaway, H. de Graaf, N. J. Brendish, I. D. Poulton, O. J. Griffiths, N. J. Edwards, J. Jin, G. M. Labbé, D. G. W. Alanine, L. Siani, S. Di Marco, R. Roberts, N. Green, E. Berrie, A. S. Ishizuka, C. M. Nielsen, M. Bardelli, F. D. Partey, M. F. Ofori, L. Barfod, J. Wambua, L. M. Murungi, F. H. Osier, S. Biswas, J. S. McCarthy, A. M. Minassian, R. Ashfield, N. K. Viebig, F. L. Nugent, A. D. Douglas, J. Vekemans, G. J. Wright, S. N. Faust, A. V. S. Hill, C. A. Long, A. M. Lawrie and S. J. Draper (2017). "Human vaccination against RH5 induces neutralizing antimalarial antibodies that inhibit RH5 invasion complex interactions." JCI Insight **2**(21).

Pei, X., X. Guo, R. Coppel, S. Bhattacharjee, K. Haldar, W. Gratzer, N. Mohandas and X. An (2007). "The ring-infected erythrocyte surface antigen (RESA) of *Plasmodium falciparum* stabilizes spectrin tetramers and suppresses further invasion." Blood **110**(3): 1036-1042.

Penny, M. A., K. Galactionova, M. Tarantino, M. Tanner and T. A. Smith (2015). "The public health impact of malaria vaccine RTS,S in malaria endemic Africa: country-specific predictions using 18 month follow-up Phase III data and simulation models." BMC Medicine **13**(1): 170.

Pertoft, H., B. Wärmegård and M. Höök (1978). "Heterogeneity of lysosomes originating from rat liver parenchymal cells. Metabolic relationship of subpopulations separated by density-gradient centrifugation." Biochem J **174**(1): 309-317.

Pinkevych, M., J. Petravic, K. Chelimo, J. W. Kazura, A. M. Moormann and M. P. Davenport (2012). "The dynamics of naturally acquired immunity to *Plasmodium falciparum* infection." PLoS computational biology **8**(10): e1002729-e1002729.

Pino, P., R. Caldelari, B. Mukherjee, J. Vahokoski, N. Klages, B. Maco, C. R. Collins, M. J. Blackman, I. Kursula, V. Heussler, M. Brochet and D. Soldati-Favre (2017). "A multistage antimalarial targets the plasmepsins IX and X essential for invasion and egress." Science **358**(6362): 522-528.

Planche, T., A. Dzeing, E. Ngou-Milama, M. Kombila and P. W. Stacpoole (2005). "Metabolic complications of severe malaria." Curr Top Microbiol Immunol **295**: 105-136.

Ponnudurai, T., A. D. Leeuwenberg and J. H. Meuwissen (1981). "Chloroquine sensitivity of isolates of Plasmodium falciparum adapted to *in vitro* culture." Trop Geogr Med **33**(1): 50-54.

Pontarotti, P. (2017). Evolutionary Biology: Self/Nonself Evolution, Species and Complex Traits Evolution, Methods and Concepts, Springer International Publishing.

Preiser, P. R., R. J. Wilson, P. W. Moore, S. McCready, M. A. Hajibagheri, K. J. Blight, M. Strath and D. H. Williamson (1996). "Recombination associated with replication of malarial mitochondrial DNA." Embo j **15**(3): 684-693.

Proellocks, N. I., L. M. Kats, D. A. Sheffield, E. Hanssen, C. G. Black, K. L. Waller and R. L. Coppel (2009). "Characterisation of PfRON6, a *Plasmodium falciparum* rhoptry neck protein with a novel cysteine-rich domain." International Journal for Parasitology **39**(6): 683-692.

Prommana, P., C. Uthaipibull, C. Wongsombat, S. Kamchonwongpaisan, Y. Yuthavong, E. Knuepfer, A. A. Holder and P. J. Shaw (2013). "Inducible Knockdown of *Plasmodium* Gene Expression Using the glmS Ribozyme." PLOS ONE **8**(8): e73783.

Proto, W. R., S. V. Siegel, S. Dankwa, W. Liu, A. Kemp, S. Marsden, Z. A. Zenonos, S. Unwin, P. M. Sharp, G. J. Wright, B. H. Hahn, M. T. Duraisingh and J. C. Rayner (2019). "Adaptation of *Plasmodium falciparum* to humans involved the loss of an ape-specific erythrocyte invasion ligand." Nature Communications **10**(1): 4512.

Qinghaosu Antimalaria Coordinating Research_Group (1979). "Antimalaria studies on qinghaosu." Chinese medical journal **92**(12): 811-816.

Ragotte, R. J., M. K. Higgins and S. J. Draper (2020). "The RH5-CyRPA-Ripr Complex as a Malaria Vaccine Target." Trends in Parasitology **36**(6): 545-559.

Rayner , J. C., E. Vargas-Serrato , C. S. Huber , M. R. Galinski and J. W. Barnwell (2001). "A *Plasmodium falciparum* Homologue of Plasmodium vivax Reticulocyte Binding Protein (PvRBP1) Defines a Trypsin-resistant Erythrocyte Invasion Pathway." Journal of Experimental Medicine **194**(11): 1571-1582.

Reddy, K. S., E. Amlabu, A. K. Pandey, P. Mitra, V. S. Chauhan and D. Gaur (2015). "Multiprotein complex between the GPI-anchored CyRPA with PfRH5 and PfRipr is crucial for *Plasmodium falciparum* erythrocyte invasion." Proc Natl Acad Sci U S A **112**(4): 1179-1184.

Reed, M. B., S. R. Caruana, A. H. Batchelor, J. K. Thompson, B. S. Crabb and A. F. Cowman (2000). "Targeted disruption of an erythrocyte binding antigen in *Plasmodium falciparum* is associated with a switch toward a sialic acid-independent pathway of invasion." Proceedings of the National Academy of Sciences **97**(13): 7509-7514.

Reininger, L., M. Garcia, A. Tomlins, S. Müller and C. Doerig (2012). "The *Plasmodium falciparum*, Nima-related kinase Pfnek-4: a marker for asexual parasites committed to sexual differentiation." Malaria Journal **11**(1): 250.

Reynolds, C. R., S. A. Islam and M. J. E. Sternberg (2018). "EzMol: A Web Server Wizard for the Rapid Visualization and Image Production of Protein and Nucleic Acid Structures." Journal of Molecular Biology **430**(15): 2244-2248.

Richard, D., L. M. Kats, C. Langer, C. G. Black, K. Mitri, J. A. Boddey, A. F. Cowman and R. L. Coppel (2009). "Identification of Rhoptry Trafficking Determinants and

Evidence for a Novel Sorting Mechanism in the Malaria Parasite *Plasmodium falciparum*." PLOS Pathogens **5**(3): e1000328.

Richard, D., C. A. MacRaild, D. T. Riglar, J.-A. Chan, M. Foley, J. Baum, S. A. Ralph, R. S. Norton and A. F. Cowman (2010). "Interaction between *Plasmodium falciparum* Apical Membrane Antigen 1 and the Rhoptry Neck Protein Complex Defines a Key Step in the Erythrocyte Invasion Process of Malaria Parasites." Journal of Biological Chemistry **285**(19): 14815-14822.

Ridley, R. G., H.-W. Lahm, B. Takács and J. G. Scaife (1991). "Genetic and structural relationships between components of a protective rhoptry antigen complex from *Plasmodium falciparum*." Molecular and Biochemical Parasitology **47**(2): 245-246.

Riglar, D. T., D. Richard, D. W. Wilson, M. J. Boyle, C. Dekiwadia, L. Turnbull, F. Angrisano, D. S. Marapana, K. L. Rogers, C. B. Whitchurch, J. G. Beeson, A. F. Cowman, S. A. Ralph and J. Baum (2011). "Super-Resolution Dissection of Coordinated Events during Malaria Parasite Invasion of the Human Erythrocyte." Cell Host & Microbe **9**(1): 9-20.

Rivadeneira, E. M., M. Wasserman and C. T. Espinal (1983). "Separation and concentration of schizonts of *Plasmodium falciparum* by Percoll gradients." J Protozool **30**(2): 367-370.

Robert-Paganin, J., J. P. Robblee, D. Auguin, T. C. A. Blake, C. S. Bookwalter, E. B. Krementsova, D. Moussaoui, M. J. Previs, G. Jousset, J. Baum, K. M. Trybus and A. Houdusse (2019). "*Plasmodium* myosin A drives parasite invasion by an atypical force generating mechanism." Nature Communications **10**(1): 3286.

Robertson, J. G. (2005). "Mechanistic Basis of Enzyme-Targeted Drugs." Biochemistry **44**(15): 5561-5571.

Rogerson, S. J. (2017). "Management of malaria in pregnancy." The Indian journal of medical research **146**(3): 328-333.

Rognan, D. (2015). "Rational design of protein–protein interaction inhibitors." MedChemComm **6**(1): 51-60.

Rosenthal, P. J. (2018). "Artemisinin Resistance Outside of Southeast Asia." The American journal of tropical medicine and hygiene **99**(6): 1357-1359.

Roy, A., A. Kucukural and Y. Zhang (2010). "I-TASSER: a unified platform for automated protein structure and function prediction." Nat Protoc **5**(4): 725-738.

Roy, A., J. Yang and Y. Zhang (2013). "Protein–ligand binding site recognition using complementary binding-specific substructure comparison and sequence profile alignment." Bioinformatics **29**(20): 2588-2595.

Sachanonta, N., K. Chotivanich, U. Chaisri, G. D. H. Turner, D. J. P. Ferguson, N. P. J. Day and E. Pongponratn (2011). "Ultrastructural and real-time microscopic changes in *P. falciparum*-infected red blood cells following treatment with antimalarial drugs." Ultrastructural pathology **35**(5): 214-225.

Sagara, I., A. Dicko, R. D. Ellis, M. P. Fay, S. I. Diawara, M. H. Assadou, M. S. Sissoko, M. Kone, A. I. Diallo, R. Saye, M. A. Guindo, O. Kante, M. B. Niambele, K. Miura, G. E. Mullen, M. Pierce, L. B. Martin, A. Dolo, D. A. Diallo, O. K. Doumbo, L. H. Miller and A. Saul (2009). "A randomized controlled phase 2 trial of the blood stage AMA1-C1/Alhydrogel malaria vaccine in children in Mali." Vaccine **27**(23): 3090-3098.

Salamanca, D. R., M. Gómez, A. Camargo, L. Cuy-Chaparro, J. Molina-Franky, C. Reyes, M. A. Patarroyo and M. E. Patarroyo (2019). "*Plasmodium falciparum* Blood Stage Antimalarial Vaccines: An Analysis of Ongoing Clinical Trials and New Perspectives Related to Synthetic Vaccines." Frontiers in microbiology **10**: 2712-2712.

Salazar, E., E. M. Bank, N. Ramsey, K. C. Hess, K. W. Deitsch, L. R. Levin and J. Buck (2012). "Characterization of *Plasmodium falciparum* adenylyl cyclase-β and its role in erythrocytic stage parasites." PloS one **7**(6): e39769-e39769.

Sanders, P. R., L. M. Kats, D. R. Drew, R. A. O'Donnell, M. O'Neill, A. G. Maier, R. L. Coppel and B. S. Crabb (2006). "A Set of Glycosylphosphatidyl Inositol-Anchored Membrane Proteins of *Plasmodium falciparum* Is Refractory to Genetic Deletion." Infection and Immunity **74**(7): 4330-4338.

Sandve, S. R., R. V. Rohlfs and T. R. Hvidsten (2018). "Subfunctionalization versus neofunctionalization after whole-genome duplication." Nature Genetics **50**(7): 908-909.

Sasi, P., S. Burns, C. Waruiru, M. English, C. Hobson, C. King, M. Mosobo, J. Beech, R. Iles, B. Boucher and R. Cohen (2007). "Metabolic acidosis and other determinants of hemoglobin-oxygen dissociation in severe childhood *Plasmodium falciparum* malaria." American Journal of Tropical Medicine and Hygeine **77**: 4.

Schnepf, E. and G. Deichgräber (1984). "“Myzocytosis”, a kind of endocytosis with implications to compartmentation in endosymbiosis." Naturwissenschaften **71**(4): 218-219.

Schnepf, E. and M. Elbrächter (1992). "Nutritional strategies in dinoflagellates: A review with emphasis on cell biological aspects." Eur J Protistol **28**(1): 3-24.

Schofield, L., G. R. Bushell, J. A. Cooper, A. J. Saul, J. A. Upcroft and C. Kidson (1986). "A rhoptry antigen of *Plasmodium falciparum* contains conserved and variable epitopes recognized by inhibitory monoclonal antibodies." Molecular and Biochemical Parasitology **18**(2): 183-195.

Scott, D. E., A. R. Bayly, C. Abell and J. Skidmore (2016). "Small molecules, big targets: drug discovery faces the protein–protein interaction challenge." Nature Reviews Drug Discovery **15**(8): 533-550.

Segers, K., O. Sperandio, M. Sack, R. Fischer, M. A. Miteva, J. Rosing, G. A. Nicolaes and B. O. Villoutreix (2007). "Design of protein membrane interaction inhibitors by virtual ligand screening, proof of concept with the C2 domain of factor V." Proc Natl Acad Sci U S A **104**(31): 12697-12702.

Sellers, J. R. (2000). "Myosins: a diverse superfamily." Biochimica et Biophysica Acta (BBA) - Molecular Cell Research **1496**(1): 3-22.

Shaw, M. K. and L. G. Tilney (1992). "How individual cells develop from a syncytium: merogony in *Theileria parva* (Apicomplexa)." J Cell Sci **101 (Pt 1)**: 109-123.

Sherling, E. S., E. Knuepfer, J. A. Brzostowski, L. H. Miller, M. J. Blackman and C. v. Ooij (2017). "The *Plasmodium falciparum* rhoptry protein RhopH3 plays essential roles in host cell invasion and nutrient uptake." eLife **6**: e23239.

Sherling, E. S., A. J. Perrin, E. Knuepfer, M. R. G. Russell, L. M. Collinson, L. H. Miller and M. J. Blackman (2019). "The *Plasmodium falciparum* rhoptry bulb protein RAMA plays an essential role in rhoptry neck morphogenesis and host red blood cell invasion." PLOS Pathogens **15**(9): e1008049.

Sherrard-Smith, E., J. E. Skarp, A. D. Beale, C. Fornadel, L. C. Norris, S. J. Moore, S. Mihreteab, J. D. Charlwood, S. Bhatt, P. Winskill, J. T. Griffin and T. S. Churcher (2019). "Mosquito feeding behavior and how it influences residual malaria transmission across Africa." Proceedings of the National Academy of Sciences **116**(30): 15086-15095.

Silmon de Monerri, N. C., H. R. Flynn, M. G. Campos, F. Hackett, K. Koussis, C. Withers-Martinez, J. M. Skehel and M. J. Blackman (2011). "Global identification of multiple substrates for *Plasmodium falciparum* SUB1, an essential malarial processing protease." Infection and immunity **79**(3): 1086-1097.

Siltberg, J. and D. A. Liberles (2002). "A simple covarion-based approach to analyse nucleotide substitution rates." Journal of Evolutionary Biology **15**(4): 588-594.

Singh, B., L. Kim Sung, A. Matusop, A. Radhakrishnan, S. S. Shamsul, J. Cox-Singh, A. Thomas and D. J. Conway (2004). "A large focus of naturally acquired Plasmodium knowlesi infections in human beings." Lancet **363**(9414): 1017-1024.

Sinnis, P. and B. K. Sim (1997). "Cell invasion by the vertebrate stages of *Plasmodium*." Trends in microbiology **5**(2): 52-58.

Siraj, A. S., M. Santos-Vega, M. J. Bouma, D. Yadeta, D. R. Carrascal and M. Pascual (2014). "Altitudinal Changes in Malaria Incidence in Highlands of Ethiopia and Colombia." Science **343**(6175): 1154-1158.

Smyth, M. S. and J. H. Martin (2000). "x ray crystallography." Molecular pathology : MP **53**(1): 8-14.

Sougoufara, S., S. M. Diédhiou, S. Doucouré, N. Diagne, P. M. Sembène, M. Harry, J.-F. Trape, C. Sokhna and M. O. Ndiath (2014). "Biting by *Anopheles funestus* in broad daylight after use of long-lasting insecticidal nets: a new challenge to malaria elimination." Malaria Journal **13**(1): 125.

Srinivasan, P., W. L. Beatty, A. Diouf, R. Herrera, X. Ambroggio, J. K. Moch, J. S. Tyler, D. L. Narum, S. K. Pierce, J. C. Boothroyd, J. D. Haynes and L. H. Miller (2011). "Binding of *Plasmodium* merozoite proteins RON2 and AMA1 triggers commitment to invasion." Proceedings of the National Academy of Sciences **108**(32): 13275-13280.

Staines, H. M., J. C. Ellory and K. Kirk (2001). "Perturbation of the pump-leak balance for Na+ and K+ in malaria-infected erythrocytes." American Journal of Physiology-Cell Physiology **280**(6): C1576-C1587.

Staines, H. M., C. Rae and K. Kirk (2000). "Increased permeability of the malaria-infected erythrocyte to organic cations." Biochimica et Biophysica Acta (BBA) - Biomembranes **1463**(1): 88-98.

Stoecker, D. K. (1999). "Mixotrophy among Dinoflagellates 1." Journal of eukaryotic microbiology **46**(4): 397-401.

Stubbs, J., K. M. Simpson, T. Triglia, D. Plouffe, C. J. Tonkin, M. T. Duraisingh, A. G. Maier, E. A. Winzeler and A. F. Cowman (2005). "Molecular Mechanism for Switching of *P. falciparum* Invasion Pathways into Human Erythrocytes." Science **309**(5739): 1384-1387.

Suarez, C., G. Lentini, R. Ramaswamy, M. Maynadier, E. Aquilini, L. Berry-Sterkers, M. Cipriano, A. L. Chen, P. Bradley, B. Striepen, M. J. Boulanger and M. Lebrun (2019). "A lipid-binding protein mediates rhoptry discharge and invasion in *Plasmodium falciparum* and *Toxoplasma gondii* parasites." Nature Communications **10**(1): 4041.

Svenson, J. E., J. D. MacLean, T. W. Gyorkos and J. Keystone (1995). "Imported Malaria: Clinical Presentation and Examination of Symptomatic Travelers." Archives of Internal Medicine **155**(8): 861-868.

Talman, A. M., O. Domarle, F. E. McKenzie, F. Ariey and V. Robert (2004). "Gametocytogenesis : the puberty of *Plasmodium falciparum*." Malaria Journal **3**(1): 24.

Tarning, J. (2016). "Treatment of Malaria in Pregnancy." New England Journal of Medicine **374**(10): 981-982.

Tarr, S. J., R. W. Moon, I. Hardege and A. R. Osborne (2014). "A conserved domain targets exported PHISTb family proteins to the periphery of *Plasmodium* infected erythrocytes." Molecular and Biochemical Parasitology **196**(1): 29-40.

Taylor, H. M., L. McRobert, M. Grainger, A. Sicard, A. R. Dluzewski, C. S. Hopp, A. A. Holder and D. A. Baker (2010). "The Malaria Parasite Cyclic GMP-Dependent Protein Kinase Plays a Central Role in Blood-Stage Schizogony." Eukaryotic Cell **9**(1): 37.

Taylor, S., J. Beuchler and W. Yonemoto (1990). "cAMP-Dependent protein kinase: Framework for a diverse family of regulatory enzymes." Annual Review of Biochemistry **59**.

Taylor, W. R. J., J. Hanson, G. D. H. Turner, N. J. White and A. M. Dondorp (2012). "Respiratory manifestations of malaria." Chest **142**(2): 492-505.

Teo, A., G. Feng, G. V. Brown, J. G. Beeson and S. J. Rogerson (2016). "Functional Antibodies and Protection against Blood-stage Malaria." Trends in Parasitology **32**(11): 887-898.

Tetley, L., S. M. Brown, V. McDonald and G. H. Coombs (1998). "Ultrastructural analysis of the sporozoite of *Cryptosporidium parvum*." Microbiology **144 (Pt 12)**: 3249-3255.

Tham, W.-H., D. W. Wilson, S. Lopaticki, C. Q. Schmidt, P. B. Tetteh-Quarcoo, P. N. Barlow, D. Richard, J. E. Corbin, J. G. Beeson and A. F. Cowman (2010). "Complement receptor 1 is the host erythrocyte receptor for *Plasmodium falciparum* PfRh4 invasion ligand." Proceedings of the National Academy of Sciences **107**(40): 17327.

Thomas, C. C., S. Dowler, M. Deak, D. R. Alessi and D. M. van Aalten (2001). "Crystal structure of the phosphatidylinositol 3,4-bisphosphate-binding pleckstrin homology (PH) domain of tandem PH-domain-containing protein 1 (TAPP1): molecular basis of lipid specificity." Biochem J **358**(Pt 2): 287-294.

Tilley, L., J. Straimer, N. F. Gnädig, S. A. Ralph and D. A. Fidock (2016). "Artemisinin Action and Resistance in *Plasmodium falciparum*." Trends in parasitology **32**(9): 682-696.

Tokunaga, N., M. Nozaki, M. Tachibana, M. Baba, K. Matsuoka, T. Tsuboi, M. Torii and T. Ishino (2019). "Expression and Localization Profiles of Rhoptry Proteins in *Plasmodium berghei* Sporozoites." Frontiers in Cellular and Infection Microbiology **9**(316).

Topolska, A. E., A. Lidgett, D. Truman, H. Fujioka and R. L. Coppel (2004). "Characterization of a Membrane-associated Rhoptry Protein of *Plasmodium falciparum*." Journal of Biological Chemistry **279**(6): 4648-4656.

Trager, W. and J. B. Jensen (1976). "Human malaria parasites in continuous culture." Science **193**(4254): 673.

Triglia, T., M. T. Duraisingh, R. T. Good and A. F. Cowman (2005). "Reticulocyte-binding protein homologue 1 is required for sialic acid-dependent invasion into human erythrocytes by *Plasmodium falciparum*." Molecular Microbiology **55**(1): 162-174.

Triglia, T., J. Healer, S. R. Caruana, A. N. Hodder, R. F. Anders, B. S. Crabb and A. F. Cowman (2000). "Apical membrane antigen 1 plays a central role in erythrocyte invasion by *Plasmodium* species." Mol Microbiol **38**(4): 706-718.

Trish, B. and G. Tony (2007). "Prevention of malaria in travellers." Australian Family Physician **36**.

Tse, E. G., M. Korsik and M. H. Todd (2019). "The past, present and future of anti-malarial medicines." Malaria Journal **18**(1): 93.

Tyska, M. J. and D. M. Warshaw (2002). "The myosin power stroke." Cell Motility **51**(1): 1-15.

United Nations. (2000). "United Nations Millenium Declaration." from https://www.ohchr.org/EN/ProfessionalInterest/Pages/Millennium.aspx.

Viriyavejakul, P., V. Khachonsaksumet and C. Punsawad (2014). "Liver changes in severe *Plasmodium falciparum* malaria: histopathology, apoptosis and nuclear factor kappa B expression." Malaria journal **13**: 106-106.

Volz, J. C., A. Yap, X. Sisquella, J. K. Thompson, N. T. Lim, L. W. Whitehead, L. Chen, M. Lampe, W. H. Tham, D. Wilson, T. Nebl, D. Marapana, T. Triglia, W. Wong, K. L. Rogers and A. F. Cowman (2016). "Essential Role of the PfRh5/PfRipr/CyRPA Complex during *Plasmodium falciparum* Invasion of Erythrocytes." Cell Host Microbe(1934-6069 (Electronic)).

Vulliez-Le Normand, B., M. L. Tonkin, M. H. Lamarque, S. Langer, S. Hoos, M. Roques, F. A. Saul, B. W. Faber, G. A. Bentley, M. J. Boulanger and M. Lebrun (2012). "Structural and Functional Insights into the Malaria Parasite Moving Junction Complex." PLOS Pathogens **8**(6): e1002755.

Wadsworth, P. A., O. Folorunso, N. Nguyen, A. K. Singh, D. D'Amico, R. T. Powell, D. Brunell, J. Allen, C. Stephan and F. Laezza (2019). "High-throughput screening against protein:protein interaction interfaces reveals anti-cancer therapeutics as potent modulators of the voltage-gated Na+ channel complex." Scientific Reports **9**(1): 16890.

Wall, R. J., M. Zeeshan, N. J. Katris, R. Limenitakis, E. Rea, J. Stock, D. Brady, R. F. Waller, A. A. Holder and R. Tewari (2019). "Systematic analysis of *Plasmodium* myosins reveals differential expression, localisation, and function in invasive and proliferative parasite stages." Cellular Microbiology **21**(10): e13082.

Walliker, D., I. A. Quakyi, T. E. Wellems, T. F. McCutchan, A. Szarfman, W. T. London, L. M. Corcoran, T. R. Burkot and R. Carter (1987). "Genetic analysis of the human malaria parasite *Plasmodium falciparum*." Science **236**(4809): 1661-1666.

Wang, G., C. A. MacRaild, B. Mohanty, M. Mobli, N. P. Cowieson, R. F. Anders, J. S. Simpson, S. McGowan, R. S. Norton and M. J. Scanlon (2014). "Molecular Insights into the Interaction between *Plasmodium falciparum* Apical Membrane Antigen 1 and an Invasion-Inhibitory Peptide." PLOS ONE **9**(10): e109674.

Weatherall, D. J. (2008). "Genetic variation and susceptibility to infection: the red cell and malaria." British Journal of Haematology **141**(3): 276-286.

Weiss, D. J., T. C. D. Lucas, M. Nguyen, A. K. Nandi, D. Bisanzio, K. E. Battle, E. Cameron, K. A. Twohig, D. A. Pfeffer, J. A. Rozier, H. S. Gibson, P. C. Rao, D. Casey, A. Bertozzi-Villa, E. L. Collins, U. Dalrymple, N. Gray, J. R. Harris, R. E. Howes, S. Y. Kang, S. H. Keddie, D. May, S. Rumisha, M. P. Thorn, R. Barber, N. Fullman, C. K. Huynh, X. Kulikoff, M. J. Kutz, A. D. Lopez, A. H. Mokdad, M. Naghavi, G. Nguyen, K. A. Shackelford, T. Vos, H. Wang, D. L. Smith, S. S. Lim, C. J. L. Murray, S. Bhatt, S. I. Hay and P. W. Gething (2019). "Mapping the global prevalence, incidence, and mortality of *Plasmodium falciparum*, 2000–17: a spatial and temporal modelling study." The Lancet **394**(10195): 322-331.

Weiss, G. E., B. S. Crabb and P. R. Gilson (2016). "Overlaying Molecular and Temporal Aspects of Malaria Parasite Invasion." Trends Parasitol **32**(4): 284-295.

Weiss, G. E., P. R. Gilson, T. Taechalertpaisarn, W.-H. Tham, N. W. M. de Jong, K. L. Harvey, F. J. I. Fowkes, P. N. Barlow, J. C. Rayner, G. J. Wright, A. F. Cowman and B. S. Crabb (2015). "Revealing the Sequence and Resulting Cellular Morphology of Receptor-Ligand Interactions during *Plasmodium falciparum* Invasion of Erythrocytes." PLOS Pathogens **11**(2): e1004670.

White, N. J. (2018). "Anaemia and malaria." Malaria Journal **17**(1): 371.

Williams, T. N. (2016). "Sickle Cell Disease in Sub-Saharan Africa." Hematology/Oncology Clinics of North America **30**(2): 343-358.

Wilson, D. W., B. S. Crabb and J. G. Beeson (2010). "Development of fluorescent *Plasmodium falciparum* for *in vitro* growth inhibition assays." Malaria Journal **9**(1): 152.

Wilson, D. W., C. Langer, C. D. Goodman, G. I. McFadden and J. G. Beeson (2013). "Defining the timing of action of antimalarial drugs against *Plasmodium falciparum*." Antimicrobial agents and chemotherapy **57**(3): 1455-1467.

Wong, W., R. Huang, S. Menant, C. Hong, J. J. Sandow, R. W. Birkinshaw, J. Healer, A. N. Hodder, U. Kanjee, C. J. Tonkin, D. Heckmann, V. Soroka, T. M. M. Søgaard, T. Jørgensen, M. T. Duraisingh, P. E. Czabotar, W. A. de Jongh, W.-H. Tham, A. I. Webb, Z. Yu and A. F. Cowman (2019). "Structure of *Plasmodium falciparum* Rh5–CyRPA–Ripr invasion complex." Nature **565**(7737): 118-121.

World Health Organization. (1980). "Thirty-third World Health Assembly, Geneva, 5-23 May 1980: resolution and decisions, annexes." from https://apps.who.int/iris/handle/10665/154893.

World Health Organization. (2012). "WHO policy recommendation: Seasonal malaria chemoprevention (SMC) for Plasmodium falciparum malaria control in highly seasonal transmission areas of the Sahel sub-region in Africa." Retrieved 11/05/2020, 2020, from https://www.who.int/malaria/publications/atoz/who_smc_policy_recommendation/en/.

World Health Organization. (2013). "WHO policy brief for the implementation of intermittent preventative treatment of malaria in pregnancy using sulfadoxine-pyrimethamine (IPTp-SP)." from https://www.who.int/malaria/publications/atoz/policy_brief_iptp_sp_policy_recommendation/en/.

World Health Organization. (2015). "Guidelines for the treatment of malaria." Retrieved 21/05/2020, 2020, from https://www.who.int/malaria/publications/atoz/9789241549127/en/.

World Health Organization. (2015). "World Malaria Report 2015." Retrieved 08/05/2020, 2020, from https://www.who.int/malaria/publications/world-malaria-report-2015/report/en/.

World Health Organization. (2016, 23/04/2020). "Papua New Guinea statistics summary (2002-present)." Retrieved 21/05/2020, 2020, from https://apps.who.int/gho/data/node.country.country-PNG.

World Health Organization. (2017). "Malaria prevention works: let's close the gap." from https://apps.who.int/iris/bitstream/handle/10665/254991/WHO-HTM-GMP-2017.6-eng.pdf?sequence=1.

World Health Organization. (2019). "The E-2020 initiative of 21 malaria-eliminating countries: 2019 progress report." Retrieved 03/07, 2020.

World Health Organization. (2019). "World malaria report 2019." from www.who.int/malaria/publications/world-malaria-report-2019/en/.

World Health Organization. (2019). "World Malaria Report 2019." Retrieved 08/05/2020, 2020, from https://www.who.int/malaria/publications/world-malaria-report-2019/en/.

Wright, K. E., K. A. Hjerrild, J. Bartlett, A. D. Douglas, J. Jin, R. E. Brown, J. J. Illingworth, R. Ashfield, S. B. Clemmensen, W. A. de Jongh, S. J. Draper and M. K. Higgins (2014). "Structure of malaria invasion protein RH5 with erythrocyte basigin and blocking antibodies." Nature **515**(7527): 427-430.

Wu, Y., C. D. Sifri, H. H. Lei, X. Z. Su and T. E. Wellems (1995). "Transfection of Plasmodium falciparum within human red blood cells." Proc Natl Acad Sci U S A **92**(4): 973-977.

Yahata, K., M. N. Hart, H. Davies, M. Asada, T. J. Templeton, M. Treeck, R. W. Moon and O. Kaneko (2020). "Gliding motility of *Plasmodium* merozoites." bioRxiv: 2020.2005.2001.072637.

Yang, J., A. Roy and Y. Zhang (2012). "BioLiP: a semi-manually curated database for biologically relevant ligand–protein interactions." Nucleic Acids Research **41**(D1): D1096-D1103.

Yang, J., R. Yan, A. Roy, D. Xu, J. Poisson and Y. Zhang (2014). "The I-TASSER Suite: protein structure and function prediction." Nature Methods **12**: 7.

Yao, Z., M. Zhang, H. Kobayashi, H. Sakahara, H. Nakada, I. Yamashina and J. Konishi (1995). "Improved targeting of radiolabeled streptavidin in tumors pretargeted with biotinylated monoclonal antibodies through an avidin chase." J Nucl Med **36**(5): 837-841.

Yap, A., M. F. Azevedo, P. R. Gilson, G. E. Weiss, M. T. O'Neill, D. W. Wilson, B. S. Crabb and A. F. Cowman (2014). "Conditional expression of apical membrane antigen 1 in *Plasmodium falciparum* shows it is required for erythrocyte invasion by merozoites." Cellular Microbiology **16**(5): 642-656.

Yeoh, S., R. A. O'Donnell, K. Koussis, A. R. Dluzewski, K. H. Ansell, S. A. Osborne, F. Hackett, C. Withers-Martinez, G. H. Mitchell, L. H. Bannister, J. S. Bryans, C. A. Kettleborough and M. J. Blackman (2007). "Subcellular Discharge of a Serine Protease Mediates Release of Invasive Malaria Parasites from Host Erythrocytes." Cell **131**(6): 1072-1083.

Zainabadi, K. (2016). "Malaria Parasite CLAG3, a Protein Linked to Nutrient Channels, Participates in High Molecular Weight Membrane-Associated Complexes in the Infected Erythrocyte." PLOS ONE **11**(6): e0157390.

Zanghì, G., S. S. Vembar, S. Baumgarten, S. Ding, J. Guizetti, J. M. Bryant, D. Mattei, A. T. R. Jensen, L. Rénia, Y. S. Goh, R. Sauerwein, C. C. Hermsen, J. F. Franetich, M. Bordessoulles, O. Silvie, V. Soulard, O. Scatton, P. Chen, S. Mecheri, D. Mazier and A. Scherf (2018). "A Specific PfEMP1 Is Expressed in

P. falciparum Sporozoites and Plays a Role in Hepatocyte Infection." Cell Rep **22**(11): 2951-2963.

Zenonos, Z. A., J. C. Rayner and G. J. Wright (2014). "Towards a comprehensive *Plasmodium falciparum* merozoite cell surface and secreted recombinant protein library." Malaria Journal **13**(1): 93.

Zhang, M., C. Wang, T. D. Otto, J. Oberstaller, X. Liao, S. R. Adapa, K. Udenze, I. F. Bronner, D. Casandra, M. Mayho, J. Brown, S. Li, J. Swanson, J. C. Rayner, R. H. Y. Jiang and J. H. Adams (2018). "Uncovering the essential genes of the human malaria parasite *Plasmodium falciparum* by saturation mutagenesis." Science **360**(6388).

Zhang, W., Y. Shen, G. Xiong, Y. Guo, L. Deng, B. Li, J. Yang and C. Qi (2013). "Crystal structure of human Intersectin-2L C2 domain." Biochem Biophys Res Commun **431**(1): 76-80.

Zhang, Y. (2008). "I-TASSER server for protein 3D structure prediction." BMC Bioinformatics **9**(1): 40.

Zhao, X., Z. Chang, Z. Tu, S. Yu, X. Wei, J. Zhou, H. Lu, N. Jiang and Q. Chen (2014). "PfRON3 is an erythrocyte-binding protein and a potential blood-stage vaccine candidate antigen." Malaria Journal **13**(1): 490.

Zinzalla, G. and D. E. Thurston (2009). "Targeting protein–protein interactions for therapeutic intervention: a challenge for the future." Future Medicinal Chemistry **1**(1): 65-93.

Zuccala, E. S., A. M. Gout, C. Dekiwadia, D. S. Marapana, F. Angrisano, L. Turnbull, D. T. Riglar, K. L. Rogers, C. B. Whitchurch, S. A. Ralph, T. P. Speed and J. Baum (2012). "Subcompartmentalisation of proteins in the rhoptries correlates with ordered events of erythrocyte invasion by the blood stage malaria parasite." PLoS One **7**(9): e46160.